INSTITUT FÜR RADIOCHEMIE
TECHNISCHE UNIVERSITÄT MÜNCHEN

RCM 012004

EINFLUSS VON KOLLOIDEN AUF DIE MIGRATION VON ACTINIDEN

M. A. Kim, P. J. Panak, J. I. Yun*,*
J. I. Kim, A. Priemyshev, K. Köhler*

Abschlußbericht**
30.04.04

*Institut für Nukleare Entsorgung, Forschungszentrum Karlsruhe, 76021 Karlsruhe

**Das diesem Bericht zugrunde liegende Vorhaben wurde mit Mitteln des Bundesministeriums für Wirtschaft und Arbeit (BMWA) unter dem Förderkennzeichen 02E9360 gefördert. Die Verantwortung für den Inhalt dieser Veröffentlichung liegt bei den Autoren

Contents

1 Introduction

Colloids ubiquitous in natural water are called aquatic colloids. The chemical composition, number density and size distribution of aquatic colloids vary widely depending on the geochemical conditions of their provenance [1,2]. They may be composed of inorganic elements with oxo-bridges [3-5], of organic polyelectrolytes, like humic acid loaded with inorganic elements by complexation [6-9], or of tiny inorganic particles peptized by organic molecules [10-12]. The size distribution of predominant number density has been observed in general at < 100 nm, but very often at < 50 nm, as referred to an average hard sphere diameter [2,6,7]. The number density varies widely from 10^8 to 10^{14} particles per litre water depending on the geochemical environment [6,13]. Groundwater rich in organic substances, e.g. humic acid, contains abundant aquatic colloids [6,8], whereas groundwater poor in organic substances, e.g. granite water, contains a relatively smaller number density of aquatic colloids [13,14].

Aquatic colloids may play a significant carrier role for the radionuclide migration in a variety of aquifer systems [14-16]. Particularly radioactive elements of higher oxidation states, for example actinides with their strong tendency towards oxobridge building or complexation, possess a high potential for stable incorporation into aquatic colloids [2,6,14]. The formation of such aquatic colloid-borne actinides (called pseudocolloids of actinides) has not been well understood, besides the surface complexation of actinide ions onto aquatic colloids [17-19]. In the case the actinide ions are incorporated into the chemical structure of aquatic colloids, the colloid-borne actinides may remain stable as suspended in a given natural water and migrate along the water flow path with little chemical interaction with the surface of surrounding geomatrices [8,9]. Therefore, the provenance of aquatic colloids and the generation of aquatic colloid-borne actinides have become of great interest for a better appraisal of the chemical behaviour of actinide ions in natural aquifer systems [14,15,20] and also of the colloid facilitated actinide migration in aquifer systems [15,20-22].

The present work deals with the generation of aluminosilicate colloids, which are considered as a kernel for various aquatic colloids. Formation of the aluminosilicate binding is well known [23] and incorporation of traces of trivalent lanthanides and tetravalent elements like Th, has been observed in nature abundantly [24]. However, the generation of colloidal species of aluminosilicates and the chemical incorporation of actinides in such colloids have not yet been systematically understood. As the colloidal species of aluminosilicates are omni-

present in natural aquifer systems [1], the appraisal of their chemical interaction with tri- and tetravalent actinides is the main objective of the present investigation. For this purpose, the parameters controlling the formation of aquatic colloids through condensation of groundwater constituents, i.e. Si and Al, are identified, and the optimum conditions for aluminosilicate colloid formation are determined. The behaviour of the selected actinides Am(III), Cm(III) and Th(IV), either as contestants in the nucleation process of Si and Al, or as additives to preformed aluminosilicate colloids, is analyzed.

Am is the most abundant trivalent actinide in nuclear waste to be disposed of [2,25] and its chemical homologue Cm is smaller in waste amount but spectroscopically sensitive for the unperturbed speciation [26], thus allowing the study of its chemical behaviour conveniently. Th with its stable tetravalent oxidation state is the ideal model element to investigate the geochemical reactions of actinides with multiple oxidation states like Pu, U, Np and Tc which are the main components of long-lived radionuclides in nuclear waste and expected to be reduced to the tetravalent state at low redox potentials in the near field of a nuclear repository [25].

2 Natural and actinide aquatic colloids

The two general ways in which aquatic colloids may be formed, are by building up particles from dissolved molecular or atomic units, or by breaking down particles from the solid matrix, termed respectively condensation and dispersion:

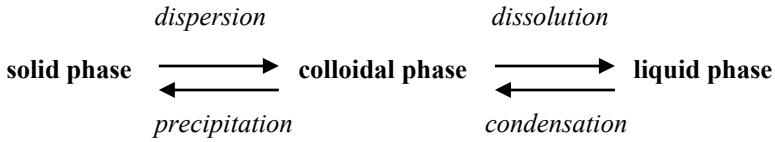

Fig. 1 (upper part) illustrates how elements with high oxidation state (≥ 3), such as Al(III), Si(IV) or actinides (An(≥III)) tend to minimize their positive charge by surrounding themselves as much as possible with oxygens through hydration, hydrolysis and polymerization. This process for colloid formation is called condensation and includes the formation of a supersaturated solution, the relieve of supersaturation by the formation of nuclei or by condensation upon nuclei already present, followed by growth to larger particles. The reverse process for colloid formation, namely dispersion (shown in Fig.1 (lower part)), involves weathering of

the parent solid material, which can be either physical disintegration or chemical decomposition, or both, and suspension of the small detached particles in the liquid phase.

Under certain optimum conditions, nanoparticles can thereby be stabilized in the colloidal phase, a process which is far from completely understood. This is partly due to the quite recent development of methods, such as ultrafiltration [6,8,9,14], laser-induced breakdown detection (LIBD) [27-32] or atomic force microscopy [33-37], which are capable to characterize small colloids (< 100 nm) in the low concentrations as they exist in nature, without perturbation. Numerous theoretical considerations concerning colloid generation and stabilization try to identify the underlying parameters and to describe their correlations in different models. Fundamental knowledge relevant to the present experimental investigations is conceptually summarized in the following.

2.1 Formation of colloids: theoretical background [1,38-43]

Colloidal interface free energy

The behavior of colloids is governed primarily by their large interfacial area. The interface is defined as the boundary between the adjoining bulk phases that comprise the colloid system, e.g. liquid/solid in the case of aquatic colloids. Within each bulk phase, forces acting on a molecule from all directions are balanced (Fig. 2). Molecules in the interface, however, interact simultaneously with molecules from both liquid and solid phases. Since forces of attraction are greater between the molecules of the solid phase than between those of the liquid phase, molecules in the interface are attracted more strongly towards the solid phase. The energy input, required to compensate for this imbalance of intermolecular forces, is the origin of the colloidal interface free energy. The high reactivity of colloids (activated solid state) stems from the tendency to minimize the free energy.

The questions are, where does this activation energy comes from, what kind of energy transfers do occur at deactivation, which mechanisms inhibit a complete deactivation so that the colloidal state, although thermodynamically unfavorable, persists over a long time span and how can we control the underlying parameters? Theoretical thermodynamic and kinetic approaches to the generation and stabilization of aquatic colloids, which might be helpful to conceive the appropriate experiments for answering such questions, are summarized in the following.

Formation of colloids through condensation

Spontaneous growth of particles out of their solution requires the formation of nuclei. The free energy of the formation of a nucleus, ΔG, consists of energy gained from making bonds and of work required to create a surface as expressed in thermodynamic terms:

$$\Delta G_j = - 4 \pi r^3 k_B T \ln S / 3 V + 4 \pi r^2 \gamma \qquad \text{Eq.1}$$

where r is the radius of the nucleus, V the molecular volume, k_B the Boltzmann constant, T the absolute temperature, S the supersaturation, ratio of actual concentration and solubility equilibrium concentration, and γ the interfacial energy (γ = = r kT ln S / 2 V). Fig. 3a shows the free energy of formation of a spherical nucleus as a function of its size, calculated for different supersaturation ratios (a/a_0). The height of the maximum, ΔG^*, is the activation barrier to the nucleation process of nuclei of radius r_j. Obviously, the activation energy ΔG^* as well as the size of the critical nucleus decrease with increasing supersaturation. Introduction of foreign solid surfaces for catalyzing the nucleation process by reducing the energy barrier of nucleation is the princip of heterogeneous nucleation, the predominant formation process for colloid and crystal formation in natural waters. If the foreign substrate is similar to the product of nucleating components, the interfacial energy between the two solids is smaller than the interfacial energy between the product and the solution, and nucleation may take place at lower supersaturation on a solid substrate surface than in solution. Temperature will also affect the value of the critical superaturation ratio.

This ratio decreases with rising temperature probably because of an increase in the number of collisions of atoms or molecules per unit concentration. The critical supersaturation ratio decreases when a system is subjected to turbulent effects, because of the probability of increasing concentration fluctuations in the form of some minute volumes of the solution with very high concentration.

The rate of formation of the nuclei, V_1, may be expressed by

$$V_1 = A \exp (- \Delta G^* / k T) \qquad \text{Eq.2}$$

where A is a factor related to the efficiency of collisions of ions or molecules. Accordingly, the rate of nucleation is controlled by the interfacial energy, the supersaturation, the collision

frequency efficiency, and the temperature. Fig.3b vizualizes the nucleation rate as a function of the critical supersaturation (ΔG^*) calculated for the following assumptions: $\gamma = 100$ mJ m^{-2}, molecular volume = 3 x 10^{-23} cm^3 and a collision frequency efficiency of 10^{30} cm^{-3} s^{-1}. At high supersaturation (low activation energy) the nucleation rate is high. Nucleation is ultimately superseded by growth of existing nuclei.

The rate of particle growth is determined by diffusion of substance from supersaturated volumes within the bulk towards those particles that are surrounded by thin envelopes of solution in equilibrium with the solid. It may be expressed by the general equation

$$V_2 = A\,(\ln S)^n \qquad \text{Eq.3}$$

where A and n are adjustable parameters.

The relative velocities of nucleation and growth, both processes competing for material in the supersaturated solution, determine the number as well as the size of the particles. At high supersaturation, the nucleation rate may be so fast that most of the excess dissolved mass is transformed in critical nuclei, leaving little material for further growth. Many small particles are formed. Few particles of huge size may be built at low supersaturation. Inhomogenity of the system with volumes of different degrees of supersaturation results in particles of various sizes (polydisperse system).

Colloidal electric double layer

Most substances acquire a surface electric charge when brought into contact with a polar (e.g. aqueous) medium, possible charging mechanisms being ionization, ion adsorption and ion dissolution. Ionization of functional groups depends strongly on the pH of the solution and leads to positively or negatively charged molecules at low pH and high pH, respectively. A net surface charge can further be acquired by the unequal adsorption of oppositely charged ions. Ion adsorption may involve positive or negative surface excess concentrations. Surfaces in contact with aqueous media are more often negatively charged than positively charged. This is a consequence of the fact that cations are usually more hydrated than anions and have the greater tendency to reside in the bulk aqueous medium, whereas the smaller, less hydrated and more polarizing anions have the greater tendency to be specifically absorbed. Surfaces which are already charged (e.g. by ionization) usually show a preferential tendency

to absorb ions of opposite charge, especially those with a high charge number. It may even cause a reversal of charge. If surfactant ions are present, their adsorption will usually determine the surface charge. In addition to specific adsorption, the net particle charge of some solids may arise either from the preferential dissolution of some ions and from lattice imperfections at the solid surface or by isomorphous replacements within the lattice.

The surface charge influences the distribution of nearby ions in the polar medium. Counter-ions are electrically attracted by the oppositely charged solids. At the same time, however, these ions have a tendency to diffuse away from the surface toward the bulk of the solution, where their concentration is lower. The net result of the two competitive tendencies is an equilibrium distribution of ions in which their concentration gradually decreases with increasing distance from the solid surface. Simultaneously, there is a deficiency of co-ions in the vicinity of the surface, since these ions, which have an electric charge with the same sign as the particle, are repelled. There is a gradual increase of co-ion concentration with the distance from the solid surface. The result is the generation of an electric double layer (EDL) at the solid-liquid interface, consisting of three regions with distinct dielectric behaviour (see Fig. 4): (1) the Stern layer, a layer of preferentially oriented water molecules in contact with the boundary, where the specific adsorbed bare ions are without their hydration shells; (2) the outer Helmholtz layer, a region of both free water molecules and molecules attached to hydrated ions, and defined by the closest approach of a fully hydrated charge ion to the boundary; (3) the Gouy-Chapman diffuse layer is the region where the concentration of the counterions decreases with increasing distance from the plane interface. The electric potential at the surface, Ψ_0, or the electric potential in the Stern plane, Ψ_δ, are not accessible by direct experimental measurement, but the surface potential can be calculated from the experimentally determined surface charge. The shear plane separates the hydrodynamically immobile liquid that moves together with the surface from the mobile liquid, which has non-zero relative velocity with respect to the surface. The electric potential in the shear plane is reflected by the measurable potential gradient that arises across the mobile part of the double layer, the electrokinetic ζ potential. The double-layer thickness is given by the reciprocal Debye length:

$$1/\kappa = (\varepsilon R T / 8 \pi F^2 c z^2)^{1/2} \qquad \text{Eq.4}$$

where ε is the dielectric constant of the medium, F is the Faraday constant, c and z are the concentration and the valence of the electrolyte, respectively. Increase of the ionic strength decreases the thickness of the double-layer.

Brownian motion of colloids

Water molecules in permanent random thermal movement hit the colloidal particles from opposite sides. The smaller the particles, the less the probability of the molecular bombardment being exactly balanced and the more intensive will be the movement. A consequence of this Brownian movement is the diffusion of colloid particles. When a certain phase is dispersed along the x axis, the mass, dm, transferred across an area O, during an interval, dt, as a result of a concentration gradient, dc/dx, is given by Fick´s first low:

$$dm/dt = - D O (dc/dx) \qquad \text{Eq.5}$$

where D is the diffusion coefficient. D depends on the properties of the disperse phase and the dispersing medium. For colloid particles D is related to the friction coefficient, B, between the particles and the dispersing medium by the expression $D = k_BT/ B$. The magnitudes of B and D depend on the dimensions and shapes of the particles. For spherical particles having a radius r, when the viscosity of the dispersing medium is η, B □□□□□□ 6 πη□ □□□.

$$D = k_BT/ 6 \pi\eta\square \qquad \text{Eq.6}$$

The Brownian motion is the dispersing energy of colloids and also the reason for frequent collisions between them. Depending upon wether the interaction forces between the particles during such collisions are attractive or repulsive, the colloids will agglomerate or stabilize (elaborated below). The movement of small colloids (e.g. < 100 nm), as they occur in the natural environment, is diffusion-limited (due to Brownian motion only). Other colloid transport mechanisms based on differential gravitational settling or caused by laminar shear being important only for large particles (≥ 1μm) are therefore not considered here.

Colloid stability: DLVO theory

Two suspended particles of like charge approaching each other as a result of their Brownian movement until their diffuse double layers interpenetrate and deform, is the basis for the quantitative description of particle-particle interaction by the DLVO (Derjagin, Landau, Verwey, Overbeek) theory. The potential energy of interaction (E_t) is calculated as the superposition of the electrostatic repulsive energy (E_R, conventionally considered positive), which is approximately an exponential function of the interparticle distance (d) with a range of the order of the thickness of the double layer ($1/\kappa$), and the van der Waals attractive energy (E_A, considered negative), which decreases as an inverse power of the interparticle distance, by the following equation (simplified and valid for thick plate particles, e.g. clay tactoids):

$$E_t = E_R + E_A = (64\ c\ R\ T\ \Gamma^2 / \kappa)\ (e^{-\kappa d}) - (K / 2\ d^2) \qquad \text{Eq.7}$$

where K is a constant depending on the nature of the dispersing medium, the particle thickness and its chemical composition, and Γ is defined as follows:

$$\Gamma = [(\exp(z\ F\ \Psi_\delta / 2RT)) - 1] / [(\exp(z\ F\ \Psi_\delta / 2RT)) + 1] \qquad \text{Eq.8}$$

Two general types of potential energy curves are presented in Fig. 5: in (a) $E_R > E_A$ and the total potential energy curve (E_t) shows a repulsive energy maximum, whereas in (b) the van der Waals attraction (E_A) predominates at any interparticle distance. The maximum in the energy curve is an energy barrier. If the potential energy maximum is large compared with the thermal energy of the particles (RT), the system should be stable; otherwise, the system should agglomerate.

The height of this energy barrier to agglomeration depends on the magnitude of Ψ_δ (and ζ) (Eq.8) and upon the repulsive forces (i.e. upon $1/\kappa$) (Eqs 4, 7). The DLVO theory to explain stabilization of colloids has been extended and may include, besides van der Waals attraction and electrostatic repulsion forces, also steric forces (generally repulsive) as well as polymer bridging forces (attractive) induced by adsorbed long-chain polymer.

Colloid stability: kinetics

Colloid stability depends on an energy barrier and is therefore also a question of kinetics and rates of agglomeration. In kinetics of the agglomeration process rapid and slow agglomerations are distinguished. In the case of rapid agglomeration so much electrolyte has been added that the energy barrier is reduced and is absent or too small to prevent particles from coming into contact (critical electrolyte concentration). Every collision results in irreversible agglomeration. In such a case the time-dependent decrease in concentration of particles (N = number of particles per cm^3) in a monodisperse suspension due to collisions by Brownian motion can be represented by

$$- dn/dt = k_p N^2 \qquad \text{Eq.9}$$

where k_p is the rate constant ($cm^3\ s^{-1}$). As given by von Smoluchowski, k_p can be expressed as

$$k_p = 8\ D\ \pi\ r \qquad \text{Eq.10}$$

The diffusion coefficient in Eq. can be subtituted in Eq.

$$- dn/dt = 4\ k_B T\ N^2 / 3\ \eta \qquad \text{Eq.11}$$

and it may be concluded that in monodisperse systems the rate of fast coagulation is not dependent on the size of the particles (r).

In practice, the right hand side of eq. is multiplied by α_p. α_p is the fraction of collisions leading to permanent agglomeration. It is an operational parameter for the stability ratio, the Fuchs-factor, $W = 1/\alpha_p$. α_p is the ratio of the slower agglomeration rate (in the presence of an energy barrier) and the fastest, diffusion controlled agglomeration rate (in the absence of an energy barrier), determined under the corresponding appropriate experimental conditions. The extended Smoluchowski theory for polydisperse systems shows that the rate of coagulation between particles of different sizes is much greater than the rate of coagulation of particles of the same size. The smaller particles disappear much more quickly than the larger one.

2.2 Actinide colloid generation pathways

Actinides may become aquatic colloids by two processes as illustrated in Fig. 6: (1) by binding to natural aquatic colloids and formation of so-called „pseudocolloids“ of actinides. The binding can proceed either by conucleation of actinides with dissolved groundwater components or by sorption of actinides to existing natural colloids; (2) by the formation of „real colloids“ either through nucleation of actinides in the order [14]

$$An^{4+} > AnO_2^{2+} > An^{3+} > AnO_2^{+}$$

or through dispersion of a solid actinide matrix.

2.3 Methods selected for actinide colloid analysis

Investigations of the geochemical behaviour of the sparingly soluble actinides (usually below 10^{-6} mol l^{-1}) in presence of ubiquitous small aquatic colloids (< 50 nm) in low concentrations (ppb range or less) require sophisticated analytical methods which have been developed in the last decade [26-35,44,45]. A brief overview of the principals of those methods, which have been used in this study for the nanoscopic analysis of aquatic actinide species under minimal perturbation of the system is presented here.

Laser spectroscopic methods

Conventional absorption spectroscopy on the transitions of the 5f-electron shell of actinides is a useful speciation method for the characterization of oxidation and complexation states. The spectroscopic resolution of actinide transition bands is in general very high but their intensity is relatively weak [46]. The low solubility of actinides under natural conditions necessitates a speciation method of high sensitivity. To that purpose, a number of spectroscopic methods have been developed in the recent past based on laser as a light source.Various laser spectroscopic techniques appropriate for the speciation of trace level actinides are illustrated schematically in Fig. 7.

The enhancement of sensitivity is attained by a direct measurement of different relaxation processes of photon excited states, instead of transmission measurement as practiced in

conventional absorption spectroscopy [47]. The methods shown in Fig. 7 can be classified in the following four categories: photo-thermal spectroscopy, luminescence spectroscopy, light-scattering and plasma generation. From those methods, TRLFS (time-resolved laser fluoresence spectroscopy) and LIBD (laser-induced breakdown detection) are used in this work. TRLFS is based on the measurement of radiative relaxation of a light induced excitaton state as illustrated in Fig. 8 for the example of Cm(III). The characteristic of this method is the selective excitation of the ground state combined with the selective time-resolved measurement of emission by an optical multichannel analyzer consisting of a polychromator and a time-gateable intensified photodiode array. All these provide a high sensitivity in the actinide speciation. However, the method is limited to the elements with fluoresence emission, to which belong some rare earth elements (REE(III)) and Cm(III) [20,26], Am(III) [48] and U [49,50] as actinides. With these elements, the aquatic chemical behaviour of trivalent and hexavalent actinides can be investigated in the nano-mole concentration range.

LIBD has been developed to quantify groundwater colloids with low number density and small average size [28,29]. The method is based on the plasma generation of colloidal particles by intense laser light absorption [30] as illustrated by Fig. 9.

The event takes place, upon multi-photon absorption, through the excitation and ionization avalanche of delocalized electrons within a colloidal composite and hence it is called breakdown. As the treshold energy density required for solid is much lower than for liquid, the plasma generation occurs with colloids selectively in their suspension medium. The breakdown event can be detected by measuring the plasma light emission with a charge-coupled-device (CCD) camera or by detecting the photo-acoustic signal with a piezo electric detector (PZT). The two-dimensional distribution of 8000 plasma events is measured in parallell as well as perpendicular to the laser beam direction (Fig. 10). The distribution width is correlated to the mean particle size (Fig. 11). By calibration of LIBD with polystyrene reference particles, a mean particle diameter and a number density of given colloids can be derived [27-32] as shown in Fig. 12. A sensitivity comparison of LIBD with that of light scattering methods, i.e. static light scattering and photon correlation spectroscopy (PCS) is shown in Fig. 13. In the low part of particle size, LIBD appears distinctively more sensitive than light scattering over many orders of magnitude.

In the course of plasma relaxation, the discrete plasma or atomic emission takes place after the recombination of electrons as shown in Fig. 9. The process can be used, as laser-induced breakdown spectroscopy (LIBS), for the characterization of colloid-borne elements

selectively in solution [31,32]. Accordingly, actinides present as ionic and colloid-borne species in aquatic systems can be differentiated by LIBS, since the colloid-borne actinides are better excited than their aqueous ions by the same laser energy intensity. This is a particular speciation method to detect pseudocolloids of actinides in groundwater, which may be used in our further continued study.

Atomic force microscopy (AFM)

AFM is a nanotopographic method scanning the repulsive and attractive forces between atoms of a SiN_3-tip, used as a sensor, and surface atoms of the sample at a separation distance of a few Å. Detection of the corresponding movements of the cantilever-tip is performed as shown in Fig.14, by sending laser light on the sample and registering the reflected light by a 4-quadrant photodetector. Interatomic force is calculated from the light intensity differences in the four quadrants. The attained resolution is 0.01 nm (0.1 Å) and the sample surface is 1nm up to 1 μm. Nano-topographical changes in the sample, e.g. during dissolution, colloid growth, sorption, etc. can be observed in situ. This is an advantage over electron microscopy requiring a vacuum resistent sample preparation.

Conclusions of section 2

Inorganic aquatic colloids in general and real colloids of actinides in particular may be generated either by condensation of dissolved elements or by dispersion of the solid matrix. The anabolic formation of inorganic aquatic colloids through condensation is based on the tendency of polyvalent cations of natural or radioactive elements such as actinides to reduce their positive charge through polymerization. The activation energy required to generate a solid surface out of dissolved elements originates from the supersaturation state of the solution. The degree of needed supersaturation varies with particle size. Supersaturation can partly be replaced by the presence of a foreign surface in the solution on which the nucleation can take place (heterogeneous nucleation). The generated particles follow the thermal movement of the water molecules, collide with one another and agglomerate. Three conditions to prevent agglomeration and to stabilize the particles at colloidal size are: (1) the generation of a particle surface charge through ionization, ion adsorption or ion dissolution; (2) the formation of an electric double layer around the charged particle with the aid of a well optimalized

ionic strength in the solution; (3) the presence of a repulsive maximum in the potential energy curve as a function of the interparticle distance (formation of an energy barrier to agglomeration) under well balanced conditions of surface charge and colloidal double layer thickness. Colloid generation as well as stabilization depend on energy barriers and are therefore not only a question of thermodynamics but also of kinetics. The underlying parameters are the parameters of solubility. The catabolic dispersive formation of inorganic aquatic colloids proceeds through the reversal of polymerization reactions. A further possibility to transfer actinides into the colloidal state is the formation of pseudocolloids of actinides either through co-condensation with natural elements in solution or through binding with preformed natural aquatic colloids.

The experimental investigation of the mentioned possible processes for the generation of natural as well as actinide aquatic colloids may rely on modern methods such as TRLFS, LIBD and AFM, which are capable to analyze the behavior of nanoconcentrations of actinides interacting with colloidal nanoparticles in ppb concentrations.

3 Synthesis of natural aquatic colloids

From the forgoing theoretical considerations (section 2.1) we have learned which parameter influence colloid formation and why they do so. We have also recognized that colloid formation and stabilization is a very complex process depending on the subtile tuning of a hughe number of parameters which can influence each other reciprocally. It is therefore not amazing that the conditions for the formation of aquatic colloids cannot be predicted theoretically but should be deduced from empirical experiences. The following section is based on colloid theory but concentrates on an experimental approach to colloid generation.

3.1 The choice of aluminosilicate colloids

The most common condensation process occurring in the hydrosphere is the hydrolysis of polyvalent cations (e.g. Si^{4+} and Al^{3+}), the formation of sparingly soluble hydroxides and hydrous oxides and the neoformation of clay minerals at coprecipitation. It seems therefore meaningful to choose clays as a representative example for answering questions about the formation of natural aquatic colloids as well as about their interaction with actinides. But

before concentrating on the synthesis of aquatic clay colloids, lets have a look on their closest relatives, the clay minerals.

Clay minerals are essentially hydrous layer aluminosilicates (phyllosilicates), with Mg and Fe acting as proxy wholly or in part for the Al in some minerals and with alkali metals and alkaline earth metals present as essential constituents in some of them. As illustrated in Fig. 15 [51], there are three types of phyllosilicates, namely, (1) the 1:1 type unit layer silicates (also known as the TO type), e.g. kaolinite, in which there is one tetrahedral sheet for every octahedral sheet, (2) the 2:1 type unit layer silicates (TOT type), e.g. smectite, illite, and (3) the 2:1:1-tape unit layer ([TOT]O[TOT], in which brucite ($Mg(OH)_2$-mineral)-type sheets lie between the parallel 2:1-type silicate layers, e.g. chlorite. The phyllosilicates are divided into groups according to the net charge of the unit layer.

A further subdivision is based on the number of available octahedral sites occupied: Those minerals containing divalent cations are called trioctahedral since all the available cation sites are filled, whereas minerals containing trivalent cations are called dioctahedral, having only two-third of the octahedral sites filled. Another subdivision is based on whether or not the stacked 1:1- or 2:1-type unit layers can be expanded and on the ease of swelling of the interlayer space either with water (compare illite and smectite) or with organic liquids. Each subgroup contains the different clay mineral species, which are distinguished by their chemical compositions. An additional group includes those clay particles with more than one type of layer present, termed mixed-layered minerals. These minerals belong to the sepiolite-palygorskite group. A further special type of highly hydrated secondary aluminosilicates are allophane and imogolite with an Si/Al-ratio of 0.5-1.0. They consist of small hollow spheres or cylindrical particles with a diameter of 3.5-5.0 nm (see Fig. 16). The AlOH outer surface is connected with the SiOH inner surface [52,53] through O-bridges. Their structure is limited to the range of very small particles (short-range order) which is in contrast to the other clay minerals. Recently much attention has been paid to aqueous hydroxy-aluminosilicates (HAS) of the imogolite type in many diverse contexts [23,54,55]. Besides their geochemical relevance, HAS play an important role in the oil industry, the paper industry, the production of zeolites, molecular sieves and catalysts. HAS seem further to be involved in biochemical reactions related to the toxicity of Al and discussed as inducers for a variety of plant, animal and human disorders, e.g. Alzheimer and Parkinson disease. The review article by Swaddle et al. [23] summarizes the present knowledge on silicate complexes of Al(III) in aqueous systems. He concludes: „The biomedical implications of the kinetic studies on Al(III)-Si(IV) interactions

at high pH by the NMR method are that simple hydroxyaluminosilicate (HAS) probably form and dissociate quickly even at low to neutral pH, so that their physiological behavior is thermodynamically controlled. However, the sequestration of Al(III) by oligomeric Si(IV), which the results of Taylor et al. [56] suggest, may be much more physiologically important, may yield kinetically inert HAS species - indeed, the apparently high stability of such complexes may well reflect the slow dissociation kinetics. Thus, a significant part of the protection afforded by silicic acid against Al(III) toxicity in biological systems may derive from the inferred kinetic inertness of ring or cage HAS structures which, once formed, may retain the Al(III) for long periods. The geological implication is that small acyclic HAS species and not the ring HAS solutes are the active agents in the hydrothermal crystallization of zeolites. The inert cage aluminosilicate solutes may act merely as reservoirs for the slow hydrolytic release of the small, active, acyclic species responsible for crystal growth."

The above statements reflect not only the high probability that very stable aqueous aluminosilicate colloids may be formed even under common environmental conditions, but at the same time they show that current knowledge, as far as colloid stability or generation mechanisms are concerned, is quite poor and that there is need for research. For this purpose, we intend in a first approach to coprecipitate Si and Al under conditions of supersaturation and to analyze in a coprecipitation parameter screening experiment whether and if yes, under which circumstances, the process is accompanied by the formation of aluminosilicate colloids.

3.2 Conditions for coprecipitation of Si and Al

Key information on how to attain supersaturation and coprecipitation of Si and Al is gained from thermodynamic solubility data for Si, Al and aluminosilicates. The main solubility parameter are temperature, pressure, pH, ionic strength, kind and concentration of water borne anions (ligands such as carbonate, sulphate, humate) and water borne cations (Na^+, K^+, Ca^{2+}, Mg^{2+}, $Fe^{2+/3+}$). Solubilities of Si, Al and some aluminosilicates as a function of pH at constant normal temperature, pressure and 0.03 mol l^{-1} NaCl are calculated from:

(1) The solubility products of the amorph solid phases of Al and Si, namely $Al(OH)_3$ and SiO_2, and of the mixed solid phases of Al and Si, namely Al_2SiO_5 (sillimanite), $Al_2Si_2O_5(OH)_4$ (kaolinite) and $NaAlSi_3O_8$ (low albite) based on the reactions:

$Al(OH)_{3(am)} + 3\ H^+ \Leftrightarrow Al^{3+} + 3\ H_2O$ $pK_{sp}^0 = -9.66$

$SiO_{2(am)} + H_2O \Leftrightarrow H_4SiO_4^0$ $pK_{sp}^0 = 2.71$

$Al_2SiO_5 + 6\ H^+ \Leftrightarrow 2\ Al^{3+} + H_4SiO_4^0 + H_2O$ $pK_{sp}^0 = -15.45$

$Al_2Si_2O_5(OH)_4 + 6\ H^+ \Leftrightarrow 2\ Al^{3+} + H_4SiO_4^0 + H_2O$ $pK_{sp}^0 = -7.30$

$NaAlSi_3O_8 + 4\ H^+ + 4\ H_2O \Leftrightarrow Na^+ + Al^{3+} + 3\ H_4SiO_4^0$ $pK_{sp}^0 = -2.76$

(2) The hydrolysis constants for the reactions:

$Al^{3+} + 2\ H_2O \Leftrightarrow Al(OH)^{2+} + H_3O^+$ $pK_{11} = 5.02$

$Al^{3+} + 4\ H_2O \Leftrightarrow Al(OH)_2^+ + 2\ H_3O^+$ $pK_{12} = 9.30$

$Al^{3+} + 6\ H_2O \Leftrightarrow Al(OH)_3^0 + 3\ H_3O^+$ $pK_{13} = 14.99$

$Al^{4+} + 8\ H_2O \Leftrightarrow Al(OH)_4^- + 4\ H_3O^+$ $pK_{14} = 23.33$

$Al^{5+} + 10\ H_2O \Leftrightarrow Al(OH)_5^{2-} + 5\ H_3O^+$ $pK_{15} = 34.24$

$2\ Al^{3+} + 4\ H_2O \Leftrightarrow Al_2(OH)_2^{4+} + 2\ H_3O^+$ $pK_{22} = 7.69$

(3) The dissociation constants for the reactions:

$H_4SiO_4^0 \Leftrightarrow H_3SiO_4^- + H^+$ $pK_{a10} = -9.71$

$H_4SiO_4^0 \Leftrightarrow H_2SiO_4^{2-} + 2\ H^+$ $pK_{a20} = -22.98$

$H_4SiO_4^0 \Leftrightarrow HSiO_4^{3-} + 3\ H^+$ $pK_{a30} = -32.85$

$H_4SiO_4^0 \Leftrightarrow SiO_4^{4-} + 4\ H^+$ $pK_{a40} = -45.95$

$4\ H_4SiO_4^0 \Leftrightarrow H_6Si_4O_{12}^{2-} + 2\ H^+ + 4\ H_2O$ $pK_{a64} = -13.32$

The given equilibrium constants [57-65] permit to calculate the concentration of each species as a function of pH, namely Al^{3+}, $Al(OH)^{2+}$, $Al(OH)_2^+$, $Al(OH)_3^0$, $Al(OH)_4^-$, $Al(OH)_5^{2-}$, $Al_2(OH)_2^{4+}$, for Al (Fig. 17); $H_4SiO_4^0$, $H_3SiO_4^-$, $H_2SiO_4^{2-}$, $HSiO_4^{3-}$, SiO_4^{4-} , $H_6Si_4O_{12}^{2-}$, for Si (Fig. 18); $H_4SiO_4^0$, Al^{3+}, $Al(OH)^{2+}$, $Al(OH)_2^+$, $Al(OH)_3^0$, $Al(OH)_4^-$, $Al(OH)_5^{2-}$, $Al_2(OH)_2^{4+}$, for aluminosilicates. Summation of the separate solubility curves gives the total solubility curve.

Fig. 19 compares the total solubility curves for Si, Al, and for the mentioned aluminosilicates. The pH range of interest, in which colloids can be formed in the course of coprecipitation, is selected according to the low solubility region of the different aluminosilicate compounds. Among them, sillimanite is the most soluble, whereas kaolinite is the least solu-

ble in the near neutral pH range, both following the similar pH dependency and showing the lowest solubility at pH 6.0. Low-albite shows the solubility behaviour different from that of sillimanite and kaolinite, decreasing sharply from pH 4.0 to 6.0 and remaining low with pH increase. Amorphous $Al(OH)_3$ is similarly soluble as sillimanite, while SiO_2 shows a constant solubility up to pH 9. Following Fig.19, the pH range for the present investigation is chosen from 4 to 9. Three initial concentrations of Si, namely 10^{-4}, 10^{-3} and 10^{-2} mol l^{-1}, below and above the saturation concentration (2 x 10^{-3} mol l^{-1}) are combined with varying Al concentrations from 10^{-7} to 10^{-3} mol l^{-1}.

3.3 Parameter screening experiment for colloid formation

The screening experimental princip, namely oversaturate solutions of Si and Al by changing the pH and trace colloid formation by observing the behaviour of ^{241}Am as a contestant in the coprecipitation process of Si and Al, is realized in three steps as shown in Fig. 20: (1) an acidic Al-solution traced with ^{241} Am (10^{-7} mol l^{-1}) is titrated with an alkaline Si-solution to a preset pH; (2) the precipitate is removed from the coprecipitation sample by filtration at 450 nm pore size and the colloids are removed from the solution (ionic+ colloidal species) by ultrafiltration at 1.8 nm pore size; (3) after different conditioning times, from 3 h to 35 days, the activity fraction in solution with and without colloids is measured by liquid scintillation counting and the activity fraction (%, related to the input activity) in solution (non-colloidal), colloids and precipitate is evaluated. The special advantage of using Am to trace colloid formation is to restrict automatically the screening to such colloids which are prone to incorporate actinides.

A typical experimental result is shown in Fig. 21, for which 10^{-3} mol l^{-1} Si, 10^{-5} mol l^{-1} Al and 4.9 x 10^{-8} mol l^{-1} Am are mixed initially at the ionic strength of 0.03 M NaCl. The Am activity fraction, evaluated as a function of pH, is shown for the first filtrate (at 450 nm pore size) normalized to the initial activity, and for the second filtrate (at10 kD-pore size) normalized to the Am activity of the first filtrate. Fig. 21a shows the pH dependent Am activity fraction, comprising the ionic and colloidal species (so called „mobile“ species), namely the Am activity fraction in the first filtrate separated from the precipitate by a filter of 450 nm pore size. The aging of the solution from 0 to 35 days does not lead to a significant change in the Am activity in solution. However, the solution pH changes slightly to acidic with time and stabilizes after some time. The lowest Am activity fraction in solution is found around pH 6,

which corresponds to the lowest solubility of aluminosilicate compounds as shown in Fig. 19 for sillimanite and kaolinite. This fact suggests the incorporation of Am into aluminosilicate formation. As the initial Al concentration taken for this experiment (Fig. 19) is at 10^{-5} mol l^{-1}, the precipitation is expected around pH 6. If the primary aluminosilicate precipitate is either sillimanite or kaolinite like (cf. Figs. 15 and 19), their solubility changes sensitively in the pH region of 4-9. The Am activity fraction observed in the solution changes sensitively in the pH range of 5-7, suggesting its incorporation into aluminosilicate formation. A separate experiment with a pure Am solution of 4.9 x 10^{-8} mol l^{-1} (also in Fig. 21a) shows a decrease of its activity fraction in the filtrate at 450 nm pore size with increasing pH and the Am activity fraction in solution remains low at pH > 6.5, being significantly different from that of aluminosilicate solutions.

The Am activity measured in the pure Am solution follows closely the solubility behaviour of an amorphous $Am(OH)_3$ precipitate (cf. Fig. 22) [66]. The difference of the Am activities between the aluminosilicate solution and its pure solution at pH > 6.5 appears another indication that Am is associated with aluminosilicate formation. Fig. 21b illustrates the colloid-borne Am activity fraction as a function of pH, which is normalized to the activity in the first filtrate from 450 nm pore size, i.e. the colloid fraction within the solution after the separation of precipitate. The colloid-borne Am in the first filtrate prevails at pH > 5 after 35 days of reaction time. At pH 4 about 20% Am appears colloid-borne and its fraction within the solution increases at pH ≥ 5 to more than 95%, then remains constant up to pH 9. Aging of the composite solution up to 35 days does not show a visible change in the colloidal Am fraction at pH > 6. Only at pH 5, the colloidal Am fraction increases with time. Fig. 21b indicates that the predominant solution species of Am at pH > 6 is colloidal and remains stable under present experimental conditions. The colloidal Am fraction in solution appears independent of different degrees of precipitation observed in Fig. 21a. The experiment shown in Fig. 21 is further conducted for a wide variety of the initial Si and Al concentrations and their different ratios in order to ascertain the conditions for the colloid formation. The main result of the screening experiment for aluminosilicate colloid formation is summarized in two time dependent contour diagrams representing the colloid-borne Am fraction (%) as a function of pH in mixture solutions of Si and Al after 3 hours up to 35 days sample conditioning time for two concentration levels of Si in the mother solution, just below (Fig. 23) and above (Fig. 24) the Si saturation concentration (2 x 10^{-3} mol l^{-1}), each of them combined with increasing concentrations of Al from 10^{-7} to 10^{-3} mol l^{-1}. Two characteristic pH regions are distinguished for

the colloid formation: around pH 5 for a minor fraction and between pH 7 and 9 for a major fraction. As the solubility of aluminosilicate compounds is lowest at pH 6 (see Fig.19), the colloid formation appears to be accordingly minimal around this pH region. The equilibrium for colloid formation is slowly reached in case that Si in the mother solution is undersaturated (Fig. 23), but the reaction of the Al^{3+} ion (also Am) with over-saturated Si as starting reactant (Fig. 24) proceeds promptly, reaches equilibrium within 3 hours and the result is not changed virtually up to 35 days and longer.

Fig. 25 illustrates an overview of the formation of colloid-borne Am as a function of pH for different Si/Al ratios in the mother solutions 35 days after mixing Si, Al and Am. Essentially three characteristic regions for optimum formation of stable colloids are differentiated. The first and second optimum arise from the slightly undersaturated Si solution at pH 5-6 and pH 8-9, respectively, and the third optimum from the 6.4 times saturated Si solution at pH 8-9, in each case a Si/Al ratio in the mother solutions of 100, namely for the following two optimalized concentration combinations:

I: $[Si] = 10^{-3}$ mol l^{-1} (0.7 x sat.) + $[Al] = 10^{-5}$ mol l^{-1} ([Si]/[Al] = 100)

II: $[Si] = 10^{-2}$ mol l^{-1} (6.4 x sat.) + $[Al] = 10^{-4}$ mol l^{-1} ([Si]/[Al] = 100)

The distinct screening patterns for colloid formation as a function of pH as well as of time, depending on whether Si in the mother solution is under- or oversaturated might be related with the expected different polymerization kinetics of Si as a function of pH and at increasing concentration [67], and prompts us to check the polymerization behaviour of Si under our experimental conditions. The understanding of the conditions for the formation of mono- and polysilanol is especially important since polysilanol is known to possess a 10^6 times higher affinity for Al than monosilanol [56]. The fact implies that the formation processes of aluminosilicate colloids and hence their interaction with Am may also be different, depending on whether monosilanol or polysilanol is involved as an initial reactant.

3.4 Mono- and polysilanol for condensation with Al

The following experiments serve the general comprehension of the generation of polysilanol under possible dynamic environmental conditions, not only out of solution through nucleation at oversaturation (polymerization of Si), but also out of the solid geoma-

trix through dispersion (depolymerization of Si). Within that study, special attention is drawn to the polymerization behaviour of Si under the previously mentioned optimum conditions for colloid formation at coprecipitation of Si, Al and Am.

The formation of polysilanol from sodium-waterglass (7.0 M Si in 4.0 M NaOH) are examined, as illustrated in Fig. 26, via two different approaches, respectively: By dilution to the alkaline pH = 12, monosilanol remains prevailed (see Fig. 19) and after subsequent adjusting the pH to neutral (pH = 5 - 9), monosilanol is converted to polysilanol under the condition of over-saturation (approach A); By dilution to the neutral pH range, polysilanol is produced by over-saturation of silanol in its low solubility region (approach B). The two approaches show the Al effect on the polymerization and depolymerization of Si in solution, respectively, and give an insight into the formation of aluminosilicate colloids.

Polymerization of Si is analyzed by approach A (Fig. 26) and made by dilution of sodium-waterglass to $2x10^{-3}$ – $4.2x10^{-2}$ mol l^{-1} Si at pH 12, in which monosilanol prevails. The solution is then neutralized to pH = 5 – 9 to make over-saturation of silanol, i.e. 1 - 21 times of the solubility saturation concentration of amorphous silica ($2x10^{-3}$mol l^{-1}) in the given pH range [68-71]. A conversion of monosilanol to polysilanol as a function of time is quantified by the molybdenum-test [67,72]. The result is illustrated in Fig. 27 and shows that the polymerization rate of silanol e.g. for the 6.4 times over-saturation (optimum conditions II) is pH dependent and completed after 5 days to a level of solubility constrains of amorphous silica, namely to about 85% mole fraction of polysilanol. Under the same condition, as expected, the polymerization does not take place in the non-saturated Si solution ($\leq 2x10^{-3}$ mol l-^{1} Si) (optimum conditions I).

The Si concentration effect on the polymerization is summarized in Fig. 28 for different pH and after different time intervals, namely 1 day (Fig.28, upper part) and 10 days (Fig. 28, lower part). At $4.2x10^{-2}$ M Si (21 x saturation concentration), the polymerization proceeds promptly and reaches a polysilanol mole fraction of 95%, as expected from the solubility of amorphous silica. A slower polymerization is observed at $1.3x10^{-2}$ M Si (6.4 times saturation concentration), especially at low pH. At $5x10^{-3}$ M Si (2.5 times saturation concentration), the completion of polymerization is considerably slow and at pH 5.5 it takes over 200 days. The upper limit of polymerization depends on the original Si concentration, which corresponds to a thermodynamic solubility level of amorphous silica, whereas the kinetics of polymerization is directly influenced by pH as well as concentration of Si. At low pH and at low Si concentration, the polymerization rate is low.

Depolymerization of Si is tested following approach B (Fig. 26). After polysilanol is produced by neutralizing dilution of sodium-waterglass to $4.2x10^{-2}$ M Si at pH = 7 (21x oversaturation, cf. Fig. 28), the depolymerization is measured, as illustrated in Fig. 29, at different degrees of dilution in the pH range of 6 - 8. By dilution of polysilanol to $5x10^{-3}$ M Si, the depolymerization takes place to a steady level of about 60%, which corresponds to the solubility of amorphous silica. The polymerization of monosilanol at the same Si concentration appears to reach the same level. At further dilution to $< 2x10^{-3}$ M Si, the depolymerization is quantitative. As is apparent from Figs. 27-29, the polymerization and depolymerization of Si are reversible processes, unless foreign metal ions of higher charged state ($2+ < z < 4+$) are present [67]. The effect of Al will be discussed later (see section 8.2).

At this point, we can further define the optimal experimental conditions for the aluminosilicate colloid formation:

I **[Si] = 10^{-3} mol l^{-1} (monosilanol = 100%) + [Al] = 10^{-5} mol l^{-1} (pH 5-6 & 8-9)**

II **[Si] = 10^{-2} mol l^{-1} (polysilanol ≤ 85%) + [Al] = 10^{-4} mol l^{-1} (pH 8-9)**

3.5 Quantification and characterization of colloids

The hitherto used methods to trace aluminosilicate colloid formation, namely separation of colloids by ultrafiltration and determination of the Am activity in the colloidal fraction, have been fast, effective and convincing. However, they are indirect methods, which cannot give any information on the quantity or type of the generated colloids. Therefore we introduce now sophisticated techniques such as LIBD, AFM and SEM-EDXS to analyze the synthetized colloids directly.

Appraisal of aluminosilicate colloid formation by LIBD

To ascertain how the colloidal Am species is formed, the colloid formation in aluminosilicate solutions without addition of Am is examined by LIBD. As shown in Fig. 30, the acidic Al solution of 10^{-5} mol l^{-1} is titrated by an alkaline Si solution of 10^{-3} mol l^{-1} (optimum conditions I). The maximum colloid formation emerges at pH 5.5, the minimum at pH 6.5, and at pH ≥ 8.0 the colloid generation increases again. The results of the LIBD experiment are comparable to the screening experiment made by filtration with addition of Am as shown in

Figs. 23 and 25. Around pH 6.5, the absolute amount of generated colloids is found to be minimal, being in accordance with the lowest solubility of aluminosilicate compounds (e.g. sillimanite) as appeared in Fig. 19. A relatively low amount of colloids observed at pH 4.0 may be ascribed to an acidic pH effect that asserts oxygenbridge breaking and hence less colloid formation. This is comparable to the colloid-borne Am fraction shown in Fig. 21(b). Since all chemical solutions for laboratory use contain more or less colloids as impurities, their influence on the present experiment is examined separately.

The original Al and Si solutions are pH titrated separately, both in about 10^{-3} mol l^{-1}, in order to ascertain whether they contain colloids originally or colloids are generated on the pH change that are detectable by LIBD. The results are shown in Fig.30. The Al solution shows a realtively small amount of colloid generation by changing pH from 4 to 7 and above 7 no colloids can be detected. The initial Al concentration of 10^{-3} mol l^{-1} may undergo precipitation of $Al(OH)_3$ with increasing pH and its solubility is the lowest at pH 6 (cf. Fig. 19). Therefore, the colloid generation, as confirmed by LIBD, in the pH region of 4-7 may be attributed to an oversaturation of Al that is conducive to polynucleation. The Al concentration of 10^{-5} mol l^{-1} with addition of Am (4.9×10^{-8} mol l^{-1}) also indicates, as shown in Fig.25 (down part), the generation of colloidal species in a small amount at pH 4-7 even in the absence of Si. The pure Si solution shows the presence of colloids in a relatively small amount in the whole pH range investigated. As the effect of pH change on the colloid concentration is only marginal, it is supposed that the original Si solution contains colloidal impurities. The element analysis indicates about 10 ppb of Al as an impurity in the original Si solution, which may induce a trace amount of aluminosilicate colloids detectable by LIBD as shown in Fig.30. As a conclusion, the original Al and Si solutions are also found to generate colloids or contain colloidal impurities for different reasons. However the amounts detectable by LIBD are distinctively lower than the colloid generation taken place in aluminosilicate solutions (Fig. 30). Such difference corroborates the formation of aluminosilicate colloids.

Particle size, number density and Si/Al ratio

The average size of corresponding aluminosilicate colloids is determined at pH values 6.0 and 7.5. The experimental results of LIBD are shown in Fig. 31. Two-dimensional distributions of optical detection of plasma generated on colloid breakdown are shown in the upper part of Fig. 31, which are concentrated in the centre of effective laser focal volume. Counting

of all breakdown events at each given pH is then made as a statistical distribution on the z-axis as shown in the lower part of Fig. 31. A twice value of the full width at half maximum (FWHM) is taken for the evaluation of an avergae colloid size in hard sphere diameter according to the previous calibration [28]. The average size is found to be 13± 1 nm at pH 6.0 and 11± 2nm at pH 7.5. The two values are virtually the same within the experimental precision. The average size remains unchanged with time, indicating the stability of aluminosilicate colloids in the investigated pH range. The AFM measurement is also performed as shown in Fig. 32. Therefore the supernatant of the colloidal precipitate at pH 7 is brought onto a mica plate for the AFM study under non-contact mode. The particle analysis results in 5-10 nm height and 10-50 nm length for the spherical or egg shaped particles of preponderance as shown in Fig. 32. This value closely corroborates LIBD results of the present experiment as evaluated for a hard sphere diameter. Breakdown events scattered mostly around a narrow sphere of y-z axes in Fig. 31 suggest a small range of the colloid size distribution. The colloid number density determined by LIBD ranges from $10^{11} – 10^{14}$ particles per litre water depending on the experimental condition (pH, Al and Si concentrations). The analog analysis of aluminosilicate colloids generated under the optimum conditions II shows a comparable average size of 10-20 nm as well as number density. The atomic Si/Al ratio of aluminosilicate colloids from conditions I and II is determined by SEM-EDXS and found to be 0.71±0.05 and 1.23±0.03, respectively. It is amazing that the Si/Al ratio in the colloids is almost independent on the degree of polymerization of Si in the mother solution. The atomic ratio of about one is evocative for a kaolinite or imogolite like composition of the aluminosilicate colloids [59] such as hydroxy aluminosilicate colloids also called HAS [54,55]. Taking into account the Si/Al ratio of HAS colloids approximately one, their formation from polysilanol can be presumed as

$$n\ Al(OH)_{3-y}^{y} + Si_nO_{n-1}(OH)_{2n+2} \quad \Leftrightarrow \quad Al_nSi_nO_{4n+2-x}(OH)_x^{x-n-4} + (7+ny-x)\ H^+ + (2n-ny-1)\ H_2O$$

where the y value varies from –1 to +3 following the degree of hydrolysis within the present experimental pH range (4 – 9) and the x value determines the anionic charge of HAS colloids. Polynuclear species of hydrolysed Al ions become important only at pH < 5 [62,63]. Whereas the Al^{3+} ion undergoes hydrolysis, thus forming different hydroxyl species in the given pH range [62-65], the predominant silanol species appears to be $Si(OH)_4$, unless the Si concentration is over-saturated [23,38,56,59,67] (see section 3.4). Therefore, a general polysilanol form

of neutral charge is envisaged as a reactant for the above-formulated reaction. The n value is too complicated to be ascertained. This formulation may correspond to the formation of the Cm-HAS(III) species via isomorphic substitution of Cm to a multidentate oxo-bridging of Al.

Because only a small amount of colloids is generated in the present experiments (10-50 ppb), their structure characterization is not directly possible. It is important to note that the characteristic values for the aluminosilicate colloids we have synthesized are typical for aluminosilicate colloids as they are found in the nature:

	Natural system	Present system
• Particle size	very often < 50 nm	10 - 50 nm
• Number density	10^8 - 10^{14} particles l^{-1}	10^{11} - 10^{14} particles l^{-1}
• Si/Al ratio	imogolite: 0.5 - 1.0	0.7 - 1.2

Conclusions of section 3

In an elaborated parameter screening experiment, optimum conditions for aluminosilicate colloid formation have been recognized from their capability to incorporate Am, which has been added in a tracer concentration as contestant in the condensation process of Si and Al. The optima correspond to mother solutions made at pH 5-6 and pH 8-9, with a Si/Al concentration ratio of 100, but at two different Si concentration levels, namely in a slightly undersaturated and in a 6.5 times oversaturated solution.

The corresponding colloids, as analyzed by LIBD, AFM and SEM-EDXS, all belong to a unique colloid type which is very similar to the natural aquatic colloids of the imogolite type with a Si/Al atomic ratio of ca 1, namely hydroxy aluminosilicate (HAS) colloids. They are small colloids (10 - 50 nm) with a low number density (10^{11} – 10^{14} particles $^{l-1}$).

Different optimum formation conditions for a solely colloid type may reflect different colloid generation mechanisms with distinct interaction potentials for Am. Such differences may be connected with pH and concentration of Si in the mother solutions, which have been shown to influence the degree of polymerization of Si. The hypothesis urges us to further investigate the interaction of Am with HAS colloids in the moment of formation, also called HAS colloids in statu nascendi.

4 Interaction of trivalent actinides with aluminosilicate colloids in statu nascendi

The study of the interaction of trivalent actinides with aluminosilicate colloids in the course of their generation by coprecipitation, also called aluminosilicate colloids in statu nascendi, comprises the following steps: (1) identify and characterize the binding state of Am(Cm) within the colloids; (2) analyze the underlying reasons for differentiated incorporation of Am(Cm) into colloids; (3) test the stability of the colloid-borne Am(Cm); (4) determine the capacity of the aluminosilicate colloids to incorporate increasing amounts of Cm(Am).

4.1 Speciation of colloid-borne Cm by TRLFS

TRLFS is the method par excellence to follow the binding state of trace amounts (up to 10^{-8} mol l^{-1}) of Cm in vivo, e.g. at the titration experiment for condensation of Si and Al. The optimal conditions I and II (cf. section 3) for the formation of aluminosilicate colloids from monosilanol and polysilanol, respectively, are selected for the purpose.

Formation of aluminosilicate colloid-borne Cm from monosilanol (condition I)

Typical TRLFS spectra of colloid-borne Cm are shown in Fig. 33, for which the initial concentrations of Si and Al are taken 10^{-3} and 10^{-5} mol l^{-1}, respectively, with an addition of a Cm concentration at 4.9×10^{-8} mol l^{-1}. The acidic Al solution containing Cm is titrated by the alkaline Si solution. The pH dependent evolution of the fluorescence spectrum is illustrated in the upper part of Fig. 33, whereas the deconvolution of a composite spectrum is shown in the middle part of Fig. 33. The spectroscopic speciation shows the presence of three different Cm species: the free Cm^{3+} aquo-ion with the emission peak at 593.8 nm and two different colloid-borne Cm species, indicated as HAS (hydrated aluminosilicate) species I and II, with the emission peaks at 598.5 and 601.8 nm, respectively. The red shift of the emission band is attributed to the formation of inner-sphere complexes. An exchange of water molecules of the inner coordination sphere by complexing ligands causes a change in the ligand field of the aquo Cm^{3+} ion, which results in a bathochrome shift of the fluorescence spectrum [26,44].

All spectra recorded at pH 2-8 are deconvoluted and individual species present at each pH are quantified. The fractions of each Cm species thus evaluated are shown in Fig. 33

(lower part) as a function of pH, in which the formation of colloidal Cm species can be appraised. The species Cm-HAS(I) is formed between pH 3 and pH 8 with its maximum around pH 6, while the Cm-HAS(II) species appears at pH 5 onwards to higher pH and becomes the prevailing colloidal species at pH > 7.

The characterization of the two colloidal species, Cm-HAS(I) and Cm-HAS(II), is further pursued by measuring their relaxation times of fluorescence at 598.5 and 601.8 nm, respectively, as designed for the colloidal species in Fig.33, to ascertain the number of hydration water molecules bound to Cm. The species Cm-HAS(I) and Cm-HAS(II) show a relaxation time of 83.5±3.7 μs and 88.3±5.2 μs, respectively. Based on these data and relative to the free Cm^{3+} ion, which is assumed to contain 9 coordinated water molecules [73] and has a fluoresence relaxation time of 65±2 μs, the numbers of hydrated water molecules are calculated according to Horrocks [74] and Kimura et al. [75]. According to Kimura et al., the remaining water molecules of Cm for the colloidal species Cm-HAS(I) and Cm-HAS(II) are calculated to be 7±0.5 and 6±0.5, respectively. This fact infers that the colloid-borne Cm has either bidentate oxygen bridges or tridentate oxygen bridges to Al-O- and Si-O- moieties within HAS colloids. According to Fig. 33, Cm appears colloid-borne in the near neutral pH region. This result supports the Am colloid formation as ascertained by filtration experiments given in Figs. 23 and 25.

For the purpose of comparison, the Cm speciation is also made in a pure Si solution of 10^{-3} mol l^{-1} without the addition of Al and in a pure Al solution of 10^{-3} mol l^{-1} without the addition of Si, to both of which 4.9x10-8 mol l^{-1} Cm is added. Fig. 34b shows Cm emission spectra measured as a function of pH in the pure Si solution. As Al impurity is present ($3.7x10^{-7}$ mol l^{-1}) in the original Si solution, a certain amount of latent aluminosilicate colloids is expected, in which Cm may be incorporated and become colloid-borne species. However, as the Si concentration is 10^{-3} mol l^{-1}, while the Al impurity concentration is so low, the plausible assumption is that the interaction of Cm with silanol groups may prevail in this solution. The radiometric assay shows that Am(III) added to the pure Si solution without Al addition becomes partially colloid-borne species with pH between 5 and 9 (Fig. 25) and the rest remains as ionic species, either Am^{3+} aquo-ion or Am-silicate complex. Cm is, therefore, expected to behave accordingly. The emission peaks of Cm observed in the pure Si solution are the same as in the Si/Al solution (Fig. 34a) at 593.8 nm, 598.5 nm and 601.8 nm. Fluorescence lifetimes of the three emission peaks are nearly the same as well, suggesting that the prevailing interaction of Cm takes place with Si in both solutions. The number of hydrated

waters appears the same as well in both solutions, i.e. 7 H_2O for the complex species (I) and about 6 H_2O for the complex species (II). These numbers surmise the bidentate and tridentate bindings to oxo-bridges, respectively.

The speciation results shown in Fig. 34c indicate that in the pure Al solution Cm is incorporated into Al hydroxides, which slowly undergo precipitation. The Cm emission peak is changing with pH from the Cm aquoion at 593.8 nm via gradual bathochrome shift to a new species at 604.1 nm. This species has a longer lifetime of 110.5 μs, being distinctively different from the interaction of Cm with Si. The total emission intensity of Cm in the Al solution is decreasing with increasing pH in the course of time. This fact infers the coprecipitation of Cm in Al hydroxide, because the Al concentration of 10^{-3} mol l^{-1} under investigation is substantially higher than its solubility in the pH region 5-9 [62,63]. Therefore, the spectra shown in Fig. 34 are recorded while stirring the solution. This experiment is to demonstrate that the incorporation of Cm in aluminosilicate colloids (Fig. 34a) shows the spectroscopic properties clearly different from its incorporation into Al hydroxide precipitate. The fact that the emission peak at 604.1 nm appears only in the pure Al solution, not in the mixed solution of Si and Al (Fig. 34a), means the non-attendance of Al hydroxide precipitation in the presence of Si, exceeding the Al concentration. The species fractions as a function of pH are evaluated for the pure Si solution and compared with the species distribution for the mixed solution.

Fractional appearances of the two Cm complex species (I) and (II) in Fig. 33 as a function of pH are found to be nearly the same for the two solutions. The fluoresence lifetimes of the two complexes in the two solutions are nearly the same for each corresponding species (Table 1) and hence the number of hydration water molecules for Cm can be assigned to seven and six for the complex species (I) and (II) in both solutions, respectively. The only difference is the amount of colloid-borne Cm species that is significantly larger in the mixed solution of Si and Al than in the pure Si solution (cf. Fig. 25). In the former solution, Cm undergoes incorporation into aluminosilicate colloids as a contestant of Al, whereas in the latter solution Cm is complexing with silanol moieties and thus results in either colloidal or ionic complex state, in which partial precipitation of Cm-silicate complex takes place.

Formation of aluminosilicate colloid-borne Cm from polysilanol (condition II)

Titration of an acidic Al solution containing Cm by an alkaline Si solution with the final concentrations 1.34×10^{-2} M Si, 1×10^{-4} M Al and 4.8×10^{-8} M Cm, which is accompanied by

the formation of polysilanol (cf. Fig. 26, approach A and Fig. 27), is traced for colloid-borne Cm by recording the TRLFS spectra at pH 2-8. The speciation results for Cm are shown in Fig. 35. The upper part of Fig. 35 demonstrates a pH-dependent evolution of fluorescence spectra as a function of pH, while the down part of Fig. 35 illustrates the deconvoluted emission spectra of four different Cm species present in the solution. The emission peak for the Cm^{3+} aquo-ion appears at 593.8 nm with a lifetime of 67.1±2.5 μs, corroborating the known value [26,44,45]. The first colloid-borne Cm species, entitled as Cm-HAS(I), becomes visible at 598.5 nm with a lifetime of 83.5±3.7 μs and the second colloid-borne Cm species Cm-HAS(II) emerges at 601.8 nm with a lifetime of 88.3±5.2 μs. The third colloid-borne Cm species: Cm-HAS(III), comes forward at 606.8 nm with a longer lifetime of 518±25 μs, which appears to be unique for Cm in the aluminosilicate colloid formation from polysilanol and has not been observed in its reaction with monosilanol.

The titration of polysilanol interacting with Cm in the absence of Al under the same condition gives rise to nearly identical speciation results. The emission spectral evolution shown in Fig. 36, i.e. peak positions and each corresponding lifetime, are the same as in Fig. 35. The observed species are named Cm-HPSi(I) (hydroxy-polysilanol), Cm-HPSi(II) and CmHPSi(III). These species come out as three different kinds of complexation of Cm with polysilanol moieties. Their similar spectroscopic characteristics to the Cm-HAS species indicate that in the aluminosilicate colloids Cm interacts preferentially with silanol moieties as a substitution to Al. From the lifetime measurement of each emission peak, one may deduce the number of water molecules, which remain coordinated with Cm in colloids. Cm-HAS(I) and CmHAS(II) are found to have 7 and 6 coordinated water molecules, whereas Cm-HAS(III) has one or none. The number of coordinated water molecules of each colloid-borne Cm species puts forward that the oxo-bridging state of Cm in aluminosilicate coilloids is a bidentate for Cm-HAS(I) and a tridentate for Cm-HAS(II). A complete structural incorporation of Cm is then conceivable for the Cm-HAS(III) species, as Cm in this species has virtually no hydration water. The same interpretation can be made for the species Cm-HPSi(I), Cm-HPSi(II) and Cm-HPSi(III) as well, according to the similar number of hydration water molecules appraised for each of these species based on their lifetimes.

Overall speciation results are summarized in Fig. 37 for all species of Cm-HAS and Cm-HPSi as a function of pH. In the upper part of Fig. 37, the Cm-HAS(I) species comes into view only in the low pH region as a minor fraction with the maximum of 23% at pH 5.8. The second species, Cm-HAS(II) emerges gradually from pH 5 to a maximum fraction of 35%

around pH 6.5. From pH 6.5, the Cm-HAS(II) species disappears rapidly and the third species, Cm-HAS(III), suddenly built at pH 6.5, becomes predominating in the whole pH range under investigation increasing its fraction with an increase of pH and becoming prevalent at pH > 7. A comparable formation pattern can be observed in the lower part of Fig.37 for the species: Cm-HPSi(I), Cm-HPSi(II) and Cm-HPSi(III). The similarity of the two-speciation results is a direct corroboration for the same kind of chemical bindings of Cm, either in Cm-HAS or in Cm-HPSi species. This fact infers that the oxo-bridging of Cm in aluminosilicate colloids converges rather on silanol moieties than on alumina oxygen. The speciation results shown in Fig. 37 are totally different from the speciation performed on the Cm-HAS species (also Cm-silanol) in the previous experiment, which are produced from monosilanol as an initial state (see Fig.33).

4.2 Isomorphic substitution of Al for Am(Cm)

Fig. 38 summarizes the hitherto results and illustrates the correlation between the binding strength of Cm to aluminosilicate colloids (colloid-borne Cm species) and the polymerization of Si (Si-species). The presence of polysilanol in the mother solution at pH ≥ 7 is a condition for isomorphic substitution of Al for Am(Cm) in HAS colloids. Since the polymerization of Si depends on pH as well as on the concentration of Si, which are not only thermodynamic but also kinetic parameter (see section 3.4), it becomes obvious that the binding strength of Am(Cm) to HAS colloids is also a question of kinetics. The experimental fact can be understood in the light of theory, saying that activation energy is necessary to bring about nucleation. Activation energy can be delivered at the allivation of supersaturation in solution. At low degrees of supersaturation an activation barrier to the nucleation (conucleation of Am(Cm)(Al) with Si) persists, which can be annihilated whenever a foreign solid surface (e.g. polysilanol) with interfacial free energy is already present as a catalyzer. The logic consequence of such an explanation for the isomorphic substitution of Si for Al and even for Am(Cm) would be that, instead of a catalyzer, increased temperature or very long aging times might also be appropriate to overcome the activation barrier to the conucleation of Si, Al, Am(Cm)).

In order to test the hypothesis, a coprecipitation sample is prepared at 25°C on the basis of mono-silanol by mixing an alkaline solution of Si (10^{-3} mol l^{-1}) with an acid solution of Al (10^{-4} mol l^{-1}) and Cm ($5.0x10^{-8}$ mol l^{-1}). The pH is adjusted to 7.5, and the temperature of the

sample is increased to 90°C. After different conditioning times at 90°C, from 5 up to 87 days, aliquots are taken and cooled to 25°C for analysis by TRLFS and LIBD in order to speciate the colloid-borne Cm and simultaneously characterize the colloid formation.

The Cm fluorescence spectra after different heating periods compared with the spectrum before heating are illustrated by Fig. 39. It is obvious that increased temperature effectuates a strong red shift of the emission band at 601.9 nm with a lifetime of 87.7±4.8 μs, which is characteristic for the Cm-HAS(II) species, (cf. section 4.1) to 606.7, 607.7 and 608.5 nm after periods of 5, 16 and 39 up to 87 days, respectively. The shifted emission bands have a composite lifetime. Fitting the data to a biexponential law, the two lifetimes 86.2±4.8 μs and 306.1±30.0 μs are derived. They are attributed to the Cm-HAS(II) with 6.7 H_2O and the Cm-HAS(III) species with 1.8±0.5 H_2O in the inner coordination sphere of Cm, respectively. The result corroborates our hypothesis, that the activation energy to incorporate Cm completely into the structure of aluminosilicate colloids, can be provided by either increased temperature or with the catalytic aid of the polysilanol surface as outlined above.

The question whether the observed temperature effect on the Cm(Am) binding to HAS colloids is equivalent with aging time, as the Arrhenius equation [77]

$$\ln k_2/k_1 = E_a / R\ (1/T_1 - 1/T_2) \qquad \text{Eq.12}$$

where k_1 and k_2 are the rate constants at temperatures T_1 and T_2, E_a is the Arrhenius activation energy (e.g. 80 KJ/mol), and R is the gas constant, suggests, or overlapping processes other than aging have also taken place, cannot be answered by this experiment. A more intensive investigation including experiments at different temperatures is required to obtain such information.

Fig.40 summarizes the results of the speciation of colloid-borne Cm and indicates the influencing parameters: the higher the pH, the concentration of Si and the temperature, the stronger the binding of Cm to HAS colloids.

4.3 Stability of colloid-borne Cm(Am)

Irreversible bindings of actinides to stable aquatic colloids may lead to an unhindered actinide migration along the water flow path. The question whether Cm-HAS(I), Cm-HAS(II) and Cm-HAS(III) correspond to „irreversible bindings“ and „stable colloids“ seems to be a

question of definition and related to eventually changing environmental conditions such as pH, temperature, the presence of anionic ligands etc.. Within this study, 3 different stability tests are considered: (1) change from radioactive to inactive medium and measuring radiometrically the desorption of Am activity from the colloidal fraction; (2) change from high to low pH environment and determining the colloid-borne Cm distribution as a function of pH with TRLFS; (3) change from ambient to increased temperature and monitoring the colloidal average size with LIBD.

Activity in colloids after desorption with inactive medium

In a first stability test for Am binding to HAS colloids, two desorption experiments for Am are performed on Am-HAS colloids. One experiment uses colloids generated under condition I and another uses colloids formed under condition II , based on the conucleation of Am and Al with prevailing monosilanol and polysilanol, respectively. The chosen pH´s of colloid formation for each experiment are 5, 7 and 9. In all cases, the sample conditioning time is seven days. For desorption, the colloidal fraction is first separated from the mother solutions by ultrafiltration and than brought into contact with a similarly prepared inactive ultrafiltrate during one day. The procedure is repeated three times. A fourth desorption is performed with bidistilled water at pH 6. The colloid-borne Am fraction remained in the colloids after the accumulated washing procedures in relation to the initial colloid-borne Am fraction before desorption is evaluated. Fig. 41 shows the result of the stability tests for the pseudocolloids of Am in question, namely generated at three different pH´s on the basis of HAS-monosilanol (upper part of Fig. 41) and on the basis of HAS-oligosilanol (lower part of Fig. 41). The least desorption of Am from HAS colloids is observed at pH 9 indicating over 90% of Am remained stable as colloid-borne species for both HAS-monosilanol and HAS-polysilanol. At pH 7, the value decreases slightly but remains still over 80% for HAS-monosilanol and 70% for HAS-polysilanol. However, at pH 5 only 33% and 50% of the initially incorporated Am remains in the colloids from HAS-mono- and -polysilanol, respectively, suggesting that the colloid-borne Am species is chemically unstable. Compared to the speciation of Cm at interaction with HAS colloids, as shown in Figs. 33, 37 and 38, the results of the desorption experiment can be interpreted as forming the colloidal species Am-HAS(I) at pH 5 and Am-HAS(II) or Am-HAS(III) from pH 7 to pH 9 in accordance with the formation of Cm-HAS(I) and Cm-HAS(II) or Cm-HAS(III). According to Fig.41, the colloidal spe-

cies Am-HAS(II) (tridentate) as well as Am-HAS(III) (isomorphically substituted) seems to be structurally stable in solution, in which Am or Cm appears irreversibly incorporated under given conditions.

Cm-HAS(III) species at decreasing pH

A second stability test investigates the pH-reversibility behaviour of the Cm-HAS(III) species. Therefore the Cm-HAS(III) species is formed at pH 9 by titration of an alkaline solution of Si (1.34×10^{-2} mol l^{-1}) with an acid solution of Al (1×10^{-4} mol l^{-1}) and Cm (4.8×10^{-8} mol l^{-1}) as previously described for colloid formation on the basis of polysilanol, condition II (see section 3.4). The mixed sample at pH 9 is divided in 8 aliquots, each of which are titrated with HCl to a lower pH unit (inverse titration), namely from pH 9 down to pH 2 in accompany with the spectroscopic speciation. A dilution of the elements concentration upon titration is maintained within 3%. The speciation results for colloid-borne Cm as a function of pH in the course of the inverse titration of the sample containing Cm-HAS(III), are shown in Fig. 42 (lower part). The formation pattern for the species Cm-HAS(I), Cm-HAS(II) and Cm-HAS(III) is similar to that for the direct titration (see Fig. 42, upper part), except that Cm-HAS(III) becomes the predominating colloid-borne Cm species in the whole pH range under investigation, increasing gradually its fraction with an increase of pH and becoming prevalent at pH > 7. A decrease of pH from 9 down to 2 converts the Cm-HAS(III) species to Cm-HAS(II) gradually. Both Cm-HAS(III) and Cm-HS(II) disappear slowly at pH < 6, while Cm-HAS(I) is appearing at lower pH. The Cm^{3+} aquo-ion fraction increases on the other hand with decreasing pH, suggesting ist dissociation from colloids. The dissociation of Cm with lowering pH is not directly from Cm-HAS(III) but takes place from Cm-HAS(II) at first and than from Cm-HAS(I).

The stability of the Cm-HAS(III) species at each pH is observed as a function of time up to 63 days, as shown in Fig. 43. At pH 9, only the Cm-HAS(III) species prevails and remains stable with time. The fraction of Cm-HAS(III) decreases with lowering pH but at each pH the corresponding Cm-HAS(III) fraction remains stable with time again after 15 days. At pH ≤ 5, the initial fraction of Cm-HAS(III) decreases with time for the first few days and then remains constant. At pH 3, Cm-HAS(III) disappears almost after a few days.

HAS colloidal size at increasing temperature

The stability of HAS colloids made at room temperature from monosilanol at pH 7.5 and heated to 90°C (see section 4.2) is monitored by LIBD as a function of heating time (up to 7 days) by determining the average colloidal size from two-dimensional recordings of plasma light emission generated by breakdown of colloids within the laser beam focus volume. The result is given in Fig. 44. The unchanged 2-D distribution (x,z-plane) of the breakdown events around the center of the optical focus of the laser beam, before and after prolonged heating periods, proves that periods of increased temperature do not irreversibly change the colloidal state.

4.4 Capacity of colloids to incorporate Am(Eu)

The maximal amount of trivalent actinides which can possibly be incorporated into HAS colloids in statu nascendi either formed from monosilanol (formation condition I) as well as from polysilanol (formation condition II) is determined. To this purpose, increasing amounts of Eu up to $5x10^{-4}$ mol l^{-1} are included in the colloid generation process in addition to a constant tracer amount of Am ($5x10^{-8}$ mol l^{-1}). A similar behaviour of Am and the somewhat better soluble Eu is thereby assumed. The fraction of Am activity in the three phases (ionic, colloids and precipitate) is measured as a function of pH and also as a function of time, from 3 hours to 35 days. Blank experiments without Si and Al are also performed in order to trace separately the colloid formation behaviour of Am(Eu) by itself, without the binding to HAS colloids. The result for the Am(Eu) fraction incorporated into the colloidal phase of the coprecipitation samples after 35 days conditioning time as a function of the (Am+Eu) concentration is given by Fig.45. The following observations are made:

(1) The maximum concentration of incorporated Am(Eu) amounts to ca. 90% of $5x10^{-5}$ mol l^{-1} in HAS colloids formed at pH 7-9 out of a mother solution containing $1.3x10^{-2}$ mol l^{-1} Si (85% polysilanol at pH $\geq$ 7) and $1.5x10^{-4}$ mol l^{-1} Al. In that case, about one out of two or three Al in the colloids is isomorphically substituted for Am(Eu). A further increase of the Am(Eu) concentration destroys the HAS colloidal state;

(2) HAS colloids in statu nascendi generated out of a mother solution, consisting of a $1x10^{-3}$ mol l^{-1} monosilanol and $1x10^{-5}$ mol l^{-1} Al, have a somewhat lower capacity to hold Am(Eu). In that case, the maximum is observed at pH 9 for a Am(Eu) concentration of $2x10^{-6}$

mol l^{-1}. Thereby 1 out of 5 Al in HAS colloids is poorly replaced by Eu(Am) in a tridendate binding;

(3) The binding capacity of HAS colloids (from mono- as well as from polysilanol) for trivalent actinides decreases with decreasing pH and is in line with the An(III)- colloid binding strength.

(4) At pH 4 to 6, the activity in the colloidal phase has not to rely on HAS, since the colloidal Am(Eu), which is formed in the presence of Si and Al is found to the same amount in the blank experiment with Am(Eu) only, without HAS colloids. Another mechanism for colloid formation is postulated. The phenomenon will be discussed later (section 9).

Conclusions of section 4

Trivalent actinides such as Am(III) or Cm(III) are incorporated into HAS colloids in statu nascendi and undergo thereby oxo-bridging into the structural position of Al(III). The different incorporation patterns as well as kinetics of Am(Cm), depending on whether HAS colloids are built from mono- or polysilanol, reflect correspondingly different incorporation mechanisms. The binding strength of Am(Cm) to the HAS colloids increases with increasing concentration of Si and increasing pH and is shown to be related with the faster polymerization kinetics of Si. HAS colloids, formed from a slightly undersaturated Si-solution (monosilanol) mixed with Al (Si/Al ratio = 100) in the presence of tracer amounts of Am(Cm), build the colloid-borne Cm species Cm-HAS(I) at pH 5 – 6 and Cm-HAS(II) at pH 8 – 9 corresponding to bidentate and tridendate bindings to the colloids, respectively. HAS colloids, generated from an oversaturated Si-solution (polysilanol), which is mixed with Al (Si/Al ratio = 100) at pH 7 – 9, form the colloid-borne Cm species Cm-HAS(III) where Cm(Am) substitutes isomorphically for Al in the aluminosilicate colloid structure. The result is explained by the interfacial energy of polysilanol, which seems to be necessary to overcome the activation energy barrier for the complete incorporation of Am(Cm). The explanation is corroborated by the fact, that isomorphic substitution of Am(Cm) can also take place without polysilanol surface, e.g. from monosilanol and Al, at increased temperature, e.g. 5 days at 90°C, which is another way to provide activation energy.

The generated pseudocolloids of Am(Cm), corresponding to the Cm-HAS(II) or Cm-HAS(III) species, are extremely stable as a function of time, against desorption with inactive medium (irreversible Am(Cm)-colloid bindings), and at increased temperature. Their forma-

tion is, however, pH reversible, and in line with the lower stability of the Cm-HAS(I) species built at pH 5 – 6.

The maximum capacity of HAS colloids to incorporate Am(Eu) is reached for HAS colloids generated from polysilanol at pH 8-9, when about one third of the Al in colloids is substituted by Am(Eu) and the HAS colloids have lost their original identity.

Am in the colloidal fraction at pH 4 – 6 is due to a process for colloid formation, which is different from the binding with HAS colloids. The corresponding mechanism will be further discussed and is still under investigation.

5 Interaction of tetravalent actinides with aluminosilicate colloids in statu nascendi

Follows now the interesting question whether Th(IV), present at the conucleation of Si and Al, will follow the behavior of Si(IV) and incorporate irreversibly into HAS colloids in statu nascendi just like Am(III) served as a substitute for Al(III). Although no direct spectroscopic speciation of colloid-borne Th like by TRLFS is possible for tetravalent actinides, we expect that, on the basis of the acquired knowlegde about the pseudocolloid formation of Am(Cm), an intelligent comparative tracing of the activity of Th in the liquid, colloidal and solid phases may provide us a conclusive answer to that question. Starting from the preparation of ^{234}Th through separation from natural ^{238}U, the study includes the determination of the Th incorporation kinetics into HAS colloids in statu nascendi as a function of the pH, of the Si concentration and of the Th concentration, as well as the analysis of the reversibility of the process.

5.1 Separation of Th from U

As obvious from the ^{238}U decay scheme (Fig. 46, upper part), ^{234}Th ($T_{1/2}$= 24.1 d) may be prepared by milking natural uranium. The separation of Th is performed in two consecutive steps [78,79]:

(1): 25 g $UO_2(NO_3)_2.6\ H_2O$ (p.a, Merck) is brought into the chloride form UO_2Cl_2 by addition of conc. HCl, evaporation to dryness, dissolution in 8 M HCl and applied to a column (4.4 cm ø, 72 cm length) filled with 750 ml of the anion exchange resin Dowex®1-X8 (100-200 mesh). Th(IV), unlike U(VI) and Pa(V), does not form anionic chlorocomplexes and is eluted with 8 M HCl. The eluate is evaporated, dissolved in conc. HNO_3 and H_2O_2 and

evaporated 3 times until all organics are destroyed. The residue is dissolved in 8 M HNO_3 for the second purification step.

(2): The hexanitratocomplex of Th is now sorbed on a small column filled with 80 µl anion exchange resin Dowex®1-X8. Remaining U and Pa impurities are washed out with 8 M HNO_3. Th is eluted with 8 M HCl. The eluate is evaporated several times with conc. HNO_3 to dryness and redissolved in 0.1 M HCl, resulting in about 150 kBq ^{234}Th. A typical elution diagram is shown in Fig. 46.

5.2 Incorporation of Th(IV) and Am(III): comparison

Similarly to the foregoing experiments for the estimation of incorporation of Am(III) in HAS colloids in statu nascendi, a constant tracer amount of Th, dissolved in acid, is added to an acid Al solution in 0.03 mol l^{-1} HCl and titrated with an alkaline Si solution in 0.03 mol l^{-1} NaOH to a preset pH, to give the following end concentrations in six series of mother solutions, each serie including six samples with different pH in the range from 4 to 9:

(1) Only Th: [Th] = $5x10^{-8}$ mol l^{-1}
(2) Th+Al: [Th] = $5x10^{-8}$ mol l^{-1}, [Al] = 10^{-5} mol l^{-1} (also [Al] = 10^{-4} mol l^{-1})
(3) Th+monosilanol.: [Th] = $5x10^{-8}$ mol l^{-1}, [Si] = 10^{-3} mol l^{-1}
(4) Th+monosilanol+Al: [Th] = $5x10^{-8}$ mol l^{-1}, [Si] = 10^{-3} mol l^{-1}, [Al] = 10^{-5} mol l^{-1}
(5) Th+polysilanol: [Th] = $5x10^{-8}$ mol l^{-1}, [Si] = 10^{-2} mol l^{-1}
(6) Th+polysilanol+Al: [Th] = $5x10^{-8}$ mol l^{-1}, [Si] = 10^{-2} mol l^{-1}, [Al] = 10^{-4} mol l^{-1}

The mother solutions (4) and (6) generate HAS colloids on the basis of monosilanol and polysilanol, respectively (cf. section 3.4: optimum conditions I and II), whereas the other solutions serve the blank experiments for the purpose of comparing the behaviour of Th with and without HAS colloid formation. From each sample, aliquots are taken after different conditioning times from 3 hours up to 35 days, and the partition of Th over the three phases, ionic, colloidal and precipitate, is determined. The result for the fraction of Th incorporated in the colloidal phase after 35 days of sample conditioning time as a function of pH is illustrated in a contour diagram (Fig. 47, left part) and compared with the previous results for the incorporation of Am (Fig. 47, right part). As far as Th is concerned, we make the following observations.

Th blank without any addition (1) is not in the colloidal phase but in the precipitate in the whole pH region. After addition of either only Al (2) or only monosilanol (3), Th persists in the precipitate. The presence of both, Al as well as monosilanol (4) (condition I for colloid formation) is necessary to transfer Th from the precipitate into the colloidal phase at neutral pH (7 – 9). The shift of the equilibrium $Th_{soln} \Leftrightarrow Th_{coll} \Leftrightarrow Th_{prec}$ from the right to the left can only be explained by the binding of Th to the HAS colloids. Polysilanol without addition of Al (5) is also capable to incorporate Th at neutral pH. Polysilanol with addition of Al (6) and forming of HAS colloids (condition II for colloid formation) is mostly efficient for transferring Th into the colloidal fraction in the broad pH region from 4 to 9, with a maximum at pH 7. The fact that almost 100% of the Th input is found in the colloidal fraction is amazing. If we assume that Th behaves just like Si, we would expect that only 1% of Th in the mother solution may become colloid-borne Th, since Si/Al concentration ratio in the mother solution is 100 and the Si/Al atomic ratio in the colloids is ca 1. The observed result infers that the affinity of the Al cation for the Th-oxyhydroxide ligand is at least 100 times higher than for the polysilanol ligand.

The incorporation patterns for Th in the HAS colloids are different depending on whether the colloids are generated on the basis of mono- or polysilanol. They reflect correspondingly different incorporation mechanisms. The comparison of the respective incorporation patterns of Th with those of Am (Fig. 47, right part) further indicates distinct incorporation pathways for tri- and tetravalent actinides.

The kinetics for the incorporation of Th and Am into HAS colloids from mono- as well as polysilanol are also compared and the result is given in Fig.48. In the case of HAS-monosilanol (Fig. 48, lower part), the colloid-borne Th fraction as well as the colloid-borne Am fraction decreases with time in the pH region of 6 to 8 or remains constant at pH 9. In the case of HAS-polysilanol (Fig. 48, upper part), the colloid-borne Am fraction at pH = 6 - 9 remains unchanged as a function of time, whereas Th grows into the colloids with time. This special behaviour of Th appears to reflect the polymerization kinetics of Si (cf. Figs 27 and 28). The differences in incorporation kinetics for Th and for Am in HAS from mono- and polysilanol are, besides the different incorporation patterns as mentioned above, further indications of correspondingly distinct incorporation mechanisms.

5.3 Stability of pseudocolloids of Th

The reversibility of Th incorporation into HAS colloids is tested in desorption experiments on 2 series of samples resulting from the titration of an acid solution of Th and Al with an alkaline solution of monosilanol and polysilanol, respectively. Each series contains 3 samples, namely at pH 5, 7 and 9, respectively. After a conditioning time of seven days, the colloids are separated and washed four times, 3x with a similar but inactive ultrafiltrate and 1x with bidistilled water, pH 6. The contact time with the wash water is one day for each desorption. The stable colloid-borne Th fraction (%) is evaluated and shown in Fig. 49. It is obvious, that Th has been irreversibly incorporated in the whole pH range. Merely at pH 5, a slight desorption can be remarked. The repetition of the experiment for Th desorption after a sample conditioning time of 35 days, shows a further stabilization of Th colloidal incorporation, even at pH 5, with a remaining colloid-borne Th fraction after desorption of 98%. The result shows that Th is irreversibly incorporated into both colloids, HAS-poly- as well as HAS-monosilanol in the whole investigated pH range. It suggests that colloid-borne Th is more stable than colloid-borne Am. The result is in agreement with the previously demonstrated higher affinity of Th for Al as compared with Si (see section 5.2). It is therefore assumed that Th is isomorphically substituted into the aluminosilicate structure of colloids.

5.4 Capacity of colloids to incorporate Th

The Th concentration incorporable into HAS colloids in statu nascendi, which are generated from either mono- or polasilanol (cf. section 3.4), is evaluated as a function of Th concentration. This is realized by determining the distribution of Th activity (initial activity from 1.3×10^{-12} mol l^{-1} ^{234}Th) in the ionic, the colloidal and the solid phase as a function of conditioning time of the titration sample (3 hours – 35 days) for several pH´s (6 – 9) and at each pH, for several Th concentrations (7×10^{-9} mol l^{-1} - 1×10^{-3} mol l^{-1}). Blank experiments without Si and Al are also included in order to distinguish between Th colloids and colloid-borne Th. Fig. 50 shows the Th activity fraction (%) in colloids after 35 days sample conditioning time as a function of the Th concentration for different pH´s. We observe the following facts:

(1) The incorporable amount of Th depends on the formation conditions of HAS colloids, namely on the pH as well as on the Si species in the mother solution (mono- or polysilanol).

(2) The maximal colloid-borne Th is found at pH 9 for HAS colloids formed from polysilanol, a result which is similar to that for the maximal incorporation of Am(Eu) (Fig. 45). This maximal amount corresponds to about 80 % of $1.6x10^{-4}$ mol l^{-1}, i.e. $1.3x10^{-4}$ mol l^{-1} Th. The amount of Si in colloids with a Si/Al atomic ratio of 1.2 (section 3.5) is 1.2% of the Si concentration in the mother solution ($1.3x10^{-2}$ mol l^{-1}), which is $1.6x10^{-4}$ mol l^{-1} Si. It means that about 80% of the Si in HAS is substituted for Th. Four out of five (Si+Th) colloidal atoms are Th. This relation is reversed at pH 6: one out of five (Si+Th) colloidal atoms is Th.

(3) HAS colloids formed from monosilanol have a much lower capacity for incorporating Th. The maximal incorporated Th incorporation is at pH 9 and a hundred times lower as for HAS from polysilanol.

(4) At low pH (pH 4), Th starts to generate colloids by itself when its concentration depasses 10^{-5} mol l^{-1}, as obvious from the blank experiment without HAS colloids. A similar observation has been made for Am, but at a lower concentration and a broader pH region (cf. Fig. 45). The possible generation of „real“ Th colloids is discussed later (see section 9).

Conclusions of section 5

Tetravalent actinides such as Th(IV) are incorporated into HAS colloids in statu nascendi and undergo thereby oxo-bridging into the structural position of Si(IV). The growing of Th in colloids with time reflects the polymerization kinetics of Si and is therefore promoted in presence of Al, at increased pH and at increased Si concentration (more Th incorporation in HAS-polysilanol than in HAS-monosilanol). The fraction of Th migrating from the mother solution into the colloids is a hundred times higher than that of Si, namely 100% and 1%, respectively. The observed facts indicate that the affinity of anionic ligands for trivalent cations is in the order:

Th-oxyhydroxide > polysilanol > monosilanol > OH.

The generated pseudocolloids of Th are extremely stable as a function of time as well as highly resistent against desorption with inactive medium (irreversible Th-colloid bindings) or bidistilled water at pH 6.

The maximum capacity of HAS colloids to incorporate Th is given for HAS colloids formed out of polysilanol at neutral pH (6 – 9) after a conditioning time of several days, and correspond almosts to the Al concentration in the mother solution which also determines the Si concentration in the colloids (Si/Al = ca. 1). In that case about 80% of Si in colloids is substituted by Th.

The different incorporation patterns as well as kinetics of Th, depending on whether HAS colloids are built from mono- or polysilanol, reflect correspondingly distinct incorporation mechanisms. The incorporation processes of Th into HAS colloids in statu nascendi also differ from those of Am as far as pH dependency, kinetics, quantity as well stability are concerned. The general tendency is that, unlike colloid-borne Am, colloid-borne Th enhances the overall HAS colloid stability.

At low pH (4) and at high concentration (≥ 10^{-5} mol l^{-1}) Th becomes colloidal without the aid of HAS colloids. The corresponding mechanism will be discussed later and is still under investigation.

6 Simultaneous interaction of tri- and tetravalent actinides with aluminosilicate colloids in statu nascendi

So far we have learned that tri- and tetravalent actinides substitute for Al(III) and Si(IV), respectively, in stable HAS colloids at the moment of their formation through heterogeneous nucleation. In the real situation, actinides (or other elements) of different oxidation state might occur simultaneously and we want to know what do actinides decide in such a situation. Do they still behave independently or does an eventual mutual interaction provides them with a new incorporation character? An answer to that question is aimed in the following investigation.

6.1 Incorporation of the (Am(III)+Th(IV)) mixture

Trace amounts of Am and Th, each at a concentration of 5×10^{-8} mol l^{-1} , are together integrated into the HAS colloid generation process, and their behaviour of incorporation into colloids is first observed radiometrically. Therefore, an acid solution of Am+Th+Al is titrated with Si in base to a preset pH in the range of 4 – 9 under the optimum colloid formation conditions I (monosilanol species) as well as conditions II (polysilanol, prevailing from pH 6) to

give „mixed“ samples. After different time intervals, from 3 hours up to 35 days, filtration and ultrafiltration procedures are applied on the samples, and the respective distributions of Am and Th activities between solution, colloids and precipitate are determined. Figs. 51 and 52 show the distribution of Th (left part of the figs) and of Am (right part) in the three phases of 35 days old samples from condition I (HAS-monosilanol) and II (HAS-polysilanol) as a function of pH, respectively. In each figure, the results for the mixed samples containing both Th and Am (Fig. 52, lower part) are compared with previous results for the corresponding separate samples with either only Th or only Am (Fig. 52, upper part). It is obvious, that the originally distinct patterns for the separate incorporation of Th and Am (upper part of Figs. 51 and 52) become more similar to one another if colloids are generated in the presence of a Th+Am mixture (lower part of Figs. 51 and 52). This characteristic is mostly pronounced in the neutral pH range 6 – 9. In this pH region, a general decrease of activity (Am or Th) in the colloidal fraction is found for the mixed samples. In the low pH region 4 to 6, however, an increased activity (Th or Am) is observed in the presence of HAS-polysilanol (Fig. 52, lower part) in comparison with the separately incorporated Th and Am (Fig. 52, upper part).

In the special case of HAS-polysilanol (Fig. 52) formed at pH 9, we also observe that Th as well as Am are partly driven from the colloidal phase (separate samples) (Fig. 52, upper part) to the solution (mixed samples) (Fig. 52, lower part) only through the fact that the actinide of the different oxidation state is also present.

$$Th(Am)_{solution} \Leftrightarrow Th(Am)_{colloid} \Leftrightarrow Th(Am)_{precipitation}$$

The shift of the equilibrium from the right to the left means that the polymerization of Th is inhibited by Am and vice versa. It also indicates that Th and Am become not only bound to HAS colloids but also to one another. This findings clamour for speciation of Cm in the presence of Th by TRLFS.

6.2 Speciation of colloid-borne Cm in presence of Th by TRLFS

TRLFS spectra of Cm, without and with the presence of Th, are recorded at the abovementioned titrations for the generation of HAS-monosilanol and HAS-polysilanol. The result is illustrated in Fig. 53. Spectra shift due to Th are observed (compare in Fig. 53 the

upper part (Cm) with the lower part (Cm+Th)) in both cases, at generation of HAS-monosilanol as well as at the formation of HAS-polysilanol (compare left and right part of Fig. 53) and reflect an interaction of Th with Cm.

Peak deconvolution of a composite spectrum as illustrated by Fig. 54 clarifies the appearance of different Cm species. In the presence of Th and HAS-monosilanol (lower part, left), three Cm species, the free Cm^{3+} aquo-ion (emission peak at 593.8 nm) and two colloid-borne Cm-species, named as Cm-Th(I) at 598,0 nm and Cm-Th(II) at 603,6 nm are identified. Exactly the same species are found if, instead of monosilanol, polysilanol is used for colloid generation (lower part, right). The result is in clear contrast to the behaviour of Cm without the presence of Th (upper part), which also shows the species at 593.8 nm and 598.5 nm, namely the Cm^{3+} aquo-ion and the Cm-HAS(I) but two further different colloid-borne Cm-species, one at 601.8 nm, named Cm-HAS(II), and another at 606.8 nm, unique for HAS-polysilanol and corresponding to the completely incorporated Cm species, namely Cm-HAS(III).

The fraction of each Cm species as a function of pH, as shown in Fig. 55, indicates roughly similar incorporation patterns for Cm with or without Th after replacing Cm-Th(II) either by Cm-HAS(II) or by Cm-HAS(III) depending on the original Si species at HAS formation.

A further characterization of Cm-Th(I) and Cm-Th(II) is made by the measurement of the fluoresence relaxation time which can be related with the number of Cm coordinated water molecules. Cm-Th(I) and Cm-Th(II) have a relaxation time of 134.0±1.8 μs and 342.9±8.6 μs (mean values for HAS-monosilanol- and HAS-polysilanol colloid-borne Cm) respectively, which correspond to four and one or no water molecules remaining in the coordination sphere of Cm.

Table 2 gives an overview of the characteristics of the different Cm-species. Therefrom we conclude that the affinity of Cm(III) for Th(IV) is higher than for mono- or even polysilanol. It infers a binding of Cm to Th and corroborates the above outlined results from radiometric measurements (see section 6.2). We postulate that a complexed form of Cm and Th is conucleating with Si and Al at colloid formation. The Cm-Th complex has a complex or „mixed“ behaviour at its interaction with HAS colloids in statu nascendi. The ambivalent behaviour of Cm+Th seems to resemble more that of Am at low pH from 4 to 6 and that of Th at neutral pH from 6 to 9. In the latter case, Cm is incorporated indirectly into the colloids via its

strong binding with Th and becomes more stably incorporated into colloids, in line with the stronger binding of Al with Th as compared with Si (cf. section 5.3).

6.3 Stability of pseudocolloids of (Am+Th)

The fact that the simultaneous interaction of Th and Am with HAS colloids in statu nascendi leads on the one side to a general somewhat lower quantity of incorporated activity in the colloidal fraction (cf. section 6.1), but on the other side to a stronger binding of Cm to the colloids (cf. section 6.2), encourages us to test the stability of the corresponding pseudocolloids of (Th+Am) by means of desorption experiments. The pseudocolloids are therefore generated at pH 5, 7 and 9 on the basis of mono- and polysilanol, conditioned in their mother solution for 7 days, and separated by ultrafiltration. The desorption consists of four washing procedures, three of them restore the original samples through addition of separately prepared inactive ultrafiltrates of the same composition as well as pH, and one uses bidistilled water at pH 6. The contact time with each wash-water is 1 day. The activity fraction remained in colloids after desorption and related to the originally incorporated fraction is evaluated. The result is shown in Figs. 56 and 57 for pseudocolloids from HAS-monosilanol and HAS-polysilanol, respectively, and compares the stable colloid-borne activity fraction (%) of Am (upper part) and of Th (lower part) in the separate samples (only Am or only Th) with that in the mixed sample (Am+Th). The conclusion of irreversible binding of Th as well as Am to HAS colloids remains valid, independently of their separate or simultaneous incorporation.

Conclusions of section 6

Tri- and tetravalent actinides such as Am(Cm) and Th, participating simultaneously in the HAS colloid generation, either on the basis of mono- or polysilanol, show a „mixed" behaviour of incorporation into the colloids. The underlying reason is the high affinity of Th for Cm, in line with its high affinity for Al. This characteristic is indirectly visible from the activity distribution in the 3 phases, ionic, colloids and precipitate, and directly proven by comparing the TRLFS speciation of Cm without and in the presence of Th at incorporation in HAS colloids in statu nascendi. Differences in incorporation patterns as well as in type and number of Cm species, as previously observed at the conucleation of Cm (without Th), Al and either mono- or polysilanol, are cancelled out if Cm is accompanied with Th. In the case of

(Cm+Th), only two Th-borne Cm species, namely Cm-Th(I) at 590 nm and Cm-Th(II) at 603.6 nm, with fluorescence life times of 134.0 μs and 342.9 μs, corresponding to four and no waters in the coordination sphere of Cm, respectively, are identified for both, HAS-mono- as well as HAS-polysilanol. The interaction behaviour of the Cm-Th complexes with HAS colloids resembles more that of Cm(Am) at low pH from 4 to 6 and more that of Th at neutral pH from 6 to 9.

The stability of the generated pseudocolloids against desorption with inactive medium remains, notwithstanding Cm-Th complex formation and altered incorporation mechanism, almost unchanged. Consequently, the statement of irreversible Am(Cm)- and Th- colloid bindings remains valid, also in the case of their simultaneous incorporation.

7 Behaviour of aged aluminosilicate colloids in presence of tri- or tetravalent actinides

The interaction of actinides with aluminosilicate colloids in statu nascendi has been used to simulate the formation of pseudocolloids through conucleation. An appropriate model to study the generation of pseudocolloids by the alternative way of actinide sorption to colloids may be the use of aged aluminosilicate colloids. Fig. 58 illustrates the corresponding experimental pathways.

7.1 Influence of colloid age on incorporation of Am and Th

HAS colloids are synthesized through conucleation of Si and Al on the basis of mono- as well as polysilanol under the optimum conditions I and II (see section 4.3) at six different pH´s from 4 to 9. After different sample conditioning or colloid aging times, namely 1, 7 and 24 days, each co-nucleation sample is spiked either with Am or with Th to achieve a final concentration of $5x10^{-8}$ mol l^{-1}. After activity contact time from 3 hours up to 35 days, the Am or Th fraction incorporated in colloids is determined. Fig. 59 illustrates the result of the incorporation of either Am (left part) or Th (right part) into the HAS-monosilanol (upper part) as well as HAS-polysilanol colloids (lower part) of different age after an activity contact time of 35 days and includes the corresponding results for HAS colloids in statu nascendi for the purpose of comparison. Aged colloids (e.g. from 7 days) are not tied up to bind Am, but the af-

finity for Th is unchanged or even higher, suggesting a displacement mechanism of Si in HAS.

The influence of the activity contact time on sorption into the colloids is further analyzed by comparing the status after 3 hours with that after 35 days (Fig. 60). Fig. 60 shows the result for Am and Fig. 61 the result for Th. As far as Am is concerned, we observe that aged HAS-monosilanol colloids (Fig. 60, upper part) loose their sorption capacity for Am from the very beginning, e.g. already after 7 days aging and 3 h activity contact time, whereas 7 days aged HAS-polysilanol colloids (Fig. 60, lower part) initially sorb Am, desorbing it again with time. As far as Th is concerned (Fig. 61), different sorption patterns as well as kinetics for Th sorption into HAS-mono- and HAS-polysilanol (compare upper and lower part of Fig. 61) reflect correspondingly different sorption mechanisms. In the case of HAS-monosilanol (Fig. 61, upper part), the Th incorporation mechanisms either through sorption or condensation (compare aged HAS with HAS in statu nascendi) are very similar. Aged HAS-polysilanol colloids, however, (Fig. 61, lower part) sorb Th much faster than HAS-polysilanol colloids in statu nascendi, which may be related with the omitted waiting time of colloid formation.

7.2 Influence of colloid age on stability of pseudocolloids of Am(Th)

Activity desorption with inactive medium

The pseudocolloids of Am and Th, which have been generated from 27 days aged HAS-polysilanol colloids at pH 5, 7 and 9 after a contact with activity during ≥35 days, are subjected to a desorption procedure consisting of three one-day-equilibrations with ultrafiltrate from duplicate but inactive samples. The stable colloid-borne activity fractions (%) are evaluated and the result is shown for Am and Th in Fig. 62b and Fig. 62c, respectively. Obviously, a small amount of incorporated Am fraction as well as the almost quantitatively incorporated Th fraction (cf. Fig. 59) are irreversibly bound. An exception is the association of Am at pH 5, which is a completely desorbed. Less aged pseudocolloids of Am at pH 5, e.g. 7 days old at the moment of contact with activity, keep still a 65% of the incorporated Am after desorption (Fig. 62a). We assume that some Am which is irreversibly bound in aged colloids is nothing but a reflection of a non completed colloid formation. The irreversible incorporation of Th, however, is not dependent on conuleation. The high affinity of Th for Al immediately displaces Si out of the HAS colloids and causes the most stable incorporation at all pH.

Activity desorption with EDTA

The stability of Th sorption into aged colloids is further tested with the aid of EDTA. Desorption experiment is performed as follows. Al is condensed with monosilanol as well with polysilanol (conditions I and II) at pH 5, 7 and 9 for colloid formation and the samples are conditioned for 27 days. Th is than introduced to make a final concentration of 4.8×10^{-8} mol l^{-1}. After a contact time with Th of 35 days, aliquots of each sample are taken to evaluate the incorporated Th activity fraction related to the input Th activity, and EDTA is added to an end concentration of 1×10^{-4} mol l^{-1}. After different contact times with EDTA, the remained or „EDTA-stable" activity fraction as compared with the initially incorporated Th fraction is determined. Fig. 63 shows the result of the Th desorption kinetics from aged pseudocolloids with EDTA. Th sorbed to either aged HAS-mono- or HAS-polysilanol colloids shows fast EDTA desorption kinetics at pH 5 within the first three days. However, a $\geq$ 20% fraction of incorporated Th remains even after 30 days contact time with EDTA. At neutral pH (7-9), Th sorbed to HAS-polysilanol colloids (Fig. 63, lower part) cannot be displaced by EDTA, in contrast to Th associated with HAS-monosilanol colloids (Fig. 63, upper part), which is at least partially (a 50%) desorbable within a few days of contact time with EDTA. This and other experiments with competitive ligands for the better comprehension of the formation of different colloid-borne Th species, leading to distinct overall stabilities of the pseudocolloids of Th, are still in progress.

Conclusions of section 7

Tri- and tetravalent actinides, e.g. Am and Th, are incorporated into HAS colloids, not only at the moment of colloid generation through conucleation, but also through sorption on aged colloids as they may exist in the aquifer system either from condensation or dispersion. The sorption of Am is small and merely the result of a still proceeding colloid formation under the given experimental colloid aging times ($\leq$ 27 days). The sorption of Th into HAS colloids, however, is almost independent of the colloid age. The underlying reason is the existence of different incorporation pathways for Th. If present at the moment of colloid formation, Th follows the conucleating behaviour of either mono- or polysilanol with Al. Later, Th interacts with preformed HAS colloids by displacing Si in a very fast sorption process. Th sorption is mosty pronounced for colloids, formed from polysilanol, reflecting the stronger

affinity of the Th-oxyhydroxide anionic ligand for the Al^{3+} cation, a characteristic which has been observed from a number of other experiments as described in previous sections.

The corresponding pseudocolloids of Th are extremely stable against desorption with inactive medium, and the Th-(aged HAS colloid)-bindings are called irreversible. Their decreasing stability against desorption with EDTA with decreasing pH, e.g. from 100% and 50% at neutral pH (7-9) for HAS generated from poly- and monosilanol, respectively, to a 20% at pH 5 for both HAS after 35 days EDTA contact time, reflects the existence of several colloid-borne Th species. Isomorphic substitution of Th for Si through sorption on aged HAS-polysilanol colloids at neutral pH is ascertained.

8. Tri- and tetravalent actinides: tracers for the aluminosilicate colloid generation

In the previous considerations, actinides have been the main subject of interest. Colloids have been seen as vehicles, which may bind actinides irreversibly and transport them without hindrance in the geosphere. Now we turn our interest to the colloids and consider the irreversibly bound actinides, Am(III) and Th(IV) as tracers for Al(III) and Si(IV), respectively, in order to better understand the process of aluminosilicate colloid formation.

8.1 Colloid and pseudocolloid generation mechanisms

HAS-monosilanol colloids

In recent publications, Doucet et al.[54,55] describe two types of HAS, formed from undersaturated Si in acidic solutions at pH = 6 and differentiated by NMR spectroscopy, and visualize their structures by AFM. One is rectangular with 25 nm length and another has a discoid shape with 18 nm diameter. They correlate the different structures as well as distinct Si/Al ratios in HAS, namely 0.5 and 1.0, with different Si/Al concentratio ratios in the mother solutions, and postulate a reaction mechanism for the formation of HAS via the competitive condensation of silicic acid $Si(OH)_4$ at a hydroxylaluminum template. Our findings, e.g. HAS colloids with a Si/Al atomic ratio of 0.7 (cf. section 3.5), are in good agreement with the mentioned concept for HAS formation. Therefore, we propose a similar reaction mechanism, which has been adapted to our experimental conditions for HAS colloid generation by titration of Al dissolved in acid with Si dissolved in base to beyond acid (pH = 4 – 9), and which

selects such HAS colloids capable to incorporate trivalent actinides. Fig. 64 illustrates the template formation [54,55]: If Al is in excess, Al hydrolyzes, dimerizes and builds a hydroxy-alumino template. $Si(OH)_4$ condensates at the preformed template under formation of a hydroxy-aluminosilicate (Si/Al ratio = 0.5). If Si is in excess, HAS(I) acts as a template for further reactions with $Si(OH)_4$ and forms HAS(II) with Si/Al = 1. In HAS(II), 50% of the Al has changed from the octahedral to the tetrahedral geometry. This kind of nucleation has to build up a surface on ist own, starting from a dimeric Al template. Fig. 65 illustrates the mentioned self catalyzing reaction, less efficient to incorporate trivalent actinides (An(III)) as compared with Al, allowing only bidentate and tridendate bindings to the colloids.

HAS-polysilanol colloids

The aluminosilicate colloids, which have been synthesized from HAS-polysilanol and from HAS-monosilanol are quite similar, e.g. both, formed out of mother solutions with a Si/Al concentration ratio of 100 have a Si/Al atomic ratio of about one (cf. section 3.5). Their completely different behaviour at the interaction with actinides, however, e.g. different incorporations patterns as well as incorporation kinetics for Am and Th, different colloid-borne Cm species as identified by TRLFS, different stability characteristics, clearly reveal distinct reaction mechanisms for the HAS-monosilanol and the HAS-polysilanol colloid generation. We propose an inner surface complexation model for the formation of HAS-polysilanol colloids, which takes into account the high affinity of polysilanol for the Al^{3+} cation [56], allows for isomorphic substitution of Cm for Al in the colloidal aluminosilicate structure as well as for the growth of Th into the colloids with time. Fig. 66 shows the consecutive steps: (1) the replacement of coordination water of Al (or Cm) by Si-polysilanol-anions; (2) the strong Al-binding weakens the Si-O-binding; (3) a product with an Si/Al ratio = 1 is splitt off. Th can either copolymerize with Si and form poly-Si(Th)- anions (Fig. 67) or displace Si in the HAS product, depending on wether the interaction of Th with Si and Al is simultaneous or a posteriori.

8.2 Role of Si and Al in colloid formation

The suggestion of Exley et al. [80,81] that the mechanim of HAS formation at low pH involves the poisoning of aluminium hydroxyde polymerization by silicic acid, bases on an

older mechanistically proposal of Birchall [82] to describe the retardation of ordinary portland cement (calcium hydroxide lattice) by sugars. The applicative know-how is even older and dates back to the construction of the chinese wall and the use of rice water as an additive in the mortel. Inspired by such points of view, we postulate that the HAS colloid formation as we observed at neutral pH (≥ 7) results from the reverse effect, namely the inhibitory effect of small amounts of Al on the polymerization of Si, which is present in the mother solution in a hundredfold Al-concentration. Fig. 68 visualizes the conception. Elements with high oxidation state such as Si(IV) neutralize their positive charge by surrounding themselves to a maximum extend with oxygens in the processes of hydration, hydrolysis and polymerization. Precipitation is the inevitable consequence. In the presence of Al, an isomorphic substitution of Al for Si takes place. Negative charges are induced into the forming silicate structure. The mutual repulsion between HAS particles hinders a further aggregation, the process which corresponds to an extremely retarded polymerization of Si through the binding of Al. We may say that an Al-controlled polymerization of Si enables kinetically the thermodynamically unfavourable colloidal state. Such a stabilization of the colloidal state has been formulated in theoretical terms by the DLVO theory (see section 2.1). The Al effect is de facto a shift of the equilibrium $Si_{solution} \Leftrightarrow Si_{colloids} \Leftrightarrow Si_{precipitate}$ from the right to the left.

To test the hypothesis, the effect of Al is analyzed under our experimental working conditions for aluminosilicate colloid formation, e.g. the behaviour of a 2.5 times oversaturated Si solution ($5x10^{-3}$ mol l^{-1}) (100%) at pH 7 in presence of 100% Al ($5x10^{-3}$ M) and 1% Al ($5x10^{-5}$ M) at depolymerization and polymerization, respectively. The experimental approaches as shown in Fig. 26 and molybdenum-tests for the quantification of mono- and polysilanol are used. The result is illustrated in Fig. 69 and shows that addition of minute amounts of Al (1% of Si) enhance at first the polymerization rate of Si but shift the equilibrium between mono- and polysilanol in favour of monosilanol ($\Delta = 10\%$). The fact corroborates the hypothesis of the inhibitory effect of the Al binding on the polymerization of Si. Fig. 69 further demonstrates the instantaneous reaction of Al with polysilanol, both present in equal concentration, and the complete inhibition of the depolymerization of Si through aluminosilicate formation. The findings not only infer the formation of the aluminosilicate binding, but they also confirm that the chemical affinity of the Al^{3+} ion towards complexation is preferentially marked with polysilanol [23,56].

The Al effect is further pursued radiochemically from Am as illustrated by Fig. 70. To a constant concentration of dissolved Si ($1.3x10^{-3}$ M) in base, increasing concentrations of Al

dissolved in acid are given and the bebaviour of Am, added as a tracer, is observed. At pH 5 and low Al-concentration, Am is in the precipitate. Through addition of more and more Al, Am migrates from the precipitate into the colloids and even to the solution. The same happens at pH 8: at increasing the Al concentration, Am is transferred from the precipitate to the colloids, and than returns to the precipitate. The explanation: The equilibrium $Am(Al)_{solution} \Leftrightarrow Am(Al)_{colloids} \Leftrightarrow Am(Al)_{precipitate}$ is shifted to the left through binding of Am(Al) with Si and indirectly through the inhibition of the polymerization of Si by Al. Once Si is saturated with Al, the overlapping hydrophobic effect of excess, non-binding Al drives the colloidal HAS including the colloid-borne Am into precipitate. In theoretical terms, the process is called the „colloid destabilization by decrease of the thickness of colloidal electric double layer through increase of the ionic strength of solution“ (see section 2.1). The experiment nicely shows the dual character of Al, either inhibitor of the polymerization of Si or activator of the agglomeration of HAS colloids, and demonstrates why colloids are built only under well-tuned parameter conditions, which we have called „optimum“ conditions. In nature, such conditions are obviously not the exception but the underlying rule; otherwise we would not find colloids in all groundwater.

Conclusions of section 8

The high oxidation state of Si(IV) induces polymerization. Doping the Si(IV) mother solution with Al(III) programms the end of polymerization at colloidal size. Stabilization of the colloidal state is due to isomorphic substitution of Si for Al, inducing thereby negative charges into the silica structure. Repulsion of the negatively charged particles and an extreme retardation of the Si polymerization is the consequence.

Two different mechanisms for colloid formation are postulated on the basis of the interaction of tri- and tetravalent actinides with HAS colloids in statu nascendi. One model starts from monosilanol condensing with Al in a self catalyzing template mechanism, which is not very efficient to bind tri- or tetravalent actinides. The other is an inner surface complexation model which starts from a preformed and very effective polysilanol surface for catalyzing the conucleation of Si and Al and proceeds under expulsion of the HAS product. In such a process, tri- and tetravalent actinides easily substitute isomorphically for Al and Si, respectively.

9 Actinide analogs of aluminosilicate colloids

The controlled polymerization of Si to the colloidal size through binding with Al is understood as a play of elements with high and different oxidation state and the induction of charge. The question whether such a mechanism is unique for Si and Al or generally valid, for example also for tri-and tetravalent actinides, motivates us to search for colloid formation at the coprecipitation of Th and Am.

9.1 Parameter screening for colloid formation of Th and Am

Solubility data for amorphous (am) $Th(OH)_4$ [83] and $Am(OH)_3$ [66] as a function of pH are given in Fig. 71, lower and upper part, respectively. Oversaturation with colloid formation within the pH range from 4 to 9 might be expected in a rather broad concentration range of about 10^{-9} to 10^{-6} mol l^{-1} for Th and 10^{-9} and 10^{-7} mol l^{-1} for Am. A screening experiment to ascertain conditions for colloid formation is conducted for a corresponding variety of the initial Th and Am concentrations and their different ratios (from 0.1 to 6.5). Each coprecipitation sample is prepared by titrating an acid solution of Th and Am in 3x 10^{-2} mol l^{-1} HCl with 3x 10^{-2} mol l^{-1} NaOH (suprapur, Merck) to a preset pH. After different conditioning times, the distribution of Th as well as of Am in the three phases (ionic, colloids and precipitate) is determined. Blanks with only Th or only Am are also made for the purpose of comparison.

Figs. 72-75 show the result for 4 levels of Th concentration, i.e. at 1x10^{-9}, 7.0x10^{-9}, 4.6x10^{-8}, 3.2x10^{-7} mol l^{-1}, each of them combined with Am to cover the above indicated screening area, as well as for the corresponding separate samples (only Am or only Th). The figures represent the activity fraction (%) in the colloidal phase after 3 hours conditioning time for the mixed and the separate samples of Th and Am, as a function of the pH. Under all analyzed conditions, the changing behaviour of „only Th“ as well as „only Am“ when accompanied by Am (measurement of Th in (Th+Am) sample) or Th (measurement of Am in (Th+Am) sample), respectively, is striking. Especially at pH = 6 – 9, Th starts to behave like Am and vice versa. What more is, Th as well as Am, are transferred from the precipitate to the colloidal state, only through mutual interaction. This is a clear indication for the binding of Th with Am, which will be verified with TRLFS (see next section 9.2). It is also the expression of the mutual inhibitory effect on their polymerization. The patterns for incorpora-

tion into the colloidal phase for the mixed and single samples of Th and Am are also different in the acidic region pH = 4 to 6. In this region, Am is well soluble and Th shows a sharp solubility decrease (see Fig. 71). It is therefore amazing to find some Th and even Am in the colloidal phase of the separate samples. The effect might be partly due to „impurities“ in the samples. Ubiquitous elements like Si may be present in concentrations, which are comparable to the solubility concentrations of actinides, and therefore not negligible. However, the comparison of the behaviour of Am and Th, separately, with that of the (Am+Th)-mixture under the exactly same conditions is still allowed and can give useful information.

Fig. 76 summarizes the results given in Figs. 72-75 without the blanks and shows the activity in the colloidal fraction (%) after 3 hours (Fig. 76, left part) and after 35 days (Fig. 76, right part) in order to allow a better comparison of colloid formation, not only at different concentration levels and ratios, but also after an increased sample conditioning time. The view of activity incorporation into the colloidal phase after 3 hours (Fig. 76, left part) clearly shows the similar behaviour of Th and Am in the mixed samples at neutral pH at all concentration levels of Th. At pH = 4 – 6, however, Th and Am behave differently. At increasing concentration, Th is oscillating between the colloidal phase and the precipitate, whereas Am is oscillating between the colloidal phase and the solution. The view of activity in colloids after 35 days (Fig. 76, right part) reveals that the colloids, which have been generated at neutral pH at relatively high concentrations of Th and Am as compared with their solubilty concentrations are quite unstable as a function of time. The fact may be due to the lower induced polarization by substituting Th(IV) for Am(III) as compared with Si(IV) substitution for Al(III), or reverse. Another reason for the low colloid stability may be related with the concentration levels of actinides we have used: too high to form stable colloids, but too low as compared with system impurities, which interactions become visible now.

In the region of higher solubility of Th and Am, namely at pH = 4 - 5, we observe an interesting colloid stabilization with time. Let us take the example of the sample with Th at $10^{-7.3}$ mol l^{-1} and Am at $10^{-8.1}$ mol l^{-1} (ratio Th/Am = 6.122) at pH = 4. Colloid stabilization (compare corresponding left and right parts of Fig. 76) is expressed not only by an increased activity in the colloidal fraction with time but also by a synchronization of the polymerization of Am and Th as expressed by a pH shift for the maximal Am-activity after 35 days. Fig.77 illustrates the corresponding kinetics and illustrates the partition of the activity in the three phases (soln / coll. / prec.). The upper part of Fig. 77 shows the behaviour of the separate Th and Am samples (Th at the left and Am at the right part of Fig. 77). Th is fully precipitated at

all times. Am is dissolved at 60% but becomes 60% colloidal with time. The middle part of Fig. 77 gives the kinetic behaviour of Th and Am in the mixed sample and shows that Th is transferred from the precipitate to the colloidal phase and even to the solution only through mixing (binding) with Am. The effect of mixing Th with Am is the partial inhibition of polymerization (precipitation) of Am in favour of Am in colloids Am and in solution. After some days, the polymerization kinetics of Th and Am become synchronized, both with a 60% in the colloidal phase. After 89 days we calculate a colloidal Th/Am atomic ratio = 7.88, reflecting almost the Th/Am concentration ratio in the mother solution, which is 6.12.

The possibility to achieve a better colloid stabilization by substituting tri- or tetravalent cations for divalent cations in order to increase the induced polarization is further analyzed. Therefore Mg is added in a concentration of 10^{-2} mol $l^{-}1$ to the mixed (Th+Am) sample (Fig. 77, middle part) at pH = 4 with Th at $10^{-7.3}$ mol l^{-1} and Am at $10^{-8.1}$ mol l^{-1}. The Mg-effect is shown in the lower part of Fig. 77. The equilibrium of Th in the mixture is shifted in favour of the precipitate. Only 20% instead of 60% of the original Th remains colloidal, but very stable with time. Am is colloidal at about 60% and shows a synchronized behaviour with Th from the very beginning. The colloids have now an atomic Th/Am ratio, e.g. after 111 days of 2.17, instead of 7.88 for the analog sample without Mg. The experiment clearly demonstrates that the colloid composition and the related colloid stability can be directed by divalent cations in the medium. This interesting effect will be further analyzed.

9.2 Interaction of Th with Cm analyzed by TRLFS

From the previous radiometric experiments coupled with ultrafiltration, we have found conditions where Th and Am conucleate, and by doing so, stabilize actinides into the colloidal state. We now want to verify spectroscopically the interaction of Cm with Th with the aid of TRLFS, directly at the titration of an acid solution ($3.5x10^{-7}$ mol l^{-1} Th and $5x10^{-8}$ mol l^{-1} Cm in 0.03 mol l^{-1} HCl) with 0.03 M NaOH (suprapure, Merck). The fluoresence spectra in the course of the titration are shown in Fig. 78 (upper part) and the deconvoluted spectra in Fig. 78 (middle part). Two Th-borne Cm species are observed, namely Cm-Th(I) and Cm-Th(II) with emission peaks at 598.0 nm and 604.8 nm, respectively. The fluorescence life times are also measured to ascertain the number of hydration waters molecules bound to Cm. Cm-Th(I) and Cm-Th(II) have a relaxation time of 135.5 μs and 331.0 μs, corresponding to 3.9 and 1.1 remaining water molecules of Cm, respectively. The pentadentate binding for the Cm-Th(I)

species and the complete incorporation of Cm into the structure of Th for the Cm-Th(II) species are thereby ascertained. Overall speciation results are summarized in Fig. 78 (lower part) for the free Cm ion as well as the Th bound Cm species as a function of pH. The Cm^{3+}-aquo-ion is predominating in the low pH region from 1 to 4. At the same time the Cm-Th(I) species is built to a maximum of 25% at pH = 5 – 6. The incorporated species Cm-Th(II) emerges from pH 4 and increases its fraction sharply at pH 6 to more than 95% in the pH region from 6 to 9. The colloid-borne Cm species, as identified by TRLFS, correspond to the optimum regions for colloid formation, as identified in the screening experiment (cf. Fig. 76), which corroborates spectroscopically the indications from radiometric measurements (section 9.1) that „americiothoronate“ colloids are generated. We also remark that Cm-Th(I) and Cm-Th(II) without HAS are very similar, although not completely same, as compared to the Cm-Th(I) and Cm-Th(II) which are found in presence of HAS (see section 6.2, Table 2).

The question whether the americiothoronate binding is a conditio sine qua non for colloid formation is still open. We expect more information from the analysis of actinide colloid formation with LIBD, as described in the following.

9.3 Interaction of Th with Eu traced by LIBD

In a similar titration experiment as performed for the TRLFS measurement, we trace colloid formation directly at the titration of 6.5×10^{-7} mol l^{-1} Th with 1×10^{-7} mol l^{-1} Eu in the pH range of 1 to 10. Eu is used as inactive substitute for Am(Cm). We compare the breakdown probability as a function of pH for four samples: (1) blank without Th and Am; (2) Eu only; (3) Th only; (4) mixture of Th+Eu. Fig. 79 shows the result. The relatively high background at pH ≥ 6 resulting even from suprapure chemicals or from leaching of the vessel walls of the LIBD instrumentation limits the observation window to the low pH region. However, the result is clear. At pH = 4 – 5, the generation of colloids by mixing Th and Eu, clearly surpasses a certain colloid formation in the separate Th and Eu samples and corroborates the previous findings of colloid generation through polarization at heterogeneous nucleation (polymerization) of elements with different oxidation state and therefore with different rates of polymerization (see section 8.2). Comparing the present result with the result of radiometric measurement as shown in Fig. 7 and Fig. 77, we may even assume that the europiothoronate colloids as detected by LIBD are similar to the americiothoronate colloids formed at pH 4 after 3 hours with a Th/Am activity fraction ratio of 59.4% / 6.4%, multiplied with the Th/Am

concentration ratio in the original solution, namely 6.12, giving the atomic Th/Am ratio in colloids: $(Th/Am)_{colloids} = 57$. Investigations on this subject are currently pursued. The important result leads to a new view of actinide colloids and also to a new definition of „real colloids“, which might quite different from what we have been used to in the past.

Conclusions of section 9

Americio- and europiothoronate colloids have been synthesized in analogy with aluminosilicate colloids. The colloid generation is explained as a controlled polymerization of actinides of one oxidation state through conucleation with actinides of different oxidation state. The control consists of the retardation of polymerization through mutual binding, as confirmed by TRLFS, and the stabilization of the colloidal state, as shown by LIBD, through polarization of the particles. The hypothesis that one element, present in a single oxidation state, cannot build „real colloids“ of actinides will be further verified.

The Th/Am atomic ratio in the americiothoronate colloids is, in contrast to that in HAS colloids, the same as the Th/Am concentration ratio in the mother solution. Divalent cations, such as Mg can alter the Th/Am atomic ratio in the colloids and influence the colloid stability correspondingly.

10 Summary

Migration of colloid-borne actinides in the geosphere is a well recognized, but hitherto non-quantifiable fact, that still questions the safety of nuclear repositories. The underlying reason is pour knowledge about the mechanisms of colloid formation, colloid stabilization and hence of colloid/actinide interaction. The present investigation concentrates on whether and how tri- and tetravalent actinides are incorporated into the colloidal phase, either through formation of real colloids or by binding to natural aquatic colloids, e.g. aluminosilicate colloids. The irreversibility of such processes is a conditio sine qua non for the colloid facilitated actinide migration and therefore a central question in this study.

The first part of the work deals with the synthesis of aluminosilicate colloids under normal conditions of temperature and pressure from supersaturated mother solutions through conucleation of Si(IV) and Al(III). It includes the identification, analysis and intercorrelation of the thermodynamical and kinetic solubility parameter of Si and Al on theoretical and ex-

perimental basis, as well as the characterization of the generated colloids. In an elaborated parameter screening experiment, optimum conditions for the formation of aluminosilicate colloids are recognized from the behaviour of Am, added as a tracer in the condensation process of Si and Al. The optima are reflected by maxima of Am activity in the colloidal fraction of mother solutions made at pH 5 - 6 and pH 8 - 9, with a Si/Al concentration ratio of 100, but at two different Si concentration levels, namely in a slightly undersaturated and in a 6.5 times oversaturated solution, containing monosilanol and polysilanol, respectively. The corresponding colloids, as characterized by LIBD, AFM and SEM-EDXS, all belong to a unique colloid type which is very similar to the natural aquatic colloids of the imogolite type with a Si/Al atomic ratio of ca. 1, namely hydroxy aluminosilicate (HAS) colloids. The particle size is 10 - 50 nm and the number density amounts to $10^{11} – 10^{14}$ particles per litre.

The second part of this study investigates the interaction of trivalent actinides with HAS colloids in formation (in statu nascendi) and comprises the speciation of colloid-borne Cm with TRLFS, stability tests of the generated pseudocolloids of Am(Cm) by means of LIBD and desorption experiments, and determination of the capacity of HAS colloids to bind Am(Cm). The TRLFS analysis shows a red shift of the typical fluorescence emission band of the Cm^{3+} aquo-ion at 593.8 nm to 598.5 nm, 601.8 nm and 606.8 nm indicating the formation of three colloid-borne Cm species, namely Cm-HAS(I), Cm-HAS(II) and Cm-HAS(III), respectively. The spectral shift is proven to be characteristic for the interaction of Cm with Si. The respective increased fluorescence relaxation times from 65.2 μs for the Cm aquo-ion to 83.5 μs, 88.3 μs and 518.0 μs, are correlated with the number of replaced Cm coordination waters through silanols, and reveal the three colloid-borne Cm species as a bidentate, a tridentate and a completely incorporated Cm into the aluminosilicate structure of colloids. The relative Cm species distribution as a function of pH at the two above mentioned concentrations of Si for optimum colloid formation shows that the binding strength of Am(Cm) to HAS colloids increases with increasing pH and increasing concentration of Si. The effect is correlated with the faster polymerization kinetics of Si at high pH and high Si concentration, as demonstrated by a number of molybdenum tests for the quantification of the polysilanol fraction as a function of time under our experimental conditions for colloid generation. The isomorphic substitution of Am(Cm) for Al in the aluminosilicate colloid structure is further correlated with the interfacial energy of polysilanol, which seems to be necessary to overcome the activation energy barrier for the complete incorporation of Am(Cm). The explanation is corroborated by the fact that Cm-HAS(III) is also built at increased temperature, e.g. 5 days at 90°C, from

undersaturated Si (monosilanol) as an alternative way to provide activation energy. The generated pseudocolloids of Am(Cm), corresponding to the Cm-HAS(II) and Cm-HAS(III) species are extremely stable as a function of time, against desorption with inactive medium (irreversible Am(Cm)-colloid binding), and at increased temperature. Their formation is, however, pH reversible, and in line with the relatively low stability of Cm-HAS(I) built at pH 5-6. The maximum capacity of HAS colloids to incorporate Am(Eu) is reached for HAS colloids, generated from polysilanol at pH 8 - 9 when about one third of the Al in colloids is substituted by Am(Eu) and the HAS colloids start loosing their original identity.

The third topic of investigation is the interaction of tetravalent actinides with HAS colloids in statu nascendi, and includes the determination of the activity incorporation patterns as well as kinetics for Th, stability tests of the generated pseudocolloids of Th, and determination of the capacity of HAS colloids to bind Th. The incorporation of Th into HAS colloids increases with increasing time, pH and Si concentration, and reflects the polymerization kinetics of Si. The behaviour of Th is yet different from that of Si: the fraction of Th migrating from the mother solution into the colloids is a hundred times higher than that of Si, namely 100% and 1%, respectively, indicating a much higher affinity of Th-oxyhydroxide for the Al^{3+} cation in comparison with mono- and even polysilanol. The pseudocolloids of Th show a high resistance against desorption with inactive medium. The Th-HAS bindings are therefore considered to be irreversible. The incorporation of Th differs from that of Am as far as pH dependency, kinetics, quantity as well as stability are concerned. The general tendency ist that Th incorporates slower, more and in a broader pH region as compared with Am. Colloid-borne Th, unlike colloid-borne Am, stabilizes the HAS colloids. The highest concentration of Th, possibly hold by HAS colloids, is given at colloid formation from polysilanol at neutral pH from 6 to 9, and after a conditioning time of several days. In that case about 80% of the Si in colloids is substituted by Th. Since the Si/Al atomic ratio in colloids is ca. 1, the Al concentration in the mother solution can serve as an indicator for the amount of potentially incorporated Th in the colloids.

The fourth part of this study analyzes the interaction behaviour of a mixture of tri- and tetravalent actinides with HAS colloids in statu nascendi by comparing it with their separate behaviour. To this purpose, Am(Cm) and Th activity phase distribution patterns, time-resolved laser fluoresence spectra shifts, Cm species distributions and activity desorption measurements are evaluated. Incorporation of Am as well as of Th out of their mixture still takes place. Differences in incorporation patterns as well as in type and number of Cm spe-

cies, as previously observed at the formation of HAS colloids, either from mono- or polysilanol, are cancelled out if Cm is accompanied with Th. Only two colloid-borne Cm species, namely the Th-borne Cm species, Cm-Th(I) at 590.0 nm, and Cm-Th(II) at 603.6 nm, with fluorescence life times of 134.0 μs and 342.9 μs, corresponding to four and no waters in the coordination sphere of Cm, respectively, are now identified. They reflect the interaction behaviour of Cm-Th complexes with HAS colloids. This interaction resembles more that of Cm(Am) at low pH from 4 to 6, and more that of Th at neutral pH from 6 to 9. The stability of the generated pseudocolloids against desorption with inactive medium remains, notwithstanding the Cm-Th complex formation, almost unchanged. Consequently, the (Cm+Th)-HAS bindings are irreversible.

The fifth topic of this work concerns the incorporation behaviour of tri- and tetravalent actinides into aged HAS colloids through sorption, and comprises the evaluation of Am and Th activity incorporation patterns as well as stability tests of the corresponding pseudocolloids. Aged colloids are not tied up to sorb Am. Their capability to sorb Th, however, is high, and comparable to that of HAS colloids in statu nascendi. The high stability of the pseudo-(aged)-colloids of Th against desorption with inactive medium corresponds to irreversible Th-(aged HAS colloid)-bindings. A gradually decreasing stability against desorption with EDTA, from 100% to a 20% after 35 days EDTA contact time, reveals different colloid-borne Th species with decreasing Th-colloid binding strength in the order: Th-HAS-polysilanol (pH 7-9) (containing Th isomorphically substituted for Si) > Th-HAS-monosilanol (pH 7-9) > Th-HAS-poly-silanol or Th–monosilanol (pH 5).

The sixt part of the work is the trial to find out how colloids are thinking by reviewing the gained results from the standpoint of colloids, traced by actinides, and to postulate mechanisms for colloid formation. Key words of colloidal language are „controlled polymerization“ through „polarization“ and „optimal conditions“. They are elaborated in the experimentally corroborated conception. The high oxidation state of Si(IV) induces polymerization. Doping the Si(IV) mother solution with Al(III) programms the end of polymerization at colloidal size. Stabilization of the colloidal state is due to isomorphic substitution of Si for Al, inducing thereby negative charges into the silica structure. Repulsion of the negatively charged particles and an extreme retardation of the Si polymerization is the consequence. An optimal Si/Al ratio in the mother solution is prerequisite to stable HAS colloids. An excess of Al promotes colloid agglomeration through solvation effect. Two different mechanisms for colloid formation are postulated on the basis of the interaction of tri- and tetravalent actinides with HAS

colloids in statu nascendi. One model starts from monosilanol condensing with Al in a self-catalyzing template mechanism, which is not very efficient to bind tri- or tetravalent actinides. The other is an inner surface complexation model which starts from a preformed and very effective polysilanol surface for catalyzing the conucleation of Si and Al and proceeds under expulsion of the HAS product. In such a process, tri- and tetravalent actinides easily substitute isomorphically for Al and Si, respectively.

The seventh and last part of this study is devoted to the question whether actinide analogs of aluminosilicate colloids such as americiothoronate colloids do exist, also without the aid of Si or Al. This part contains a parameter screening experiment for colloid formation out of supersaturated solutions of Th and Am, based on activity measurements in the ionic, colloidal and precipitated fraction, speciation of colloid-borne Cm with TRLFS, and monitoring of colloid formation by LIBD. Optimum conditions for the formation of stable amerciothoronate colloids are found at pH 4 – 6, for several Th concentration levels between 10^{-9} and 10^{-6} mol l^{-1} , and at pH 9, for one Th concentration namely 10^{-9} mol l^{-1}, each of them combined with Am to give a Th/Am ratio in the mother solutions between 0.1 and 6.5. The optima are correlated with two colloid-borne Cm species, Cm-Th(I) at 598.0 nm and Cm-Th(II) at 604.8 nm, with fluoresence life times of 135.5 μs and 331.0 μs, corresponding to four and no water molecules in the coordination sphere of Cm, respectively. The species are very similar to those found at simultaneous incorporation of Am(Cm) and Th in HAS colloids in statu nascendi. LIBD measurements corroborate that precipitating Th, mixed with precipitating Eu, are transferred into the colloidal state through Th-Eu-binding. The Th/Am atomic ratio in the americiothoronate colloids is the same as the Th/Am concentration ratio in the mother solutions. We propose therefore a simple conucleation of Th with Am(Cm, Eu) as a binding mechanism. This is in contrast to the nucleation mechanism of Si with Al, namely the formation of a solid solution, with ($Si/Al_{coll.} = 1$) << ($Si/Al_{soln} = 100$). Divalent cations, such as Mg, can alter the Th/Am atomic ratio in the colloids and influence the colloids stability correspondingly. The Mg effect is shown to be an effect on the polymerization rate of Th (retardation through binding) as well as on the polymerization rate of Am (acceleration through solvation effect). Investigations on this subject are continued, since they may lead to a new view of actinide colloids, to a new definition of „real colloids“, which is quite different from the one we have been used to in the past, and especially to a better understanding of the fundamental rules for colloid stabilization in general.

11 References

[1] S. Yariv, H. Cross, Geochemistry of Colloid Systems, Springer, Berlin, 1979.

[2] J.F. McCarthy and C. Degueldre, in: J. Buffle and H.P. Van Leeuwen (Eds.), Environmental Particles, Lewis publishers, Boca Raton, 1993, p. 248

[3] P. Cloos, A.J. Leonard, J.P. Moreau, A. Habillon, J.J. Fripiat, Clays Clay Miner. 17 (1969) 270.

[4] C. Clark-Monk and B. Ellis, J. Colloid Interface Sci. 44 (1979) 37.

[5] J. Duan, J. Gregory, Colloids Surf. A 107 (1996) 309.

[6] J.I. Kim, Radiochim. Acta 52/53 (1991) 71.

[7] M. Bouby, T. Ngo Manh, H. Geckeis, F. Sherbaum, J.I. Kim, Radiochim. Acta 90 (2002) 727.

[8] J.I. Kim, P. Zeh, B. Delakowitz, Radiochim. Acta 58/59 (1992) 147.

[9] J.I. Kim, B. Delakowitz, P. Zeh, D. Klotz, D. Lazik, Radiochim. Acta 66/67 (1994) 165.

[10] M. Schnitzer and S.U. Kahn, Humic Substances in the Environment, Marcel Dekker, New York, 1972.

[11] M. Buleva, I. Petkanchin, Colloids Surf. A 151 (1999) 225.

[12] J.I. Kim, D.S. Rhee, G. Buckau, A. Morgenstern, Radiochim. Acta 79 (1997) 173.

[13] C. Degueldre, I. Triay, J.I. Kim, P. Vilks, M. Laaksoharju, N. Miekeley, Appl. Geochem. 15 (2000) 1043.

[14] J.I. Kim, MRS Bulletin 19 (1994) 47.

[15] J.I. Kim, Nuclear Engineering and Design 202 (2000) 143.

[16] A.B. Kersting, D.W. Erfurd, D.L. Finnegan, D.J. Rokop, D.K. Smith, J.L. Thompson, Nature 397 (1999) 56.

[17] H. Geckeis, R. Klenze, J.I. Kim, Radiochim. Acta 87 (1999) 13.

[18] Th. Stumpf, A. Bauer, F. Coppin, J.I. Kim, Environ. Sci. Technol. 35 (2001) 3691.

[19] Th. Rabung, Th. Stumpf, H. Geckeis, R. Klenze, J.I. Kim, Radiochim. Acta 88 (2000) 711.

[20] J.I. Kim, Mater. Res. Soc. Symp. Proc. 294 (1993) 3.

[21] R. Artinger, W. Schüßler, T. Schäfer, J.I.Kim, Environ. Sci. Technol. 36 (2002) 4358.

[22] R. Artinger, Th. Rabung, J.I. Kim, S. Sachs, K. Schmeide, K.H. Heise, G. Bernhard, H. Nitsche, J. Contam. Hydrol. 58 (2002) 1.

[23] T.W. Swaddle, Coord. Chem. Rev. 219-221 (2001) 665.
[24] W. Bernotat, X. Le Gal, J.L. Crovisier, European Union of Geosciences, J. Conf. Abstracts, Vol. 6 No. 1, EUG XI Strasbourg, France, 6-12 April 2001, p. 660.
[25] J.I. Kim, K. Gompper, K.D. Closs, G. Kessler, D. Faude, J. Nucl. Mater. 238 (1996) 1.
[26] J.I. Kim, R. Klenze, H. Wimmer, Eur. J. Solid State Inorg. Chem. 28 (1991) 347.
[27] F.J. Scherbaum, R. Knopp, J.I. Kim, Appl. Phys. B - Lasers and Optics 63(3) (1996) 299.
[28] T. Bundshuh, W. Hauser, J.I. Kim, R. Knopp, F.J. Scherbaum, Colloid. Surf. A 180 (2001) 285.
[29] T. Bundshuh, R. Knopp, J.I. Kim, Colloids Surf.A 177 (1) (2001) 47.
[30] K. Kitamori, K. Yokose, M. Sakagami, T. Sawada, Jpn. J. Appl. Phys. 28 (7) (1989) 1195.
[31] C. Walther, C. Bitea, W. Hauser, J.I. Kim, F.J. Scherbaum, Nucl. Instrum. Methods Phys. Res. B 195 (2002) 374.
[32] C. Bitea, C. Walther, J.I. Kim, H. Geckeis, T. rabung, F.J. Sherbaum, D.G. Cacuci, Colloids Surf. A, in press.
[33] R.J. Hamers, J. Phys. Chem. 100 (1996) 13103.
[34] F.J. Giessibl, Science 267 (1995) 68.
[35] M. Plaschke, J. Römer, J.I. Kim, Ultramicroscopy 75 (1998) 77.
[36] M. Plaschke, T. Schäfer, T. Ngo Manh, R. Knopp, H. Geckeis, J.I. Kim, Anal. Chem. 73 (2001) 4338.
[37] M. Plaschke, J. Römer, J.I. Kim, Environ. Sci. Technol. 36 (2002) 4483.
[38] M. Stumm, Aquatic Chemistry, Wiley-Interscience, New York, 1981.
[39] M. Stumm, Chemistry of the Solid-Water interface, Wiley-Interscience, New York, 1992.
[40] K.S. Birdi, Surface and Colloid Chemistry, CRC, New York, 1997.
[41] H.-D. Dörfler, Grenzflächen- und Kolloidchemie, VCH, Weinheim, 1994.
[42] D.J. Shaw, Introduction to Colloid and Surface Chemistry, Butterworth-Heinemann, Oxford, 1991.
[43] D.F. Evans, H. Wennerström, The Colloidal Domain – Where Physics, Biology and Technology Meet, VCH, Weinheim, 1994.
[44] R. Klenze, J.I. Kim, H. Wimmer, Radiochim. Acta 52/53 (1991) 97.
[45] Th. Fanghänel, J.I. Kim, J. Alloys Compd. 271-273 (1998) 728.

[46] J.V. Beitz, Similarities and differences in trivalent lanthanide- and actinide molecules, in Handbook of Physics and Chemistry of the Actinides, Vol.18, K.A. Gschneider, Jr, L. Eyring, G.R. Choppin, G.H. Lander (Eds), North-Holland Phys. Publ., Amsterdam, p.120, 1994.

[47] D.S. Kliger, Ultrasensitive Laser Spectroscopy, Academic Press, New York, 1983.

[48] A.B. Yusov, J. Radioanal. Nucl. Chem. Articles 143 (1990) 287.

[49] Y. Kato, G. Meinrath, T. Kimura, Z. Yoshida, Radiochim. Acta 64 (1994) 107.

[50] Ch. Moulin, P. Decambox, V. Moulin, J.G. Decaillon, Anal. Chem. 67 (1995) 348.

[51] P. Schachtschabel, H.-P. Blume, C. Brümmer, K.-H. Hartge, U. Schwertmann, Lehrbuch der Bodenkunde, Ferdinand Enke Verlag Stuttgart, 1992.

[52] K. Wada, in J.B. Dixon, S.B. Weed (Eds.), Minerals in Soil Environments, Soil. Sci. Soc. Am., Madison (Wisc.), 1989.

[53] V.C. Farmer, M.J. Adams, A.R. Fraser, F. Palmieri, Clay Min. 18 (1983) 459.

[54] F.J. Doucet, C. Schneider, S.J. Bones, A. Kretchmer, I. Moss, P. Tekely, C. Exley, Geochim. Cosmochim. Acta 65 (2001) 2461.

[55] F.J. Doucet, M.E. Rotov, C. Exley, J. Inorg. Biochem. 87 (2001) 71.

[56] P.D. Taylor, R. Jugdaoshing, J.J. Powell, J. Amer. Soc. 119 (1997) 8852.

[57] J.D. Rimstidt, H.L. Barnes, Geochim. Cosmochim. Acta 44 (1980) 1683.

[58] M. Sadiq, W.L. Lindsay, Colo. State Univ. Exp. Stn. Tech. Bull., 134 (1979) 1.

[59] W.L. Lindsay, Chemical Equilibria in Soils, Wiley-Interscience, New York, 1979.

[60] H.M. May, D.G. Kinniburgh, P.A. Helmke, M.L. Jackson, Geochim. Cosmochim. Acta 50 (1986) 1667.

[61] H.C. Helgeson, J.M. Delany, H.W. Nesbitt, D.K. Bid, Am. J. Sc. 278 (1978) 1.

[62] C.F. Baes, Jr, R.E. Mesmer, the Hydrolysis of Cations, Wiley-Interscience, New York, 1976.

[63] R.M. Smith, A.E. Martell, Critical Stability Constants, Vol.4, Plenum Press, New York, 1978.

[64] Th. Stumpf, Th. Rabung, R. Klenze, H. Geckeis, J.I. Kim, J. Colloid Interf. Sci. 238 (2001) 219.

[65] W.I. Bourcier, K.G. Knauss, K.J. Jackson, Geochim. Cosmochim. Acta 57 (1993) 747.

[66] V. Neck, Th. Fanghänel, J.I. Kim, Report: FZKA 6110, Forschungszentrum Karlsruhe, 1998.

[67] R.K. Iler, The Chemistry of Silica, Wiley-Interscience, New York, 1997.

[68] G. Lagerstrom, Acta Chem. Scand. 13 (1959) 722.
[69] R. Siever, Amer. Mineral. 42 (1957) 826.
[70] N. Ingri, Acta Chem. Scand. 13 (1959) 758.
[71] S.M. Elgawhary, L. Lindsay, Soil Sci. Soc. Am. Proc. 36 (1972) 439.
[72] G.B. Alexander, J. Am. Chem. Soc. 75 (1953) 5655.
[73] E.N. Rizkalla, G.R. Choppin in: K.A. Gschneider Jr, L. Eyring, G.R. Choppin, G.H. Lander (Eds), Lanthanides and Actinides Hydration and Hydrolysis, Handbook on the Physics and Chemistry of Rare Earths, Vol. 18, Elsevier Science B. V., p. 529, 1994.
[74] W.De, Jr. Horrocks, D.R. Sudnick, J. Am. Chem. Soc. 101 (1979) 334.
[75] T. Kimura, G.R. Choppin, J. Alloys and Comp. 213/214 (1994) 313.
[76] K.H. Chung, R. Klenze, K.K. Park, P. Paviet-Hartmann, J.I. Kim, Radiochim. Acta 82 (1998) 215.
[77] H.M. Kingston, S.J. Haswell, Microwave-Enhanced Chemistry, Fundamentals, Sample Preparation and Applications, Am. Chem. Soc., Washington, D.C., p.314, 1997.
[78] S.W. Sill, Anal. Chem. 36 (1964) 675.
[79] O. Alhassanieh, A. Abdul-Hadi, M. Ghafar, A. Aba, Appl. Rad. Isotop. 51 (1999) 493.
[80] C. Exley, J.D. Birchall, Polyhedron 11 (1992) 1901.
[81] C. Exley, J.D. Birchall, Polyhedron 12 (1993) 1007.
[82] J.D. Birchall, N.L. Thomas, Brit. Ceram. Proc. 35 (1984) 305.
[83] V. Neck, J.I. Kim, Radiochim. Acta 89 (2001) 1.

12 Publications, Reports, Conferences

Publications

[1] M.A. Kim, P.J. Panak, J.I. Yun, J.I. Kim, R. Klenze, K. Köhler: „Interaction of Actinides with Aluminosilicate Colloids in Statu Nascendi, Part I: Generation and Characterization of Actinide(III)-Pseudocolloids“; Colloids and Surfaces A: Physicochem. Eng. Aspects 216 (2003) 97-108.
[2] P.J. Panak, M.A. Kim, J.I. Yun, J.I. Kim: „Interaction of Actinides with Aluminosilicate Colloids in Statu Nascendi, Part II: Spectroscopic Speciation of Colloid-borne Actinides(III); Colloids and Surfaces A: Physicochem. Eng. Aspects 227 (2003) 93-103.

[3] M.A. Kim, P.J. Panak, J.I. Yun, A. Priemyshev, J.I. Kim: „Interaction of Actinides with Aluminosilicate Colloids in Statu Nascendi, Part III: Colloid Formation from Monosilanol and Polysilanol“; Colloids and Surfaces A: Physicochem. Eng. Aspects, in press.

[4] M.A.Kim, P.J. Panak, J.I. Yun, A. Priemyshev, J.I. Kim: “Interaction of tetravalent Actinides with Aluminosilicate Colloids: Generation of Th-Pseudocolloids”, in preparation.

[5] M.A. Kim, P.J. Panak, J.I. Yun, A. Priemyshev, J.I. Kim: “Interaction of Actindes with Aquatic Colloids and Generation of Actinide Pseudocolloids”; Annual Rep. BMWA (2003).

[6] M.A, Kim, P.J. Panak, J.I. Yun, A. Priemyshev, J.I. Kim: “Interaction of Actinides with Aquatic Colloids and Generation of Actinide Pseudocolloids; IAEA Waste Management Research Abstracts (WMRA), Vol. 28, Abstarct No. 4959.

[7] P.J. Panak, M.A. Kim, R. Klenze, J.I. Kim, Th. Fanghänel: “Interaction of Cm(III) with Aqueous Mono- and Polysilicates studied by Time-resolved Laser Fluorescence Spectroscopy (TRLFS); Colloids and Surfaces A: Physicochem. Eng. Aspects, submitted.

Ph.D. Thesis

[1] A. Priemyshev; “Colloid Formation of Americium and Thorium in the Water / Aluminosilicate Systems”, Fakultät für Chemie, Technische Universität München (2004).

Conferences

[1] 8th International Conference on the Chemistry and Migration Behaviour of Actinides and Fission Products in the Geosphere, Bregenz, Österreich (2001):
M.A. Kim, P.J. Panak, J.I. Yun, J.I. Kim, R. Klenze, K. Köhler, “Interaction of Actinides with Aluminosilicate Colloids in Statu Nascendi”.

[2] GDCh-Jahrestagung Chemie 2001, Würzburg (2001):
M.A. Kim, P.J. Panak, J.I. Yun, J.I. Kim, R. Klenze, K. Köhler, “Interaction of Actinides with Aluminosilicate Colloids in Statu Nascendi”.

[3] 6. Projektstatusgespräch zu BMBF/BMWA-geförderten FuE-Vorhaben auf dem Gebiet der Entsorgung gefährlicher Abfälle in tiefen geologischen Formationen, Karlsruhe, "Einfluß von Kolloiden auf die Migration von Actiniden".

[4] 9th International Conference on the Chemistry and Migration Behaviour of Actinides and Fission Products in the Geosphere, Gyeongju, Korea (2003):
M.A. Kim, P.J. Panak, A. Priemyshev, J.I. Kim, "Actinides on the Track of Groundwater Colloids".
M.A. Kim, P.J. Panak, J.I. Yun, A. Priemyshev, J.I. Kim, K. Köhler, "Interaction of Tetravalent Actinides with Aluminosilicate Colloids: Generation of Thorium Pseudocolloids".
P.J. Panak, M.A. Kim, J.I. Yun, J.I. Kim, "Interaction of Actinides with Aluminosilicate Colloids "in Statu Nascendi"; Spectroscopic Speciation of Colloid-borne Cm(III)."

[5] GDCh-Jahrestagung Chemie 2003, München (2003):
M.A. Kim, P.J. Panak, J.I. Yun, A. Priemyshev, J.I. Kim, K. K. Köhler, "Interaction of Actinides with Aluminosilicate Colloids: Colloid Formation by Mono-Silanol and Oligo-Silanol".
M.A. Kim, P.J. Panak, J.I. Yun, A. Priemyshev, J.I. Kim, K. Köhler, "Intercation of Tetravalent Actinides with Aluminosilicate Colloids: Generation of Thorium Pseudocolloids".
P.J. Panak, M.A. Kim, J.I. Yun, J.I. Kim, "Interaction of Actinides with Aluminosilicate Colloids in "Statu Nascendi": Spectroscopic Speciation of Colloid-borne Cm(III)".

[6] "Plutonium Futures – the Science Conference", Albuquerque, New Mexico, USA (2003):
J.I. Kim, M.A. Kim, P.J. Panak, J.I. Yun, "Aquatic Colloids of Actinides: How are they generated under natural Aquifer Conditions?".

[7] American Chemical Society, 22th National Meeting & Exposition, Anaheim, CA, USA (2004):
J.I. Kim, P.J. Panak, J.I. Yun, M.A. Kim, "Actinides on the Track of Aquatic Colloids: Speciation of Colloid-borne Cm(III)".

Acknowledgements

Thanks are due to Drs. D. Schild and J.Römer for XPS and EDX analyses, M.Plaschke for AFM analyses, H. Geckeis for ICP-MS measurements, C.M. Marquardt for providing the isotopes Am and Cm and C. Dardenne for the thermodynamic solubility calculation.

Annexe: Figures and Tables

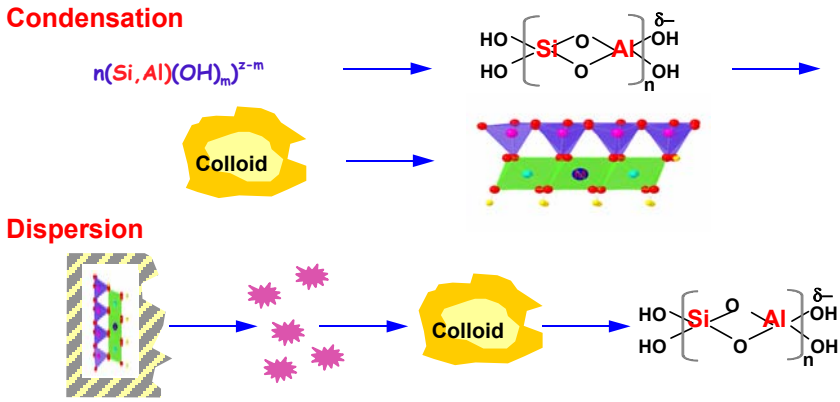

Fig. 1: General pathways for the formation of inorganic aquatic colloids such as aluminosilicate colloids.

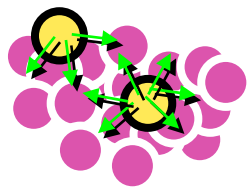

Fig. 2: Colloidal free energy stems from the imbalance of intermolecular forces exerted on molecules at the interface.

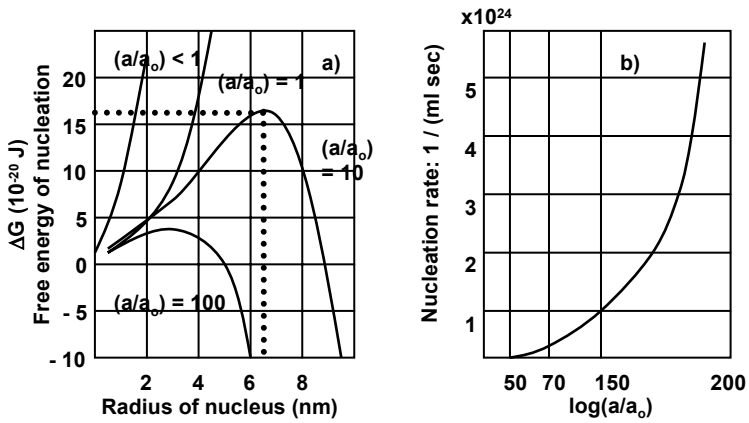

Fig. 3: (a) Free energy of nucleus formation calculated as a function of the radius for different supersaturated ratios (Eq.1). The maximum ΔG^* is the activation barrier to the generation of nuclei of radius r_j; (b) Nucleation rate calculated as a function of the critical supersaturation.

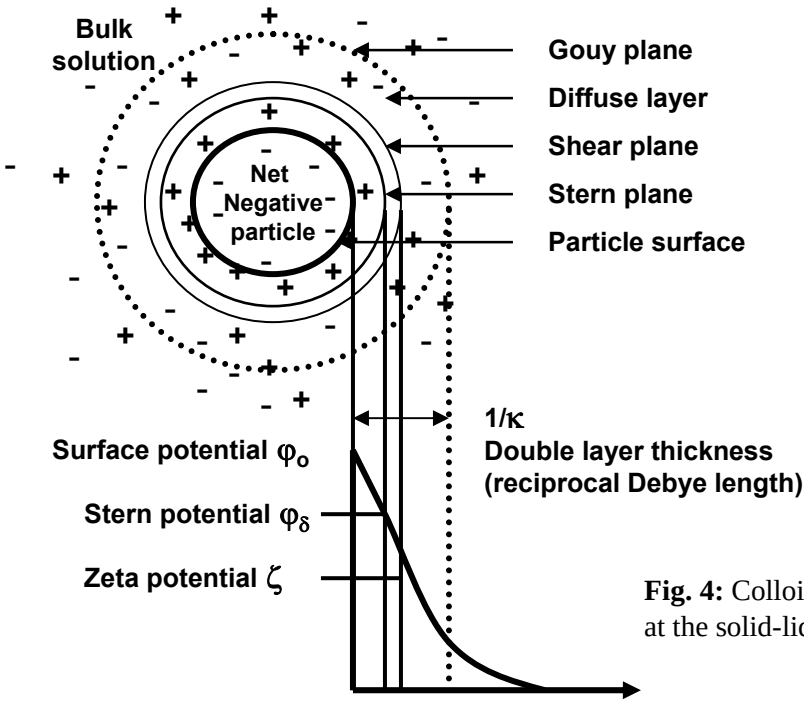

Fig. 4: Colloidal electric double layer at the solid-liquid interface.

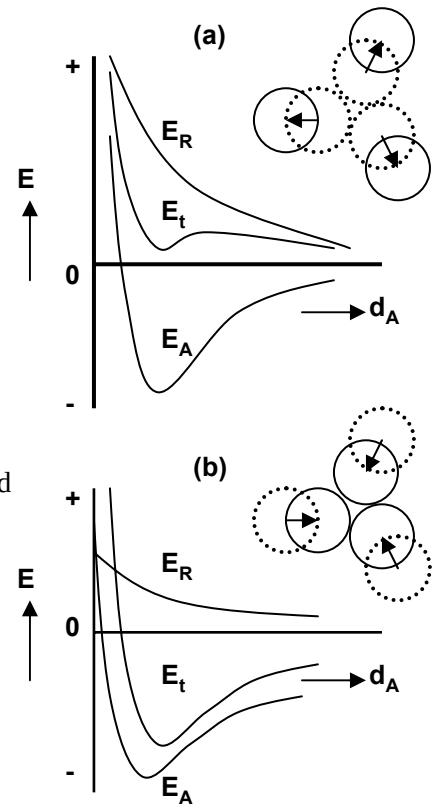

Fig. 5: Potential energy of particle-particle interaction (E_t) calculated as the sum of the electrostatic repulsive energy (E_R) and the van der Waals attractive energy (E_A) (Eqs. 7 and 8): (a) $E_R > E_A$: particle repulsion and colloid stabilization; (b) $E_A > E_R$: particle attraction and colloid agglomeration.

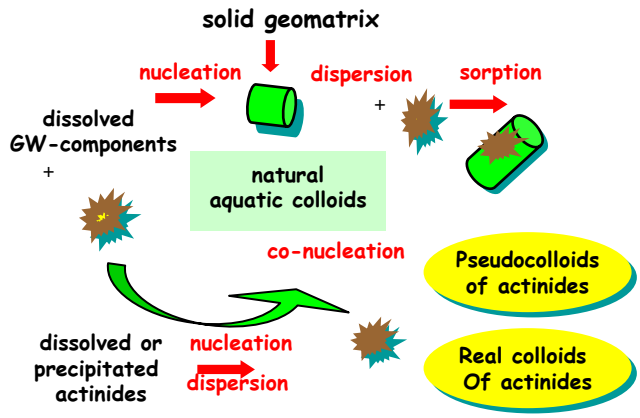

Fig. 6: General pathways for the transferation of actinides into the colloidal state by the formation of either real or pseudocolloids of actinides.

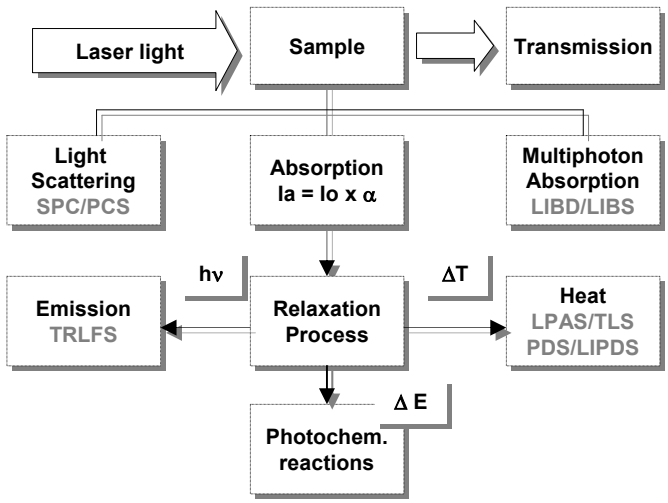

Fig. 7: Scheme of the basic principles of highly sensitive laser spectroscopic methods. Four categories are summarized as follows:

Photo-thermal spectroscopy
- LPAS: Laser-induced photo-acoustic spectroscopy
- LIPDS: Laser-induced photo-thermal displacement spectroscopy
- TLS: Thermal lensing spectroscopy
- PDS: Photo-thermal deflection spectroscopy

Luminescence spectroscopy
- TRLFS: Time-resolved laser fluorescence spectroscopy

Light scattering
- SPC: Single particle counting
- PCS: Photon correlation spectroscopy

Plasma generation
- LIBD: Laser-induced breakdown detection
- LIBS: Laser-induced breakdown spectroscopy

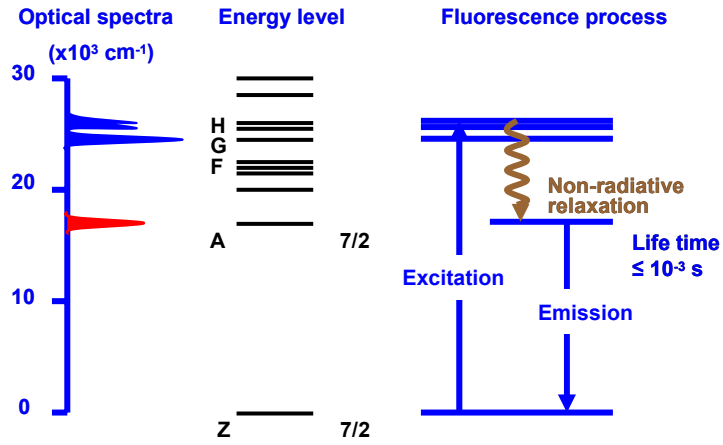

Fig. 8: TRLFS is based on the measurement of radiative relaxation of a light induced state e.g. of Cm(III).

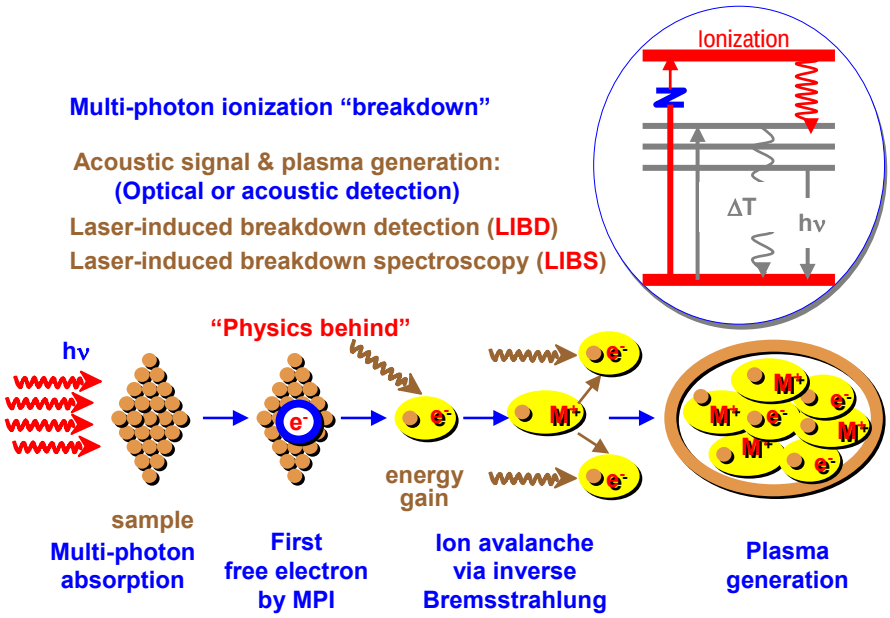

Fig. 9: Plasma generation of colloidal particles followed by plasma relaxation and ion-electron recombination accompanied by emission of white light (LIBD) and followed by atomic light emission of discrete wavelengths (LIBS).

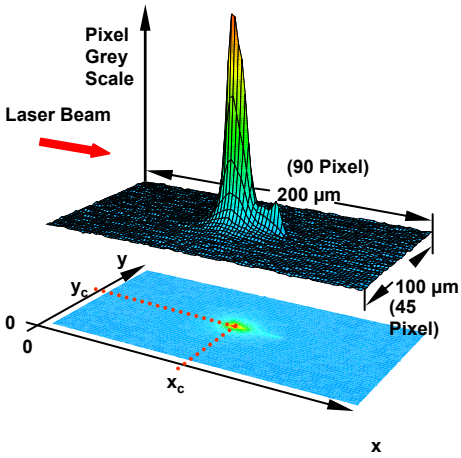

Fig. 10: A plasma light intensity contour of a single particle breakdown event (ø = 19 nm).

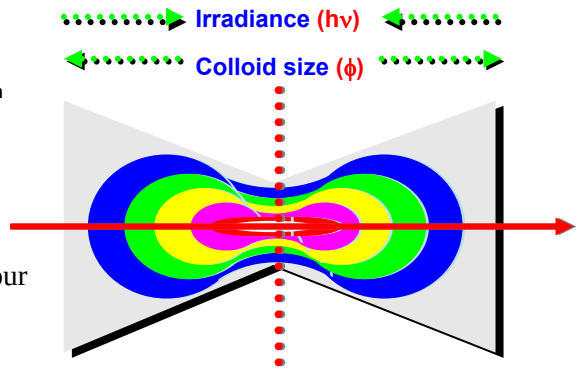

Fig. 11: Breakdown plasma generation in the laser beam focus area.

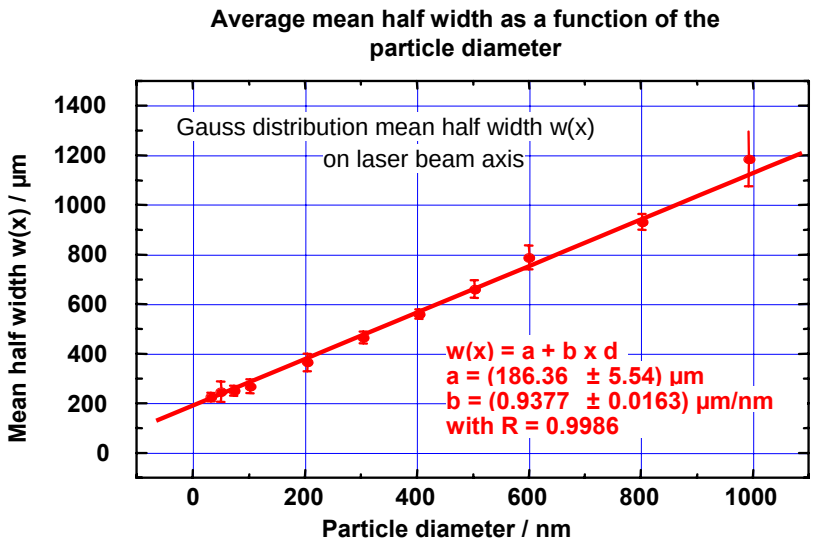

Fig. 12: LIBD particle size calibration with polystyrene reference particles.

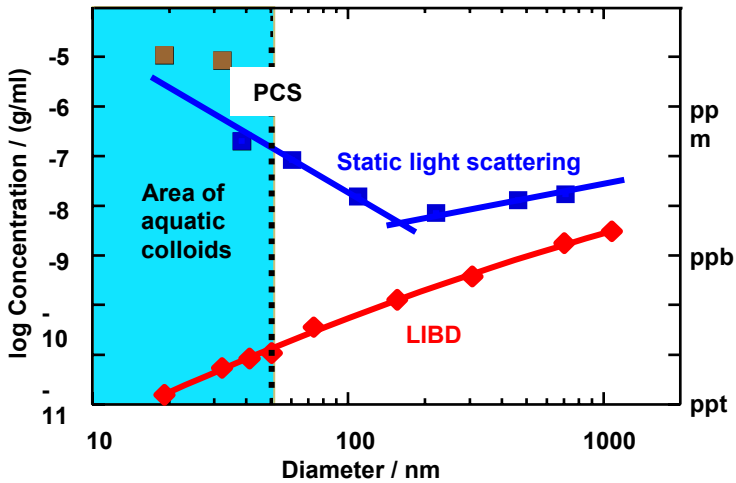

Fig. 13: The LIBD sensitivity: 10^4 – 10^7 times superior to light scattering methods. for aquatic colloids < 50 nm

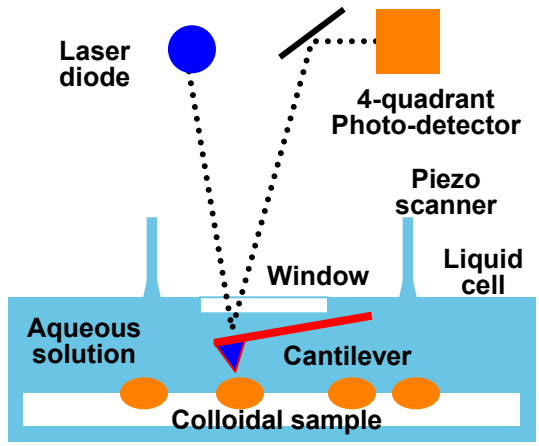

Fig. 14: Non-contact-mode atomic force microscopy (AFM) in aqueous solution with a laser-optical tip-sample distance control.

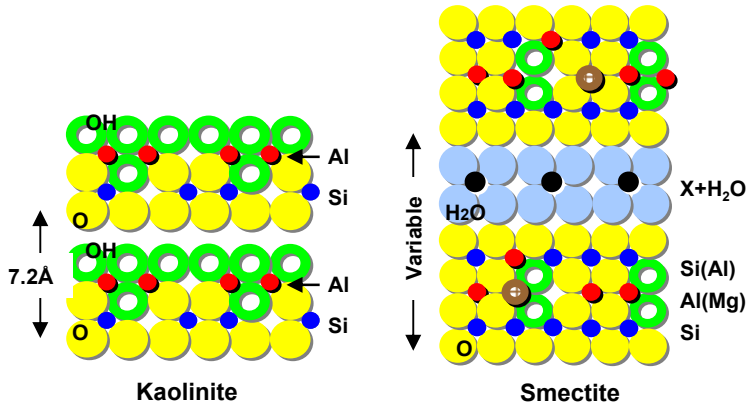

Fig. 15: Types of clay minerals based on the number and the sequence of tetrahadral (Si) and octahedral (Al) sheets: [TO]-kaolinite type; [TOT]-smectite type.

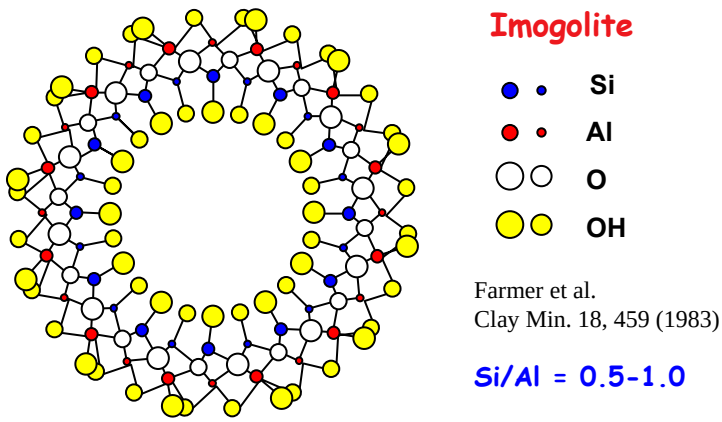

Fig. 16: Structure of imogolite (hydroxy-aluminosilicate or HAS) [53].

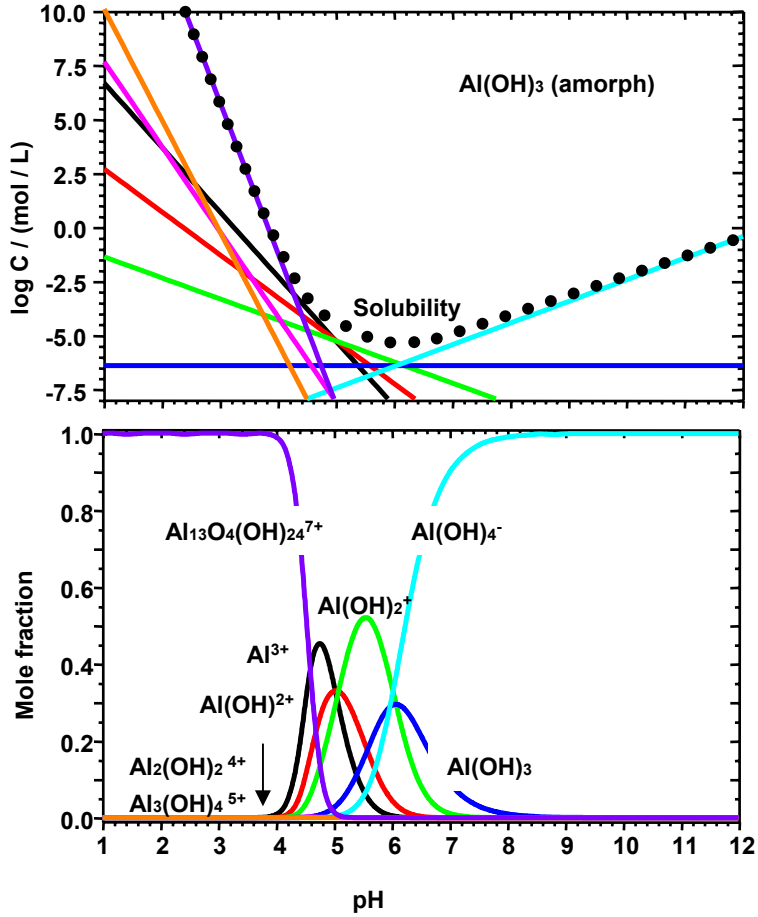

Fig. 17: Solubility of Al-hydroxide calculated by the data in refs [32-39] (upper part): Al species distribution as a function of pH (lower part).

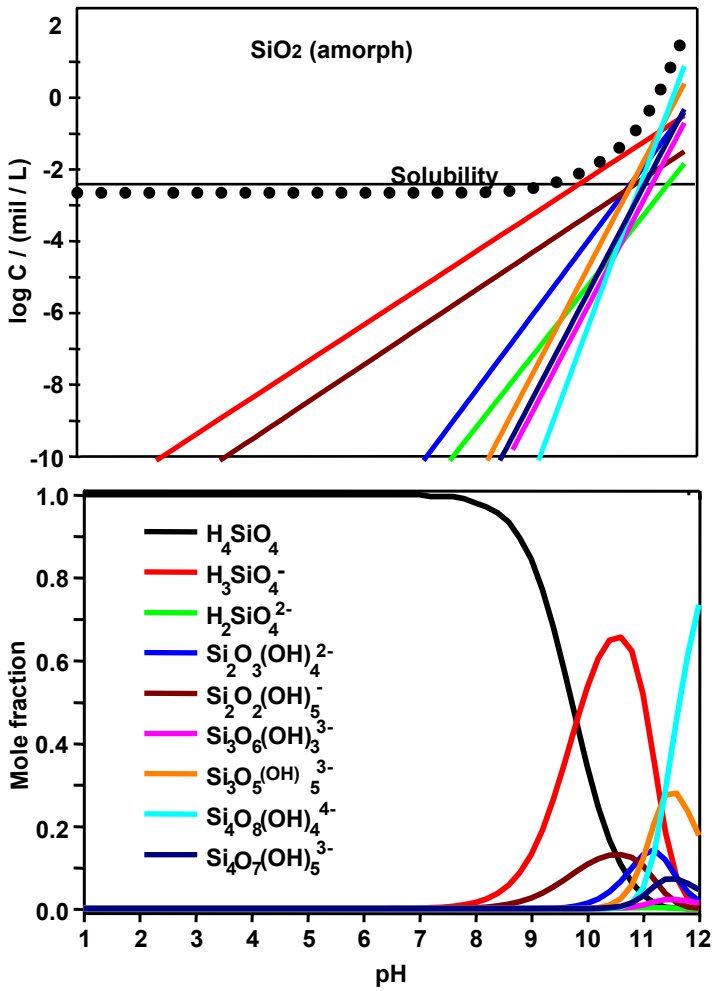

Fig. 18: Solubility of silica (amorph) calculated from the data in refs [32-39] (upper part); Si species distribution as a function of pH (lower part).

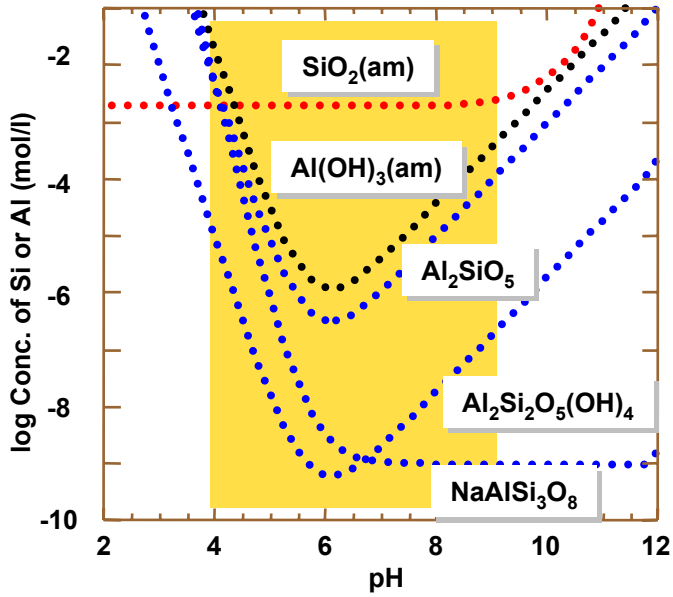

Fig. 19: Thermodynamic solubility of amorphous SiO_2, $Al(OH)_3$ and of some aluminosilicates calculated based on the available data in refs [32-39]: Al_2SiO_5 for sillimanite, $Al_2Si_2O_5(OH)_4$ for kaolinite and $NaAlSi_3O_8$ for low albite; the selected parameter screening area for aluminosilicate colloid formation is Indicated as coloured zone. Selection is made for the highest an lowest solubility of aluminosilicates.

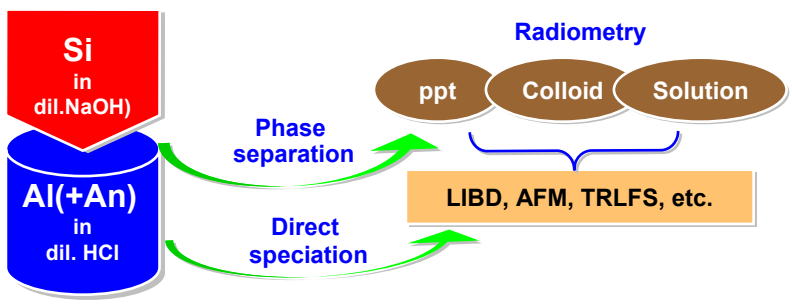

Fig. 20: Experiment of the parameter screening for the HAS colloid formation in the presence of Am(III) or Th(IV) by varying the individual element concentration and pH.

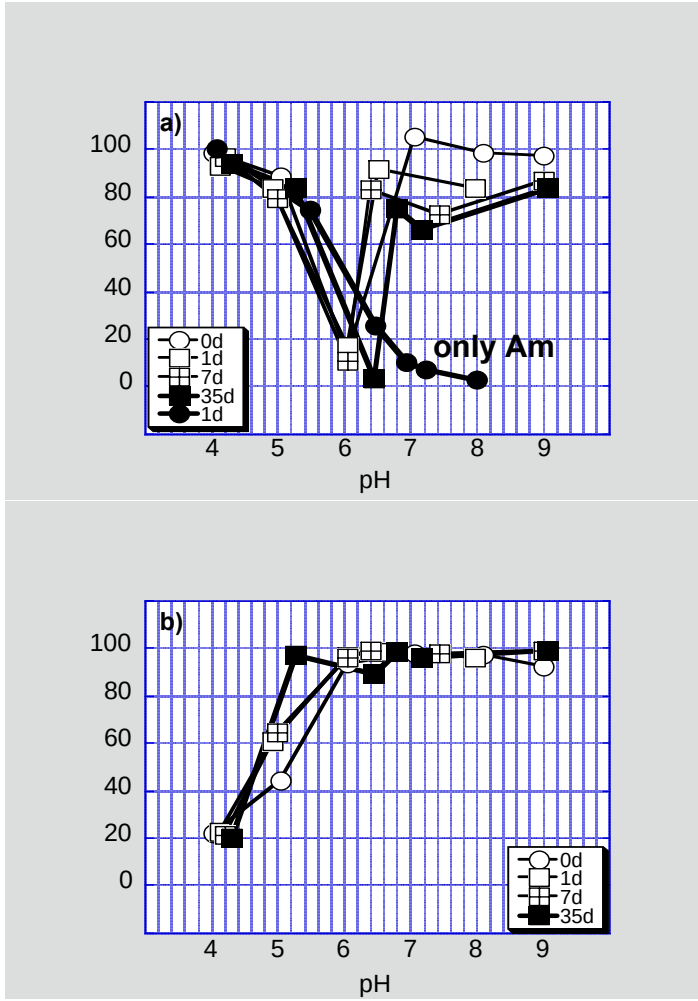

Fig. 21: The Am fraction in the filtrate from a 450 nm pore size filter as a function of pH (a) (normalized to the initial Am concentration); the colloid-borne Am fraction in the same filtrate (b). The sample solution is a mixture of 10^{-3} mol l^{-1} Si, 10^{-5} mol l^{-1} Al and 4.9x 10^{-8} mol l^{-1} Am, which is conditioned at different time. For comparison, the pure Am solution of 4.9x 10^{-8} mol l^{-1}, filtered at 450 nm pore size, is also shown for its fraction in solution.

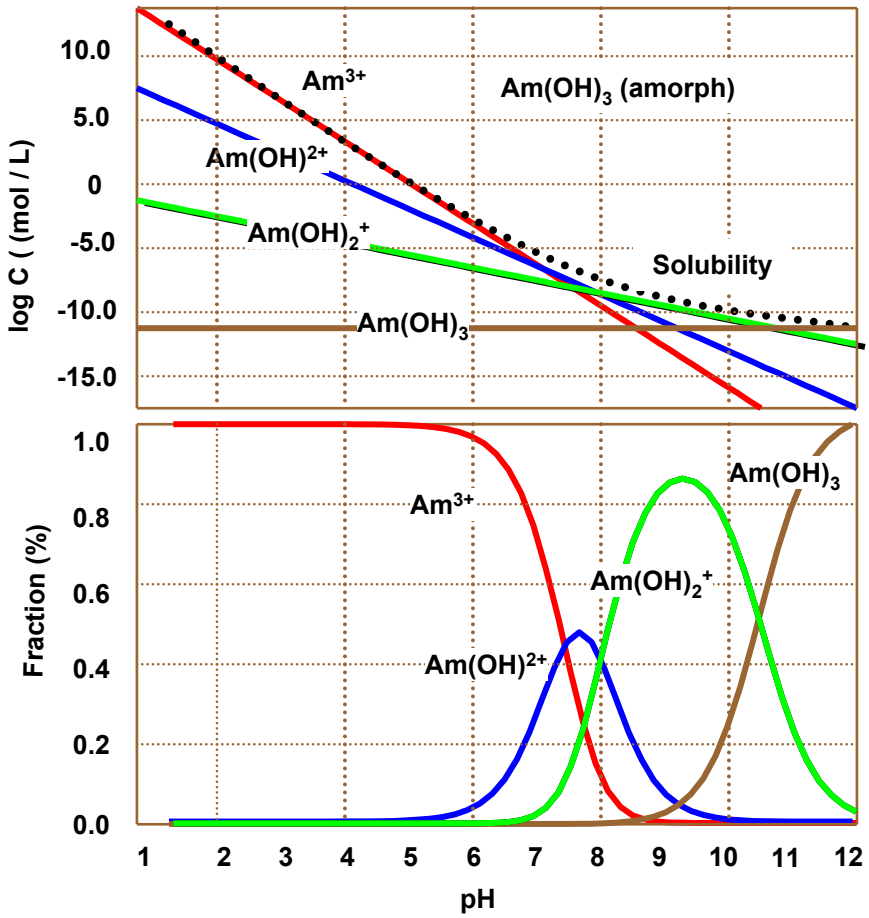

Fig. 22: Thermodynamic solubility and speciation of Am hydroxide calculated from the data in ref. [66]

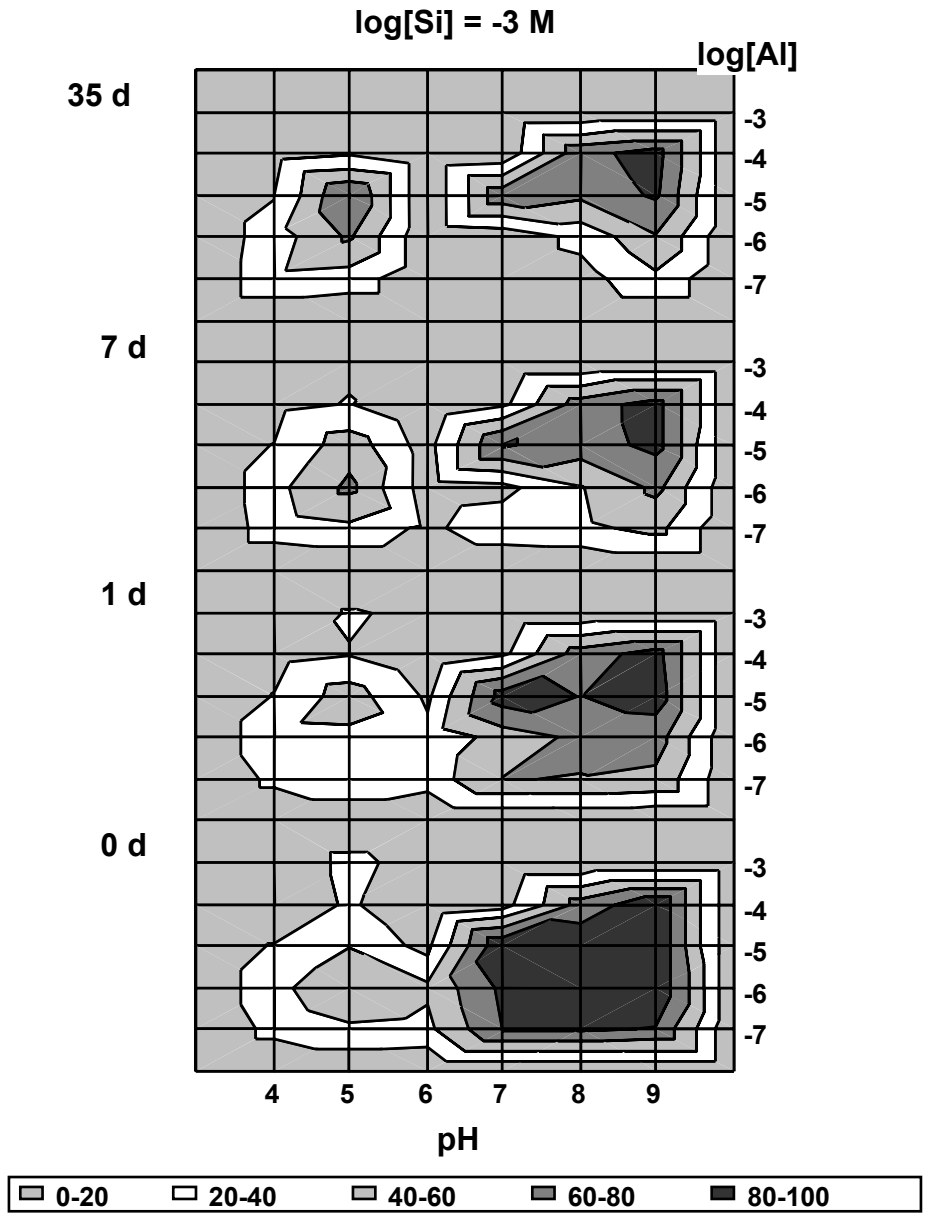

Fig. 23: Screening experimental results given as contour diagrams for the colloid-borne Am fraction (%) in mixture solutions of Al and Si. The Si concentration is maintained constant at 10^{-3} mol l^{-1}, while varying the Al concentration from 10^{-7} to 10^{-3} mol l^{-1} in the pH range 4-9.

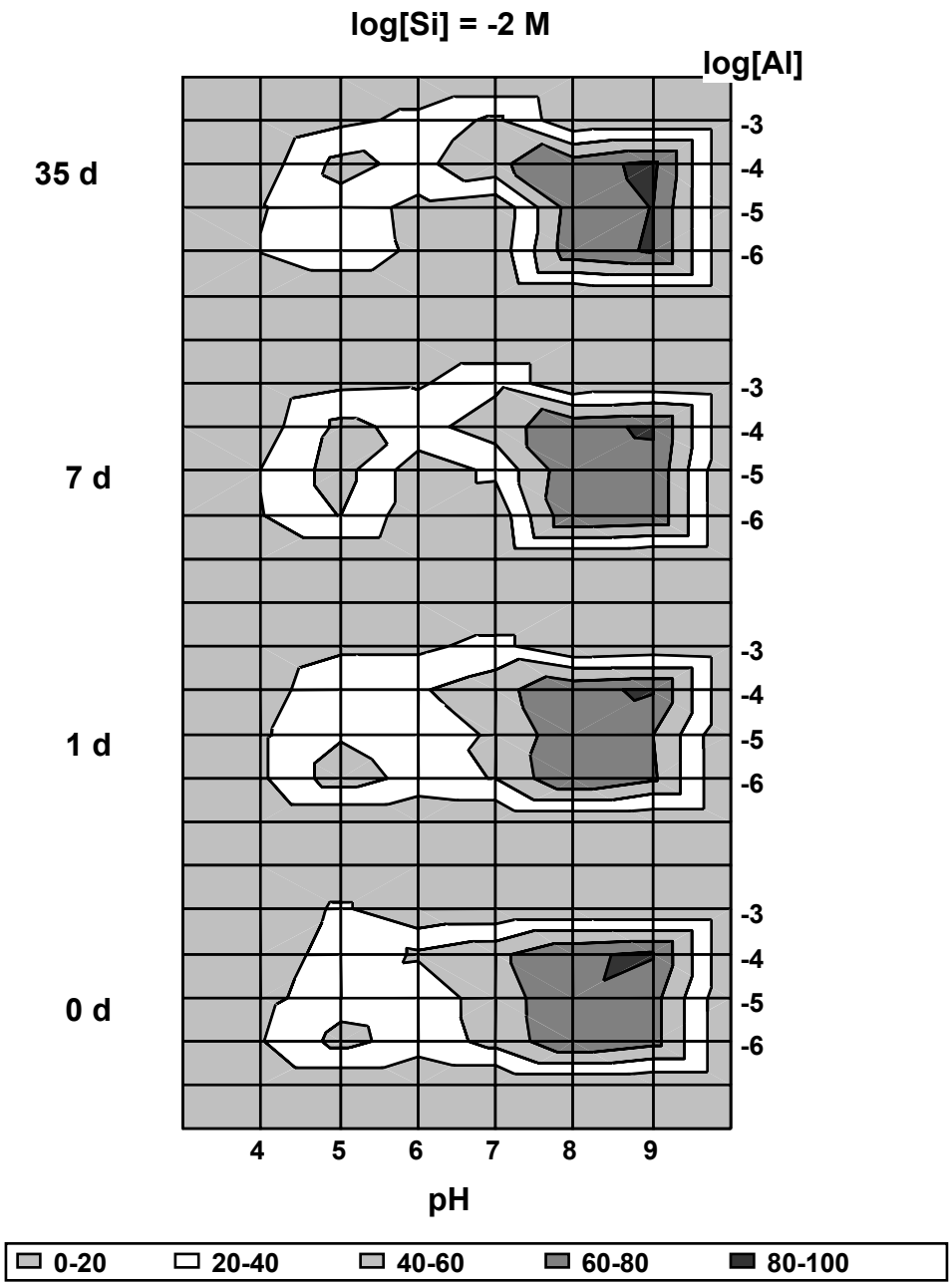

Fig. 24: Screening experimental results given as contour diagrams for the colloid-borne Am fraction (%) in mixture solutions of Al and Si. The Si concentration is maintained constant at 10^{-2} mol l^{-1}, while varying the Al concentration from 10^{-6} to 10^{-3} mol l^{-1} in the pH range 4-9.

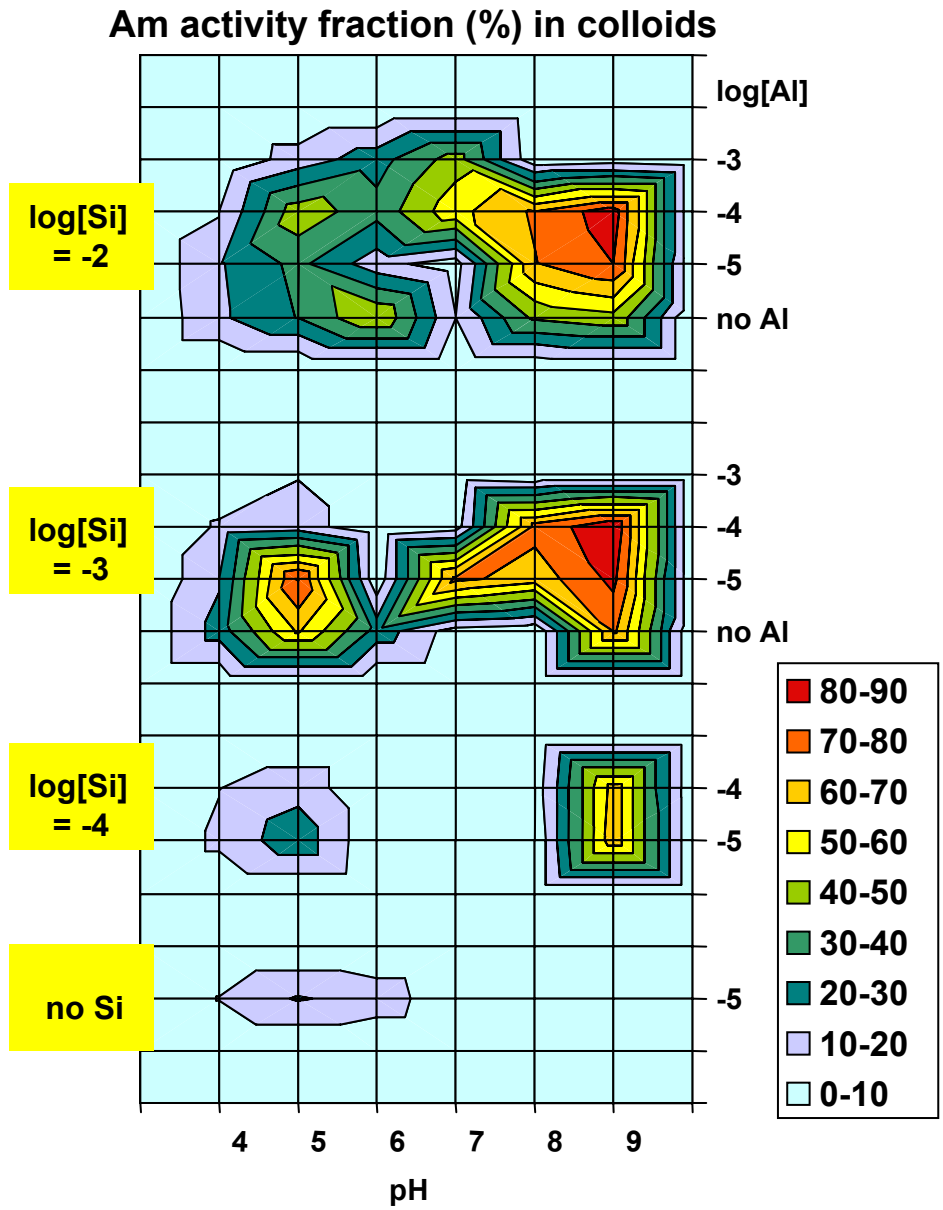

Fig. 25: A contour diagram of the colloid-borne Am fraction (z-axis) normalized to the initial Am concentration after 35 days of conditioning in different pH. Different Si and Al concentrations are indicated on the left and on the right y-axis, respectively.

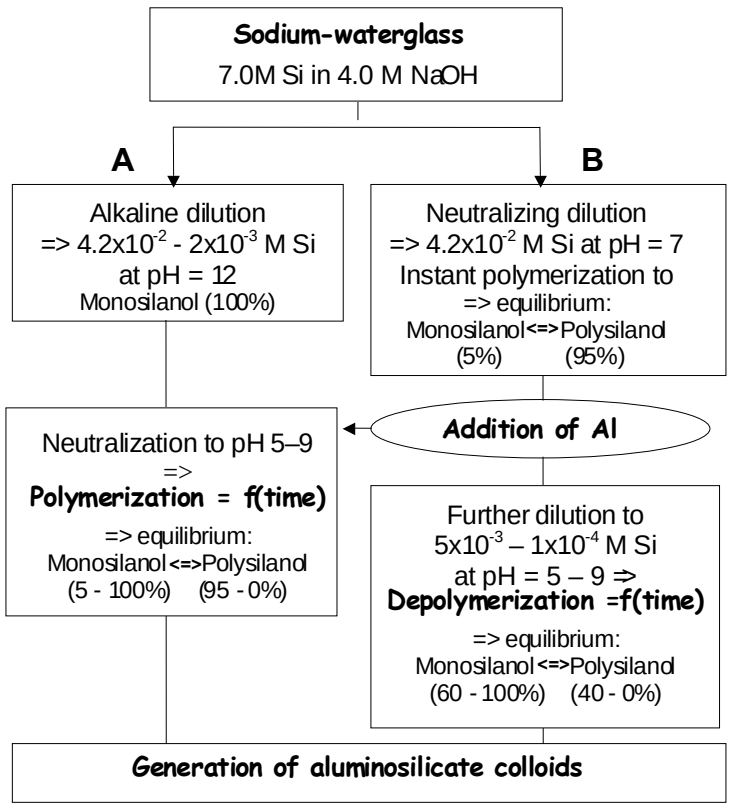

Fig. 26: Two experimental pathways for the generation of polysilanol and of hydroxy aluminosilicate (HAS) colloids from sodium-waterglass by (A): alkaline dilution and neutralization or (B): neutralization and dilution.

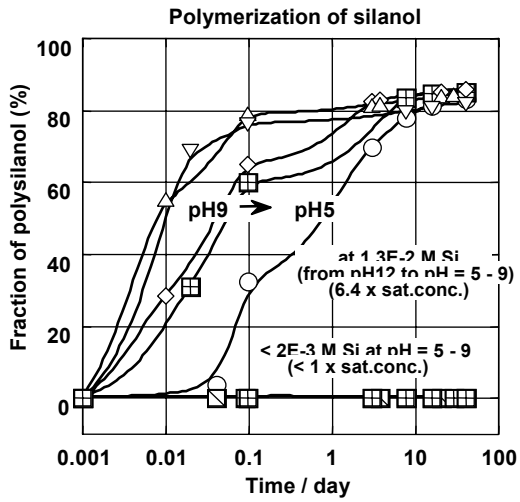

Fig. 27: The time dependent polymerization of silanol (silicic acid) at different pH for the Si concentration of $1.3x10^{-2}$ mol l^{-1} (6.4 times the saturation concentration of amorphous silica) (cf. approach A in Fig.26).

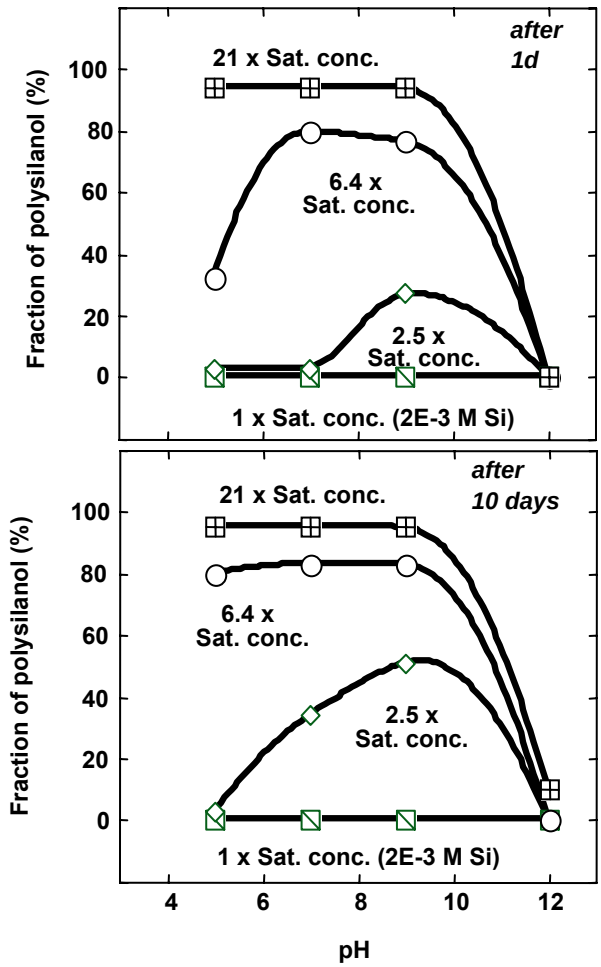

Fig. 28: The pH dependent polymerization of silanol at different initial concentrations after one day and 10 days of pH adjusting (the original solution at pH 12) (approach A in Fig.26)

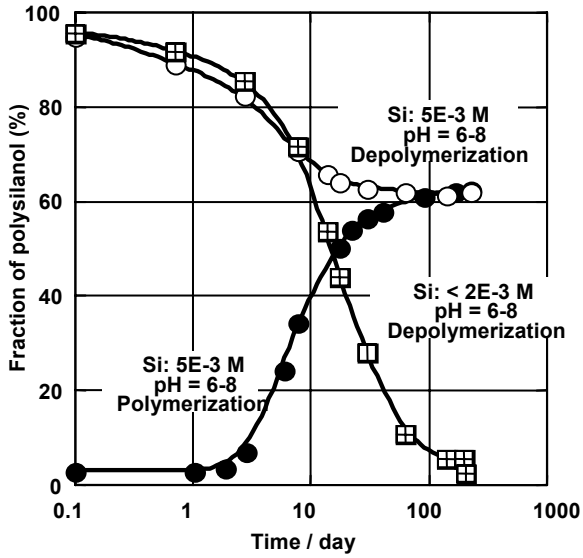

Fig. 29: Polymerization of silanol and depolymerization by dilution (approach A and B in Fig.25, respectively): an illustration of the reversibility under present experimental conditions.

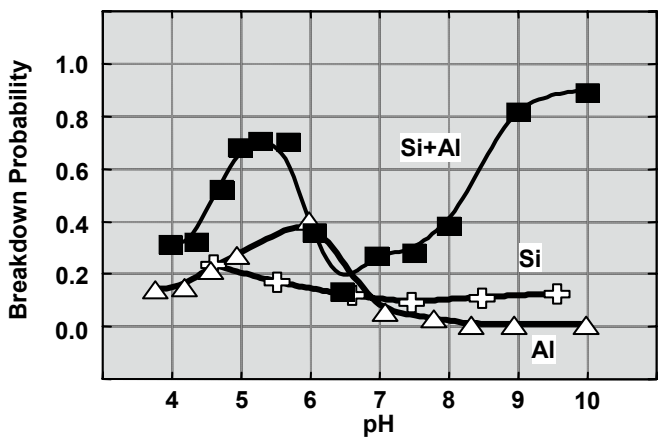

Fig. 30: Colloid generation observed by laser-induced breakdown detection (LIBD); (Si+Al): a titration of 10^{-5} mol l^{-1} Al in 0.03 M HCl with 10^{-3} mol l^{-1} Si in 0.03 M NaOH; (Si) and (Al): a titration of 0.03 M HCl with 10^{-3} mol l^{-1} Si in 0.03 M NaOH and of 10^{-3} mol l^{-1} Al in 0.03M HCl with 0.03 M NaOH

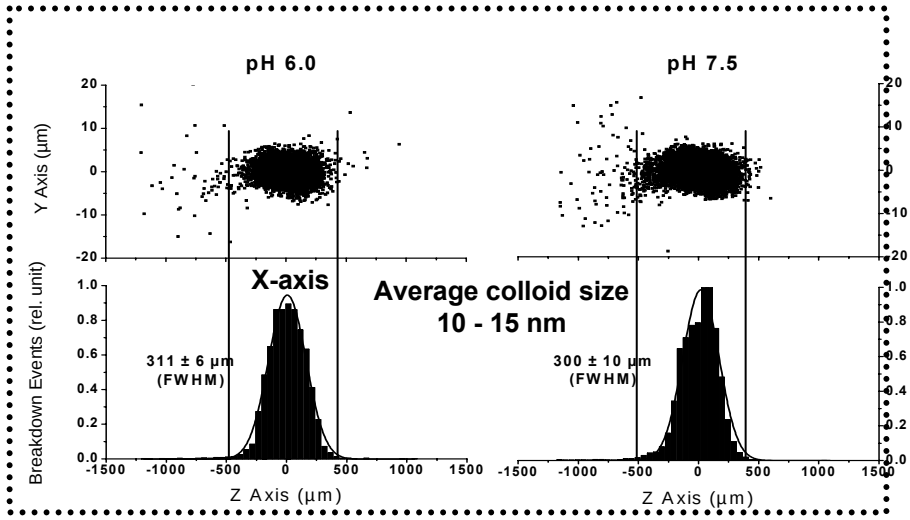

Fig. 31: LIBD experiment for the quantification of an average size of HAS colloids at pH 6.0 and 7.5: two-dimensional recordings of plasma light emission generated by breakdown of colloids within the laser beam focus volume (upper part) and statistical distribution of breakdown events on the z-axis. FWHM of breakdown event distribution is directly related to the average size of colloids of preponderance in solution.

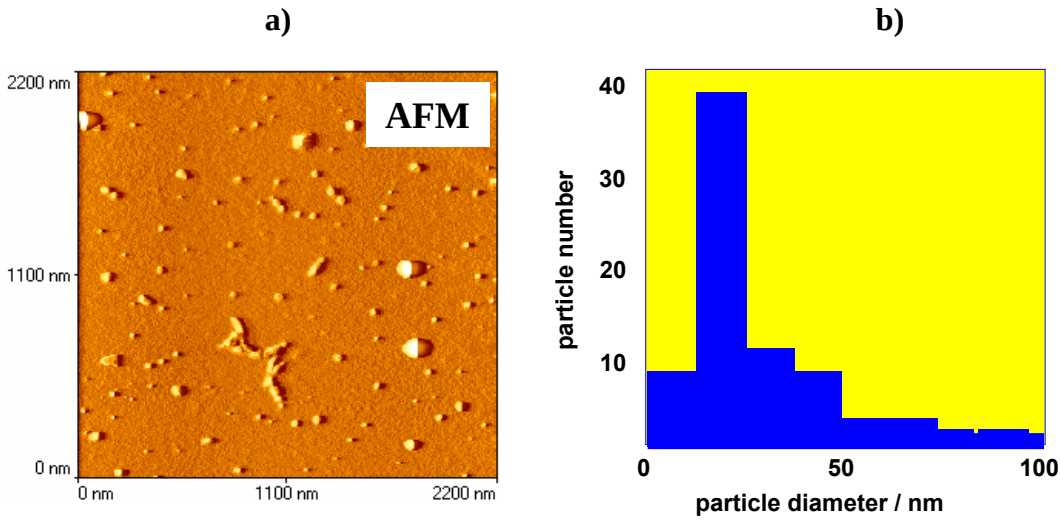

Fig. 32: Atomic force microscopic (AFM) characterization of colloids generated in a sample mixture of 10-3 mol l-1 Si and 10-4 mol l-1 Al at pH 7: (a) a non-contact mode AFM image of hydroxy aluminosilicate (HAS) colloids; (b) Size distribution of 70 particles (a mean particle diameter at about 27 nm and the maximal number at 19 nm).

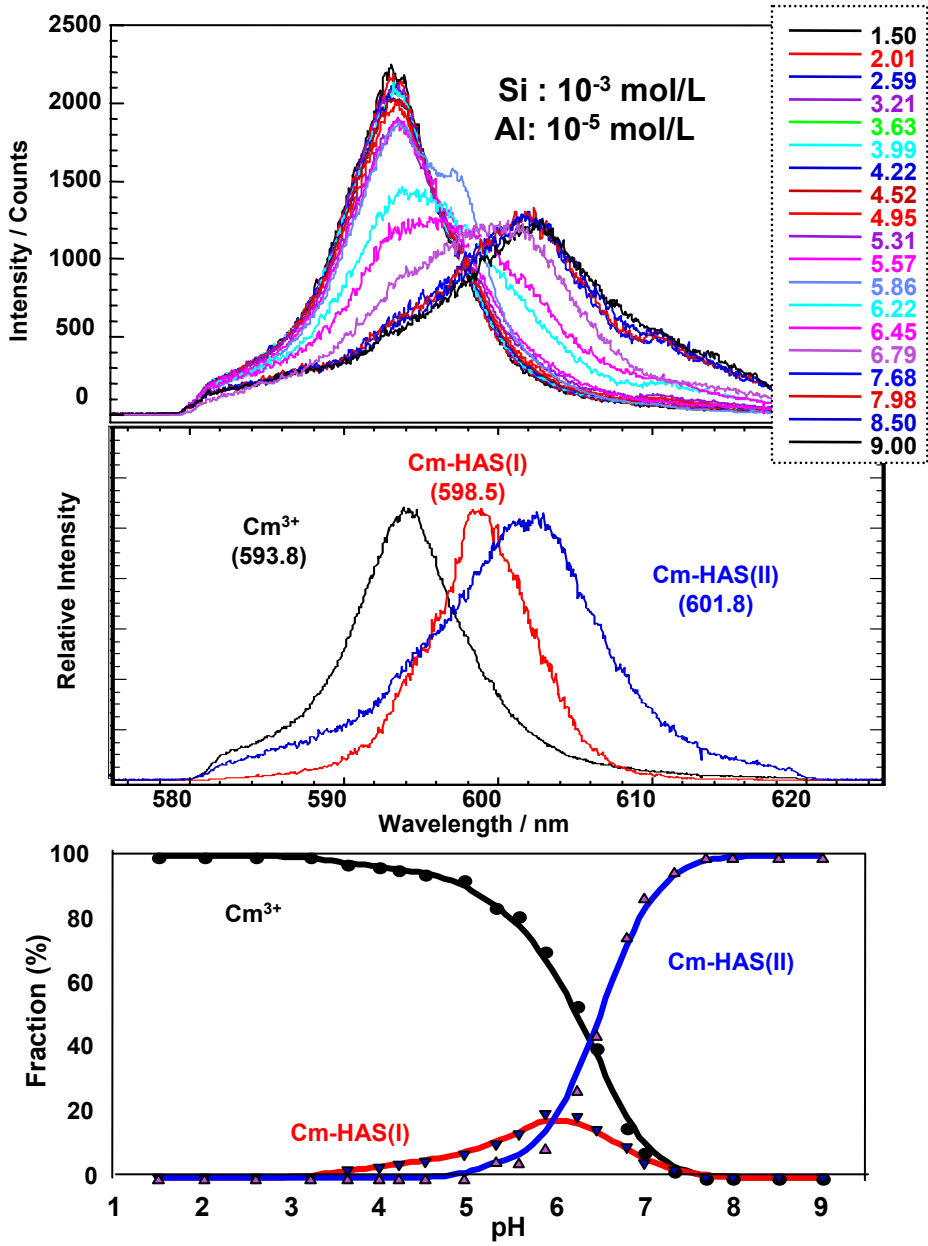

Fig. 33: Speciation of HAS colloid-borne Cm by TRLFS on the pH titration from 1 to 9 in a mixture solution containing 10^{-3} mol l^{-1} Si, 10^{-5} mol l^{-1} Al and 4.9×10^{-8} mol l^{-1} Cm: the pH dependent spectrum evolution (upper part) and the deconvoluted spectra of different Cm species present in the solution (middle part). The species distribution as a function of pH is illustrated in the lower part.

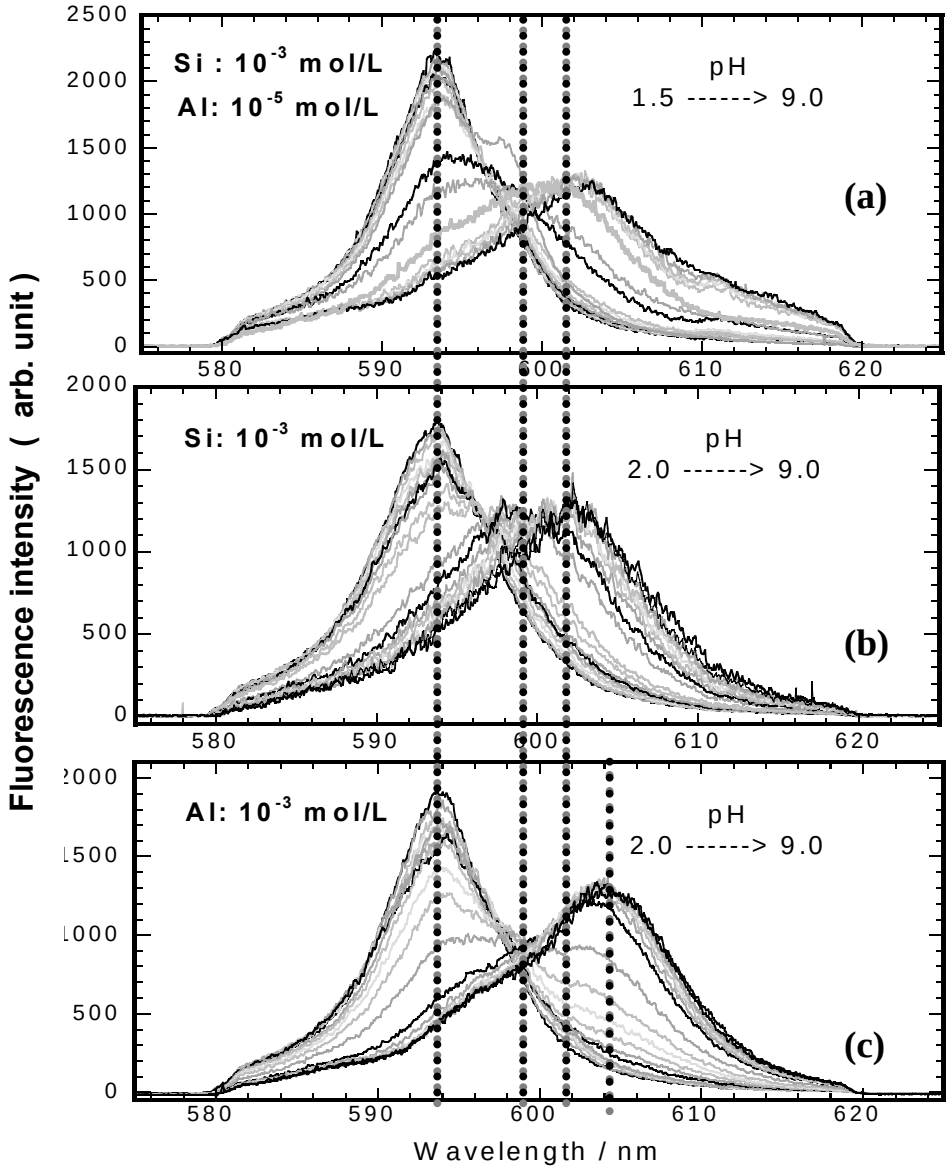

Fig. 34: Speciation of Cm by TRLFS in a mixture solution of 10^{-3} mol l^{-1} Si and 10^{-5} mol l^{-1} Al (a), in a pure Si solution of 10^{-3} mol l^{-1} (b) and in a pure Al solution of 10^{-3} mol l^{-1} (c). The solution pH is varied from 1.5 or 2.0 upwards to 9.0.

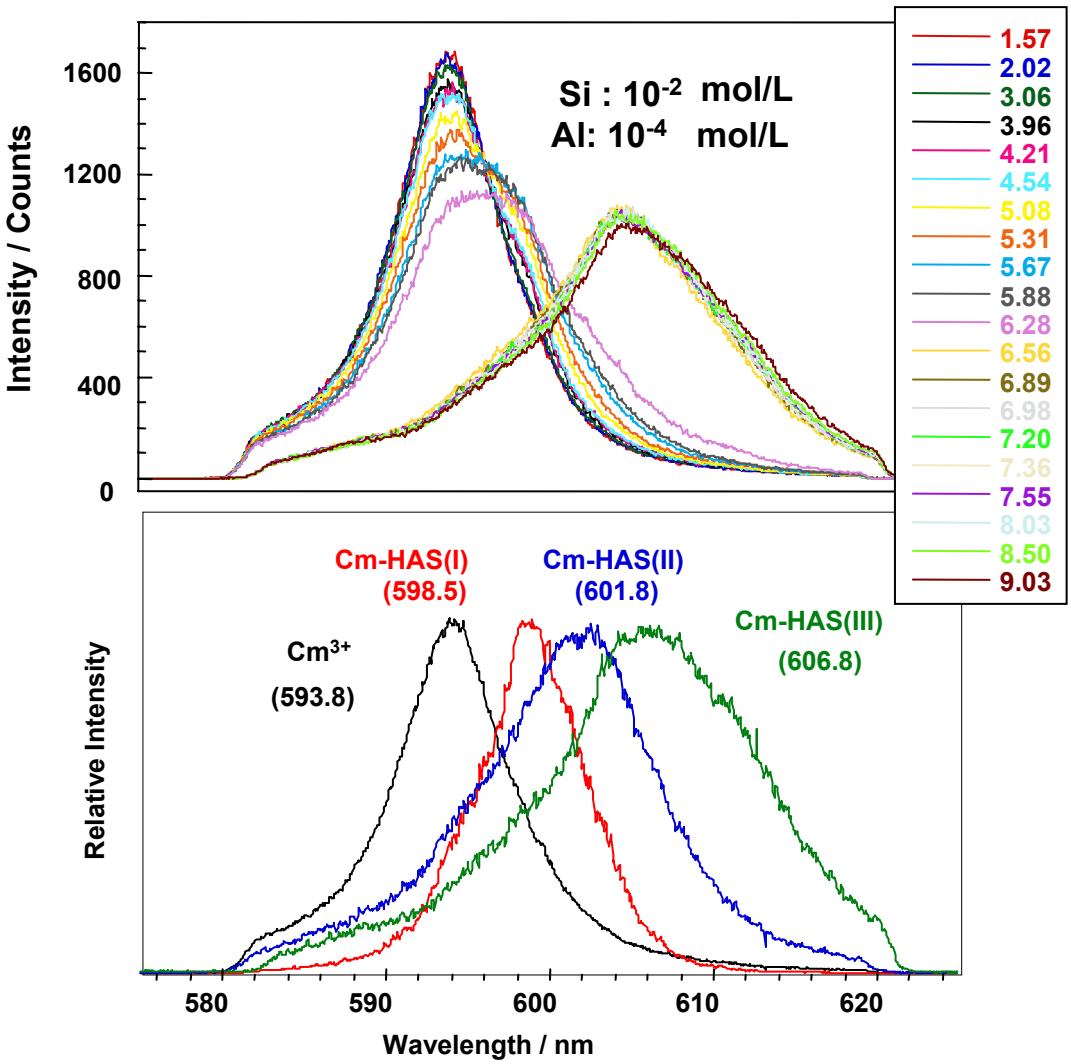

Fig. 35: Speciation of HAS colloid-borne Cm by TRLFS upon the pH titration from 1 to 9 in a mixture solution containing 10^{-2} mol l^{-1} Si, 10^{-4} mol l^{-1} Al and 4.9×10^{-8} mol l^{-1} Cm: the pH dependent spectrum evolution (upper part) and the deconvoluted spectra of different Cm species present in the solution (lower part).

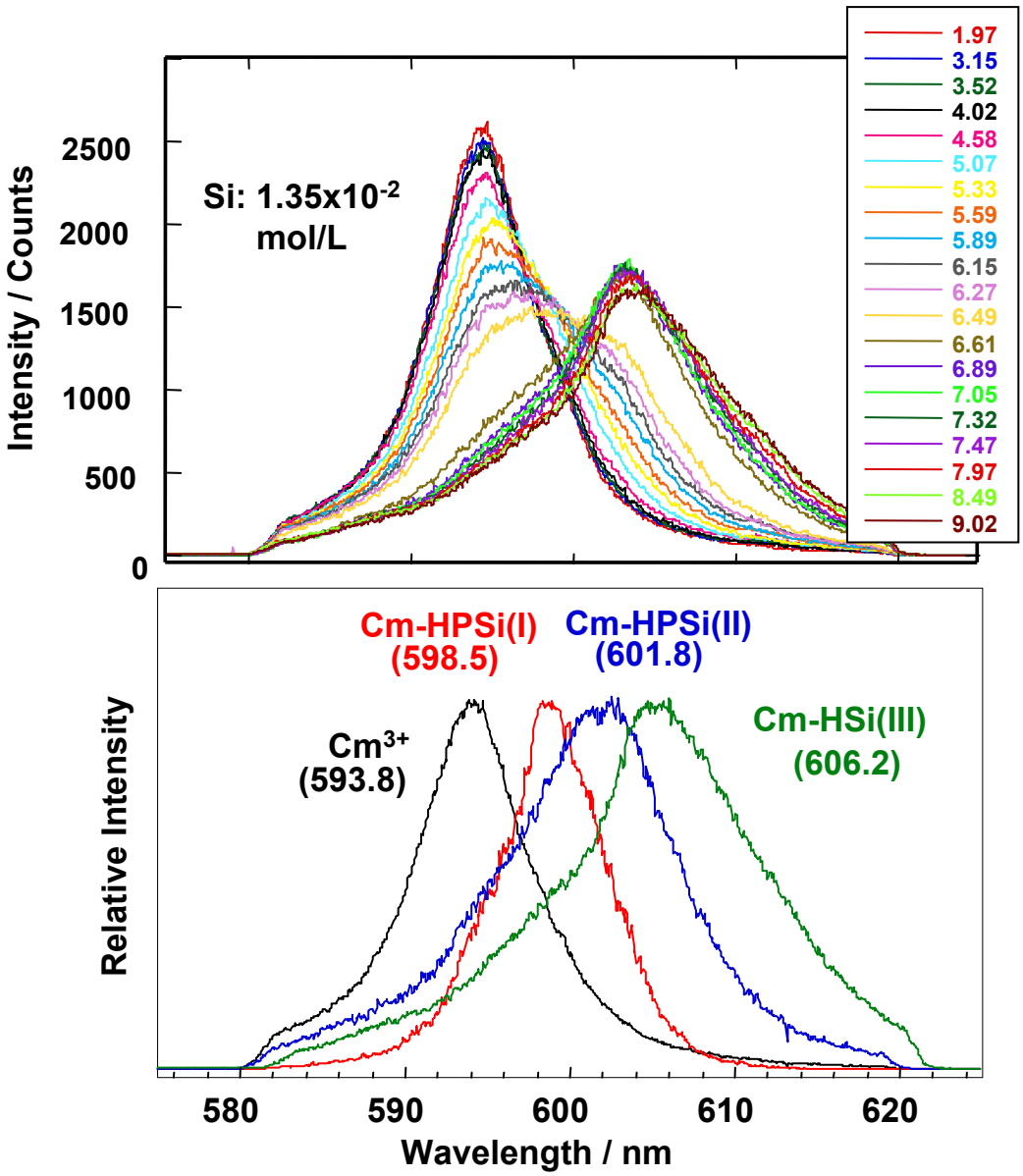

Fig.36: Speciation of Cm by TRLFS in a pure Si solution of 1.35×10^{-2} mol l^{-1}. The solution pH is varied from 2.0 upwards to 9.0: the pH dependent spectrum evolution (upper part) and the deconvoluted spectra of different Cm species (lower part).

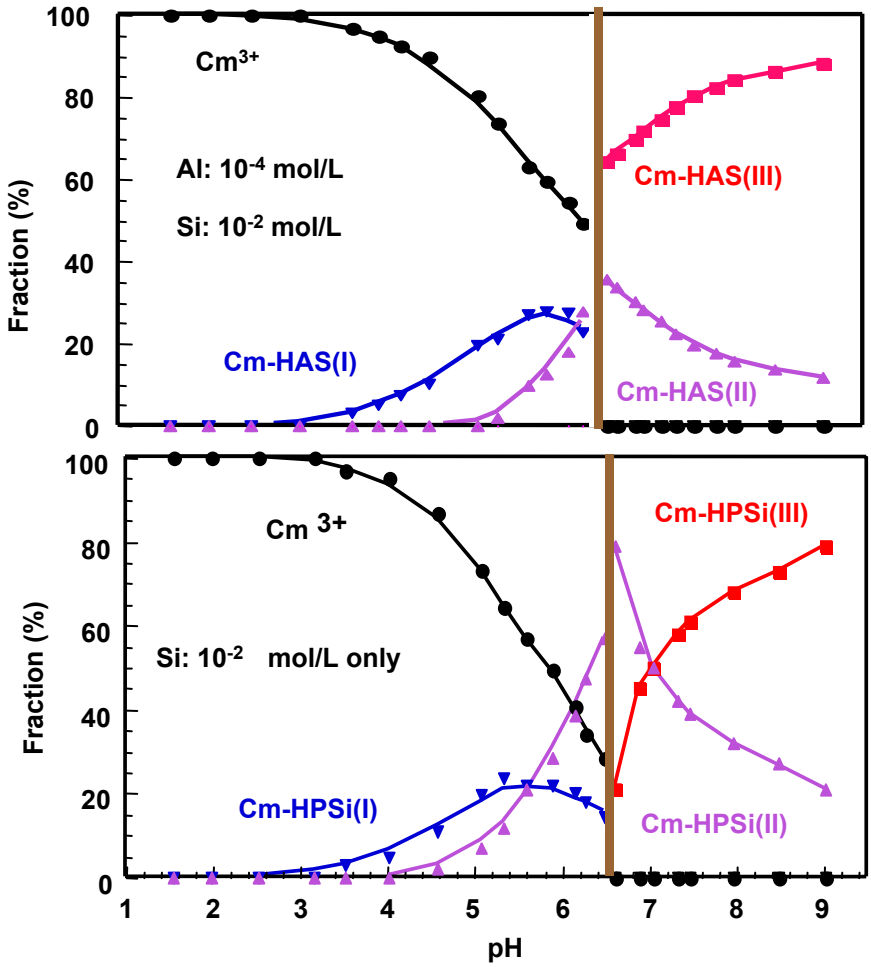

Fig. 37: The relative Cm species distribution as a function of pH in a mixture solution of 10^{-2} mol l^{-1} Si and 10^{-4} mol l^{-1} Al (upper part) and compared with that of a pure solution of 10^{-2} mol l^{-1} Si (lower part).

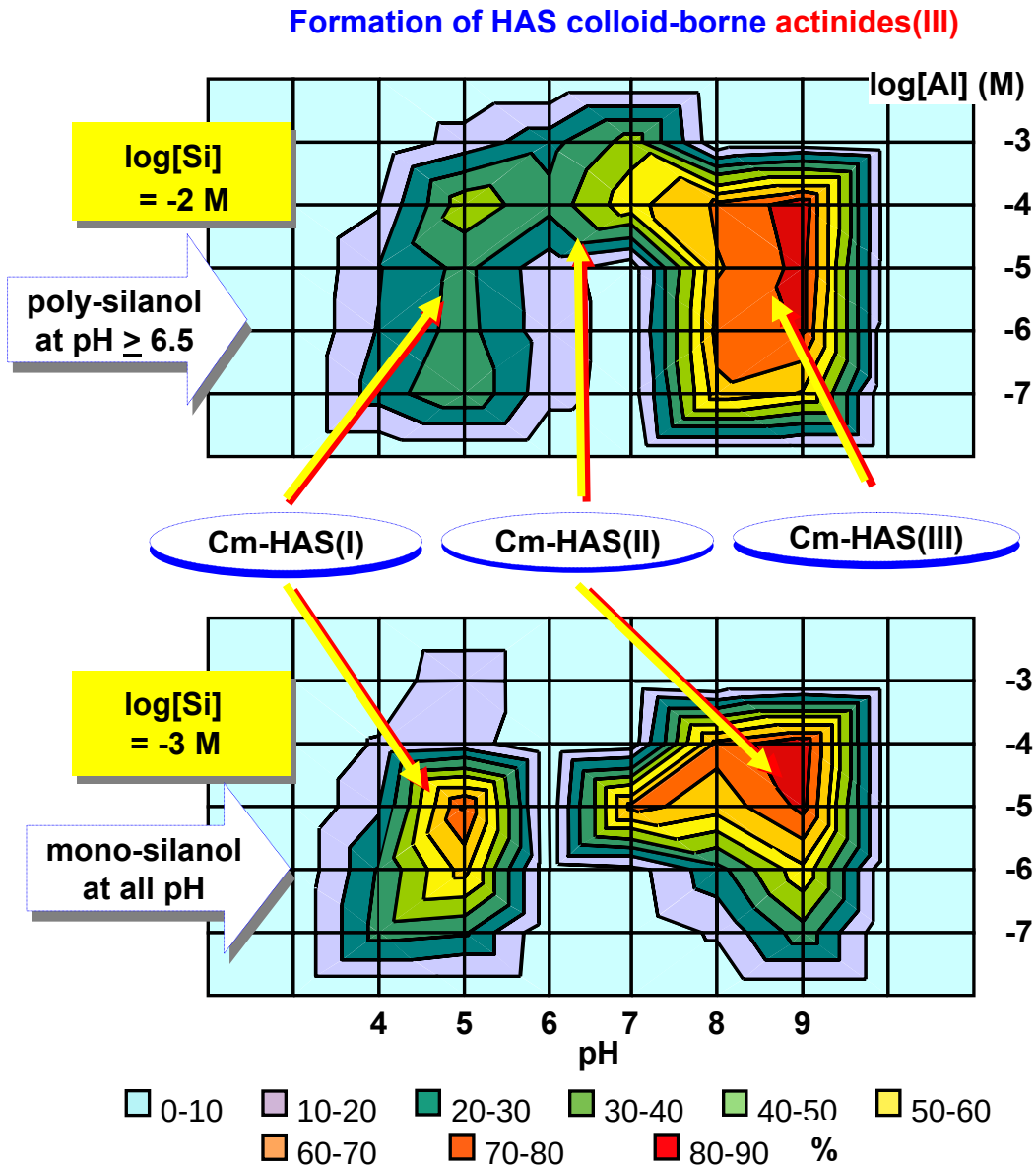

Fig. 38: : A contour diagram of the colloid-borne Am fraction (z-axis) normalized to the initial Am concentration after 35 days of conditioning in different pH. Different Si and Al concentrations are indicated on the left and on the right y-axis, respectively. The regions for the formation of different colloid-borne Cm(III) species, namely Cm-HAS(I) as a bidentate, Cm-HAS(II) as a tridendate, and Cm-HAS(III) as isomorphically substituted, are indicated by blue ellipses. The regions for the formation of different Si species, namely mono- and polysilanol are indicated by yellow arrows.

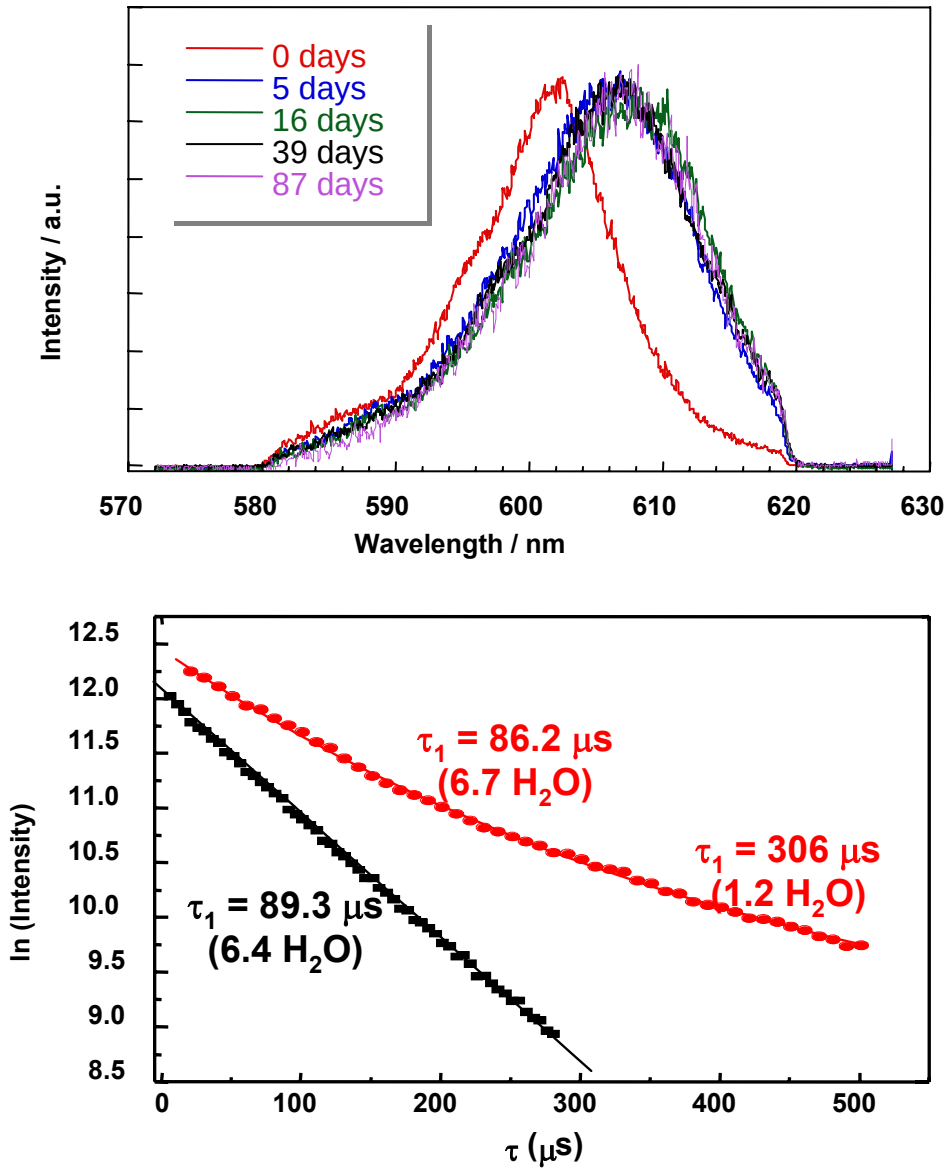

Fig. 39: Speciation of HAS colloid-borne Cm by TRLFS upon heating at 90°C from 5 up to 87 days of a mixture solution containing 10^{-3} mol l^{-1} Si, 10^{-4} mol l^{-1} Al and $5.0x10^{-8}$ mol l^{-1} cm: The time dependent spectrum evolution (upper part) and the fluorescence life times (lower part) before and after heating the sample.

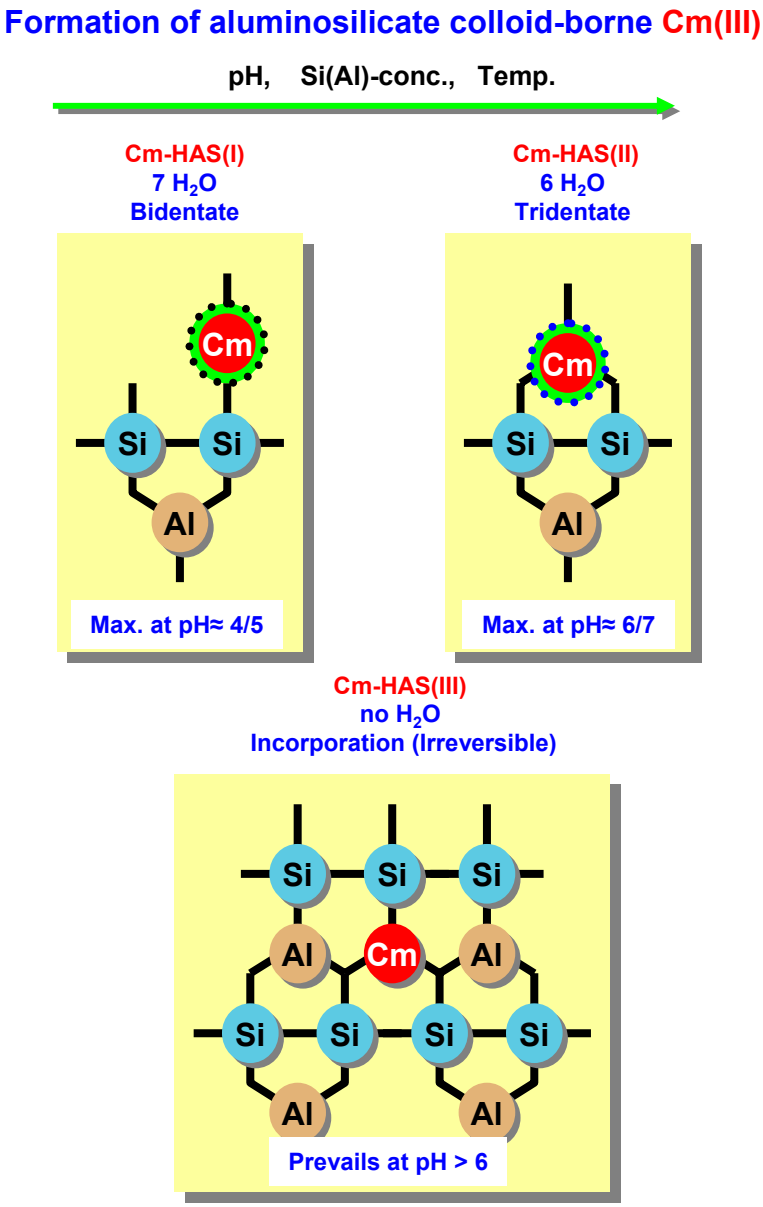

Fig.40: Illustrative overview for the formation of three colloid-borne Cm species.

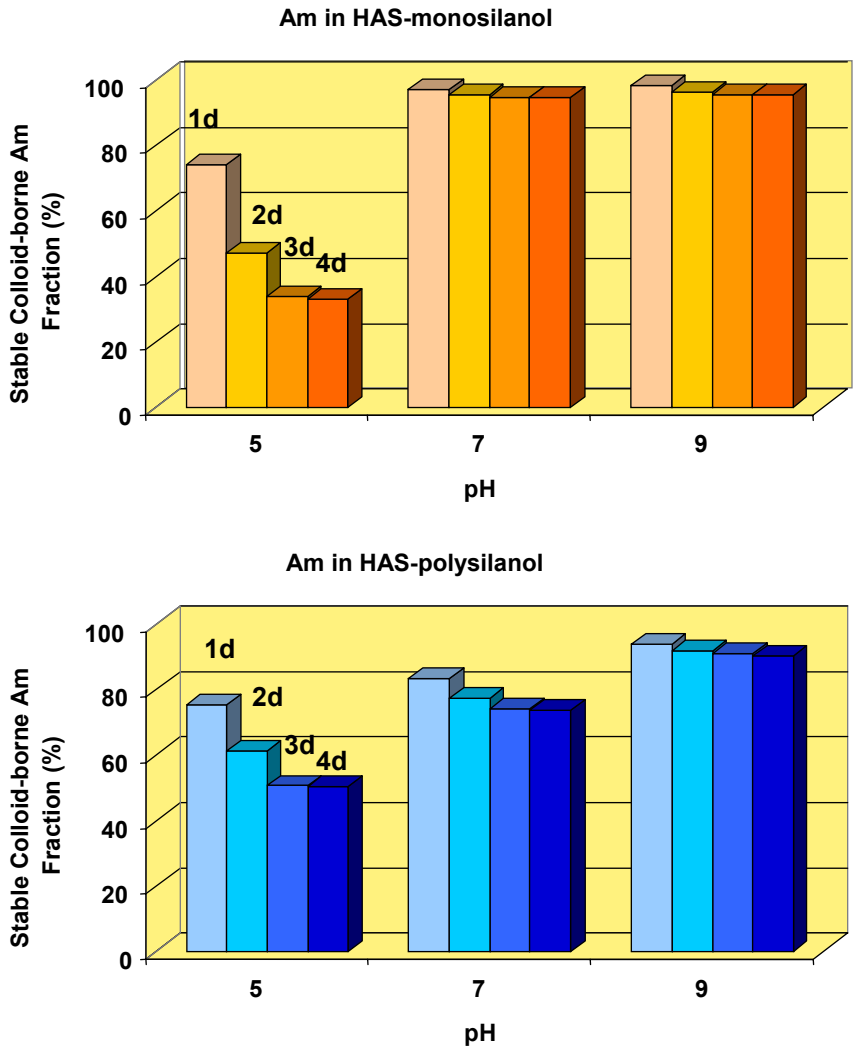

Fig.41: Colloid-borne Am fraction (%) in a sample after the desorption experiment. The initial sample is prepared at different pH with 10^{-3} mol l^{-1} Si, 10^{-5} mol l^{-1} Al and $5x10^{-8}$ mol l^{-1} Am (upper part) and 10^{-2} mol l^{-1} Si, 10^{-4} mol l^{-1} Al and $5x10^{-8}$ mol l^{-1} Am (lower part) and conditioned for 7 days prior to desorption experiment.

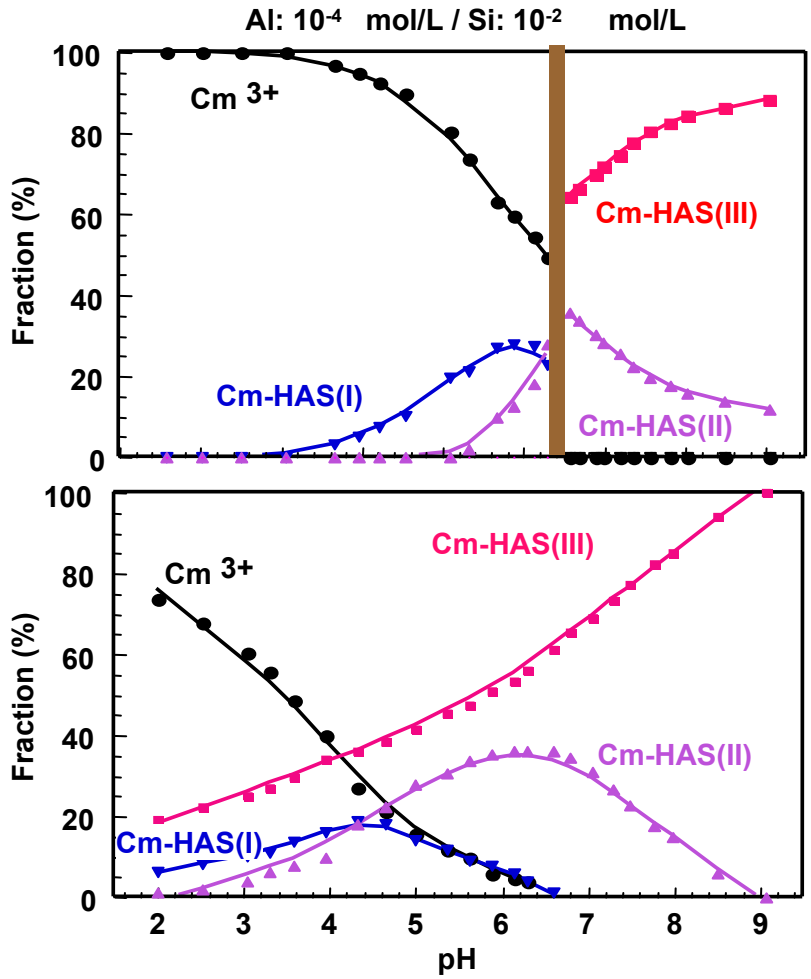

Fig. 42: The relative Cm species distribution upon pH titration from 9 to 2 (inverse titration) (lower part) and from 2 to 9 (upper part) in a mixture solution containing 1.3×10^{-2} mol l^{-1} Si, 10^{-4} mol l^{-1} Al and 4.9×10^{-8} mol l^{-1} Cm.

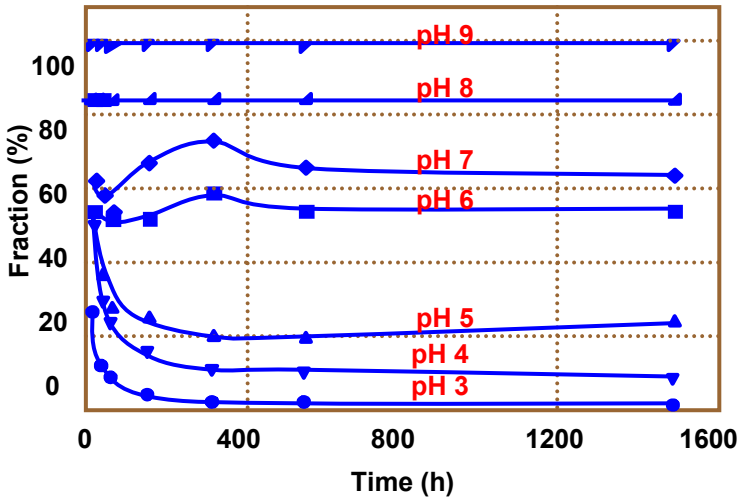

Fig. 43: Stability of the HAS colloid-borne Cm: Cm-HAS(III) as a function of time at different pH (cf. Fig.42).

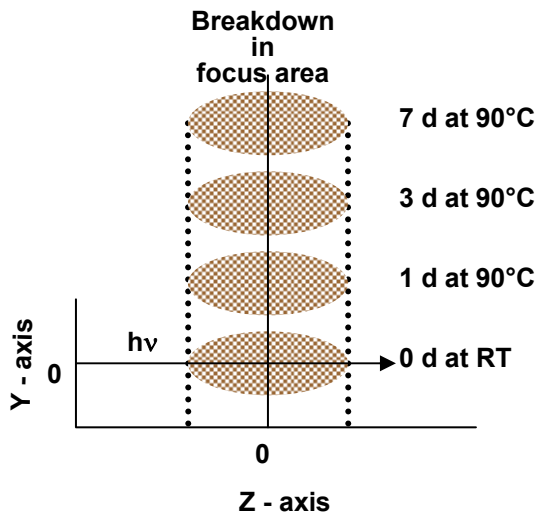

Fig. 44: LIBD experiment for the quantification of an average size of HAS colloids at pH 7.5 after heating to 90°C for different periods of time: two-dimensional recordings of plasma light emission generated by breakdown of colloids within the laser beam focus volume on which basis the average size of colloids of preponderance in solution can be estimated. The average size remains unchanged with time.

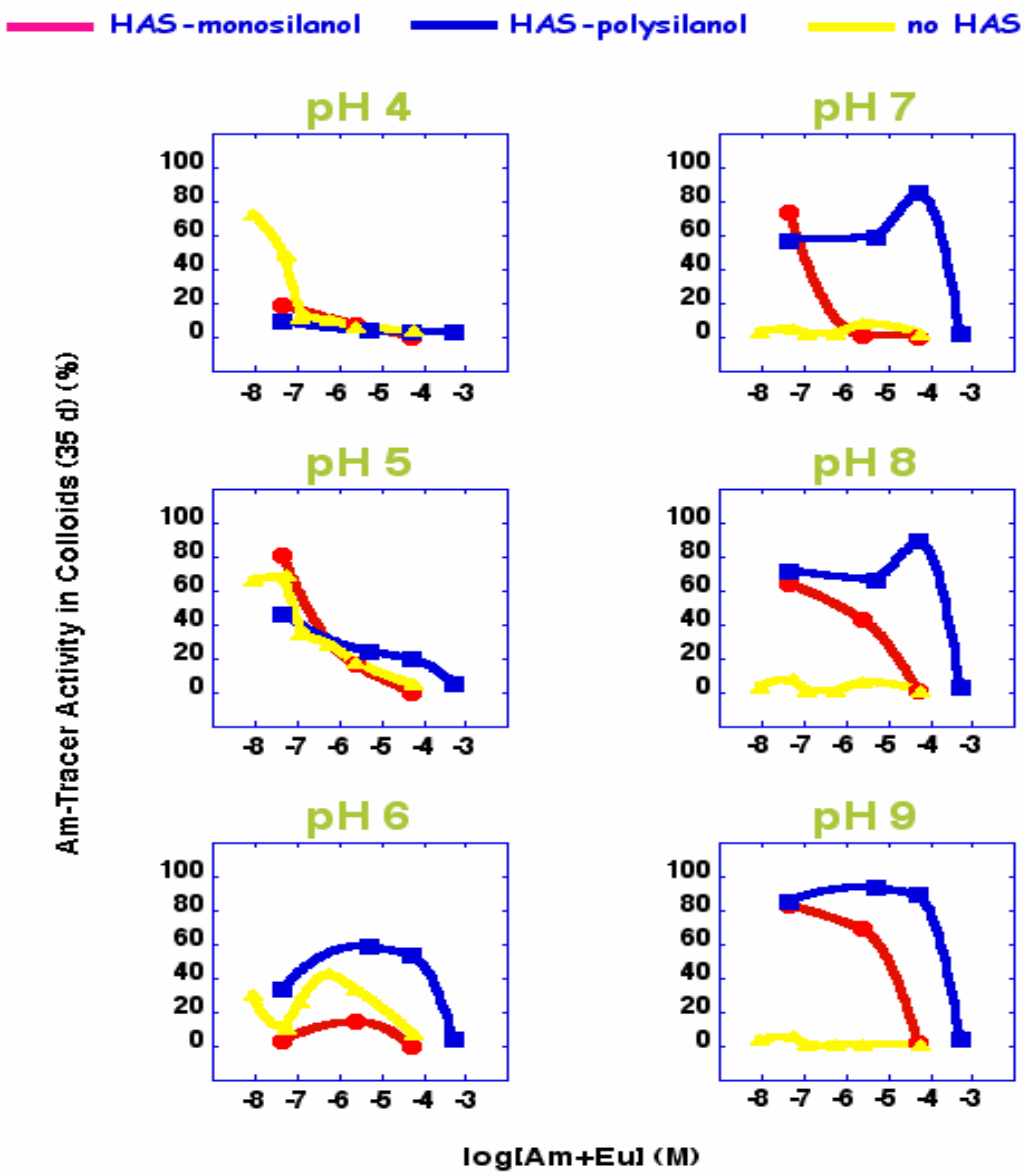

Fig. 45: Colloid-borne Am-activity fraction (%) as a function of the (Am+Eu)-concentration for different pH´s in three series of samples indicated as HAS-monosilanol, HAS-polysilanol and no HAS, respectively, and containing mixture solutions of:
(1): 10^{-3} mol l^{-1} Si, 10^{-5} mol l^{-1} Al, $5x10^{-8}$ mol l^{-1} Am, varied concentration of Eu;
(2): $1.3x10^{-2}$ mol l^{-1} Si, $1.5x10^{-4}$ mol l^{-1} Al, $5x10^{-8}$ mol l^{-1} Am, varied concentration of Eu;
(3): $5x10^{-8}$ mol l^{-1} Am, varied concentration of Eu.

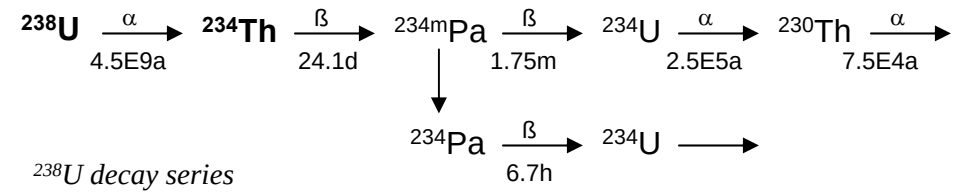

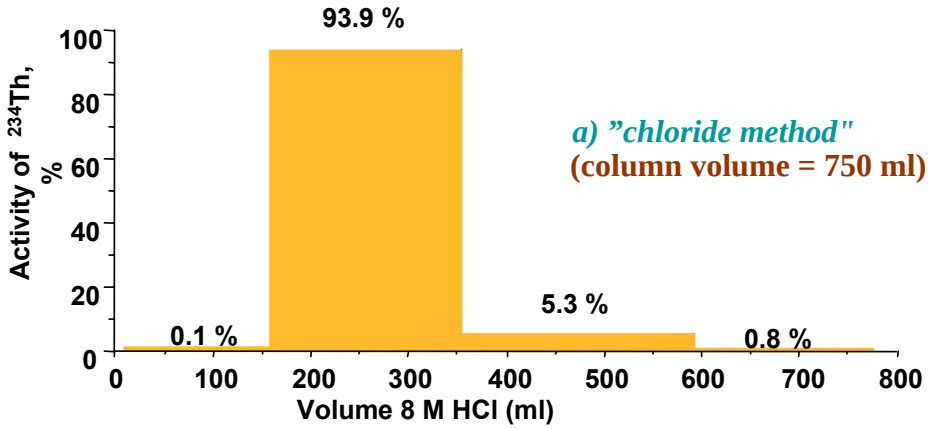

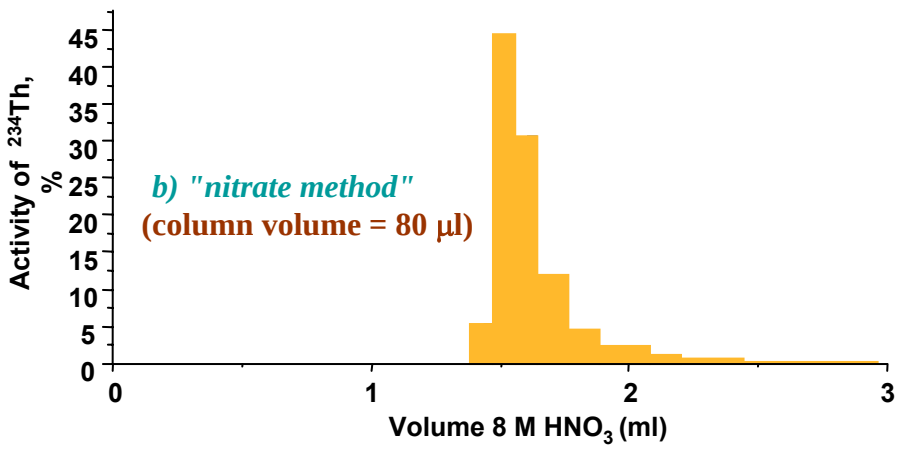

Fig. 46: Typical elution diagrams of 150 kBq 234Th at separation from 25 g uranylnitrate by chloride anion exchange (upper part) followed by nitrate anion exchange (lower part).

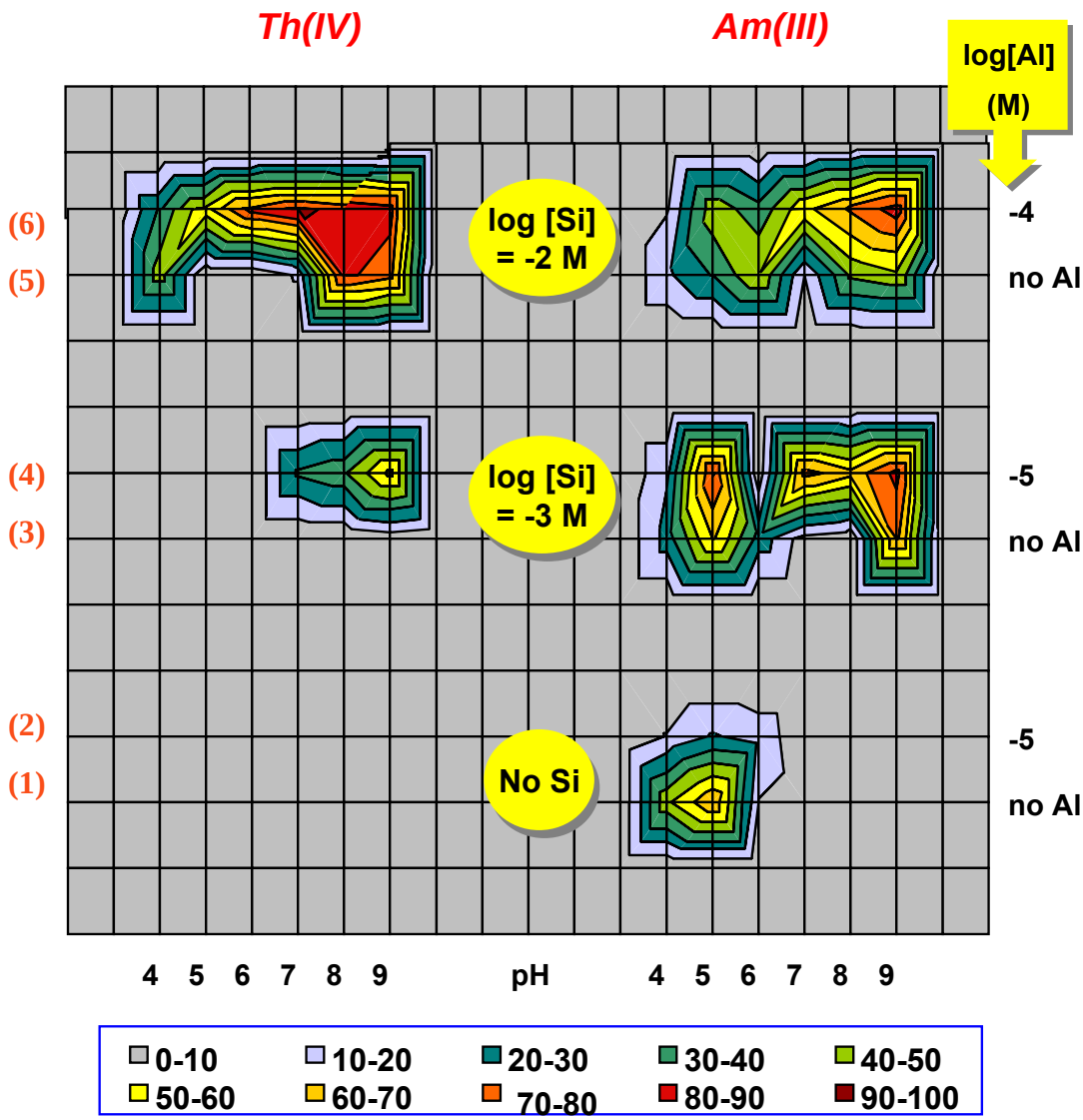

Fig, 47: A contour diagram of the colloid-borne activity fraction (%) (z-axis) normalized to the initial input activity after 35 days of sample conditioning time in different pH for Th (left part) and for Am (right part). Different Si and Al concentrations are indicated in the middle part of the fig. and on the right y-axis, respectively.

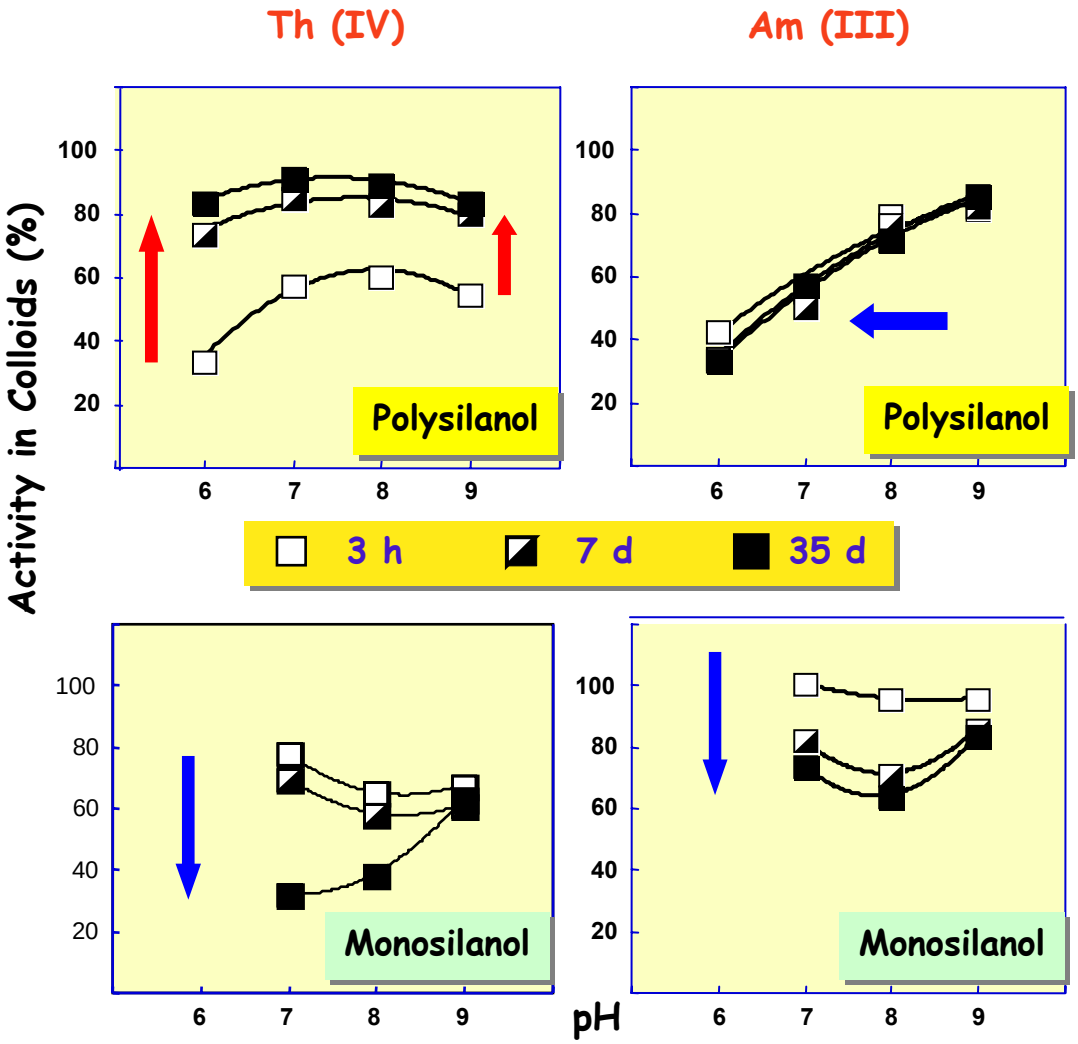

Fig. 48: Colloid-borne activity fraction (%) normalized to the initial activity as a function of pH after different sample conditioning times: Th- (left part) and Am- (right part) incorporated into HAS colloids generated from mono- (lower part) and from polysilanol (upper part).

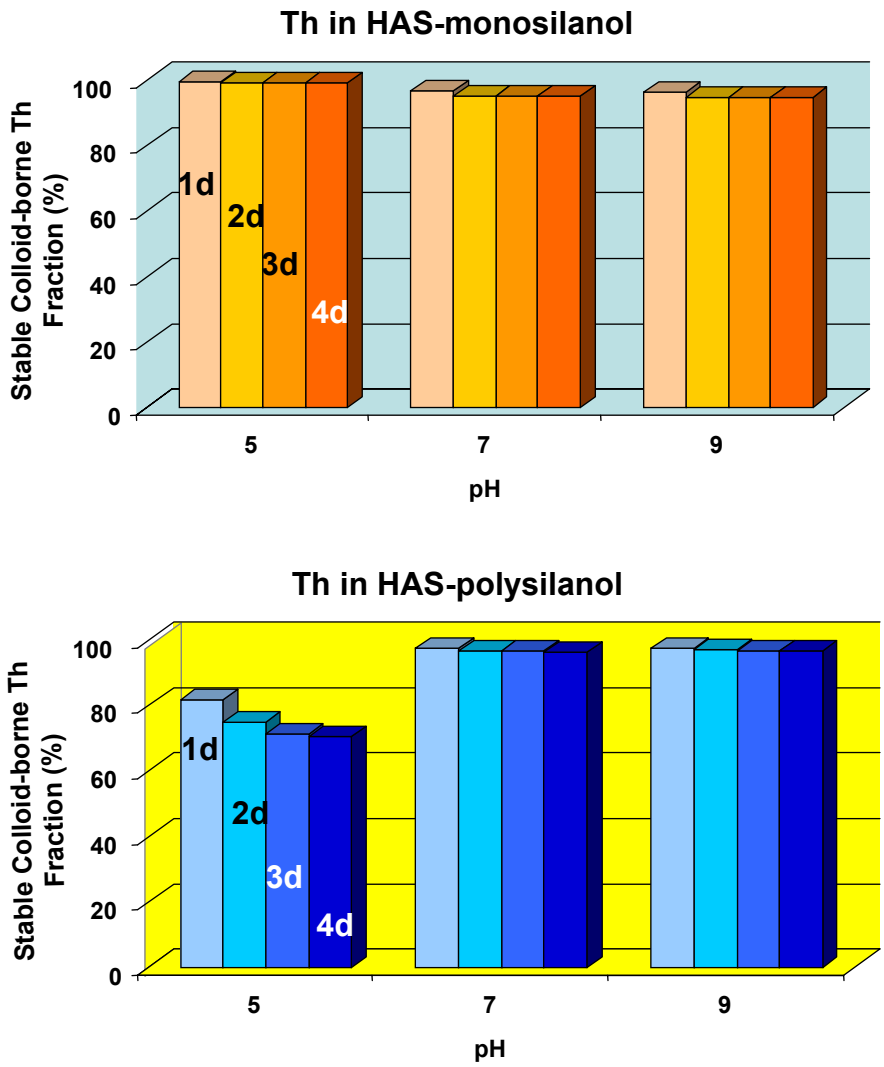

Fig. 49: Colloid-borne Th fraction (%) in a sample after the desorption experiment. The initial sample is prepared at different pH with 10^{-3} mol l^{-1} Si, 10^{-5} mol l^{-1} Al and $5x10^{-8}$ mol l^{-1} Th (upper part) and 10^{-2} mol l^{-1} Si, 10^{-4} mol l^{-1} Al and $5x10^{-8}$ mol l^{-1} Th (lower part) and conditioned for 7 days.

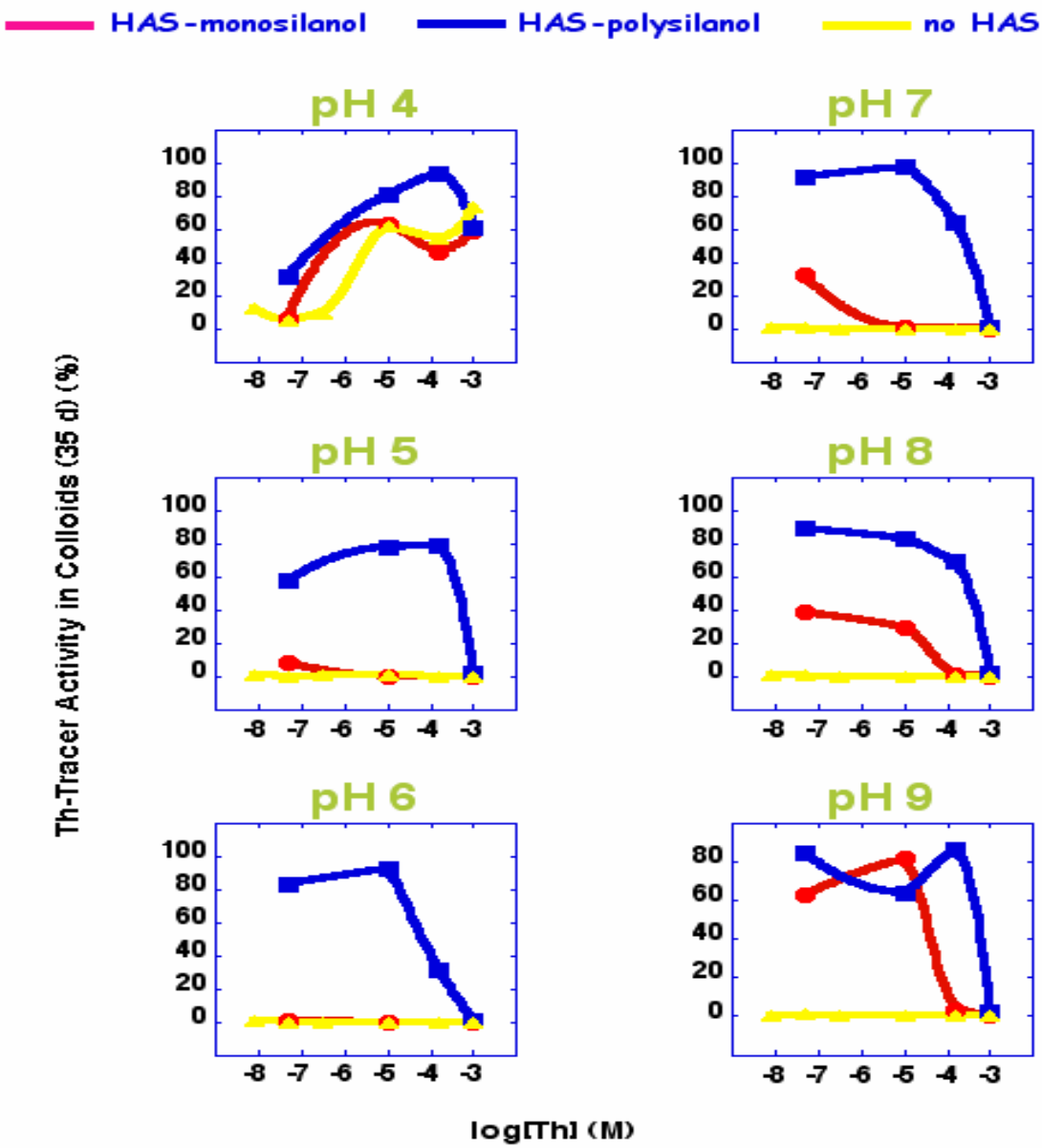

Fig. 50: Colloid-borne Th-activity fraction (%) as a function of the Th concentration for different pH´s in three series of samples indicated as HAS-monosilanol, HAS-polysilanol and no HAS, respectively, and containing mixture solutions of:
(1): 10^{-3} mol l^{-1} Si, 10^{-5} mol l^{-1} Al, $5x10^{-8}$ mol l^{-1}, varied concentration of Th;
(2): $1.3x10^{-2}$ mol l^{-1} Si, $1.5x10^{-4}$ mol l^{-1} Al, $5x10^{-8}$ mol l^{-1} Am, varied concentration of Th;
(3): Varied concentration of Th.

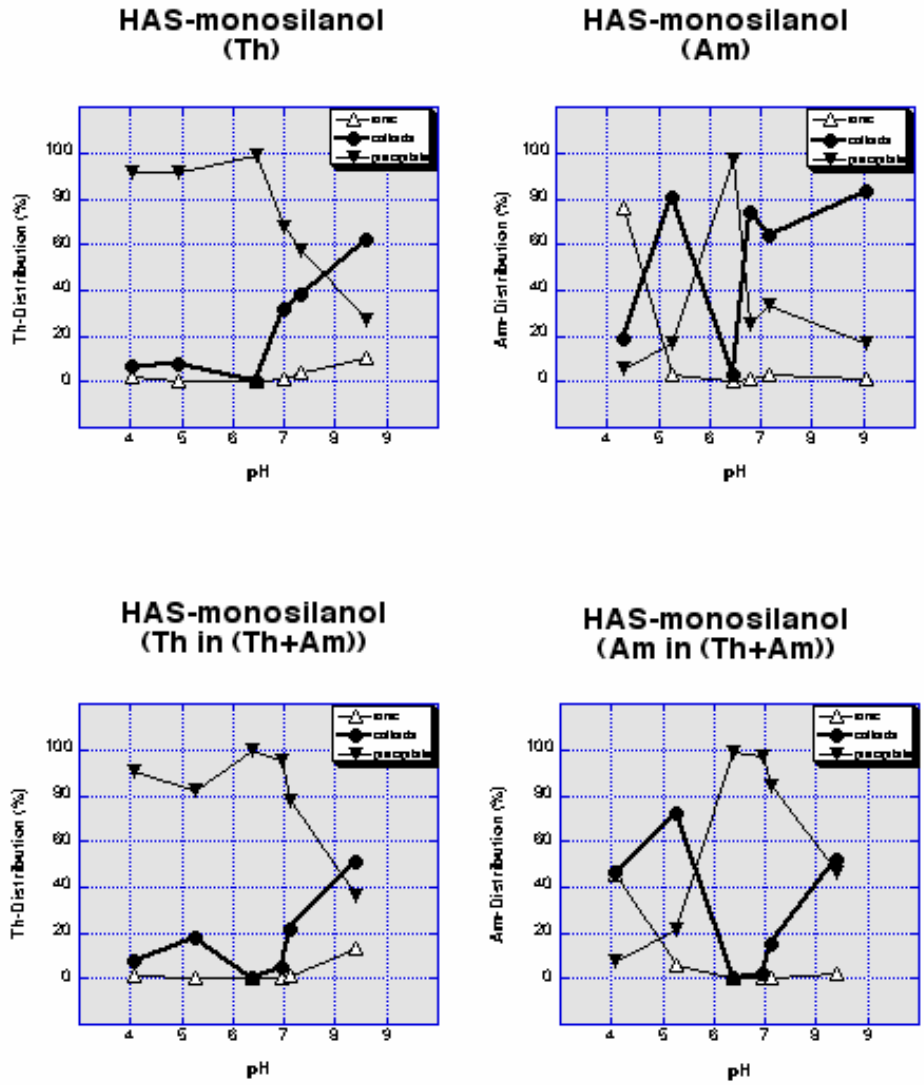

Fig.51: Activity fraction (%) in solution, colloids and precipitate as a function of pH for samples formed from HAS-monosilanol and containing solutions of:
(1): 10^{-3} mol l^{-1} Si, 10^{-5} mol l^{-1} Al, $5x10^{-8}$ mol l^{-1} Th (upper left part)
(2): 10^{-3} mol l^{-1} Si, 10^{-5} mol l^{-1} Al, $5x10^{-8}$ mol l^{-1} Am (upper right part)
(3): 10^{-3} mol l^{-1} Si, 10^{-5} mol l^{-1} Al, $5x10^{-8}$ mol l^{-1} Th, $5x10^{-8}$ mol l^{-1} Am (upper left and upper right part for Th and Am measurement, respectively).

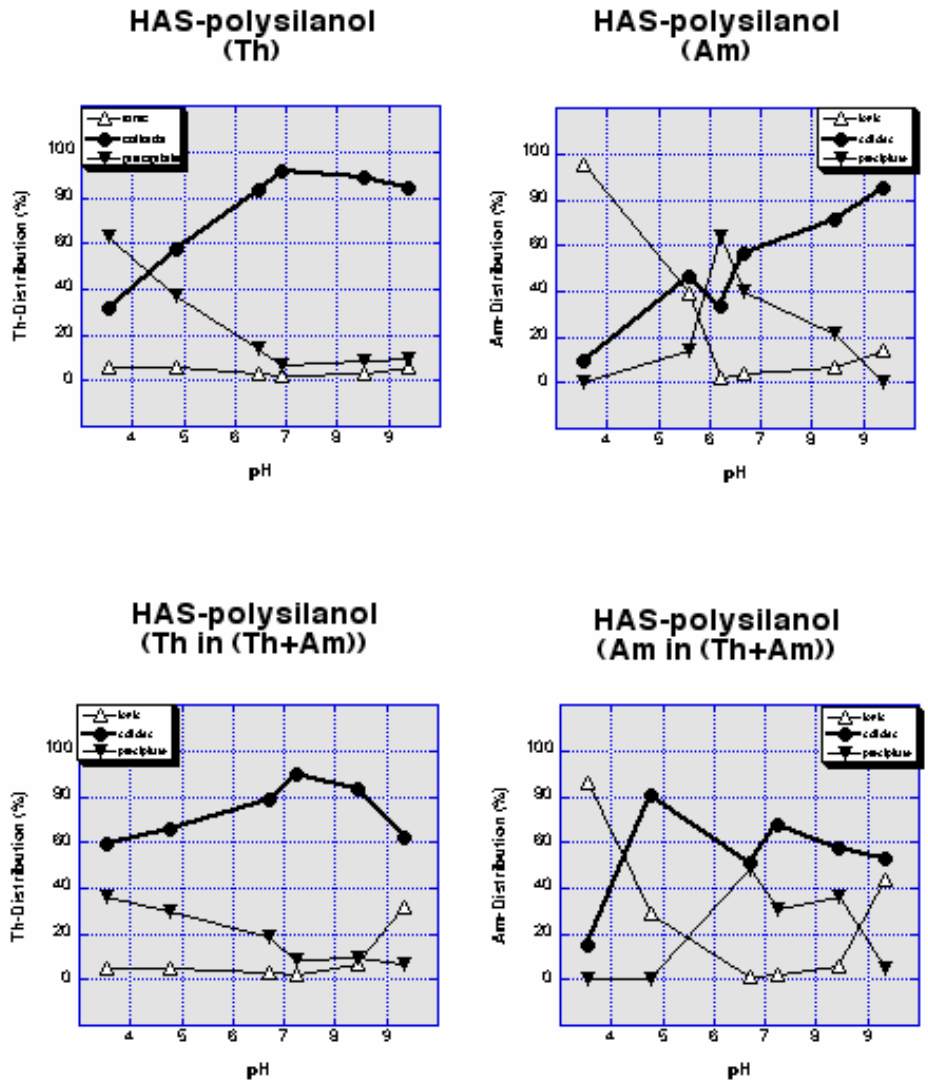

Fig.52: Activity fraction (%) in solution, colloids and precipitate as a function of pH for samples formed from HAS-polysilanol and containing solutions of:
(1): 1.3×10^{-2} mol l^{-1} Si, 1.5×10^{-4} mol l^{-1} Al, 5×10^{-8} mol l^{-1} Th (upper left part)
(2): 1.3×10^{-2} mol l^{-1} Si, 1.5×10^{-4} mol l^{-1} Al, 5×10^{-8} mol l^{-1} Am (upper right part)
(3): 1.3×10^{-2} mol l^{-1} Si, 1.5×10^{-4} mol l^{-1} Al, 5×10^{-8} mol l^{-1} Th, 5×10^{-8} mol l^{-1} Am (upper left and upper right part for Th and Am measurement, respectively).

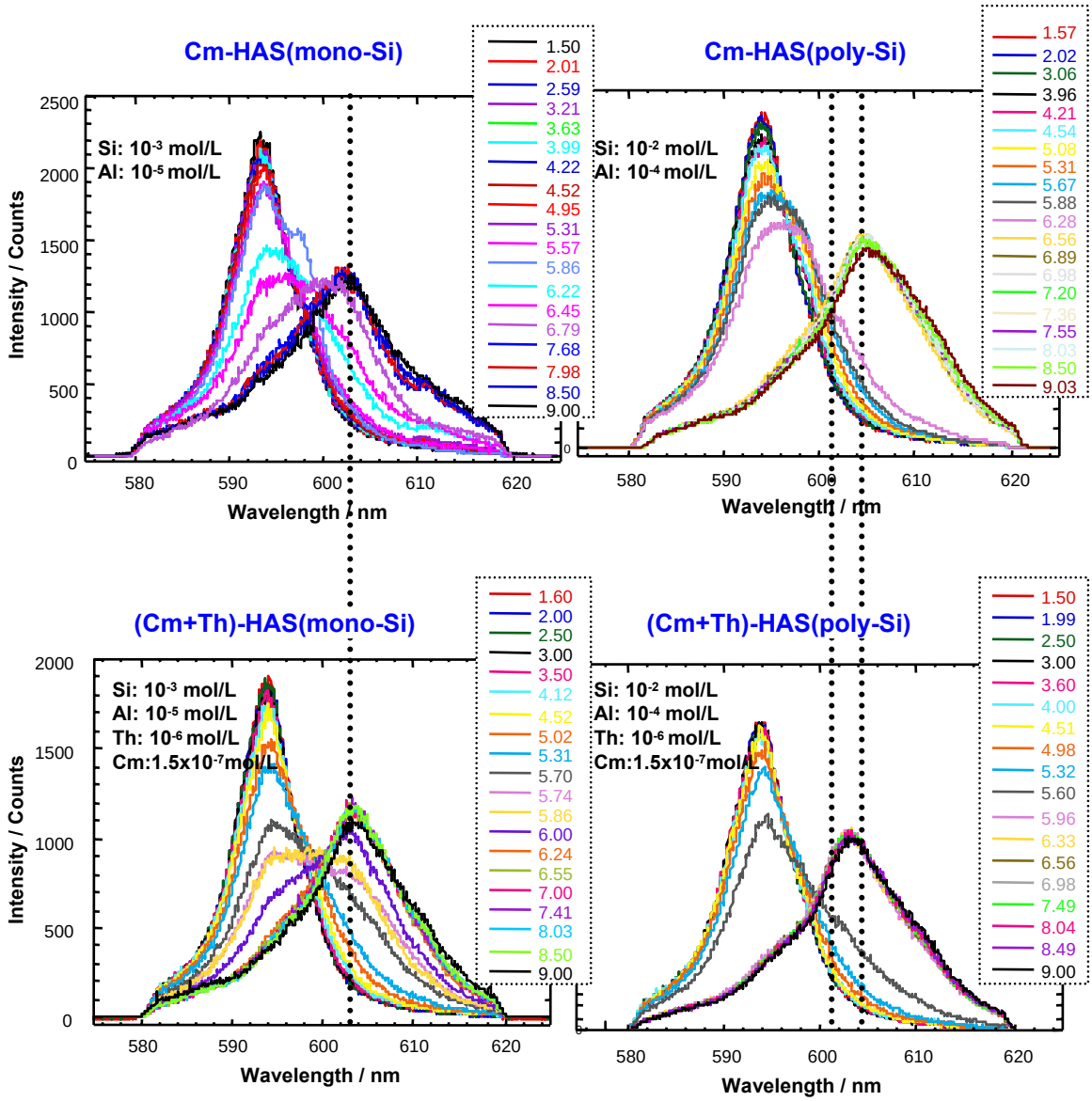

Fig.53: Speciation of HAS colloid-borne Cm by TRLFS on the pH titration from 1 to 9 in a solution containing mono-ilanol (left part) and in a solution containing polysilanol (right part) without (upper part) and with (lower part) Th addition: the pH dependent spectrum evolution.

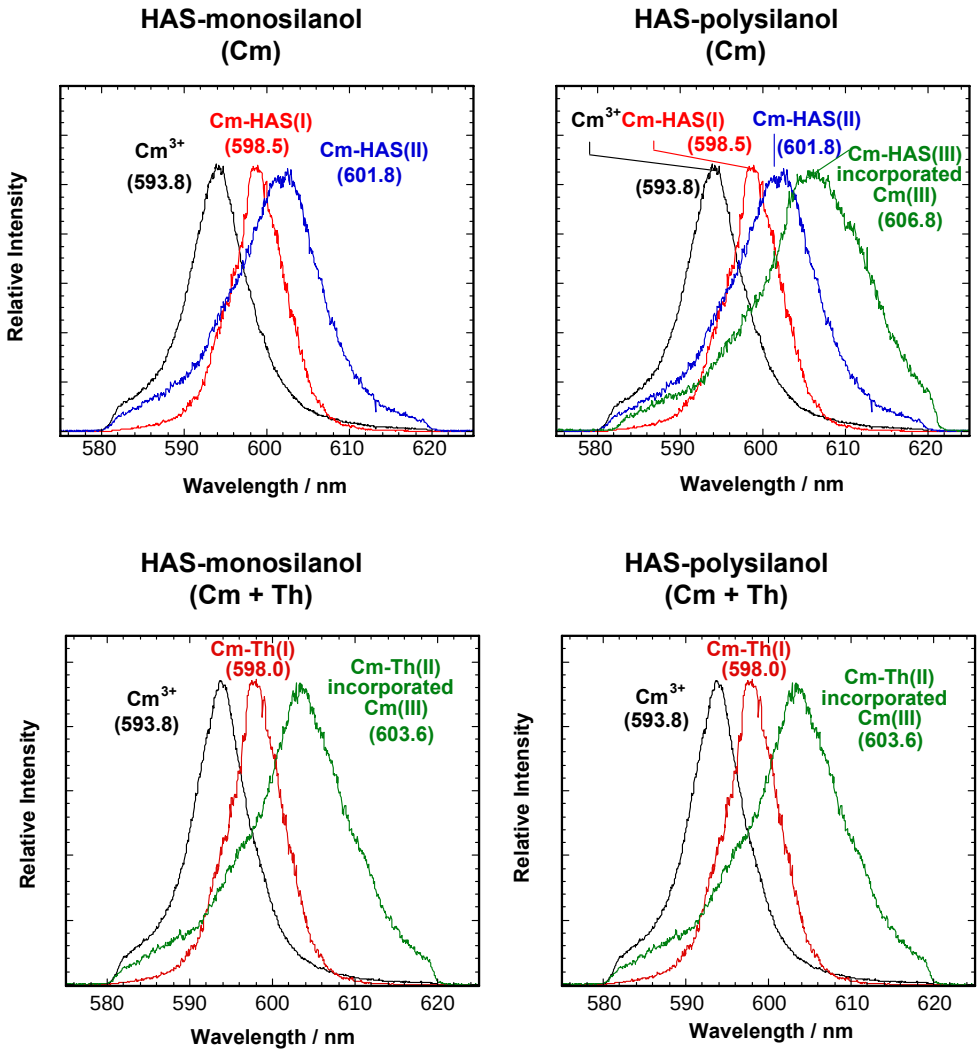

Fig.54: Deconvoluted spectra of different Cm species present in the solution (cf. Fig.53).

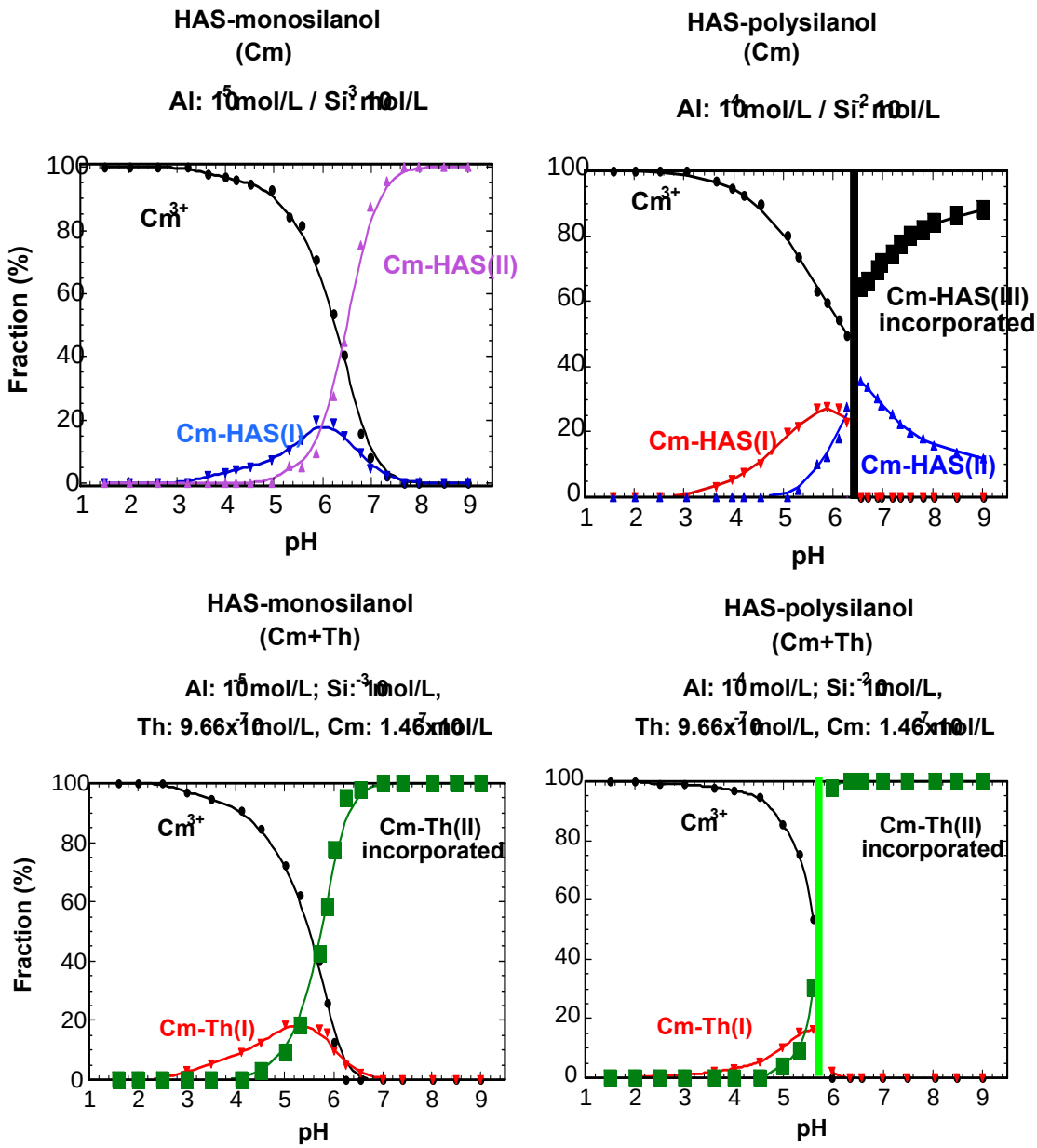

Fig.55: The relative Cm species distribution as a function of pH (cf. Figs 53 and 54).

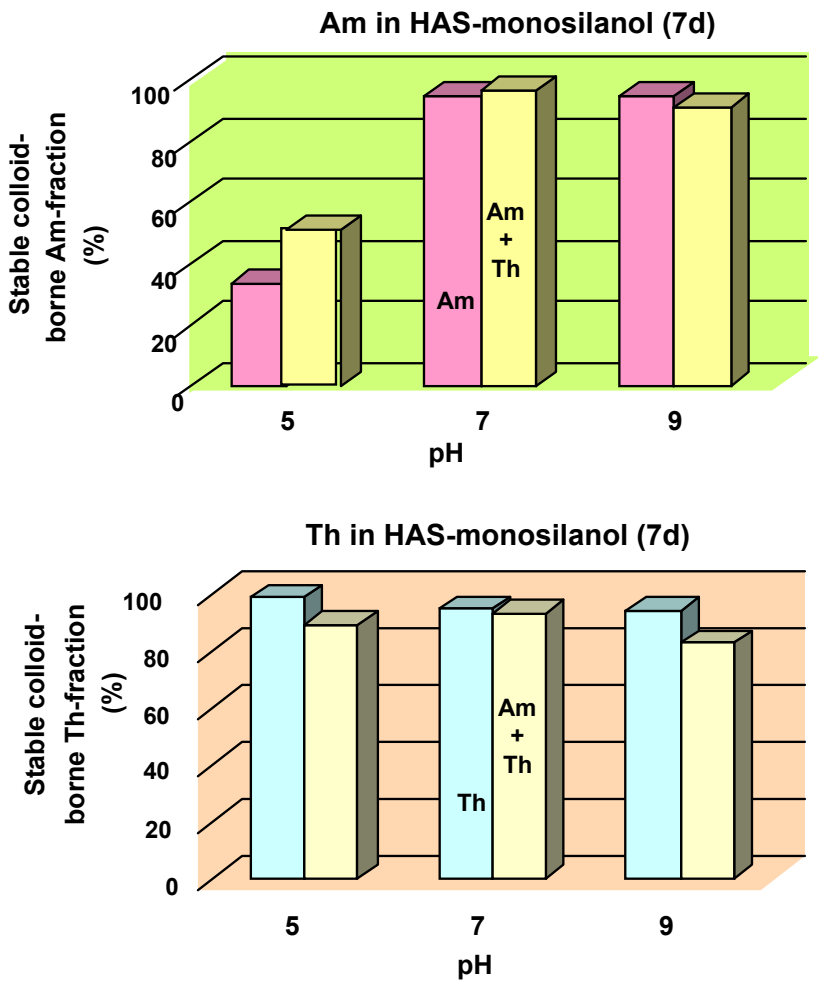

Fig. 56: Colloid-borne activity fraction (%) in a sample after the desorption experiment. The initial sample is prepared at different pH with 10^{-3} mol l^{-1} Si (monosilanol), 10^{-5} mol l^{-1} Al and $5x10^{-8}$ mol l^{-1} Am or Th or Th+Am and conditioned for seven days.

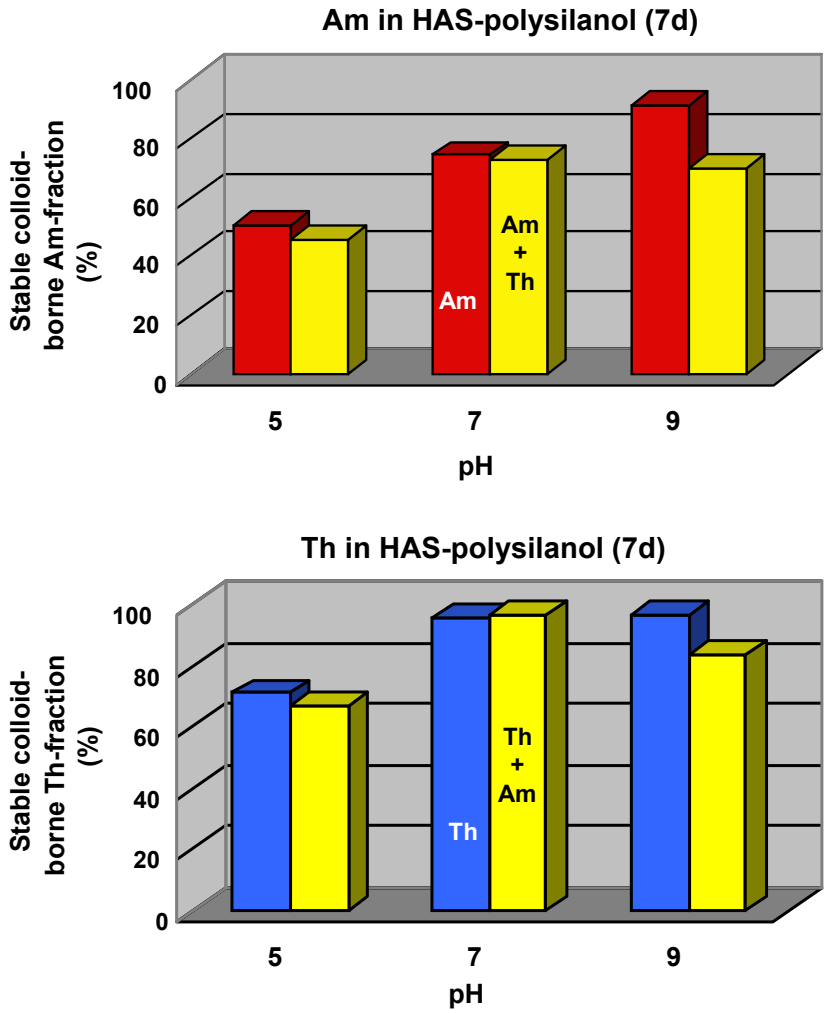

Fig. 57: Colloid-borne activity fraction (%) in a sample after the desorption experiment. The initial sample is prepared at different pH with 10^{-2} mol l^{-1} Si (polysilanol), 10^{-4} mol l^{-1} Al and $5x10^{-8}$ mol l^{-1} Am or Th or Th+Am and conditioned for seven days.

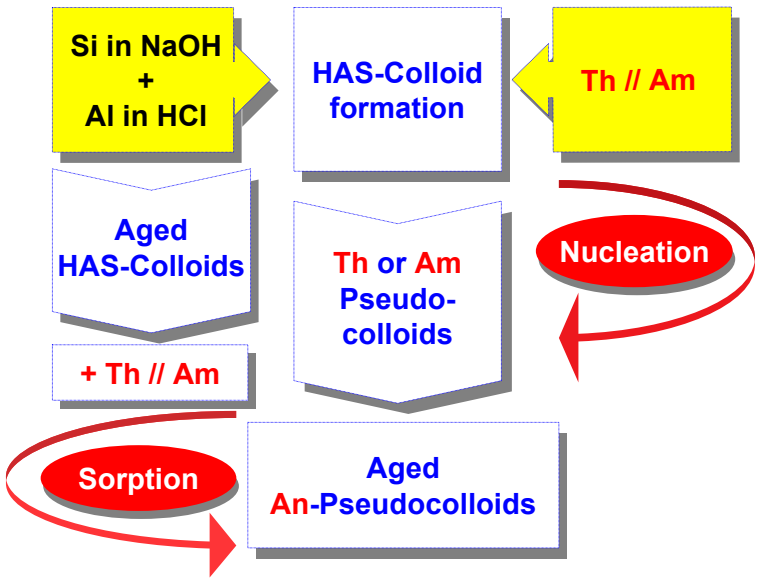

Fig. 58: Experimental interactions pathways of actinides with HAS colloids.

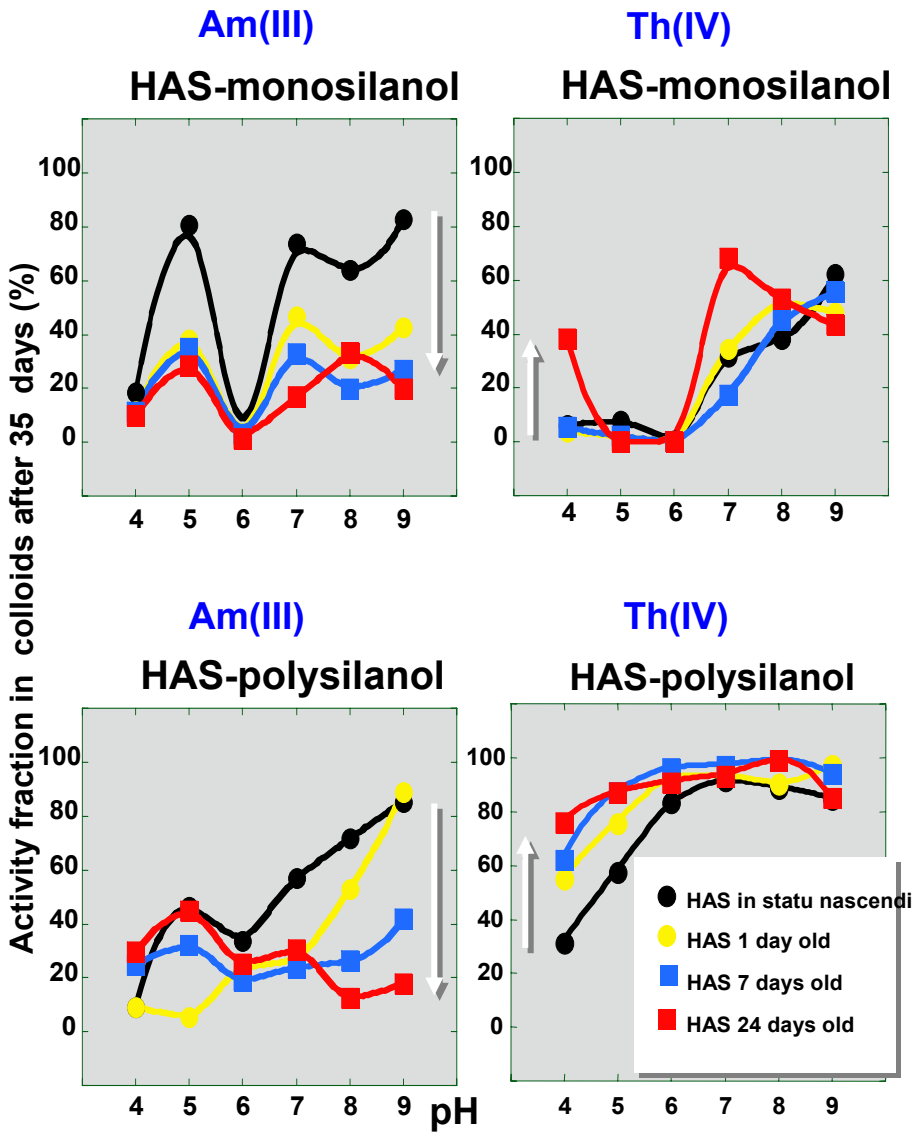

Fig. 59: Colloid-borne activity fraction (%) normalized to the initial activity as a function of pH after 35 days sample conditioning time for colloids of different ages (from 0 to 24 days): for Am (left part) and Th (right part) incorporation into colloids generated from HAS-monosilanol (upper part) and from HAS-polysilanol (lower part).

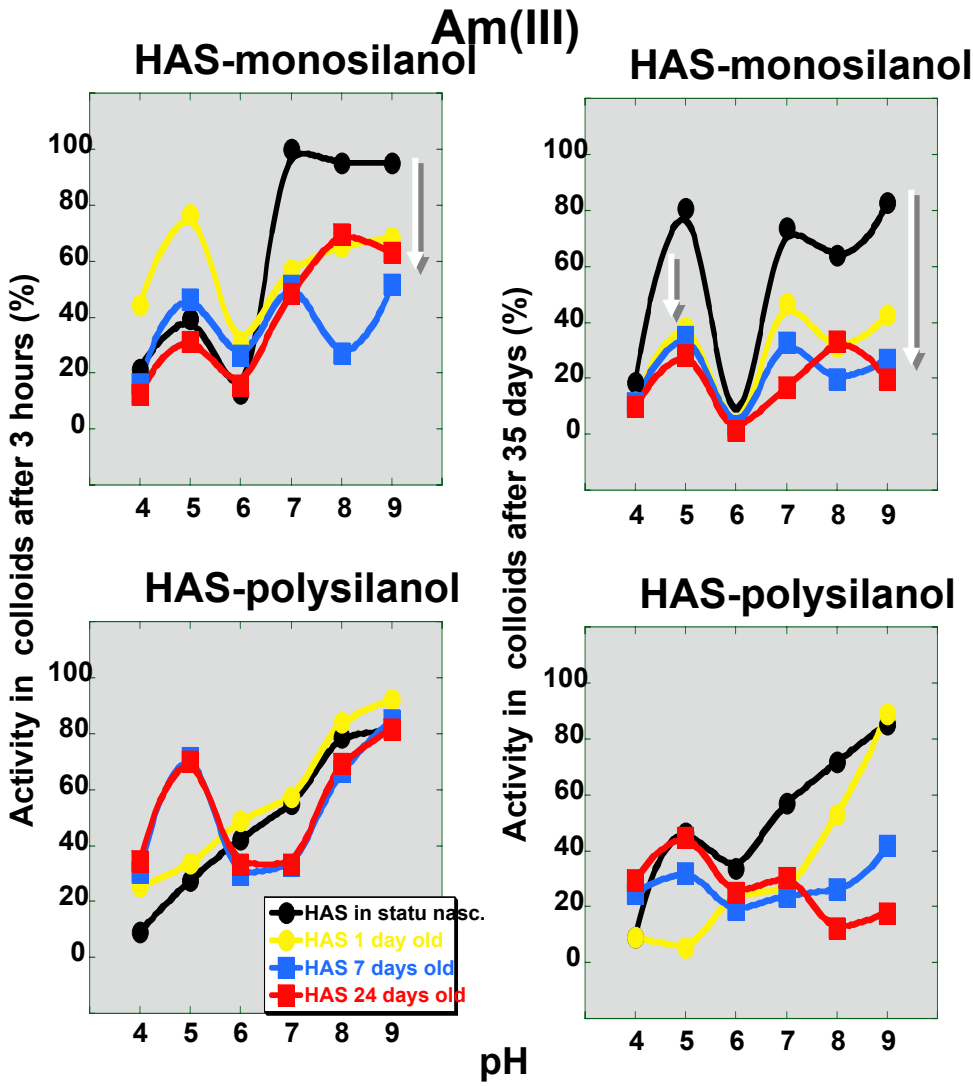

Fig. 60: Colloid-borne Am fraction (%) normalized to the initial activity as a function of pH after 3 hours and 35 days activity contact time (left and right part, respectively) for colloids of different ages (from 0 to 24 days) generated from HAS-monosilanol (upper part) and from HAS-polysilanol (lower part).

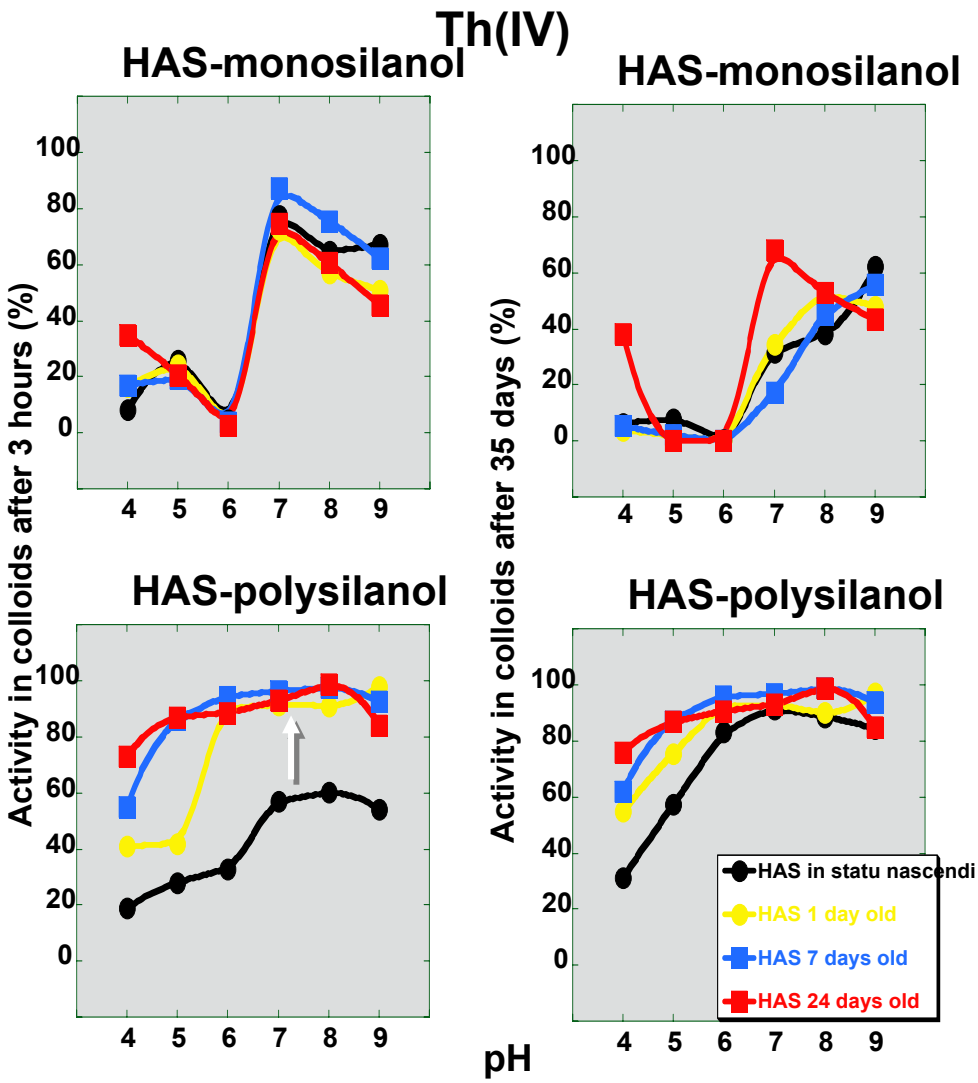

Fig. 61: Colloid-borne Th fraction (%) normalized to the initial activity as a function of pH after 3 hours and 35 days activity contact time (left and right part, respectively) for colloids of different ages (from 0 to 24 days) generated from HAS-monosilanol (upper part) and from HAS-polysilanol (lower part).

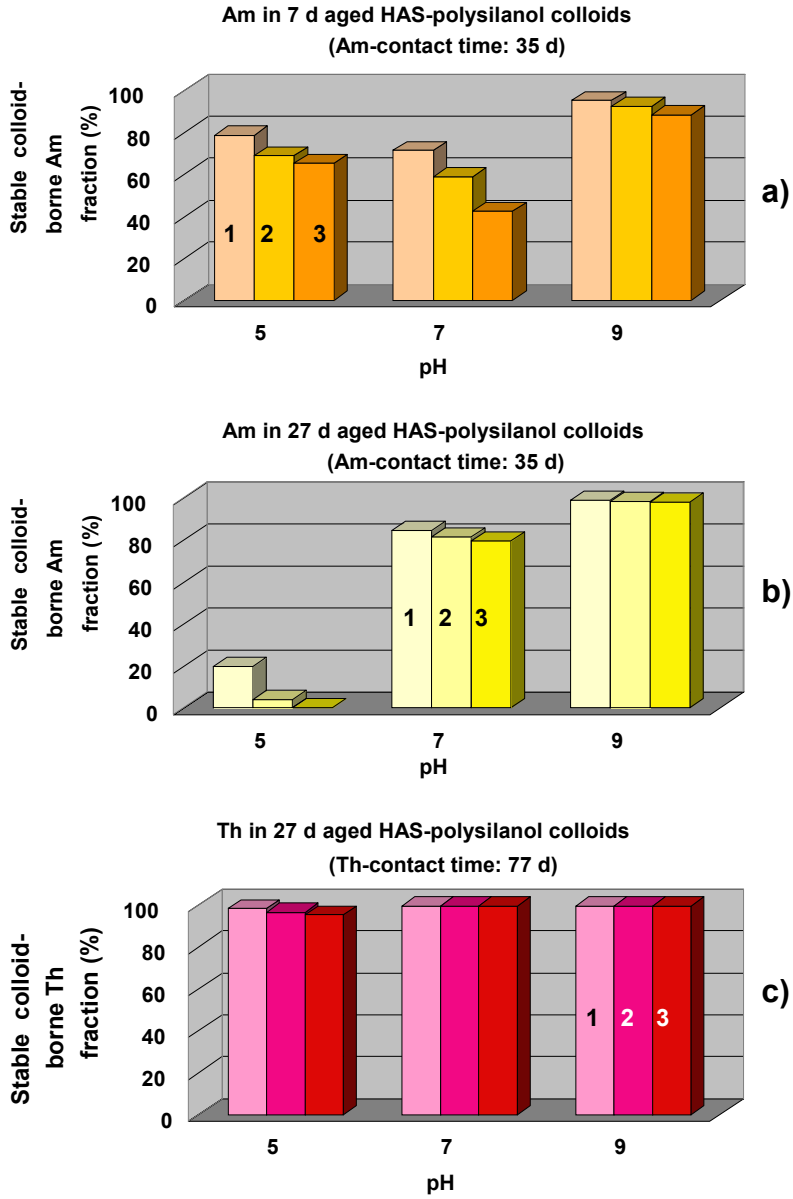

Fig. 62: Colloid-borne activity fraction (%) in a sample after the desorption experiment. The initial sample is prepared at different pH with 10^{-2} mol l^{-1} Si (polysilanol), 10^{-4} mol l^{-1} Al: (a) $5x10^{-8}$ mol l^{-1} Am is added after 7 days aging time and the Am contact time is 35 days; (b) $5x10^{-8}$ mol l^{-1} Am is added after 27 days aging time and the Am contact time is 35 days; (c) $5x10^{-8}$ mol l^{-1} Th is added after 27 days aging time and the Am contact time is 77 days. Desorption experiment is performed in three sequential equilibria each with fresh solution.

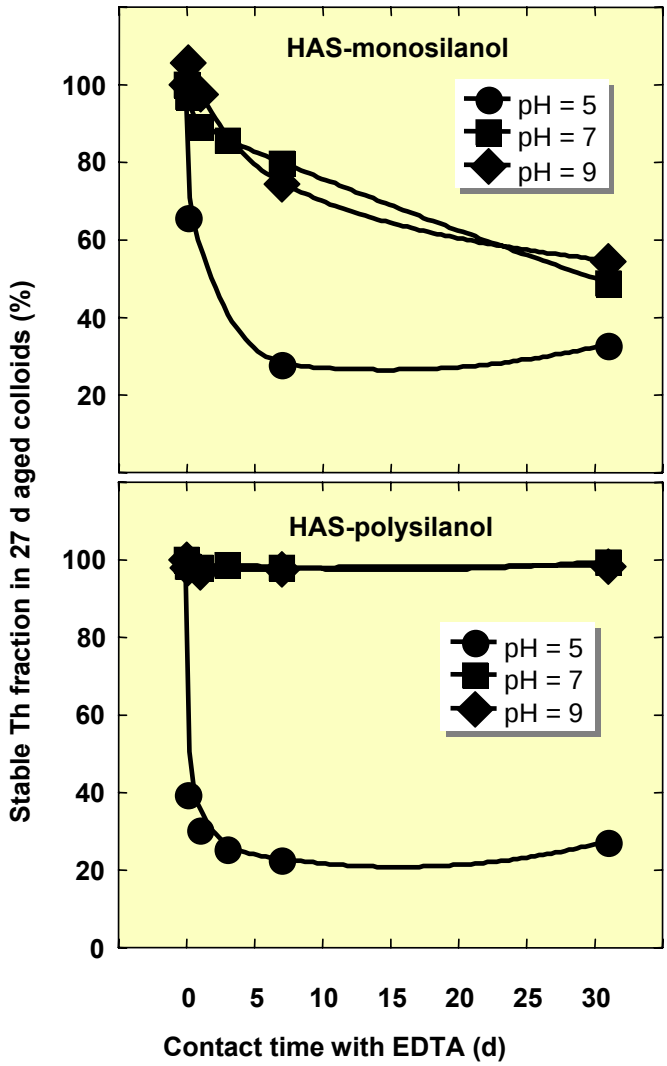

Fig. 63: Colloid-borne Th activity fraction (%) in a sample at desorption with $1x10^{-4}$ mol l^{-1} EDTA as a function of time. The initial sample is prepared at different pH with
(upper part): 10^{-3} mol l^{-1} Si (monosilanol), 10^{-5} mol l^{-1} Al
(lower part): 10^{-2} mol l^{-1} Si (polysilanol), 10^{-4} mol l^{-1} Al
After an aging time of 27 days, $4.8x10^{-8}$ mol l^{-1} Th is added; The Th contact time is 35 days.

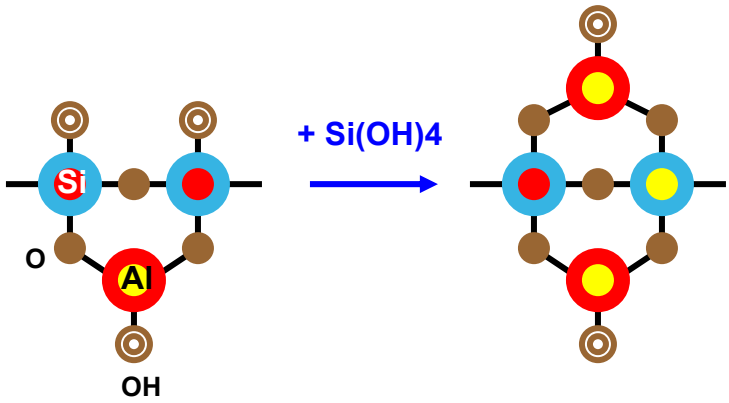

Fig. 64: Template mechanism for the formation of hydroxy aluminosilicates as proposed by Doucet et al. [Geochim. Cosmochim. Acta 65 (15) 2461 (2001)].

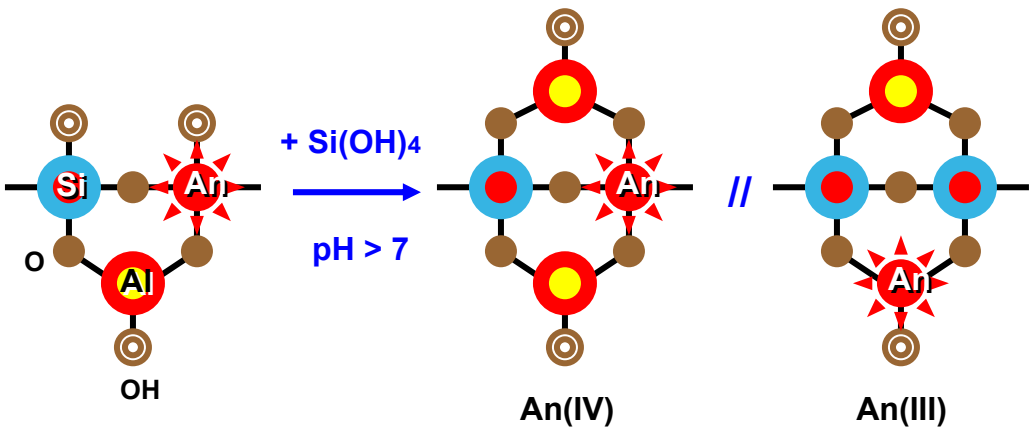

Fig. 65: Postulated mechanism for the formation of colloid-borne An(III) or An(IV) in HAS(monosilanol) colloids.

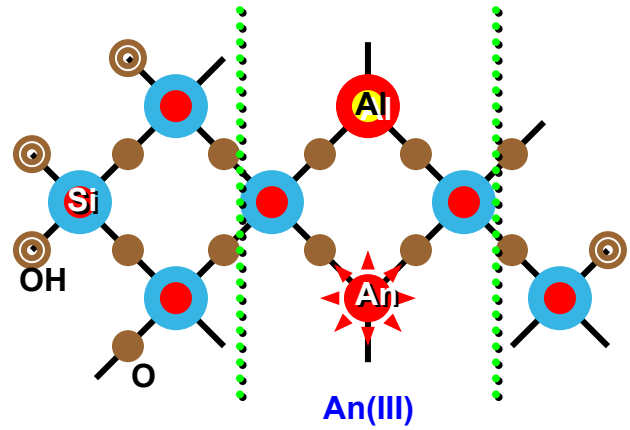

Fig. 66: Postulated mechanism for the formation of colloid-borne Am(Cm) from HAS(polysilanol) colloids with Si/Al atomic ratio: ca 1.

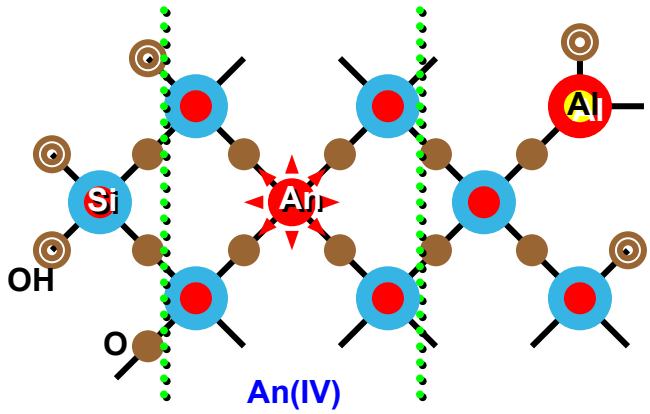

Fig. 67: Postulated mechanism for the formation of colloid-borne Th(IV) by heterogeneous nucleation with Si.

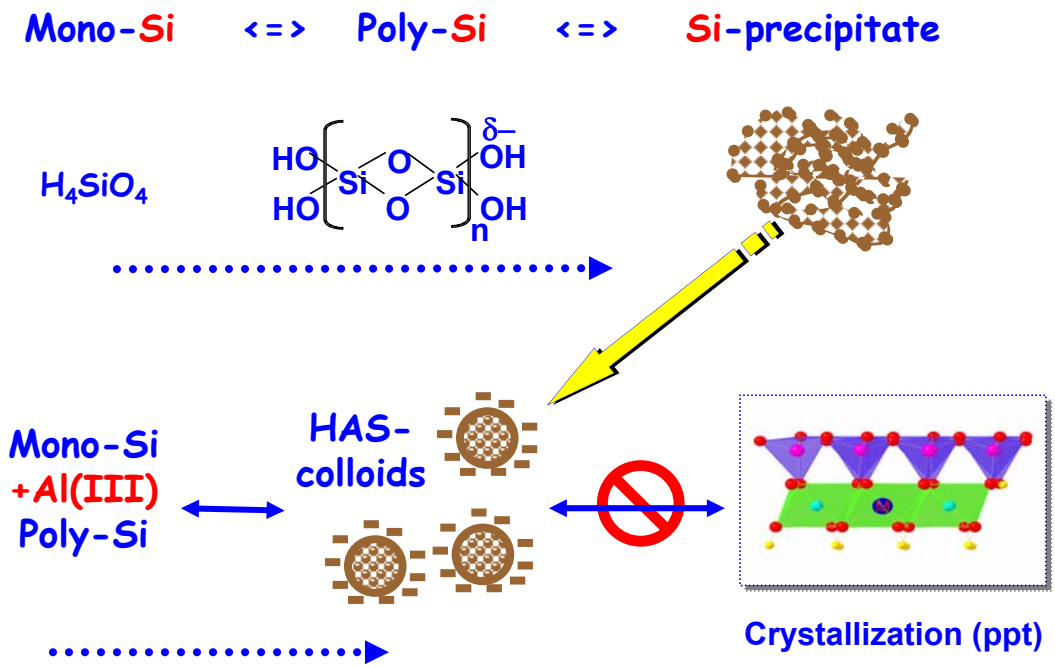

Fig. 68: Stabilization of HAS colloids through Al-controlled polymerization of Si.

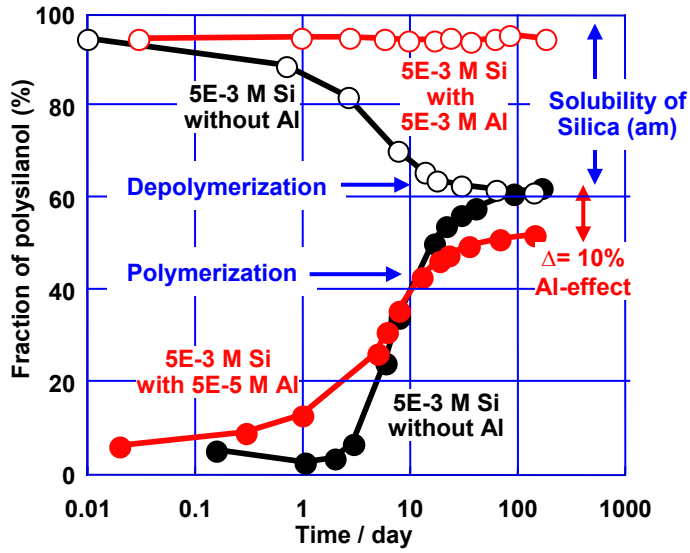

Fig. 69: The Al ion effect on the polymerization and depolymerization of Si, monitored by molybdenum tests.

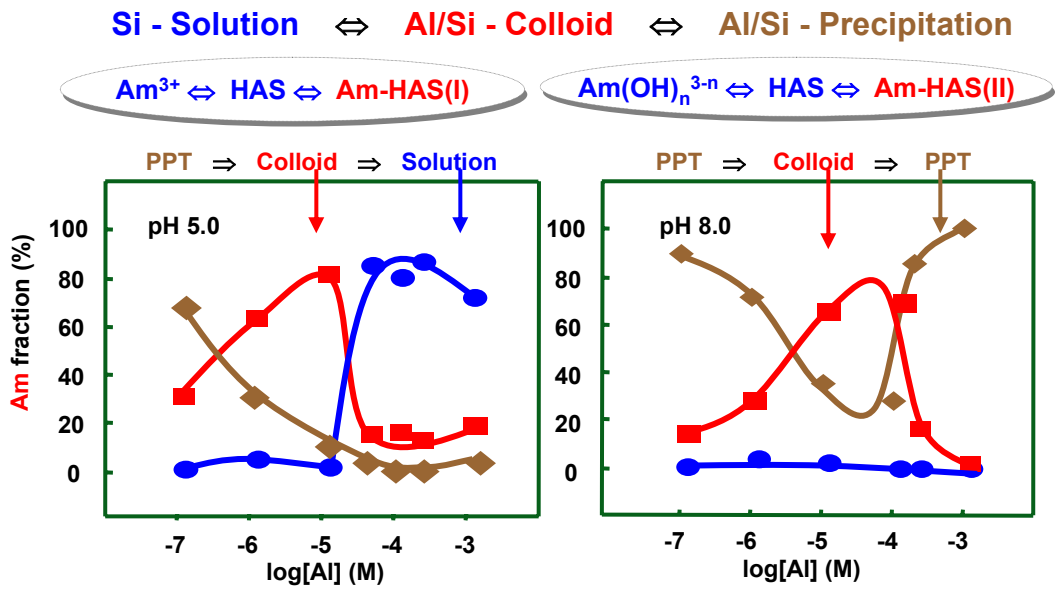

Fig. 70: Dual effects of Al on the formation of colloid-borne Am: (1) Binding with Si and HAS colloid formation (pH 5); (2) HAS colloid agglomeration via hydrophobic process.

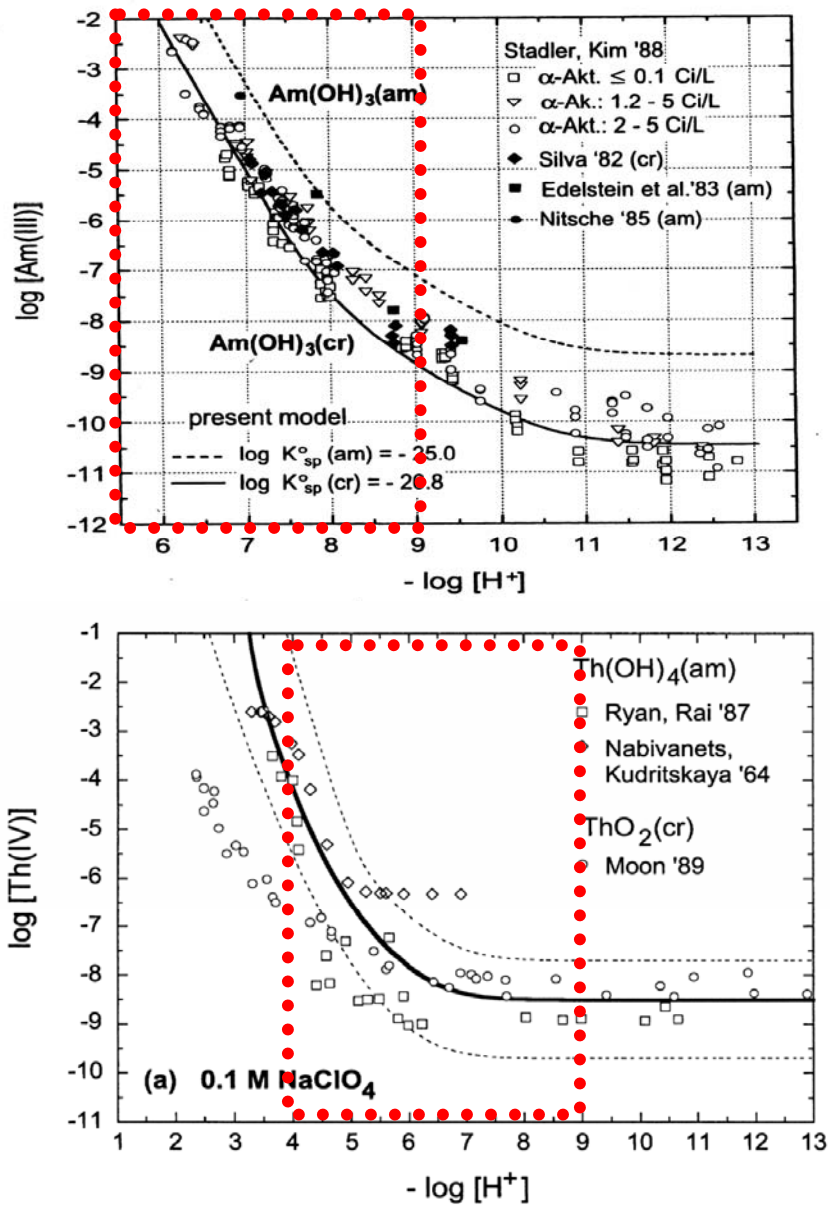

Fig. 71: Thermodynamic solubility of $Th(OH)_4$ (am) and $Am(OH)_3$ as a function of pH from literature. Conditions expected for colloid formation are indicated by dotted area.

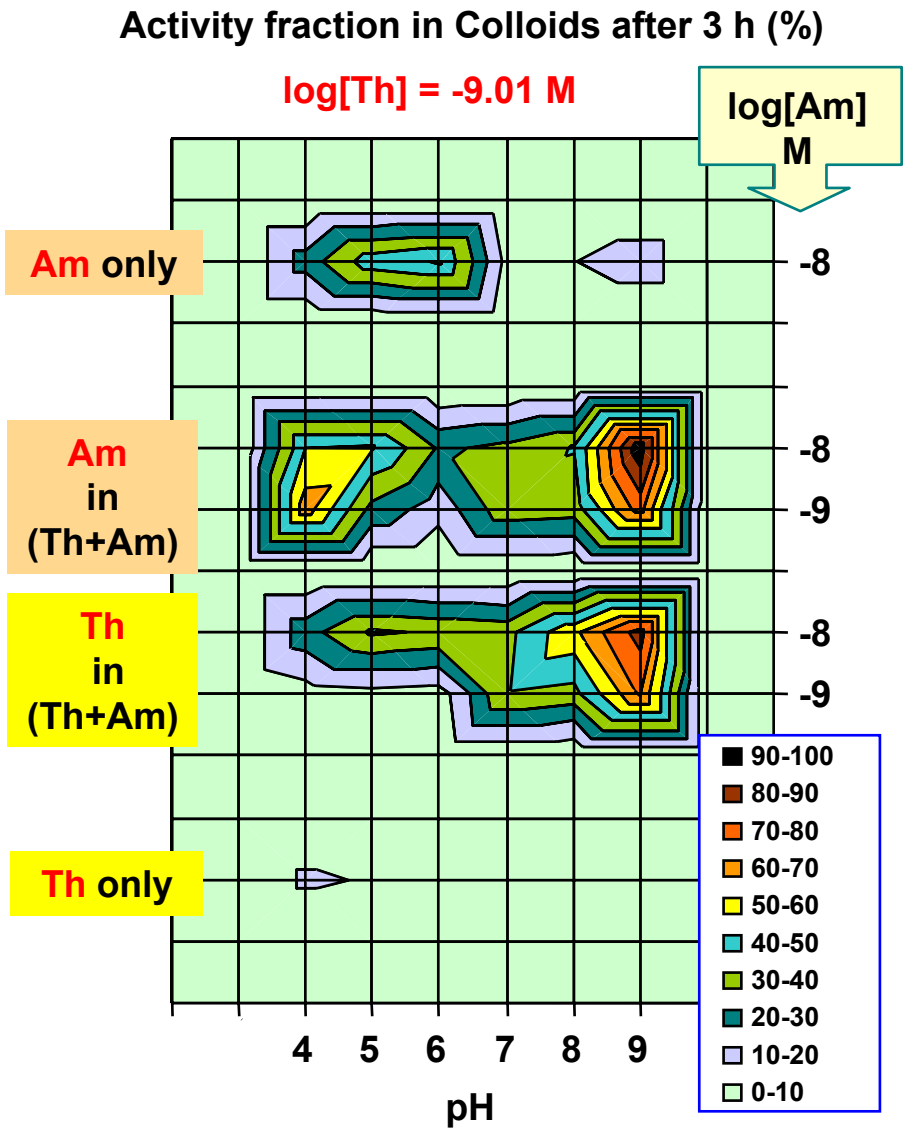

Fig. 72: Th and Am colloid-borne activity fraction (%) after 3 hours conditioning time in four sample series at different pH: two mixed samples containing $1x10^{-9}$ mol l^{-1} Th and $1x10^{-9}$ or $8x10^{-9}$ mol l^{-1} Am (Th+Am) and two separate samples containing $1x10^{-10}$ mol l^{-1} Th (Th only) and $8x\ 10^{-9}$ mol l^{-1} Am (Am only).

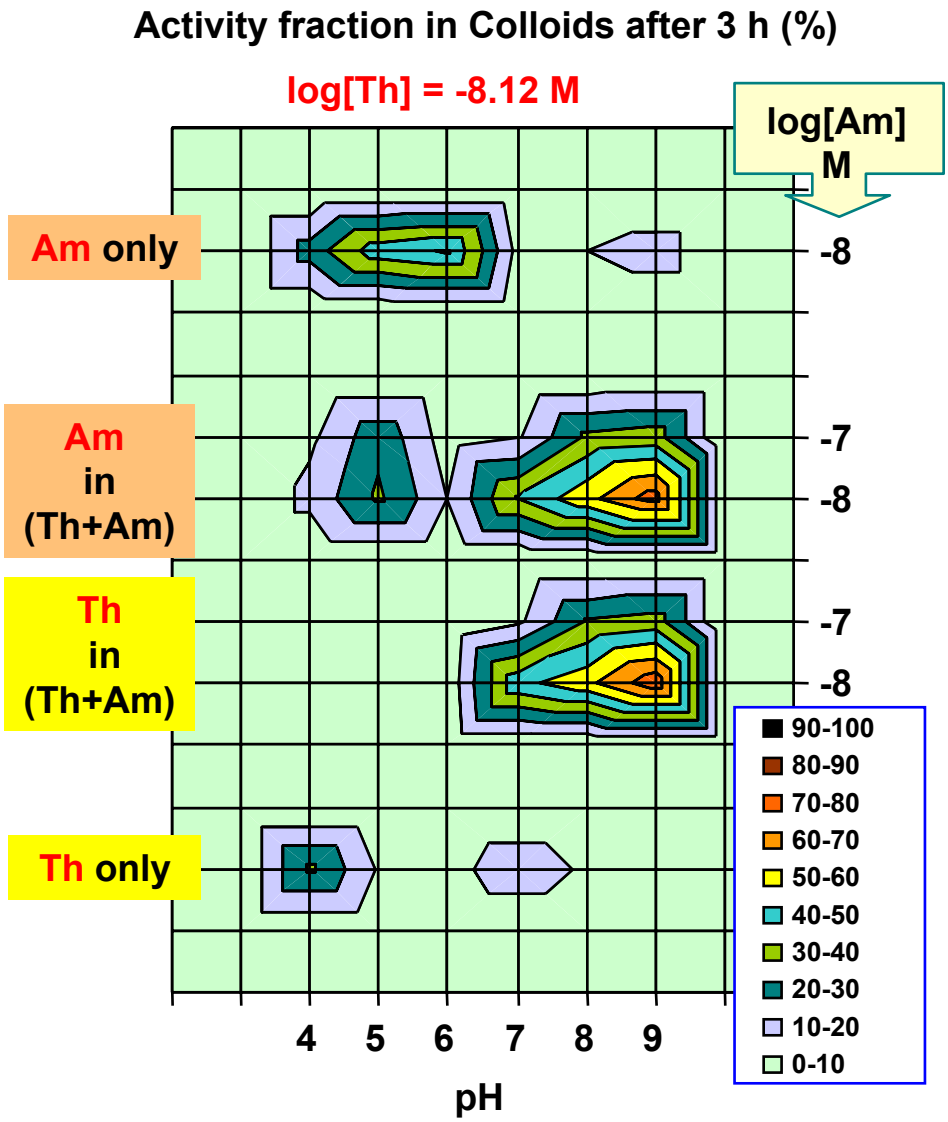

Fig. 73: Th and Am colloid-borne activity fraction (%) after 3 hours conditioning time in four sample series at different pH: two mixed samples containing $7x10^{-9}$ mol l^{-1} Th and $8x10^{-9}$ or $5.4x10^{-8}$ mol l^{-1} Am (Th+Am) and two separate samples containing $7x10^{-9}$ mol l^{-1} Th (Th only) and $8x10^{-9}$ mol l^{-1} Am (Am only).

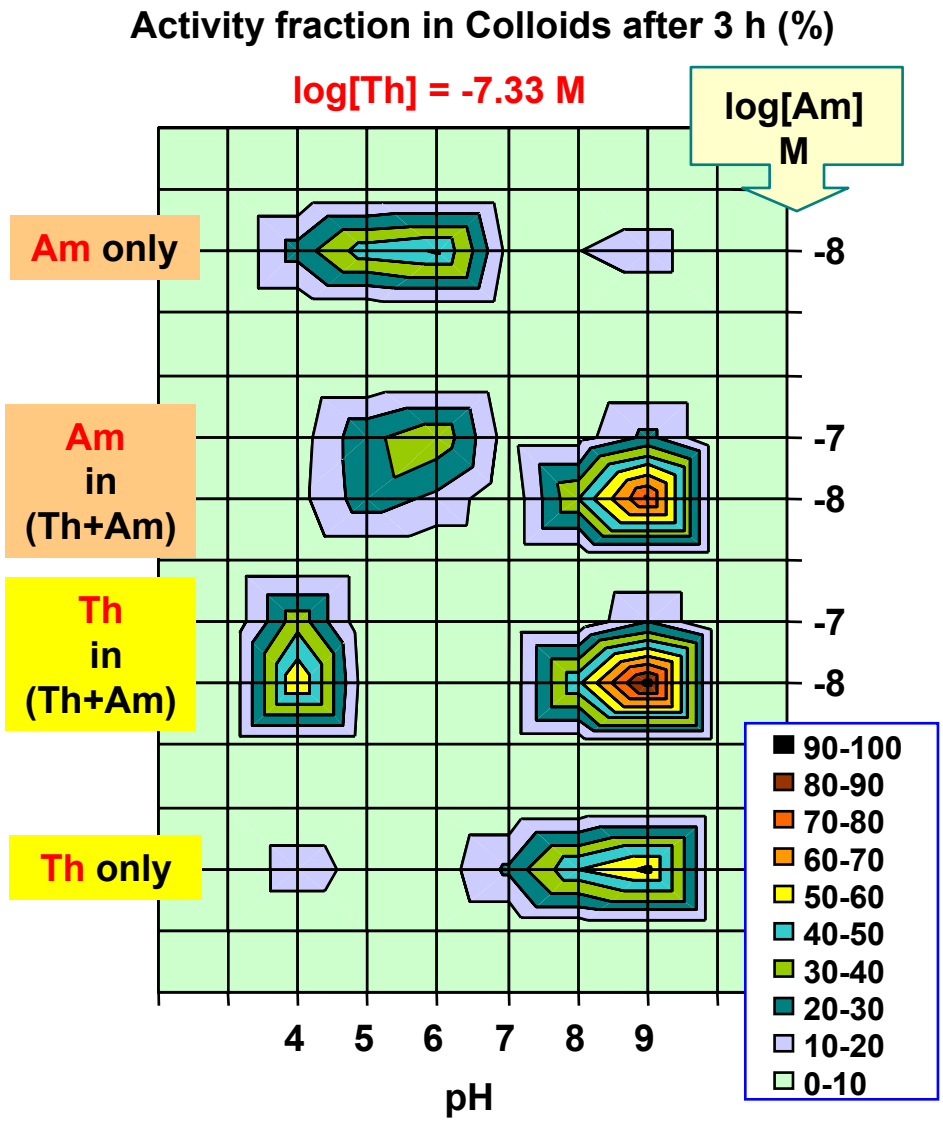

Fig. 74: Th and Am colloid-borne activity fraction (%) after 3 hours conditioning time in four sample series at different pH: two mixed samples containing 4.6×10^{-8} mol l^{-1} Th and 7×10^{-9} or 6×10^{-8} mol l^{-1} Am (Th+Am) and two separate samples containing 4.6×10^{-8} mol l^{-1} Th (Th only) and 1×10^{-8} mol l^{-1} Am (Am only).

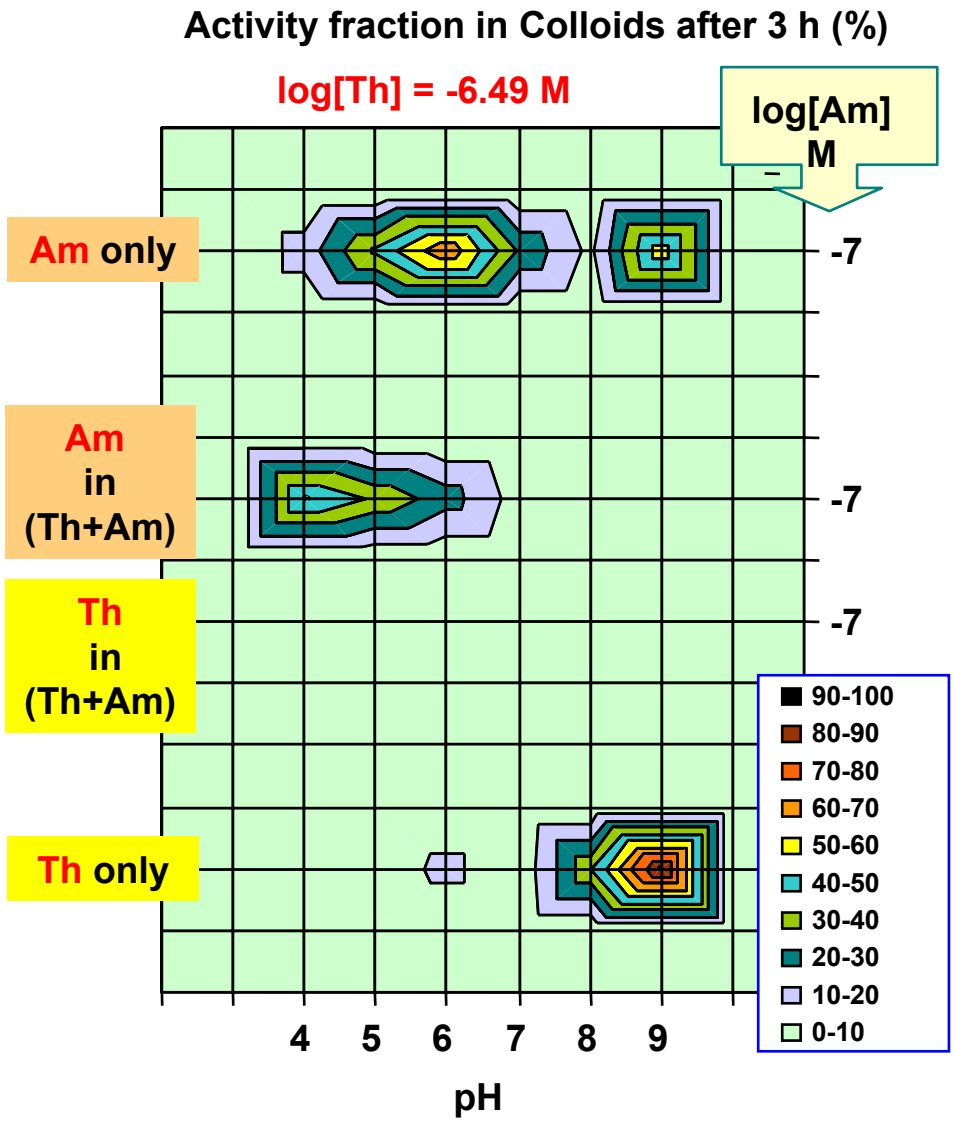

Fig. 75: Th and Am colloid-borne activity fraction (%) after 3 hours conditioning time in three sample series at different pH: two mixed samples containing 3.2×10^{-7} mol l^{-1} Th and 5×10^{-8} mol l^{-1} Am (Th+Am) and two separate samples containing 3.2×10^{-7} mol l^{-1} Th (Th only) and 5×10^{-8} mol l^{-1} Am (Am only).

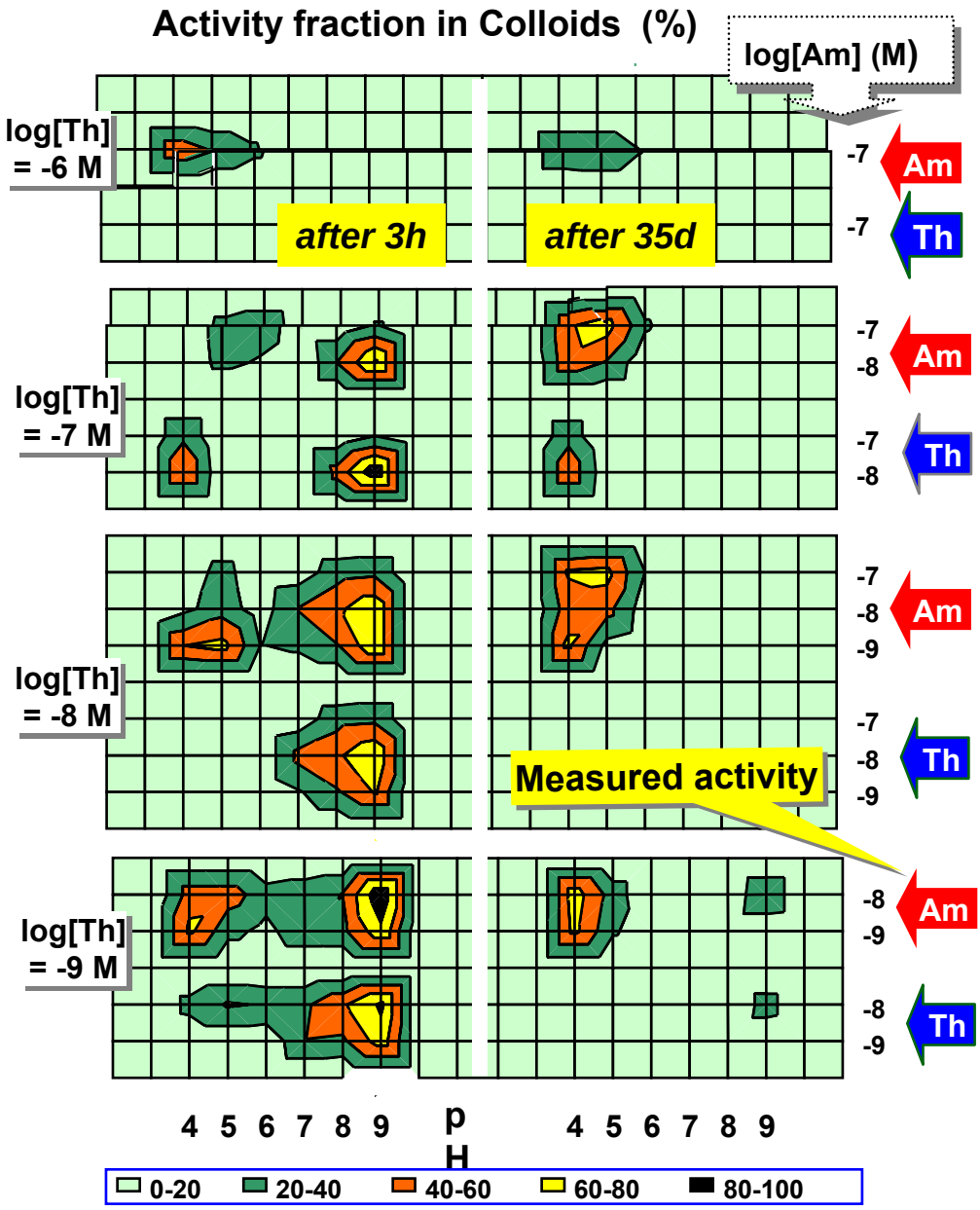

Fig. 76: Overview of Th and Am colloid-borne activity fraction (%) as shown in Figs. 72-75 (series of mixed samples (Th+Am), separate samples (Th or Am only)) at different pH after different sample conditioning times, 3 hours and 35 days as illustrated in the left and the right part of the figure.

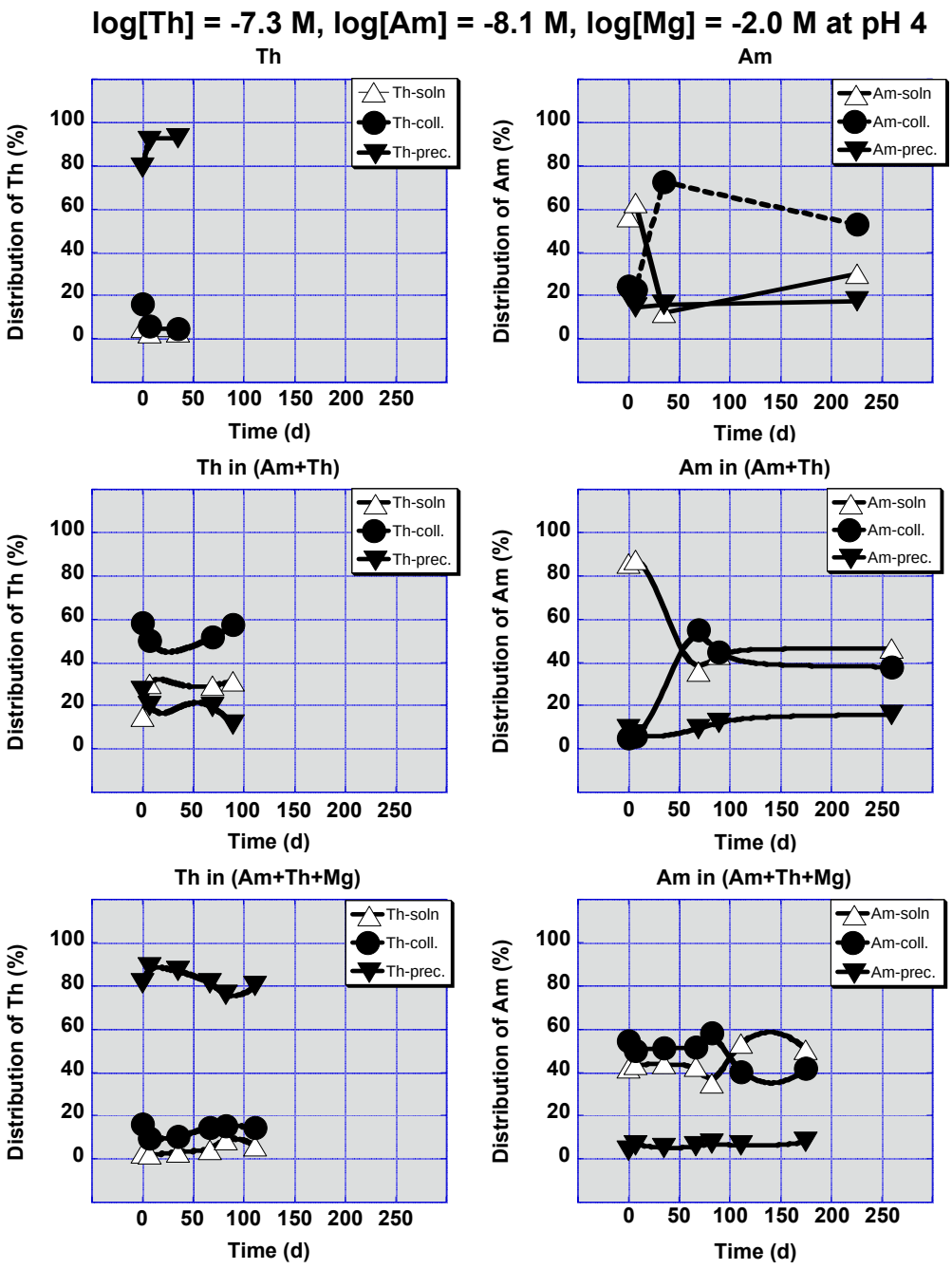

Fig.77: Colloid-borne activity fraction (%) as a function of the conditioning time without and with Mg: one mixed and two separate samples containing 4.6×10^{-8} mol l^{-1} Th and 7×10^{-9} mol l^{-1} Am (cf. Fig.76) at pH 4 (middle and upper parts) and for the mixed sample with addition of 10^{-2} mol l^{-1} Mg (lower part).

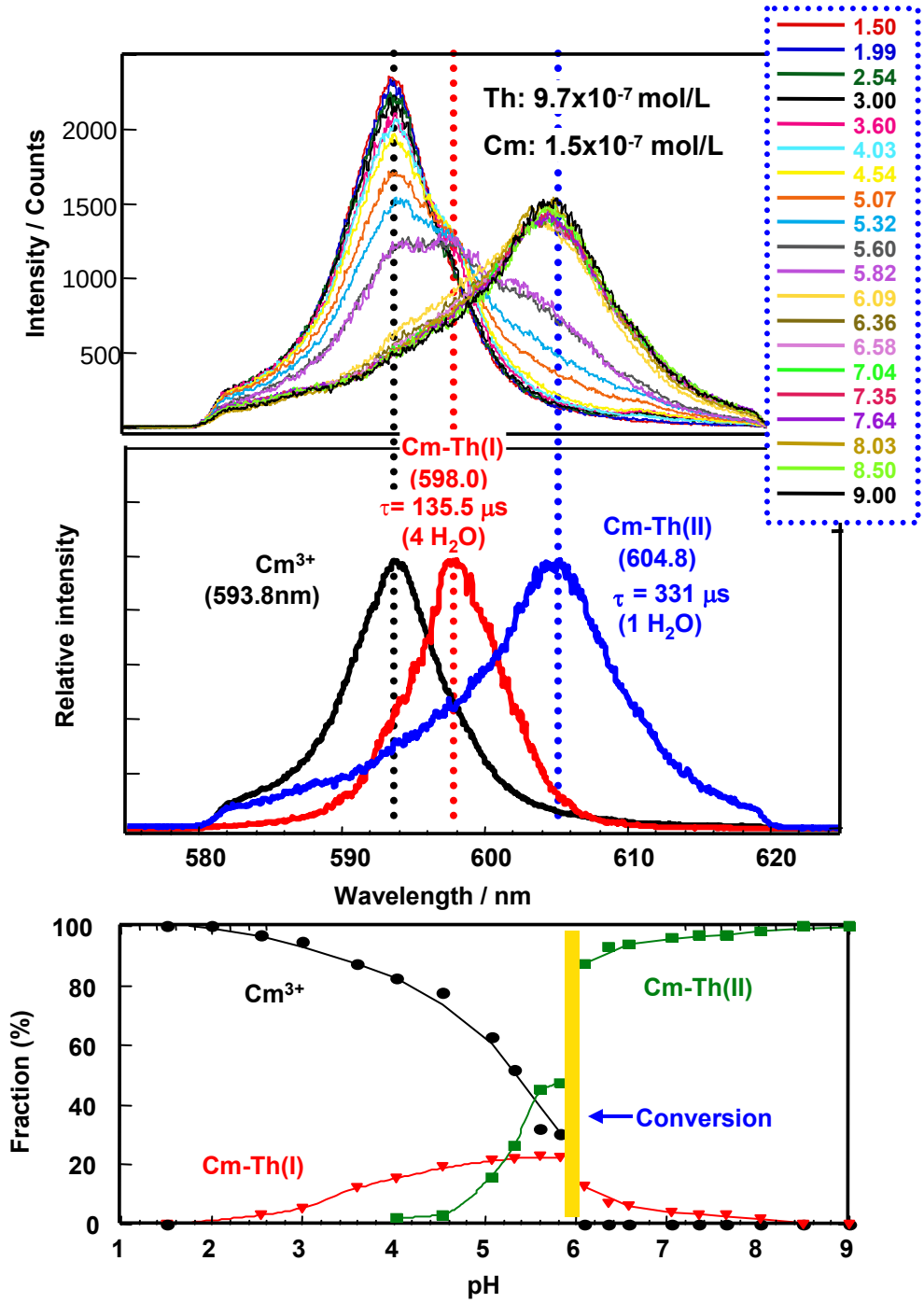

Fig. 78: Speciation of Th-borne Cm by TRLFS on the pH titration from 1 to 9 in a mixture solution containing 3.5×10^{-7} mol l^{-1} Th and 5×10^{-8} mol l^{-1} Cm: the pH dependent spectrum evolution (upper part) and the deconvoluted spectra of different Cm species present in the solution (middle part). The species distribution is given in the lower part.

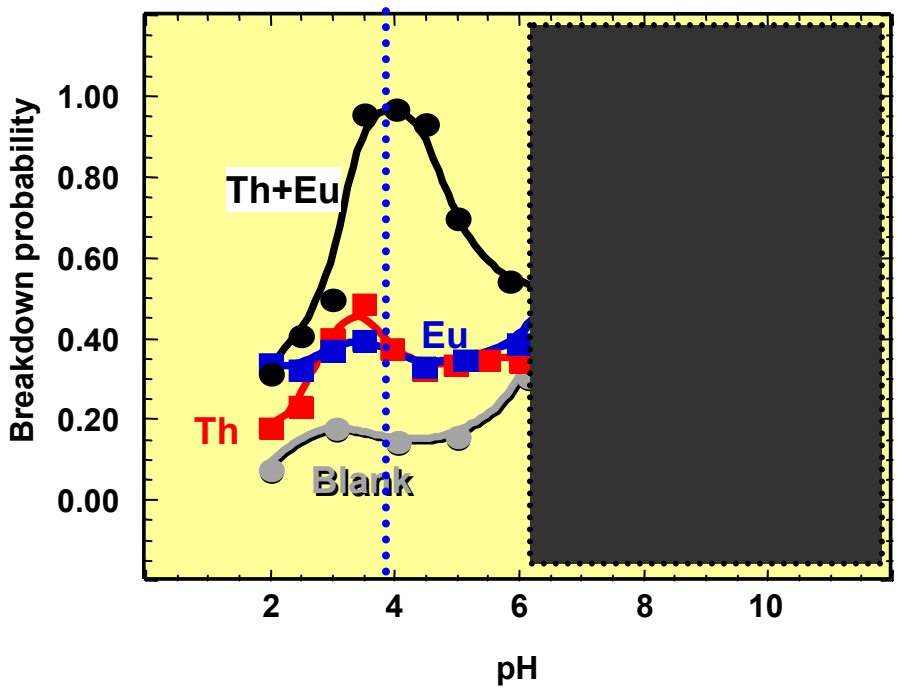

Fig. 79: Colloid generation observed by LIBD on the pH titration from 1 to 10 in a mixture solution containing 3.5×10^{-7} mol l^{-1} Th and 5×10^{-8} mol l^{-1} Eu (cf. Fig.78). Blank is water titrated by diluted HCl and NaOH. The latter contains colloidal impurities, which are however scavenged by Th for partial precipitation.

Table 1: Fluorescence emission properties of Cm in different solutions: a comparison. The Cm^{3+} aquoion has a emission peak at 593.8 nm with a life time of 65 μs and 9 inner sphere hydration water molecules

Solution	Parameter	Species (I)	Species (II)	Reference
Mixture of	Emission peak (nm)	598.5	601.8	this work
10^{-3} mol/l Si	Life time (μs)	83.5±3.7	88.3±5.2	
10^{-5} mol/l Al	H_2O molecule	6.9	6.4	
10^{-3} mol/l Si	Emission peak (nm)	598.5	601.9	this work
	Life time (μs)	85.5±6.1	88.1±8.5	
	H_2O molecule	6.8	6.5	
10^{-3} mol/l Al	Emission peak (nm)	598.2	604.1	this work
	Life time (μs)	82.0±2.9	110.5±6.7	
	H_2O molecule	7.1	5.0	
Colloidal	Emission peak (nm)	601.2	603.3	ref. 64
γ-Alumina	Life time (μs)	110	110	
	H_2O molecule	5.0	5.0	
Suspension	Emission peak (nm)	598.8	603.3	ref. 18
of smectite	Life time (μs)	110	110	
& kaolinte	H_2O molecule	5.0	5.0	
Colloidal	Emission peak (nm)	602.3	604.9	ref. 76
Silica	Life time (μs)	220±14	740±35	
	H_2O molecule	2.1	0	

Table 2: Comparison of colloid-borne Cm species without and with Th								
	HAS-Monosilanol					HAS-Polysilanol		
	Cm Species	Peak Max. (nm)	Relax. Time (μs)	Coord. Water (number)		Cm Species	Peak Max. (nm)	Relax. Time (nm)	Coord. Water (number)
Cm	Cm-HAS(I)	598.0	83.5	7		Cm-HAS(I)	598.5	83.5	7
	Cm-HAS(II)	601.8	88.5	6		Cm-HAS(II)	601.8	88.3	6
						Cm-HAS(III)	605.2	518.5	0-1
Cm+Th	Cm-Th(I)	598.0	132.8	4		Cm-Th(I)	598.5	135.3	4
	Cm-Th(II)	603.6	336.9	0-1		Cm-Th(II)	603.6	349.0	0-1

INSTITUT FÜR RADIOCHEMIE
TECHNISCHE UNIVERSITÄT MÜNCHEN

RCM 012004

EINFLUSS VON KOLLOIDEN AUF DIE MIGRATION VON ACTINIDEN

M. A. Kim, P. J. Panak, J. I. Yun*,*
J. I. Kim, A. Priemyshev, K. Köhler*

Abschlußbericht**
30.04.04

*Institut für Nukleare Entsorgung, Forschungszentrum Karlsruhe, 76021 Karlsruhe

**Das diesem Bericht zugrunde liegende Vorhaben wurde mit Mitteln des Bundesministeriums für Wirtschaft und Arbeit (BMWA) unter dem Förderkennzeichen 02E9360 gefördert. Die Verantwortung für den Inhalt dieser Veröffentlichung liegt bei den Autoren

Contents

1 Introduction

Colloids ubiquitous in natural water are called aquatic colloids. The chemical composition, number density and size distribution of aquatic colloids vary widely depending on the geochemical conditions of their provenance [1,2]. They may be composed of inorganic elements with oxo-bridges [3-5], of organic polyelectrolytes, like humic acid loaded with inorganic elements by complexation [6-9], or of tiny inorganic particles peptized by organic molecules [10-12]. The size distribution of predominant number density has been observed in general at < 100 nm, but very often at < 50 nm, as referred to an average hard sphere diameter [2,6,7]. The number density varies widely from 10^8 to 10^{14} particles per litre water depending on the geochemical environment [6,13]. Groundwater rich in organic substances, e.g. humic acid, contains abundant aquatic colloids [6,8], whereas groundwater poor in organic substances, e.g. granite water, contains a relatively smaller number density of aquatic colloids [13,14].

Aquatic colloids may play a significant carrier role for the radionuclide migration in a variety of aquifer systems [14-16]. Particularly radioactive elements of higher oxidation states, for example actinides with their strong tendency towards oxobridge building or complexation, possess a high potential for stable incorporation into aquatic colloids [2,6,14]. The formation of such aquatic colloid-borne actinides (called pseudocolloids of actinides) has not been well understood, besides the surface complexation of actinide ions onto aquatic colloids [17-19]. In the case the actinide ions are incorporated into the chemical structure of aquatic colloids, the colloid-borne actinides may remain stable as suspended in a given natural water and migrate along the water flow path with little chemical interaction with the surface of surrounding geomatrices [8,9]. Therefore, the provenance of aquatic colloids and the generation of aquatic colloid-borne actinides have become of great interest for a better appraisal of the chemical behaviour of actinide ions in natural aquifer systems [14,15,20] and also of the colloid facilitated actinide migration in aquifer systems [15,20-22].

The present work deals with the generation of aluminosilicate colloids, which are considered as a kernel for various aquatic colloids. Formation of the aluminosilicate binding is well known [23] and incorporation of traces of trivalent lanthanides and tetravalent elements like Th, has been observed in nature abundantly [24]. However, the generation of colloidal species of aluminosilicates and the chemical incorporation of actinides in such colloids have not yet been systematically understood. As the colloidal species of aluminosilicates are omni-

present in natural aquifer systems [1], the appraisal of their chemical interaction with tri- and tetravalent actinides is the main objective of the present investigation. For this purpose, the parameters controlling the formation of aquatic colloids through condensation of groundwater constituents, i.e. Si and Al, are identified, and the optimum conditions for aluminosilicate colloid formation are determined. The behaviour of the selected actinides Am(III), Cm(III) and Th(IV), either as contestants in the nucleation process of Si and Al, or as additives to preformed aluminosilicate colloids, is analyzed.

Am is the most abundant trivalent actinide in nuclear waste to be disposed of [2,25] and its chemical homologue Cm is smaller in waste amount but spectroscopically sensitive for the unperturbed speciation [26], thus allowing the study of its chemical behaviour conveniently. Th with its stable tetravalent oxidation state is the ideal model element to investigate the geochemical reactions of actinides with multiple oxidation states like Pu, U, Np and Tc which are the main components of long-lived radionuclides in nuclear waste and expected to be reduced to the tetravalent state at low redox potentials in the near field of a nuclear repository [25].

2 Natural and actinide aquatic colloids

The two general ways in which aquatic colloids may be formed, are by building up particles from dissolved molecular or atomic units, or by breaking down particles from the solid matrix, termed respectively condensation and dispersion:

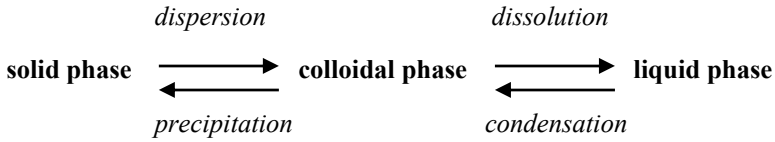

Fig. 1 (upper part) illustrates how elements with high oxidation state (≥ 3), such as Al(III), Si(IV) or actinides (An(≥III)) tend to minimize their positive charge by surrounding themselves as much as possible with oxygens through hydration, hydrolysis and polymerization. This process for colloid formation is called condensation and includes the formation of a supersaturated solution, the relieve of supersaturation by the formation of nuclei or by condensation upon nuclei already present, followed by growth to larger particles. The reverse process for colloid formation, namely dispersion (shown in Fig.1 (lower part)), involves weathering of

the parent solid material, which can be either physical disintegration or chemical decomposition, or both, and suspension of the small detached particles in the liquid phase.

Under certain optimum conditions, nanoparticles can thereby be stabilized in the colloidal phase, a process which is far from completely understood. This is partly due to the quite recent development of methods, such as ultrafiltration [6,8,9,14], laser-induced breakdown detection (LIBD) [27-32] or atomic force microscopy [33-37], which are capable to characterize small colloids (< 100 nm) in the low concentrations as they exist in nature, without perturbation. Numerous theoretical considerations concerning colloid generation and stabilization try to identify the underlying parameters and to describe their correlations in different models. Fundamental knowledge relevant to the present experimental investigations is conceptually summarized in the following.

2.1 Formation of colloids: theoretical background [1,38-43]

Colloidal interface free energy

The behavior of colloids is governed primarily by their large interfacial area. The interface is defined as the boundary between the adjoining bulk phases that comprise the colloid system, e.g. liquid/solid in the case of aquatic colloids. Within each bulk phase, forces acting on a molecule from all directions are balanced (Fig. 2). Molecules in the interface, however, interact simultaneously with molecules from both liquid and solid phases. Since forces of attraction are greater between the molecules of the solid phase than between those of the liquid phase, molecules in the interface are attracted more strongly towards the solid phase. The energy input, required to compensate for this imbalance of intermolecular forces, is the origin of the colloidal interface free energy. The high reactivity of colloids (activated solid state) stems from the tendency to minimize the free energy.

The questions are, where does this activation energy comes from, what kind of energy transfers do occur at deactivation, which mechanisms inhibit a complete deactivation so that the colloidal state, although thermodynamically unfavorable, persists over a long time span and how can we control the underlying parameters? Theoretical thermodynamic and kinetic approaches to the generation and stabilization of aquatic colloids, which might be helpful to conceive the appropriate experiments for answering such questions, are summarized in the following.

Formation of colloids through condensation

Spontaneous growth of particles out of their solution requires the formation of nuclei. The free energy of the formation of a nucleus, ΔG, consists of energy gained from making bonds and of work required to create a surface as expressed in thermodynamic terms:

$$\Delta G_j = - 4 \pi r^3 k_B T \ln S / 3 V + 4 \pi r^2 \gamma \qquad \text{Eq.1}$$

where r is the radius of the nucleus, V the molecular volume, k_B the Boltzmann constant, T the absolute temperature, S the supersaturation, ratio of actual concentration and solubility equilibrium concentration, and γ the interfacial energy (γ = = r kT ln S / 2 V). Fig. 3a shows the free energy of formation of a spherical nucleus as a function of its size, calculated for different supersaturation ratios (a/a_0). The height of the maximum, ΔG^*, is the activation barrier to the nucleation process of nuclei of radius r_j. Obviously, the activation energy ΔG^* as well as the size of the critical nucleus decrease with increasing supersaturation. Introduction of foreign solid surfaces for catalyzing the nucleation process by reducing the energy barrier of nucleation is the princip of heterogeneous nucleation, the predominant formation process for colloid and crystal formation in natural waters. If the foreign substrate is similar to the product of nucleating components, the interfacial energy between the two solids is smaller than the interfacial energy between the product and the solution, and nucleation may take place at lower supersaturation on a solid substrate surface than in solution. Temperature will also affect the value of the critical superaturation ratio.

This ratio decreases with rising temperature probably because of an increase in the number of collisions of atoms or molecules per unit concentration. The critical supersaturation ratio decreases when a system is subjected to turbulent effects, because of the probability of increasing concentration fluctuations in the form of some minute volumes of the solution with very high concentration.

The rate of formation of the nuclei, V_1, may be expressed by

$$V_1 = A \exp (- \Delta G^* / k T) \qquad \text{Eq.2}$$

where A is a factor related to the efficiency of collisions of ions or molecules. Accordingly, the rate of nucleation is controlled by the interfacial energy, the supersaturation, the collision

frequency efficiency, and the temperature. Fig.3b vizualizes the nucleation rate as a function of the critical supersaturation (ΔG^*) calculated for the following assumptions: $\gamma = 100$ mJ m^{-2}, molecular volume = 3 x 10^{-23} cm^3 and a collision frequency efficiency of 10^{30} cm^{-3} s^{-1}. At high supersaturation (low activation energy) the nucleation rate is high. Nucleation is ultimately superseded by growth of existing nuclei.

The rate of particle growth is determined by diffusion of substance from supersaturated volumes within the bulk towards those particles that are surrounded by thin envelopes of solution in equilibrium with the solid. It may be expressed by the general equation

$$V_2 = A\,(\ln S)^n \qquad \text{Eq.3}$$

where A and n are adjustable parameters.

The relative velocities of nucleation and growth, both processes competing for material in the supersaturated solution, determine the number as well as the size of the particles. At high supersaturation, the nucleation rate may be so fast that most of the excess dissolved mass is transformed in critical nuclei, leaving little material for further growth. Many small particles are formed. Few particles of huge size may be built at low supersaturation. Inhomogenity of the system with volumes of different degrees of supersaturation results in particles of various sizes (polydisperse system).

Colloidal electric double layer

Most substances acquire a surface electric charge when brought into contact with a polar (e.g. aqueous) medium, possible charging mechanisms being ionization, ion adsorption and ion dissolution. Ionization of functional groups depends strongly on the pH of the solution and leads to positively or negatively charged molecules at low pH and high pH, respectively. A net surface charge can further be acquired by the unequal adsorption of oppositely charged ions. Ion adsorption may involve positive or negative surface excess concentrations. Surfaces in contact with aqueous media are more often negatively charged than positively charged. This is a consequence of the fact that cations are usually more hydrated than anions and have the greater tendency to reside in the bulk aqueous medium, whereas the smaller, less hydrated and more polarizing anions have the greater tendency to be specifically absorbed. Surfaces which are already charged (e.g. by ionization) usually show a preferential tendency

to absorb ions of opposite charge, especially those with a high charge number. It may even cause a reversal of charge. If surfactant ions are present, their adsorption will usually determine the surface charge. In addition to specific adsorption, the net particle charge of some solids may arise either from the preferential dissolution of some ions and from lattice imperfections at the solid surface or by isomorphous replacements within the lattice.

The surface charge influences the distribution of nearby ions in the polar medium. Counter-ions are electrically attracted by the oppositely charged solids. At the same time, however, these ions have a tendency to diffuse away from the surface toward the bulk of the solution, where their concentration is lower. The net result of the two competitive tendencies is an equilibrium distribution of ions in which their concentration gradually decreases with increasing distance from the solid surface. Simultaneously, there is a deficiency of co-ions in the vicinity of the surface, since these ions, which have an electric charge with the same sign as the particle, are repelled. There is a gradual increase of co-ion concentration with the distance from the solid surface. The result is the generation of an electric double layer (EDL) at the solid-liquid interface, consisting of three regions with distinct dielectric behaviour (see Fig. 4): (1) the Stern layer, a layer of preferentially oriented water molecules in contact with the boundary, where the specific adsorbed bare ions are without their hydration shells; (2) the outer Helmholtz layer, a region of both free water molecules and molecules attached to hydrated ions, and defined by the closest approach of a fully hydrated charge ion to the boundary; (3) the Gouy-Chapman diffuse layer is the region where the concentration of the counterions decreases with increasing distance from the plane interface. The electric potential at the surface, Ψ_0, or the electric potential in the Stern plane, Ψ_δ, are not accessible by direct experimental measurement, but the surface potential can be calculated from the experimentally determined surface charge. The shear plane separates the hydrodynamically immobile liquid that moves together with the surface from the mobile liquid, which has non-zero relative velocity with respect to the surface. The electric potential in the shear plane is reflected by the measurable potential gradient that arises across the mobile part of the double layer, the electrokinetic ζ potential. The double-layer thickness is given by the reciprocal Debye length:

$$1/\kappa = (\varepsilon R T / 8 \pi F^2 c z^2)^{1/2} \qquad \text{Eq.4}$$

where ε is the dielectric constant of the medium, F is the Faraday constant, c and z are the concentration and the valence of the electrolyte, respectively. Increase of the ionic strength decreases the thickness of the double-layer.

Brownian motion of colloids

Water molecules in permanent random thermal movement hit the colloidal particles from opposite sides. The smaller the particles, the less the probability of the molecular bombardment being exactly balanced and the more intensive will be the movement. A consequence of this Brownian movement is the diffusion of colloid particles. When a certain phase is dispersed along the x axis, the mass, dm, transferred across an area O, during an interval, dt, as a result of a concentration gradient, dc/dx, is given by Fick´s first low:

$$dm/dt = - D O (dc/dx) \qquad \text{Eq.5}$$

where D is the diffusion coefficient. D depends on the properties of the disperse phase and the dispersing medium. For colloid particles D is related to the friction coefficient, B, between the particles and the dispersing medium by the expression $D = k_BT/ B$. The magnitudes of B and D depend on the dimensions and shapes of the particles. For spherical particles having a radius r, when the viscosity of the dispersing medium is η, B □□□□□□ 6 πη□ □□□.

$$D = k_BT/ 6 \pi\eta\square \qquad \text{Eq.6}$$

The Brownian motion is the dispersing energy of colloids and also the reason for frequent collisions between them. Depending upon wether the interaction forces between the particles during such collisions are attractive or repulsive, the colloids will agglomerate or stabilize (elaborated below). The movement of small colloids (e.g. < 100 nm), as they occur in the natural environment, is diffusion-limited (due to Brownian motion only). Other colloid transport mechanisms based on differential gravitational settling or caused by laminar shear being important only for large particles (≥ 1μm) are therefore not considered here.

Colloid stability: DLVO theory

Two suspended particles of like charge approaching each other as a result of their Brownian movement until their diffuse double layers interpenetrate and deform, is the basis for the quantitative description of particle-particle interaction by the DLVO (Derjagin, Landau, Verwey, Overbeek) theory. The potential energy of interaction (E_t) is calculated as the superposition of the electrostatic repulsive energy (E_R, conventionally considered positive), which is approximately an exponential function of the interparticle distance (d) with a range of the order of the thickness of the double layer ($1/\kappa$), and the van der Waals attractive energy (E_A, considered negative), which decreases as an inverse power of the interparticle distance, by the following equation (simplified and valid for thick plate particles, e.g. clay tactoids):

$$E_t = E_R + E_A = (64\ c\ R\ T\ \Gamma^2 / \kappa)\ (e^{-\kappa d}) - (K / 2\ d^2) \qquad \text{Eq.7}$$

where K is a constant depending on the nature of the dispersing medium, the particle thickness and its chemical composition, and Γ is defined as follows:

$$\Gamma = [(\exp(z\ F\ \Psi_\delta / 2RT)) - 1] / [(\exp(z\ F\ \Psi_\delta / 2RT)) + 1] \qquad \text{Eq.8}$$

Two general types of potential energy curves are presented in Fig. 5: in (a) $E_R > E_A$ and the total potential energy curve (E_t) shows a repulsive energy maximum, whereas in (b) the van der Waals attraction (E_A) predominates at any interparticle distance. The maximum in the energy curve is an energy barrier. If the potential energy maximum is large compared with the thermal energy of the particles (RT), the system should be stable; otherwise, the system should agglomerate.

The height of this energy barrier to agglomeration depends on the magnitude of Ψ_δ (and ζ) (Eq.8) and upon the repulsive forces (i.e. upon $1/\kappa$) (Eqs 4, 7). The DLVO theory to explain stabilization of colloids has been extended and may include, besides van der Waals attraction and electrostatic repulsion forces, also steric forces (generally repulsive) as well as polymer bridging forces (attractive) induced by adsorbed long-chain polymer.

Colloid stability: kinetics

Colloid stability depends on an energy barrier and is therefore also a question of kinetics and rates of agglomeration. In kinetics of the agglomeration process rapid and slow agglomerations are distinguished. In the case of rapid agglomeration so much electrolyte has been added that the energy barrier is reduced and is absent or too small to prevent particles from coming into contact (critical electrolyte concentration). Every collision results in irreversible agglomeration. In such a case the time-dependent decrease in concentration of particles (N = number of particles per cm^3) in a monodisperse suspension due to collisions by Brownian motion can be represented by

$$- dn/dt = k_p N^2 \qquad \text{Eq.9}$$

where k_p is the rate constant ($cm^3\ s^{-1}$). As given by von Smoluchowski, k_p can be expressed as

$$k_p = 8\ D\ \pi\ r \qquad \text{Eq.10}$$

The diffusion coefficient in Eq. can be subtituted in Eq.

$$- dn/dt = 4\ k_B T\ N^2 / 3\ \eta \qquad \text{Eq.11}$$

and it may be concluded that in monodisperse systems the rate of fast coagulation is not dependent on the size of the particles (r).

In practice, the right hand side of eq. is multiplied by α_p. α_p is the fraction of collisions leading to permanent agglomeration. It is an operational parameter for the stability ratio, the Fuchs-factor, $W = 1/\alpha_p$. α_p is the ratio of the slower agglomeration rate (in the presence of an energy barrier) and the fastest, diffusion controlled agglomeration rate (in the absence of an energy barrier), determined under the corresponding appropriate experimental conditions. The extended Smoluchowski theory for polydisperse systems shows that the rate of coagulation between particles of different sizes is much greater than the rate of coagulation of particles of the same size. The smaller particles disappear much more quickly than the larger one.

2.2 Actinide colloid generation pathways

Actinides may become aquatic colloids by two processes as illustrated in Fig. 6: (1) by binding to natural aquatic colloids and formation of so-called „pseudocolloids“ of actinides. The binding can proceed either by conucleation of actinides with dissolved groundwater components or by sorption of actinides to existing natural colloids; (2) by the formation of „real colloids“ either through nucleation of actinides in the order [14]

$$An^{4+} > AnO_2^{2+} > An^{3+} > AnO_2^{+}$$

or through dispersion of a solid actinide matrix.

2.3 Methods selected for actinide colloid analysis

Investigations of the geochemical behaviour of the sparingly soluble actinides (usually below 10^{-6} mol l^{-1}) in presence of ubiquitous small aquatic colloids (< 50 nm) in low concentrations (ppb range or less) require sophisticated analytical methods which have been developed in the last decade [26-35,44,45]. A brief overview of the principals of those methods, which have been used in this study for the nanoscopic analysis of aquatic actinide species under minimal perturbation of the system is presented here.

Laser spectroscopic methods

Conventional absorption spectroscopy on the transitions of the 5f-electron shell of actinides is a useful speciation method for the characterization of oxidation and complexation states. The spectroscopic resolution of actinide transition bands is in general very high but their intensity is relatively weak [46]. The low solubility of actinides under natural conditions necessitates a speciation method of high sensitivity. To that purpose, a number of spectroscopic methods have been developed in the recent past based on laser as a light source.Various laser spectroscopic techniques appropriate for the speciation of trace level actinides are illustrated schematically in Fig. 7.

The enhancement of sensitivity is attained by a direct measurement of different relaxation processes of photon excited states, instead of transmission measurement as practiced in

conventional absorption spectroscopy [47]. The methods shown in Fig. 7 can be classified in the following four categories: photo-thermal spectroscopy, luminescence spectroscopy, light-scattering and plasma generation. From those methods, TRLFS (time-resolved laser fluoresence spectroscopy) and LIBD (laser-induced breakdown detection) are used in this work. TRLFS is based on the measurement of radiative relaxation of a light induced excitaton state as illustrated in Fig. 8 for the example of Cm(III). The characteristic of this method is the selective excitation of the ground state combined with the selective time-resolved measurement of emission by an optical multichannel analyzer consisting of a polychromator and a time-gateable intensified photodiode array. All these provide a high sensitivity in the actinide speciation. However, the method is limited to the elements with fluoresence emission, to which belong some rare earth elements (REE(III)) and Cm(III) [20,26], Am(III) [48] and U [49,50] as actinides. With these elements, the aquatic chemical behaviour of trivalent and hexavalent actinides can be investigated in the nano-mole concentration range.

LIBD has been developed to quantify groundwater colloids with low number density and small average size [28,29]. The method is based on the plasma generation of colloidal particles by intense laser light absorption [30] as illustrated by Fig. 9.

The event takes place, upon multi-photon absorption, through the excitation and ionization avalanche of delocalized electrons within a colloidal composite and hence it is called breakdown. As the treshold energy density required for solid is much lower than for liquid, the plasma generation occurs with colloids selectively in their suspension medium. The breakdown event can be detected by measuring the plasma light emission with a charge-coupled-device (CCD) camera or by detecting the photo-acoustic signal with a piezo electric detector (PZT). The two-dimensional distribution of 8000 plasma events is measured in parallell as well as perpendicular to the laser beam direction (Fig. 10). The distribution width is correlated to the mean particle size (Fig. 11). By calibration of LIBD with polystyrene reference particles, a mean particle diameter and a number density of given colloids can be derived [27-32] as shown in Fig. 12. A sensitivity comparison of LIBD with that of light scattering methods, i.e. static light scattering and photon correlation spectroscopy (PCS) is shown in Fig. 13. In the low part of particle size, LIBD appears distinctively more sensitive than light scattering over many orders of magnitude.

In the course of plasma relaxation, the discrete plasma or atomic emission takes place after the recombination of electrons as shown in Fig. 9. The process can be used, as laser-induced breakdown spectroscopy (LIBS), for the characterization of colloid-borne elements

selectively in solution [31,32]. Accordingly, actinides present as ionic and colloid-borne species in aquatic systems can be differentiated by LIBS, since the colloid-borne actinides are better excited than their aqueous ions by the same laser energy intensity. This is a particular speciation method to detect pseudocolloids of actinides in groundwater, which may be used in our further continued study.

Atomic force microscopy (AFM)

AFM is a nanotopographic method scanning the repulsive and attractive forces between atoms of a SiN_3-tip, used as a sensor, and surface atoms of the sample at a separation distance of a few Å. Detection of the corresponding movements of the cantilever-tip is performed as shown in Fig.14, by sending laser light on the sample and registering the reflected light by a 4-quadrant photodetector. Interatomic force is calculated from the light intensity differences in the four quadrants. The attained resolution is 0.01 nm (0.1 Å) and the sample surface is 1nm up to 1 μm. Nano-topographical changes in the sample, e.g. during dissolution, colloid growth, sorption, etc. can be observed in situ. This is an advantage over electron microscopy requiring a vacuum resistent sample preparation.

Conclusions of section 2

Inorganic aquatic colloids in general and real colloids of actinides in particular may be generated either by condensation of dissolved elements or by dispersion of the solid matrix. The anabolic formation of inorganic aquatic colloids through condensation is based on the tendency of polyvalent cations of natural or radioactive elements such as actinides to reduce their positive charge through polymerization. The activation energy required to generate a solid surface out of dissolved elements originates from the supersaturation state of the solution. The degree of needed supersaturation varies with particle size. Supersaturation can partly be replaced by the presence of a foreign surface in the solution on which the nucleation can take place (heterogeneous nucleation). The generated particles follow the thermal movement of the water molecules, collide with one another and agglomerate. Three conditions to prevent agglomeration and to stabilize the particles at colloidal size are: (1) the generation of a particle surface charge through ionization, ion adsorption or ion dissolution; (2) the formation of an electric double layer around the charged particle with the aid of a well optimalized

ionic strength in the solution; (3) the presence of a repulsive maximum in the potential energy curve as a function of the interparticle distance (formation of an energy barrier to agglomeration) under well balanced conditions of surface charge and colloidal double layer thickness. Colloid generation as well as stabilization depend on energy barriers and are therefore not only a question of thermodynamics but also of kinetics. The underlying parameters are the parameters of solubility. The catabolic dispersive formation of inorganic aquatic colloids proceeds through the reversal of polymerization reactions. A further possibility to transfer actinides into the colloidal state is the formation of pseudocolloids of actinides either through co-condensation with natural elements in solution or through binding with preformed natural aquatic colloids.

The experimental investigation of the mentioned possible processes for the generation of natural as well as actinide aquatic colloids may rely on modern methods such as TRLFS, LIBD and AFM, which are capable to analyze the behavior of nanoconcentrations of actinides interacting with colloidal nanoparticles in ppb concentrations.

3 Synthesis of natural aquatic colloids

From the forgoing theoretical considerations (section 2.1) we have learned which parameter influence colloid formation and why they do so. We have also recognized that colloid formation and stabilization is a very complex process depending on the subtile tuning of a hughe number of parameters which can influence each other reciprocally. It is therefore not amazing that the conditions for the formation of aquatic colloids cannot be predicted theoretically but should be deduced from empirical experiences. The following section is based on colloid theory but concentrates on an experimental approach to colloid generation.

3.1 The choice of aluminosilicate colloids

The most common condensation process occurring in the hydrosphere is the hydrolysis of polyvalent cations (e.g. Si^{4+} and Al^{3+}), the formation of sparingly soluble hydroxides and hydrous oxides and the neoformation of clay minerals at coprecipitation. It seems therefore meaningful to choose clays as a representative example for answering questions about the formation of natural aquatic colloids as well as about their interaction with actinides. But

before concentrating on the synthesis of aquatic clay colloids, lets have a look on their closest relatives, the clay minerals.

Clay minerals are essentially hydrous layer aluminosilicates (phyllosilicates), with Mg and Fe acting as proxy wholly or in part for the Al in some minerals and with alkali metals and alkaline earth metals present as essential constituents in some of them. As illustrated in Fig. 15 [51], there are three types of phyllosilicates, namely, (1) the 1:1 type unit layer silicates (also known as the TO type), e.g. kaolinite, in which there is one tetrahedral sheet for every octahedral sheet, (2) the 2:1 type unit layer silicates (TOT type), e.g. smectite, illite, and (3) the 2:1:1-tape unit layer ([TOT]O[TOT], in which brucite ($Mg(OH)_2$-mineral)-type sheets lie between the parallel 2:1-type silicate layers, e.g. chlorite. The phyllosilicates are divided into groups according to the net charge of the unit layer.

A further subdivision is based on the number of available octahedral sites occupied: Those minerals containing divalent cations are called trioctahedral since all the available cation sites are filled, whereas minerals containing trivalent cations are called dioctahedral, having only two-third of the octahedral sites filled. Another subdivision is based on whether or not the stacked 1:1- or 2:1-type unit layers can be expanded and on the ease of swelling of the interlayer space either with water (compare illite and smectite) or with organic liquids. Each subgroup contains the different clay mineral species, which are distinguished by their chemical compositions. An additional group includes those clay particles with more than one type of layer present, termed mixed-layered minerals. These minerals belong to the sepiolite-palygorskite group. A further special type of highly hydrated secondary aluminosilicates are allophane and imogolite with an Si/Al-ratio of 0.5-1.0. They consist of small hollow spheres or cylindrical particles with a diameter of 3.5-5.0 nm (see Fig. 16). The AlOH outer surface is connected with the SiOH inner surface [52,53] through O-bridges. Their structure is limited to the range of very small particles (short-range order) which is in contrast to the other clay minerals. Recently much attention has been paid to aqueous hydroxy-aluminosilicates (HAS) of the imogolite type in many diverse contexts [23,54,55]. Besides their geochemical relevance, HAS play an important role in the oil industry, the paper industry, the production of zeolites, molecular sieves and catalysts. HAS seem further to be involved in biochemical reactions related to the toxicity of Al and discussed as inducers for a variety of plant, animal and human disorders, e.g. Alzheimer and Parkinson disease. The review article by Swaddle et al. [23] summarizes the present knowledge on silicate complexes of Al(III) in aqueous systems. He concludes: „The biomedical implications of the kinetic studies on Al(III)-Si(IV) interactions

at high pH by the NMR method are that simple hydroxyaluminosilicate (HAS) probably form and dissociate quickly even at low to neutral pH, so that their physiological behavior is thermodynamically controlled. However, the sequestration of Al(III) by oligomeric Si(IV), which the results of Taylor et al. [56] suggest, may be much more physiologically important, may yield kinetically inert HAS species - indeed, the apparently high stability of such complexes may well reflect the slow dissociation kinetics. Thus, a significant part of the protection afforded by silicic acid against Al(III) toxicity in biological systems may derive from the inferred kinetic inertness of ring or cage HAS structures which, once formed, may retain the Al(III) for long periods. The geological implication is that small acyclic HAS species and not the ring HAS solutes are the active agents in the hydrothermal crystallization of zeolites. The inert cage aluminosilicate solutes may act merely as reservoirs for the slow hydrolytic release of the small, active, acyclic species responsible for crystal growth."

The above statements reflect not only the high probability that very stable aqueous aluminosilicate colloids may be formed even under common environmental conditions, but at the same time they show that current knowledge, as far as colloid stability or generation mechanisms are concerned, is quite poor and that there is need for research. For this purpose, we intend in a first approach to coprecipitate Si and Al under conditions of supersaturation and to analyze in a coprecipitation parameter screening experiment whether and if yes, under which circumstances, the process is accompanied by the formation of aluminosilicate colloids.

3.2 Conditions for coprecipitation of Si and Al

Key information on how to attain supersaturation and coprecipitation of Si and Al is gained from thermodynamic solubility data for Si, Al and aluminosilicates. The main solubility parameter are temperature, pressure, pH, ionic strength, kind and concentration of water borne anions (ligands such as carbonate, sulphate, humate) and water borne cations (Na^+, K^+, Ca^{2+}, Mg^{2+}, $Fe^{2+/3+}$). Solubilities of Si, Al and some aluminosilicates as a function of pH at constant normal temperature, pressure and 0.03 mol l^{-1} NaCl are calculated from:

(1) The solubility products of the amorph solid phases of Al and Si, namely $Al(OH)_3$ and SiO_2, and of the mixed solid phases of Al and Si, namely Al_2SiO_5 (sillimanite), $Al_2Si_2O_5(OH)_4$ (kaolinite) and $NaAlSi_3O_8$ (low albite) based on the reactions:

$Al(OH)_{3(am)} + 3\ H^+ \Leftrightarrow Al^{3+} + 3\ H_2O$ $pK_{sp}^0 = -9.66$

$SiO_{2(am)} + H_2O \Leftrightarrow H_4SiO_4^0$ $pK_{sp}^0 = 2.71$

$Al_2SiO_5 + 6\ H^+ \Leftrightarrow 2\ Al^{3+} + H_4SiO_4^0 + H_2O$ $pK_{sp}^0 = -15.45$

$Al_2Si_2O_5(OH)_4 + 6\ H^+ \Leftrightarrow 2\ Al^{3+} + H_4SiO_4^0 + H_2O$ $pK_{sp}^0 = -7.30$

$NaAlSi_3O_8 + 4\ H^+ + 4\ H_2O \Leftrightarrow Na^+ + Al^{3+} + 3\ H_4SiO_4^0$ $pK_{sp}^0 = -2.76$

(2) The hydrolysis constants for the reactions:

$Al^{3+} + 2\ H_2O \Leftrightarrow Al(OH)^{2+} + H_3O^+$ $pK_{11} = 5.02$

$Al^{3+} + 4\ H_2O \Leftrightarrow Al(OH)_2^+ + 2\ H_3O^+$ $pK_{12} = 9.30$

$Al^{3+} + 6\ H_2O \Leftrightarrow Al(OH)_3^0 + 3\ H_3O^+$ $pK_{13} = 14.99$

$Al^{4+} + 8\ H_2O \Leftrightarrow Al(OH)_4^- + 4\ H_3O^+$ $pK_{14} = 23.33$

$Al^{5+} + 10\ H_2O \Leftrightarrow Al(OH)_5^{2-} + 5\ H_3O^+$ $pK_{15} = 34.24$

$2\ Al^{3+} + 4\ H_2O \Leftrightarrow Al_2(OH)_2^{4+} + 2\ H_3O^+$ $pK_{22} = 7.69$

(3) The dissociation constants for the reactions:

$H_4SiO_4^0 \Leftrightarrow H_3SiO_4^- + H^+$ $pK_{a10} = -9.71$

$H_4SiO_4^0 \Leftrightarrow H_2SiO_4^{2-} + 2\ H^+$ $pK_{a20} = -22.98$

$H_4SiO_4^0 \Leftrightarrow HSiO_4^{3-} + 3\ H^+$ $pK_{a30} = -32.85$

$H_4SiO_4^0 \Leftrightarrow SiO_4^{4-} + 4\ H^+$ $pK_{a40} = -45.95$

$4\ H_4SiO_4^0 \Leftrightarrow H_6Si_4O_{12}^{2-} + 2\ H^+ + 4\ H_2O$ $pK_{a64} = -13.32$

The given equilibrium constants [57-65] permit to calculate the concentration of each species as a function of pH, namely Al^{3+}, $Al(OH)^{2+}$, $Al(OH)_2^+$, $Al(OH)_3^0$, $Al(OH)_4^-$, $Al(OH)_5^{2-}$, $Al_2(OH)_2^{4+}$, for Al (Fig. 17); $H_4SiO_4^0$, $H_3SiO_4^-$, $H_2SiO_4^{2-}$, $HSiO_4^{3-}$, SiO_4^{4-} , $H_6Si_4O_{12}^{2-}$, for Si (Fig. 18); $H_4SiO_4^0$, Al^{3+}, $Al(OH)^{2+}$, $Al(OH)_2^+$, $Al(OH)_3^0$, $Al(OH)_4^-$, $Al(OH)_5^{2-}$, $Al_2(OH)_2^{4+}$, for aluminosilicates. Summation of the separate solubility curves gives the total solubility curve.

Fig. 19 compares the total solubility curves for Si, Al, and for the mentioned aluminosilicates. The pH range of interest, in which colloids can be formed in the course of coprecipitation, is selected according to the low solubility region of the different aluminosilicate compounds. Among them, sillimanite is the most soluble, whereas kaolinite is the least solu-

ble in the near neutral pH range, both following the similar pH dependency and showing the lowest solubility at pH 6.0. Low-albite shows the solubility behaviour different from that of sillimanite and kaolinite, decreasing sharply from pH 4.0 to 6.0 and remaining low with pH increase. Amorphous $Al(OH)_3$ is similarly soluble as sillimanite, while SiO_2 shows a constant solubility up to pH 9. Following Fig.19, the pH range for the present investigation is chosen from 4 to 9. Three initial concentrations of Si, namely 10^{-4}, 10^{-3} and 10^{-2} mol l^{-1}, below and above the saturation concentration (2 x 10^{-3} mol l^{-1}) are combined with varying Al concentrations from 10^{-7} to 10^{-3} mol l^{-1}.

3.3 Parameter screening experiment for colloid formation

The screening experimental princip, namely oversaturate solutions of Si and Al by changing the pH and trace colloid formation by observing the behaviour of ^{241}Am as a contestant in the coprecipitation process of Si and Al, is realized in three steps as shown in Fig. 20: (1) an acidic Al-solution traced with ^{241} Am (10^{-7} mol l^{-1}) is titrated with an alkaline Si-solution to a preset pH; (2) the precipitate is removed from the coprecipitation sample by filtration at 450 nm pore size and the colloids are removed from the solution (ionic+ colloidal species) by ultrafiltration at 1.8 nm pore size; (3) after different conditioning times, from 3 h to 35 days, the activity fraction in solution with and without colloids is measured by liquid scintillation counting and the activity fraction (%, related to the input activity) in solution (non-colloidal), colloids and precipitate is evaluated. The special advantage of using Am to trace colloid formation is to restrict automatically the screening to such colloids which are prone to incorporate actinides.

A typical experimental result is shown in Fig. 21, for which 10^{-3} mol l^{-1} Si, 10^{-5} mol l^{-1} Al and 4.9 x 10^{-8} mol l^{-1} Am are mixed initially at the ionic strength of 0.03 M NaCl. The Am activity fraction, evaluated as a function of pH, is shown for the first filtrate (at 450 nm pore size) normalized to the initial activity, and for the second filtrate (at10 kD-pore size) normalized to the Am activity of the first filtrate. Fig. 21a shows the pH dependent Am activity fraction, comprising the ionic and colloidal species (so called „mobile“ species), namely the Am activity fraction in the first filtrate separated from the precipitate by a filter of 450 nm pore size. The aging of the solution from 0 to 35 days does not lead to a significant change in the Am activity in solution. However, the solution pH changes slightly to acidic with time and stabilizes after some time. The lowest Am activity fraction in solution is found around pH 6,

which corresponds to the lowest solubility of aluminosilicate compounds as shown in Fig. 19 for sillimanite and kaolinite. This fact suggests the incorporation of Am into aluminosilicate formation. As the initial Al concentration taken for this experiment (Fig. 19) is at 10^{-5} mol l^{-1}, the precipitation is expected around pH 6. If the primary aluminosilicate precipitate is either sillimanite or kaolinite like (cf. Figs. 15 and 19), their solubility changes sensitively in the pH region of 4-9. The Am activity fraction observed in the solution changes sensitively in the pH range of 5-7, suggesting its incorporation into aluminosilicate formation. A separate experiment with a pure Am solution of 4.9 x 10^{-8} mol l^{-1} (also in Fig. 21a) shows a decrease of its activity fraction in the filtrate at 450 nm pore size with increasing pH and the Am activity fraction in solution remains low at pH > 6.5, being significantly different from that of aluminosilicate solutions.

The Am activity measured in the pure Am solution follows closely the solubility behaviour of an amorphous $Am(OH)_3$ precipitate (cf. Fig. 22) [66]. The difference of the Am activities between the aluminosilicate solution and its pure solution at pH > 6.5 appears another indication that Am is associated with aluminosilicate formation. Fig. 21b illustrates the colloid-borne Am activity fraction as a function of pH, which is normalized to the activity in the first filtrate from 450 nm pore size, i.e. the colloid fraction within the solution after the separation of precipitate. The colloid-borne Am in the first filtrate prevails at pH > 5 after 35 days of reaction time. At pH 4 about 20% Am appears colloid-borne and its fraction within the solution increases at pH ≥ 5 to more than 95%, then remains constant up to pH 9. Aging of the composite solution up to 35 days does not show a visible change in the colloidal Am fraction at pH > 6. Only at pH 5, the colloidal Am fraction increases with time. Fig. 21b indicates that the predominant solution species of Am at pH > 6 is colloidal and remains stable under present experimental conditions. The colloidal Am fraction in solution appears independent of different degrees of precipitation observed in Fig. 21a. The experiment shown in Fig. 21 is further conducted for a wide variety of the initial Si and Al concentrations and their different ratios in order to ascertain the conditions for the colloid formation. The main result of the screening experiment for aluminosilicate colloid formation is summarized in two time dependent contour diagrams representing the colloid-borne Am fraction (%) as a function of pH in mixture solutions of Si and Al after 3 hours up to 35 days sample conditioning time for two concentration levels of Si in the mother solution, just below (Fig. 23) and above (Fig. 24) the Si saturation concentration (2 x 10^{-3} mol l^{-1}), each of them combined with increasing concentrations of Al from 10^{-7} to 10^{-3} mol l^{-1}. Two characteristic pH regions are distinguished for

the colloid formation: around pH 5 for a minor fraction and between pH 7 and 9 for a major fraction. As the solubility of aluminosilicate compounds is lowest at pH 6 (see Fig.19), the colloid formation appears to be accordingly minimal around this pH region. The equilibrium for colloid formation is slowly reached in case that Si in the mother solution is undersaturated (Fig. 23), but the reaction of the Al^{3+} ion (also Am) with over-saturated Si as starting reactant (Fig. 24) proceeds promptly, reaches equilibrium within 3 hours and the result is not changed virtually up to 35 days and longer.

Fig. 25 illustrates an overview of the formation of colloid-borne Am as a function of pH for different Si/Al ratios in the mother solutions 35 days after mixing Si, Al and Am. Essentially three characteristic regions for optimum formation of stable colloids are differentiated. The first and second optimum arise from the slightly undersaturated Si solution at pH 5-6 and pH 8-9, respectively, and the third optimum from the 6.4 times saturated Si solution at pH 8-9, in each case a Si/Al ratio in the mother solutions of 100, namely for the following two optimalized concentration combinations:

I: $[Si] = 10^{-3}$ mol l^{-1} (0.7 x sat.) + $[Al] = 10^{-5}$ mol l^{-1} ([Si]/[Al] = 100)

II: $[Si] = 10^{-2}$ mol l^{-1} (6.4 x sat.) + $[Al] = 10^{-4}$ mol l^{-1} ([Si]/[Al] = 100)

The distinct screening patterns for colloid formation as a function of pH as well as of time, depending on whether Si in the mother solution is under- or oversaturated might be related with the expected different polymerization kinetics of Si as a function of pH and at increasing concentration [67], and prompts us to check the polymerization behaviour of Si under our experimental conditions. The understanding of the conditions for the formation of mono- and polysilanol is especially important since polysilanol is known to possess a 10^6 times higher affinity for Al than monosilanol [56]. The fact implies that the formation processes of aluminosilicate colloids and hence their interaction with Am may also be different, depending on whether monosilanol or polysilanol is involved as an initial reactant.

3.4 Mono- and polysilanol for condensation with Al

The following experiments serve the general comprehension of the generation of polysilanol under possible dynamic environmental conditions, not only out of solution through nucleation at oversaturation (polymerization of Si), but also out of the solid geoma-

trix through dispersion (depolymerization of Si). Within that study, special attention is drawn to the polymerization behaviour of Si under the previously mentioned optimum conditions for colloid formation at coprecipitation of Si, Al and Am.

The formation of polysilanol from sodium-waterglass (7.0 M Si in 4.0 M NaOH) are examined, as illustrated in Fig. 26, via two different approaches, respectively: By dilution to the alkaline pH = 12, monosilanol remains prevailed (see Fig. 19) and after subsequent adjusting the pH to neutral (pH = 5 - 9), monosilanol is converted to polysilanol under the condition of over-saturation (approach A); By dilution to the neutral pH range, polysilanol is produced by over-saturation of silanol in its low solubility region (approach B). The two approaches show the Al effect on the polymerization and depolymerization of Si in solution, respectively, and give an insight into the formation of aluminosilicate colloids.

Polymerization of Si is analyzed by approach A (Fig. 26) and made by dilution of sodium-waterglass to $2x10^{-3}$ – $4.2x10^{-2}$ mol l^{-1} Si at pH 12, in which monosilanol prevails. The solution is then neutralized to pH = 5 – 9 to make over-saturation of silanol, i.e. 1 - 21 times of the solubility saturation concentration of amorphous silica ($2x10^{-3}$mol l^{-1}) in the given pH range [68-71]. A conversion of monosilanol to polysilanol as a function of time is quantified by the molybdenum-test [67,72]. The result is illustrated in Fig. 27 and shows that the polymerization rate of silanol e.g. for the 6.4 times over-saturation (optimum conditions II) is pH dependent and completed after 5 days to a level of solubility constrains of amorphous silica, namely to about 85% mole fraction of polysilanol. Under the same condition, as expected, the polymerization does not take place in the non-saturated Si solution ($\leq 2x10^{-3}$ mol l-^{1} Si) (optimum conditions I).

The Si concentration effect on the polymerization is summarized in Fig. 28 for different pH and after different time intervals, namely 1 day (Fig.28, upper part) and 10 days (Fig. 28, lower part). At $4.2x10^{-2}$ M Si (21 x saturation concentration), the polymerization proceeds promptly and reaches a polysilanol mole fraction of 95%, as expected from the solubility of amorphous silica. A slower polymerization is observed at $1.3x10^{-2}$ M Si (6.4 times saturation concentration), especially at low pH. At $5x10^{-3}$ M Si (2.5 times saturation concentration), the completion of polymerization is considerably slow and at pH 5.5 it takes over 200 days. The upper limit of polymerization depends on the original Si concentration, which corresponds to a thermodynamic solubility level of amorphous silica, whereas the kinetics of polymerization is directly influenced by pH as well as concentration of Si. At low pH and at low Si concentration, the polymerization rate is low.

Depolymerization of Si is tested following approach B (Fig. 26). After polysilanol is produced by neutralizing dilution of sodium-waterglass to $4.2x10^{-2}$ M Si at pH = 7 (21x oversaturation, cf. Fig. 28), the depolymerization is measured, as illustrated in Fig. 29, at different degrees of dilution in the pH range of 6 - 8. By dilution of polysilanol to $5x10^{-3}$ M Si, the depolymerization takes place to a steady level of about 60%, which corresponds to the solubility of amorphous silica. The polymerization of monosilanol at the same Si concentration appears to reach the same level. At further dilution to $< 2x10^{-3}$ M Si, the depolymerization is quantitative. As is apparent from Figs. 27-29, the polymerization and depolymerization of Si are reversible processes, unless foreign metal ions of higher charged state ($2+ < z < 4+$) are present [67]. The effect of Al will be discussed later (see section 8.2).

At this point, we can further define the optimal experimental conditions for the aluminosilicate colloid formation:

I **[Si] = 10^{-3} mol l^{-1} (monosilanol = 100%) + [Al] = 10^{-5} mol l^{-1} (pH 5-6 & 8-9)**

II **[Si] = 10^{-2} mol l^{-1} (polysilanol ≤ 85%) + [Al] = 10^{-4} mol l^{-1} (pH 8-9)**

3.5 Quantification and characterization of colloids

The hitherto used methods to trace aluminosilicate colloid formation, namely separation of colloids by ultrafiltration and determination of the Am activity in the colloidal fraction, have been fast, effective and convincing. However, they are indirect methods, which cannot give any information on the quantity or type of the generated colloids. Therefore we introduce now sophisticated techniques such as LIBD, AFM and SEM-EDXS to analyze the synthetized colloids directly.

Appraisal of aluminosilicate colloid formation by LIBD

To ascertain how the colloidal Am species is formed, the colloid formation in aluminosilicate solutions without addition of Am is examined by LIBD. As shown in Fig. 30, the acidic Al solution of 10^{-5} mol l^{-1} is titrated by an alkaline Si solution of 10^{-3} mol l^{-1} (optimum conditions I). The maximum colloid formation emerges at pH 5.5, the minimum at pH 6.5, and at pH ≥ 8.0 the colloid generation increases again. The results of the LIBD experiment are comparable to the screening experiment made by filtration with addition of Am as shown in

Figs. 23 and 25. Around pH 6.5, the absolute amount of generated colloids is found to be minimal, being in accordance with the lowest solubility of aluminosilicate compounds (e.g. sillimanite) as appeared in Fig. 19. A relatively low amount of colloids observed at pH 4.0 may be ascribed to an acidic pH effect that asserts oxygenbridge breaking and hence less colloid formation. This is comparable to the colloid-borne Am fraction shown in Fig. 21(b). Since all chemical solutions for laboratory use contain more or less colloids as impurities, their influence on the present experiment is examined separately.

The original Al and Si solutions are pH titrated separately, both in about 10^{-3} mol l^{-1}, in order to ascertain whether they contain colloids originally or colloids are generated on the pH change that are detectable by LIBD. The results are shown in Fig.30. The Al solution shows a realtively small amount of colloid generation by changing pH from 4 to 7 and above 7 no colloids can be detected. The initial Al concentration of 10^{-3} mol l^{-1} may undergo precipitation of $Al(OH)_3$ with increasing pH and its solubility is the lowest at pH 6 (cf. Fig. 19). Therefore, the colloid generation, as confirmed by LIBD, in the pH region of 4-7 may be attributed to an oversaturation of Al that is conducive to polynucleation. The Al concentration of 10^{-5} mol l^{-1} with addition of Am (4.9×10^{-8} mol l^{-1}) also indicates, as shown in Fig.25 (down part), the generation of colloidal species in a small amount at pH 4-7 even in the absence of Si. The pure Si solution shows the presence of colloids in a relatively small amount in the whole pH range investigated. As the effect of pH change on the colloid concentration is only marginal, it is supposed that the original Si solution contains colloidal impurities. The element analysis indicates about 10 ppb of Al as an impurity in the original Si solution, which may induce a trace amount of aluminosilicate colloids detectable by LIBD as shown in Fig.30. As a conclusion, the original Al and Si solutions are also found to generate colloids or contain colloidal impurities for different reasons. However the amounts detectable by LIBD are distinctively lower than the colloid generation taken place in aluminosilicate solutions (Fig. 30). Such difference corroborates the formation of aluminosilicate colloids.

Particle size, number density and Si/Al ratio

The average size of corresponding aluminosilicate colloids is determined at pH values 6.0 and 7.5. The experimental results of LIBD are shown in Fig. 31. Two-dimensional distributions of optical detection of plasma generated on colloid breakdown are shown in the upper part of Fig. 31, which are concentrated in the centre of effective laser focal volume. Counting

of all breakdown events at each given pH is then made as a statistical distribution on the z-axis as shown in the lower part of Fig. 31. A twice value of the full width at half maximum (FWHM) is taken for the evaluation of an avergae colloid size in hard sphere diameter according to the previous calibration [28]. The average size is found to be 13± 1 nm at pH 6.0 and 11± 2nm at pH 7.5. The two values are virtually the same within the experimental precision. The average size remains unchanged with time, indicating the stability of aluminosilicate colloids in the investigated pH range. The AFM measurement is also performed as shown in Fig. 32. Therefore the supernatant of the colloidal precipitate at pH 7 is brought onto a mica plate for the AFM study under non-contact mode. The particle analysis results in 5-10 nm height and 10-50 nm length for the spherical or egg shaped particles of preponderance as shown in Fig. 32. This value closely corroborates LIBD results of the present experiment as evaluated for a hard sphere diameter. Breakdown events scattered mostly around a narrow sphere of y-z axes in Fig. 31 suggest a small range of the colloid size distribution. The colloid number density determined by LIBD ranges from $10^{11} – 10^{14}$ particles per litre water depending on the experimental condition (pH, Al and Si concentrations). The analog analysis of aluminosilicate colloids generated under the optimum conditions II shows a comparable average size of 10-20 nm as well as number density. The atomic Si/Al ratio of aluminosilicate colloids from conditions I and II is determined by SEM-EDXS and found to be 0.71±0.05 and 1.23±0.03, respectively. It is amazing that the Si/Al ratio in the colloids is almost independent on the degree of polymerization of Si in the mother solution. The atomic ratio of about one is evocative for a kaolinite or imogolite like composition of the aluminosilicate colloids [59] such as hydroxy aluminosilicate colloids also called HAS [54,55]. Taking into account the Si/Al ratio of HAS colloids approximately one, their formation from polysilanol can be presumed as

$$n\ Al(OH)_{3-y}^{y} + Si_nO_{n-1}(OH)_{2n+2} \quad \Leftrightarrow \quad Al_nSi_nO_{4n+2-x}(OH)_x^{x-n-4} + (7+ny-x)\ H^+ + (2n-ny-1)\ H_2O$$

where the y value varies from –1 to +3 following the degree of hydrolysis within the present experimental pH range (4 – 9) and the x value determines the anionic charge of HAS colloids. Polynuclear species of hydrolysed Al ions become important only at pH < 5 [62,63]. Whereas the Al^{3+} ion undergoes hydrolysis, thus forming different hydroxyl species in the given pH range [62-65], the predominant silanol species appears to be $Si(OH)_4$, unless the Si concentration is over-saturated [23,38,56,59,67] (see section 3.4). Therefore, a general polysilanol form

of neutral charge is envisaged as a reactant for the above-formulated reaction. The n value is too complicated to be ascertained. This formulation may correspond to the formation of the Cm-HAS(III) species via isomorphic substitution of Cm to a multidentate oxo-bridging of Al.

Because only a small amount of colloids is generated in the present experiments (10-50 ppb), their structure characterization is not directly possible. It is important to note that the characteristic values for the aluminosilicate colloids we have synthesized are typical for aluminosilicate colloids as they are found in the nature:

	Natural system	Present system
• Particle size	very often < 50 nm	10 - 50 nm
• Number density	10^8 - 10^{14} particles l^{-1}	10^{11} - 10^{14} particles l^{-1}
• Si/Al ratio	imogolite: 0.5 - 1.0	0.7 - 1.2

Conclusions of section 3

In an elaborated parameter screening experiment, optimum conditions for aluminosilicate colloid formation have been recognized from their capability to incorporate Am, which has been added in a tracer concentration as contestant in the condensation process of Si and Al. The optima correspond to mother solutions made at pH 5-6 and pH 8-9, with a Si/Al concentration ratio of 100, but at two different Si concentration levels, namely in a slightly undersaturated and in a 6.5 times oversaturated solution.

The corresponding colloids, as analyzed by LIBD, AFM and SEM-EDXS, all belong to a unique colloid type which is very similar to the natural aquatic colloids of the imogolite type with a Si/Al atomic ratio of ca 1, namely hydroxy aluminosilicate (HAS) colloids. They are small colloids (10 - 50 nm) with a low number density (10^{11} – 10^{14} particles $^{l-1}$).

Different optimum formation conditions for a solely colloid type may reflect different colloid generation mechanisms with distinct interaction potentials for Am. Such differences may be connected with pH and concentration of Si in the mother solutions, which have been shown to influence the degree of polymerization of Si. The hypothesis urges us to further investigate the interaction of Am with HAS colloids in the moment of formation, also called HAS colloids in statu nascendi.

4 Interaction of trivalent actinides with aluminosilicate colloids in statu nascendi

The study of the interaction of trivalent actinides with aluminosilicate colloids in the course of their generation by coprecipitation, also called aluminosilicate colloids in statu nascendi, comprises the following steps: (1) identify and characterize the binding state of Am(Cm) within the colloids; (2) analyze the underlying reasons for differentiated incorporation of Am(Cm) into colloids; (3) test the stability of the colloid-borne Am(Cm); (4) determine the capacity of the aluminosilicate colloids to incorporate increasing amounts of Cm(Am).

4.1 Speciation of colloid-borne Cm by TRLFS

TRLFS is the method par excellence to follow the binding state of trace amounts (up to 10^{-8} mol l^{-1}) of Cm in vivo, e.g. at the titration experiment for condensation of Si and Al. The optimal conditions I and II (cf. section 3) for the formation of aluminosilicate colloids from monosilanol and polysilanol, respectively, are selected for the purpose.

Formation of aluminosilicate colloid-borne Cm from monosilanol (condition I)

Typical TRLFS spectra of colloid-borne Cm are shown in Fig. 33, for which the initial concentrations of Si and Al are taken 10^{-3} and 10^{-5} mol l^{-1}, respectively, with an addition of a Cm concentration at 4.9×10^{-8} mol l^{-1}. The acidic Al solution containing Cm is titrated by the alkaline Si solution. The pH dependent evolution of the fluorescence spectrum is illustrated in the upper part of Fig. 33, whereas the deconvolution of a composite spectrum is shown in the middle part of Fig. 33. The spectroscopic speciation shows the presence of three different Cm species: the free Cm^{3+} aquo-ion with the emission peak at 593.8 nm and two different colloid-borne Cm species, indicated as HAS (hydrated aluminosilicate) species I and II, with the emission peaks at 598.5 and 601.8 nm, respectively. The red shift of the emission band is attributed to the formation of inner-sphere complexes. An exchange of water molecules of the inner coordination sphere by complexing ligands causes a change in the ligand field of the aquo Cm^{3+} ion, which results in a bathochrome shift of the fluorescence spectrum [26,44].

All spectra recorded at pH 2-8 are deconvoluted and individual species present at each pH are quantified. The fractions of each Cm species thus evaluated are shown in Fig. 33

(lower part) as a function of pH, in which the formation of colloidal Cm species can be appraised. The species Cm-HAS(I) is formed between pH 3 and pH 8 with its maximum around pH 6, while the Cm-HAS(II) species appears at pH 5 onwards to higher pH and becomes the prevailing colloidal species at pH > 7.

The characterization of the two colloidal species, Cm-HAS(I) and Cm-HAS(II), is further pursued by measuring their relaxation times of fluorescence at 598.5 and 601.8 nm, respectively, as designed for the colloidal species in Fig.33, to ascertain the number of hydration water molecules bound to Cm. The species Cm-HAS(I) and Cm-HAS(II) show a relaxation time of 83.5±3.7 μs and 88.3±5.2 μs, respectively. Based on these data and relative to the free Cm^{3+} ion, which is assumed to contain 9 coordinated water molecules [73] and has a fluoresence relaxation time of 65±2 μs, the numbers of hydrated water molecules are calculated according to Horrocks [74] and Kimura et al. [75]. According to Kimura et al., the remaining water molecules of Cm for the colloidal species Cm-HAS(I) and Cm-HAS(II) are calculated to be 7±0.5 and 6±0.5, respectively. This fact infers that the colloid-borne Cm has either bidentate oxygen bridges or tridentate oxygen bridges to Al-O- and Si-O- moieties within HAS colloids. According to Fig. 33, Cm appears colloid-borne in the near neutral pH region. This result supports the Am colloid formation as ascertained by filtration experiments given in Figs. 23 and 25.

For the purpose of comparison, the Cm speciation is also made in a pure Si solution of 10^{-3} mol l^{-1} without the addition of Al and in a pure Al solution of 10^{-3} mol l^{-1} without the addition of Si, to both of which 4.9x10-8 mol l^{-1} Cm is added. Fig. 34b shows Cm emission spectra measured as a function of pH in the pure Si solution. As Al impurity is present ($3.7x10^{-7}$ mol l^{-1}) in the original Si solution, a certain amount of latent aluminosilicate colloids is expected, in which Cm may be incorporated and become colloid-borne species. However, as the Si concentration is 10^{-3} mol l^{-1}, while the Al impurity concentration is so low, the plausible assumption is that the interaction of Cm with silanol groups may prevail in this solution. The radiometric assay shows that Am(III) added to the pure Si solution without Al addition becomes partially colloid-borne species with pH between 5 and 9 (Fig. 25) and the rest remains as ionic species, either Am^{3+} aquo-ion or Am-silicate complex. Cm is, therefore, expected to behave accordingly. The emission peaks of Cm observed in the pure Si solution are the same as in the Si/Al solution (Fig. 34a) at 593.8 nm, 598.5 nm and 601.8 nm. Fluorescence lifetimes of the three emission peaks are nearly the same as well, suggesting that the prevailing interaction of Cm takes place with Si in both solutions. The number of hydrated

waters appears the same as well in both solutions, i.e. 7 H_2O for the complex species (I) and about 6 H_2O for the complex species (II). These numbers surmise the bidentate and tridentate bindings to oxo-bridges, respectively.

The speciation results shown in Fig. 34c indicate that in the pure Al solution Cm is incorporated into Al hydroxides, which slowly undergo precipitation. The Cm emission peak is changing with pH from the Cm aquoion at 593.8 nm via gradual bathochrome shift to a new species at 604.1 nm. This species has a longer lifetime of 110.5 μs, being distinctively different from the interaction of Cm with Si. The total emission intensity of Cm in the Al solution is decreasing with increasing pH in the course of time. This fact infers the coprecipitation of Cm in Al hydroxide, because the Al concentration of 10^{-3} mol l^{-1} under investigation is substantially higher than its solubility in the pH region 5-9 [62,63]. Therefore, the spectra shown in Fig. 34 are recorded while stirring the solution. This experiment is to demonstrate that the incorporation of Cm in aluminosilicate colloids (Fig. 34a) shows the spectroscopic properties clearly different from its incorporation into Al hydroxide precipitate. The fact that the emission peak at 604.1 nm appears only in the pure Al solution, not in the mixed solution of Si and Al (Fig. 34a), means the non-attendance of Al hydroxide precipitation in the presence of Si, exceeding the Al concentration. The species fractions as a function of pH are evaluated for the pure Si solution and compared with the species distribution for the mixed solution.

Fractional appearances of the two Cm complex species (I) and (II) in Fig. 33 as a function of pH are found to be nearly the same for the two solutions. The fluoresence lifetimes of the two complexes in the two solutions are nearly the same for each corresponding species (Table 1) and hence the number of hydration water molecules for Cm can be assigned to seven and six for the complex species (I) and (II) in both solutions, respectively. The only difference is the amount of colloid-borne Cm species that is significantly larger in the mixed solution of Si and Al than in the pure Si solution (cf. Fig. 25). In the former solution, Cm undergoes incorporation into aluminosilicate colloids as a contestant of Al, whereas in the latter solution Cm is complexing with silanol moieties and thus results in either colloidal or ionic complex state, in which partial precipitation of Cm-silicate complex takes place.

Formation of aluminosilicate colloid-borne Cm from polysilanol (condition II)

Titration of an acidic Al solution containing Cm by an alkaline Si solution with the final concentrations 1.34×10^{-2} M Si, 1×10^{-4} M Al and 4.8×10^{-8} M Cm, which is accompanied by

the formation of polysilanol (cf. Fig. 26, approach A and Fig. 27), is traced for colloid-borne Cm by recording the TRLFS spectra at pH 2-8. The speciation results for Cm are shown in Fig. 35. The upper part of Fig. 35 demonstrates a pH-dependent evolution of fluorescence spectra as a function of pH, while the down part of Fig. 35 illustrates the deconvoluted emission spectra of four different Cm species present in the solution. The emission peak for the Cm^{3+} aquo-ion appears at 593.8 nm with a lifetime of 67.1±2.5 μs, corroborating the known value [26,44,45]. The first colloid-borne Cm species, entitled as Cm-HAS(I), becomes visible at 598.5 nm with a lifetime of 83.5±3.7 μs and the second colloid-borne Cm species Cm-HAS(II) emerges at 601.8 nm with a lifetime of 88.3±5.2 μs. The third colloid-borne Cm species: Cm-HAS(III), comes forward at 606.8 nm with a longer lifetime of 518±25 μs, which appears to be unique for Cm in the aluminosilicate colloid formation from polysilanol and has not been observed in its reaction with monosilanol.

The titration of polysilanol interacting with Cm in the absence of Al under the same condition gives rise to nearly identical speciation results. The emission spectral evolution shown in Fig. 36, i.e. peak positions and each corresponding lifetime, are the same as in Fig. 35. The observed species are named Cm-HPSi(I) (hydroxy-polysilanol), Cm-HPSi(II) and CmHPSi(III). These species come out as three different kinds of complexation of Cm with polysilanol moieties. Their similar spectroscopic characteristics to the Cm-HAS species indicate that in the aluminosilicate colloids Cm interacts preferentially with silanol moieties as a substitution to Al. From the lifetime measurement of each emission peak, one may deduce the number of water molecules, which remain coordinated with Cm in colloids. Cm-HAS(I) and CmHAS(II) are found to have 7 and 6 coordinated water molecules, whereas Cm-HAS(III) has one or none. The number of coordinated water molecules of each colloid-borne Cm species puts forward that the oxo-bridging state of Cm in aluminosilicate coilloids is a bidentate for Cm-HAS(I) and a tridentate for Cm-HAS(II). A complete structural incorporation of Cm is then conceivable for the Cm-HAS(III) species, as Cm in this species has virtually no hydration water. The same interpretation can be made for the species Cm-HPSi(I), Cm-HPSi(II) and Cm-HPSi(III) as well, according to the similar number of hydration water molecules appraised for each of these species based on their lifetimes.

Overall speciation results are summarized in Fig. 37 for all species of Cm-HAS and Cm-HPSi as a function of pH. In the upper part of Fig. 37, the Cm-HAS(I) species comes into view only in the low pH region as a minor fraction with the maximum of 23% at pH 5.8. The second species, Cm-HAS(II) emerges gradually from pH 5 to a maximum fraction of 35%

around pH 6.5. From pH 6.5, the Cm-HAS(II) species disappears rapidly and the third species, Cm-HAS(III), suddenly built at pH 6.5, becomes predominating in the whole pH range under investigation increasing its fraction with an increase of pH and becoming prevalent at pH > 7. A comparable formation pattern can be observed in the lower part of Fig.37 for the species: Cm-HPSi(I), Cm-HPSi(II) and Cm-HPSi(III). The similarity of the two-speciation results is a direct corroboration for the same kind of chemical bindings of Cm, either in Cm-HAS or in Cm-HPSi species. This fact infers that the oxo-bridging of Cm in aluminosilicate colloids converges rather on silanol moieties than on alumina oxygen. The speciation results shown in Fig. 37 are totally different from the speciation performed on the Cm-HAS species (also Cm-silanol) in the previous experiment, which are produced from monosilanol as an initial state (see Fig.33).

4.2 Isomorphic substitution of Al for Am(Cm)

Fig. 38 summarizes the hitherto results and illustrates the correlation between the binding strength of Cm to aluminosilicate colloids (colloid-borne Cm species) and the polymerization of Si (Si-species). The presence of polysilanol in the mother solution at pH ≥ 7 is a condition for isomorphic substitution of Al for Am(Cm) in HAS colloids. Since the polymerization of Si depends on pH as well as on the concentration of Si, which are not only thermodynamic but also kinetic parameter (see section 3.4), it becomes obvious that the binding strength of Am(Cm) to HAS colloids is also a question of kinetics. The experimental fact can be understood in the light of theory, saying that activation energy is necessary to bring about nucleation. Activation energy can be delivered at the allivation of supersaturation in solution. At low degrees of supersaturation an activation barrier to the nucleation (conucleation of Am(Cm)(Al) with Si) persists, which can be annihilated whenever a foreign solid surface (e.g. polysilanol) with interfacial free energy is already present as a catalyzer. The logic consequence of such an explanation for the isomorphic substitution of Si for Al and even for Am(Cm) would be that, instead of a catalyzer, increased temperature or very long aging times might also be appropriate to overcome the activation barrier to the conucleation of Si, Al, Am(Cm)).

In order to test the hypothesis, a coprecipitation sample is prepared at 25°C on the basis of mono-silanol by mixing an alkaline solution of Si (10^{-3} mol l^{-1}) with an acid solution of Al (10^{-4} mol l^{-1}) and Cm ($5.0x10^{-8}$ mol l^{-1}). The pH is adjusted to 7.5, and the temperature of the

sample is increased to 90°C. After different conditioning times at 90°C, from 5 up to 87 days, aliquots are taken and cooled to 25°C for analysis by TRLFS and LIBD in order to speciate the colloid-borne Cm and simultaneously characterize the colloid formation.

The Cm fluorescence spectra after different heating periods compared with the spectrum before heating are illustrated by Fig. 39. It is obvious that increased temperature effectuates a strong red shift of the emission band at 601.9 nm with a lifetime of 87.7±4.8 μs, which is characteristic for the Cm-HAS(II) species, (cf. section 4.1) to 606.7, 607.7 and 608.5 nm after periods of 5, 16 and 39 up to 87 days, respectively. The shifted emission bands have a composite lifetime. Fitting the data to a biexponential law, the two lifetimes 86.2±4.8 μs and 306.1±30.0 μs are derived. They are attributed to the Cm-HAS(II) with 6.7 H_2O and the Cm-HAS(III) species with 1.8±0.5 H_2O in the inner coordination sphere of Cm, respectively. The result corroborates our hypothesis, that the activation energy to incorporate Cm completely into the structure of aluminosilicate colloids, can be provided by either increased temperature or with the catalytic aid of the polysilanol surface as outlined above.

The question whether the observed temperature effect on the Cm(Am) binding to HAS colloids is equivalent with aging time, as the Arrhenius equation [77]

$$\ln k_2/k_1 = E_a / R\ (1/T_1 - 1/T_2) \qquad \text{Eq.12}$$

where k_1 and k_2 are the rate constants at temperatures T_1 and T_2, E_a is the Arrhenius activation energy (e.g. 80 KJ/mol), and R is the gas constant, suggests, or overlapping processes other than aging have also taken place, cannot be answered by this experiment. A more intensive investigation including experiments at different temperatures is required to obtain such information.

Fig.40 summarizes the results of the speciation of colloid-borne Cm and indicates the influencing parameters: the higher the pH, the concentration of Si and the temperature, the stronger the binding of Cm to HAS colloids.

4.3 Stability of colloid-borne Cm(Am)

Irreversible bindings of actinides to stable aquatic colloids may lead to an unhindered actinide migration along the water flow path. The question whether Cm-HAS(I), Cm-HAS(II) and Cm-HAS(III) correspond to „irreversible bindings“ and „stable colloids“ seems to be a

question of definition and related to eventually changing environmental conditions such as pH, temperature, the presence of anionic ligands etc.. Within this study, 3 different stability tests are considered: (1) change from radioactive to inactive medium and measuring radiometrically the desorption of Am activity from the colloidal fraction; (2) change from high to low pH environment and determining the colloid-borne Cm distribution as a function of pH with TRLFS; (3) change from ambient to increased temperature and monitoring the colloidal average size with LIBD.

Activity in colloids after desorption with inactive medium

In a first stability test for Am binding to HAS colloids, two desorption experiments for Am are performed on Am-HAS colloids. One experiment uses colloids generated under condition I and another uses colloids formed under condition II , based on the conucleation of Am and Al with prevailing monosilanol and polysilanol, respectively. The chosen pH´s of colloid formation for each experiment are 5, 7 and 9. In all cases, the sample conditioning time is seven days. For desorption, the colloidal fraction is first separated from the mother solutions by ultrafiltration and than brought into contact with a similarly prepared inactive ultrafiltrate during one day. The procedure is repeated three times. A fourth desorption is performed with bidistilled water at pH 6. The colloid-borne Am fraction remained in the colloids after the accumulated washing procedures in relation to the initial colloid-borne Am fraction before desorption is evaluated. Fig. 41 shows the result of the stability tests for the pseudocolloids of Am in question, namely generated at three different pH´s on the basis of HAS-monosilanol (upper part of Fig. 41) and on the basis of HAS-oligosilanol (lower part of Fig. 41). The least desorption of Am from HAS colloids is observed at pH 9 indicating over 90% of Am remained stable as colloid-borne species for both HAS-monosilanol and HAS-polysilanol. At pH 7, the value decreases slightly but remains still over 80% for HAS-monosilanol and 70% for HAS-polysilanol. However, at pH 5 only 33% and 50% of the initially incorporated Am remains in the colloids from HAS-mono- and -polysilanol, respectively, suggesting that the colloid-borne Am species is chemically unstable. Compared to the speciation of Cm at interaction with HAS colloids, as shown in Figs. 33, 37 and 38, the results of the desorption experiment can be interpreted as forming the colloidal species Am-HAS(I) at pH 5 and Am-HAS(II) or Am-HAS(III) from pH 7 to pH 9 in accordance with the formation of Cm-HAS(I) and Cm-HAS(II) or Cm-HAS(III). According to Fig.41, the colloidal spe-

cies Am-HAS(II) (tridentate) as well as Am-HAS(III) (isomorphically substituted) seems to be structurally stable in solution, in which Am or Cm appears irreversibly incorporated under given conditions.

Cm-HAS(III) species at decreasing pH

A second stability test investigates the pH-reversibility behaviour of the Cm-HAS(III) species. Therefore the Cm-HAS(III) species is formed at pH 9 by titration of an alkaline solution of Si (1.34×10^{-2} mol l^{-1}) with an acid solution of Al (1×10^{-4} mol l^{-1}) and Cm (4.8×10^{-8} mol l^{-1}) as previously described for colloid formation on the basis of polysilanol, condition II (see section 3.4). The mixed sample at pH 9 is divided in 8 aliquots, each of which are titrated with HCl to a lower pH unit (inverse titration), namely from pH 9 down to pH 2 in accompany with the spectroscopic speciation. A dilution of the elements concentration upon titration is maintained within 3%. The speciation results for colloid-borne Cm as a function of pH in the course of the inverse titration of the sample containing Cm-HAS(III), are shown in Fig. 42 (lower part). The formation pattern for the species Cm-HAS(I), Cm-HAS(II) and Cm-HAS(III) is similar to that for the direct titration (see Fig. 42, upper part), except that Cm-HAS(III) becomes the predominating colloid-borne Cm species in the whole pH range under investigation, increasing gradually its fraction with an increase of pH and becoming prevalent at pH > 7. A decrease of pH from 9 down to 2 converts the Cm-HAS(III) species to Cm-HAS(II) gradually. Both Cm-HAS(III) and Cm-HS(II) disappear slowly at pH < 6, while Cm-HAS(I) is appearing at lower pH. The Cm^{3+} aquo-ion fraction increases on the other hand with decreasing pH, suggesting ist dissociation from colloids. The dissociation of Cm with lowering pH is not directly from Cm-HAS(III) but takes place from Cm-HAS(II) at first and than from Cm-HAS(I).

The stability of the Cm-HAS(III) species at each pH is observed as a function of time up to 63 days, as shown in Fig. 43. At pH 9, only the Cm-HAS(III) species prevails and remains stable with time. The fraction of Cm-HAS(III) decreases with lowering pH but at each pH the corresponding Cm-HAS(III) fraction remains stable with time again after 15 days. At pH ≤ 5, the initial fraction of Cm-HAS(III) decreases with time for the first few days and then remains constant. At pH 3, Cm-HAS(III) disappears almost after a few days.

HAS colloidal size at increasing temperature

The stability of HAS colloids made at room temperature from monosilanol at pH 7.5 and heated to 90°C (see section 4.2) is monitored by LIBD as a function of heating time (up to 7 days) by determining the average colloidal size from two-dimensional recordings of plasma light emission generated by breakdown of colloids within the laser beam focus volume. The result is given in Fig. 44. The unchanged 2-D distribution (x,z-plane) of the breakdown events around the center of the optical focus of the laser beam, before and after prolonged heating periods, proves that periods of increased temperature do not irreversibly change the colloidal state.

4.4 Capacity of colloids to incorporate Am(Eu)

The maximal amount of trivalent actinides which can possibly be incorporated into HAS colloids in statu nascendi either formed from monosilanol (formation condition I) as well as from polysilanol (formation condition II) is determined. To this purpose, increasing amounts of Eu up to $5x10^{-4}$ mol l^{-1} are included in the colloid generation process in addition to a constant tracer amount of Am ($5x10^{-8}$ mol l^{-1}). A similar behaviour of Am and the somewhat better soluble Eu is thereby assumed. The fraction of Am activity in the three phases (ionic, colloids and precipitate) is measured as a function of pH and also as a function of time, from 3 hours to 35 days. Blank experiments without Si and Al are also performed in order to trace separately the colloid formation behaviour of Am(Eu) by itself, without the binding to HAS colloids. The result for the Am(Eu) fraction incorporated into the colloidal phase of the coprecipitation samples after 35 days conditioning time as a function of the (Am+Eu) concentration is given by Fig.45. The following observations are made:

(1) The maximum concentration of incorporated Am(Eu) amounts to ca. 90% of $5x10^{-5}$ mol l^{-1} in HAS colloids formed at pH 7-9 out of a mother solution containing $1.3x10^{-2}$ mol l^{-1} Si (85% polysilanol at pH $\geq$ 7) and $1.5x10^{-4}$ mol l^{-1} Al. In that case, about one out of two or three Al in the colloids is isomorphically substituted for Am(Eu). A further increase of the Am(Eu) concentration destroys the HAS colloidal state;

(2) HAS colloids in statu nascendi generated out of a mother solution, consisting of a $1x10^{-3}$ mol l^{-1} monosilanol and $1x10^{-5}$ mol l^{-1} Al, have a somewhat lower capacity to hold Am(Eu). In that case, the maximum is observed at pH 9 for a Am(Eu) concentration of $2x10^{-6}$

mol l^{-1}. Thereby 1 out of 5 Al in HAS colloids is poorly replaced by Eu(Am) in a tridendate binding;

(3) The binding capacity of HAS colloids (from mono- as well as from polysilanol) for trivalent actinides decreases with decreasing pH and is in line with the An(III)- colloid binding strength.

(4) At pH 4 to 6, the activity in the colloidal phase has not to rely on HAS, since the colloidal Am(Eu), which is formed in the presence of Si and Al is found to the same amount in the blank experiment with Am(Eu) only, without HAS colloids. Another mechanism for colloid formation is postulated. The phenomenon will be discussed later (section 9).

Conclusions of section 4

Trivalent actinides such as Am(III) or Cm(III) are incorporated into HAS colloids in statu nascendi and undergo thereby oxo-bridging into the structural position of Al(III). The different incorporation patterns as well as kinetics of Am(Cm), depending on whether HAS colloids are built from mono- or polysilanol, reflect correspondingly different incorporation mechanisms. The binding strength of Am(Cm) to the HAS colloids increases with increasing concentration of Si and increasing pH and is shown to be related with the faster polymerization kinetics of Si. HAS colloids, formed from a slightly undersaturated Si-solution (monosilanol) mixed with Al (Si/Al ratio = 100) in the presence of tracer amounts of Am(Cm), build the colloid-borne Cm species Cm-HAS(I) at pH 5 – 6 and Cm-HAS(II) at pH 8 – 9 corresponding to bidentate and tridendate bindings to the colloids, respectively. HAS colloids, generated from an oversaturated Si-solution (polysilanol), which is mixed with Al (Si/Al ratio = 100) at pH 7 – 9, form the colloid-borne Cm species Cm-HAS(III) where Cm(Am) substitutes isomorphically for Al in the aluminosilicate colloid structure. The result is explained by the interfacial energy of polysilanol, which seems to be necessary to overcome the activation energy barrier for the complete incorporation of Am(Cm). The explanation is corroborated by the fact, that isomorphic substitution of Am(Cm) can also take place without polysilanol surface, e.g. from monosilanol and Al, at increased temperature, e.g. 5 days at 90°C, which is another way to provide activation energy.

The generated pseudocolloids of Am(Cm), corresponding to the Cm-HAS(II) or Cm-HAS(III) species, are extremely stable as a function of time, against desorption with inactive medium (irreversible Am(Cm)-colloid bindings), and at increased temperature. Their forma-

tion is, however, pH reversible, and in line with the lower stability of the Cm-HAS(I) species built at pH 5 – 6.

The maximum capacity of HAS colloids to incorporate Am(Eu) is reached for HAS colloids generated from polysilanol at pH 8-9, when about one third of the Al in colloids is substituted by Am(Eu) and the HAS colloids have lost their original identity.

Am in the colloidal fraction at pH 4 – 6 is due to a process for colloid formation, which is different from the binding with HAS colloids. The corresponding mechanism will be further discussed and is still under investigation.

5 Interaction of tetravalent actinides with aluminosilicate colloids in statu nascendi

Follows now the interesting question whether Th(IV), present at the conucleation of Si and Al, will follow the behavior of Si(IV) and incorporate irreversibly into HAS colloids in statu nascendi just like Am(III) served as a substitute for Al(III). Although no direct spectroscopic speciation of colloid-borne Th like by TRLFS is possible for tetravalent actinides, we expect that, on the basis of the acquired knowlegde about the pseudocolloid formation of Am(Cm), an intelligent comparative tracing of the activity of Th in the liquid, colloidal and solid phases may provide us a conclusive answer to that question. Starting from the preparation of ^{234}Th through separation from natural ^{238}U, the study includes the determination of the Th incorporation kinetics into HAS colloids in statu nascendi as a function of the pH, of the Si concentration and of the Th concentration, as well as the analysis of the reversibility of the process.

5.1 Separation of Th from U

As obvious from the ^{238}U decay scheme (Fig. 46, upper part), ^{234}Th ($T_{1/2}$= 24.1 d) may be prepared by milking natural uranium. The separation of Th is performed in two consecutive steps [78,79]:

(1): 25 g $UO_2(NO_3)_2.6\ H_2O$ (p.a, Merck) is brought into the chloride form UO_2Cl_2 by addition of conc. HCl, evaporation to dryness, dissolution in 8 M HCl and applied to a column (4.4 cm ø, 72 cm length) filled with 750 ml of the anion exchange resin Dowex®1-X8 (100-200 mesh). Th(IV), unlike U(VI) and Pa(V), does not form anionic chlorocomplexes and is eluted with 8 M HCl. The eluate is evaporated, dissolved in conc. HNO_3 and H_2O_2 and

evaporated 3 times until all organics are destroyed. The residue is dissolved in 8 M HNO_3 for the second purification step.

(2): The hexanitratocomplex of Th is now sorbed on a small column filled with 80 µl anion exchange resin Dowex®1-X8. Remaining U and Pa impurities are washed out with 8 M HNO_3. Th is eluted with 8 M HCl. The eluate is evaporated several times with conc. HNO_3 to dryness and redissolved in 0.1 M HCl, resulting in about 150 kBq ^{234}Th. A typical elution diagram is shown in Fig. 46.

5.2 Incorporation of Th(IV) and Am(III): comparison

Similarly to the foregoing experiments for the estimation of incorporation of Am(III) in HAS colloids in statu nascendi, a constant tracer amount of Th, dissolved in acid, is added to an acid Al solution in 0.03 mol l^{-1} HCl and titrated with an alkaline Si solution in 0.03 mol l^{-1} NaOH to a preset pH, to give the following end concentrations in six series of mother solutions, each serie including six samples with different pH in the range from 4 to 9:

(1) Only Th: [Th] = $5x10^{-8}$ mol l^{-1}
(2) Th+Al: [Th] = $5x10^{-8}$ mol l^{-1}, [Al] = 10^{-5} mol l^{-1} (also [Al] = 10^{-4} mol l^{-1})
(3) Th+monosilanol.: [Th] = $5x10^{-8}$ mol l^{-1}, [Si] = 10^{-3} mol l^{-1}
(4) Th+monosilanol+Al: [Th] = $5x10^{-8}$ mol l^{-1}, [Si] = 10^{-3} mol l^{-1}, [Al] = 10^{-5} mol l^{-1}
(5) Th+polysilanol: [Th] = $5x10^{-8}$ mol l^{-1}, [Si] = 10^{-2} mol l^{-1}
(6) Th+polysilanol+Al: [Th] = $5x10^{-8}$ mol l^{-1}, [Si] = 10^{-2} mol l^{-1}, [Al] = 10^{-4} mol l^{-1}

The mother solutions (4) and (6) generate HAS colloids on the basis of monosilanol and polysilanol, respectively (cf. section 3.4: optimum conditions I and II), whereas the other solutions serve the blank experiments for the purpose of comparing the behaviour of Th with and without HAS colloid formation. From each sample, aliquots are taken after different conditioning times from 3 hours up to 35 days, and the partition of Th over the three phases, ionic, colloidal and precipitate, is determined. The result for the fraction of Th incorporated in the colloidal phase after 35 days of sample conditioning time as a function of pH is illustrated in a contour diagram (Fig. 47, left part) and compared with the previous results for the incorporation of Am (Fig. 47, right part). As far as Th is concerned, we make the following observations.

Th blank without any addition (1) is not in the colloidal phase but in the precipitate in the whole pH region. After addition of either only Al (2) or only monosilanol (3), Th persists in the precipitate. The presence of both, Al as well as monosilanol (4) (condition I for colloid formation) is necessary to transfer Th from the precipitate into the colloidal phase at neutral pH (7 – 9). The shift of the equilibrium $Th_{soln} \Leftrightarrow Th_{coll} \Leftrightarrow Th_{prec}$ from the right to the left can only be explained by the binding of Th to the HAS colloids. Polysilanol without addition of Al (5) is also capable to incorporate Th at neutral pH. Polysilanol with addition of Al (6) and forming of HAS colloids (condition II for colloid formation) is mostly efficient for transferring Th into the colloidal fraction in the broad pH region from 4 to 9, with a maximum at pH 7. The fact that almost 100% of the Th input is found in the colloidal fraction is amazing. If we assume that Th behaves just like Si, we would expect that only 1% of Th in the mother solution may become colloid-borne Th, since Si/Al concentration ratio in the mother solution is 100 and the Si/Al atomic ratio in the colloids is ca 1. The observed result infers that the affinity of the Al cation for the Th-oxyhydroxide ligand is at least 100 times higher than for the polysilanol ligand.

The incorporation patterns for Th in the HAS colloids are different depending on whether the colloids are generated on the basis of mono- or polysilanol. They reflect correspondingly different incorporation mechanisms. The comparison of the respective incorporation patterns of Th with those of Am (Fig. 47, right part) further indicates distinct incorporation pathways for tri- and tetravalent actinides.

The kinetics for the incorporation of Th and Am into HAS colloids from mono- as well as polysilanol are also compared and the result is given in Fig.48. In the case of HAS-monosilanol (Fig. 48, lower part), the colloid-borne Th fraction as well as the colloid-borne Am fraction decreases with time in the pH region of 6 to 8 or remains constant at pH 9. In the case of HAS-polysilanol (Fig. 48, upper part), the colloid-borne Am fraction at pH = 6 - 9 remains unchanged as a function of time, whereas Th grows into the colloids with time. This special behaviour of Th appears to reflect the polymerization kinetics of Si (cf. Figs 27 and 28). The differences in incorporation kinetics for Th and for Am in HAS from mono- and polysilanol are, besides the different incorporation patterns as mentioned above, further indications of correspondingly distinct incorporation mechanisms.

5.3 Stability of pseudocolloids of Th

The reversibility of Th incorporation into HAS colloids is tested in desorption experiments on 2 series of samples resulting from the titration of an acid solution of Th and Al with an alkaline solution of monosilanol and polysilanol, respectively. Each series contains 3 samples, namely at pH 5, 7 and 9, respectively. After a conditioning time of seven days, the colloids are separated and washed four times, 3x with a similar but inactive ultrafiltrate and 1x with bidistilled water, pH 6. The contact time with the wash water is one day for each desorption. The stable colloid-borne Th fraction (%) is evaluated and shown in Fig. 49. It is obvious, that Th has been irreversibly incorporated in the whole pH range. Merely at pH 5, a slight desorption can be remarked. The repetition of the experiment for Th desorption after a sample conditioning time of 35 days, shows a further stabilization of Th colloidal incorporation, even at pH 5, with a remaining colloid-borne Th fraction after desorption of 98%. The result shows that Th is irreversibly incorporated into both colloids, HAS-poly- as well as HAS-monosilanol in the whole investigated pH range. It suggests that colloid-borne Th is more stable than colloid-borne Am. The result is in agreement with the previously demonstrated higher affinity of Th for Al as compared with Si (see section 5.2). It is therefore assumed that Th is isomorphically substituted into the aluminosilicate structure of colloids.

5.4 Capacity of colloids to incorporate Th

The Th concentration incorporable into HAS colloids in statu nascendi, which are generated from either mono- or polasilanol (cf. section 3.4), is evaluated as a function of Th concentration. This is realized by determining the distribution of Th activity (initial activity from 1.3×10^{-12} mol l^{-1} ^{234}Th) in the ionic, the colloidal and the solid phase as a function of conditioning time of the titration sample (3 hours – 35 days) for several pH´s (6 – 9) and at each pH, for several Th concentrations (7×10^{-9} mol l^{-1} - 1×10^{-3} mol l^{-1}). Blank experiments without Si and Al are also included in order to distinguish between Th colloids and colloid-borne Th. Fig. 50 shows the Th activity fraction (%) in colloids after 35 days sample conditioning time as a function of the Th concentration for different pH´s. We observe the following facts:

(1) The incorporable amount of Th depends on the formation conditions of HAS colloids, namely on the pH as well as on the Si species in the mother solution (mono- or polysilanol).

(2) The maximal colloid-borne Th is found at pH 9 for HAS colloids formed from polysilanol, a result which is similar to that for the maximal incorporation of Am(Eu) (Fig. 45). This maximal amount corresponds to about 80 % of $1.6x10^{-4}$ mol l^{-1}, i.e. $1.3x10^{-4}$ mol l^{-1} Th. The amount of Si in colloids with a Si/Al atomic ratio of 1.2 (section 3.5) is 1.2% of the Si concentration in the mother solution ($1.3x10^{-2}$ mol l^{-1}), which is $1.6x10^{-4}$ mol l^{-1} Si. It means that about 80% of the Si in HAS is substituted for Th. Four out of five (Si+Th) colloidal atoms are Th. This relation is reversed at pH 6: one out of five (Si+Th) colloidal atoms is Th.

(3) HAS colloids formed from monosilanol have a much lower capacity for incorporating Th. The maximal incorporated Th incorporation is at pH 9 and a hundred times lower as for HAS from polysilanol.

(4) At low pH (pH 4), Th starts to generate colloids by itself when its concentration depasses 10^{-5} mol l^{-1}, as obvious from the blank experiment without HAS colloids. A similar observation has been made for Am, but at a lower concentration and a broader pH region (cf. Fig. 45). The possible generation of „real“ Th colloids is discussed later (see section 9).

Conclusions of section 5

Tetravalent actinides such as Th(IV) are incorporated into HAS colloids in statu nascendi and undergo thereby oxo-bridging into the structural position of Si(IV). The growing of Th in colloids with time reflects the polymerization kinetics of Si and is therefore promoted in presence of Al, at increased pH and at increased Si concentration (more Th incorporation in HAS-polysilanol than in HAS-monosilanol). The fraction of Th migrating from the mother solution into the colloids is a hundred times higher than that of Si, namely 100% and 1%, respectively. The observed facts indicate that the affinity of anionic ligands for trivalent cations is in the order:

Th-oxyhydroxide > polysilanol > monosilanol > OH.

The generated pseudocolloids of Th are extremely stable as a function of time as well as highly resistent against desorption with inactive medium (irreversible Th-colloid bindings) or bidistilled water at pH 6.

The maximum capacity of HAS colloids to incorporate Th is given for HAS colloids formed out of polysilanol at neutral pH (6 – 9) after a conditioning time of several days, and correspond almosts to the Al concentration in the mother solution which also determines the Si concentration in the colloids (Si/Al = ca. 1). In that case about 80% of Si in colloids is substituted by Th.

The different incorporation patterns as well as kinetics of Th, depending on whether HAS colloids are built from mono- or polysilanol, reflect correspondingly distinct incorporation mechanisms. The incorporation processes of Th into HAS colloids in statu nascendi also differ from those of Am as far as pH dependency, kinetics, quantity as well stability are concerned. The general tendency is that, unlike colloid-borne Am, colloid-borne Th enhances the overall HAS colloid stability.

At low pH (4) and at high concentration (≥ 10^{-5} mol l^{-1}) Th becomes colloidal without the aid of HAS colloids. The corresponding mechanism will be discussed later and is still under investigation.

6 Simultaneous interaction of tri- and tetravalent actinides with aluminosilicate colloids in statu nascendi

So far we have learned that tri- and tetravalent actinides substitute for Al(III) and Si(IV), respectively, in stable HAS colloids at the moment of their formation through heterogeneous nucleation. In the real situation, actinides (or other elements) of different oxidation state might occur simultaneously and we want to know what do actinides decide in such a situation. Do they still behave independently or does an eventual mutual interaction provides them with a new incorporation character? An answer to that question is aimed in the following investigation.

6.1 Incorporation of the (Am(III)+Th(IV)) mixture

Trace amounts of Am and Th, each at a concentration of 5×10^{-8} mol l^{-1} , are together integrated into the HAS colloid generation process, and their behaviour of incorporation into colloids is first observed radiometrically. Therefore, an acid solution of Am+Th+Al is titrated with Si in base to a preset pH in the range of 4 – 9 under the optimum colloid formation conditions I (monosilanol species) as well as conditions II (polysilanol, prevailing from pH 6) to

give „mixed“ samples. After different time intervals, from 3 hours up to 35 days, filtration and ultrafiltration procedures are applied on the samples, and the respective distributions of Am and Th activities between solution, colloids and precipitate are determined. Figs. 51 and 52 show the distribution of Th (left part of the figs) and of Am (right part) in the three phases of 35 days old samples from condition I (HAS-monosilanol) and II (HAS-polysilanol) as a function of pH, respectively. In each figure, the results for the mixed samples containing both Th and Am (Fig. 52, lower part) are compared with previous results for the corresponding separate samples with either only Th or only Am (Fig. 52, upper part). It is obvious, that the originally distinct patterns for the separate incorporation of Th and Am (upper part of Figs. 51 and 52) become more similar to one another if colloids are generated in the presence of a Th+Am mixture (lower part of Figs. 51 and 52). This characteristic is mostly pronounced in the neutral pH range 6 – 9. In this pH region, a general decrease of activity (Am or Th) in the colloidal fraction is found for the mixed samples. In the low pH region 4 to 6, however, an increased activity (Th or Am) is observed in the presence of HAS-polysilanol (Fig. 52, lower part) in comparison with the separately incorporated Th and Am (Fig. 52, upper part).

In the special case of HAS-polysilanol (Fig. 52) formed at pH 9, we also observe that Th as well as Am are partly driven from the colloidal phase (separate samples) (Fig. 52, upper part) to the solution (mixed samples) (Fig. 52, lower part) only through the fact that the actinide of the different oxidation state is also present.

$$Th(Am)_{solution} \Leftrightarrow Th(Am)_{colloid} \Leftrightarrow Th(Am)_{precipitation}$$

The shift of the equilibrium from the right to the left means that the polymerization of Th is inhibited by Am and vice versa. It also indicates that Th and Am become not only bound to HAS colloids but also to one another. This findings clamour for speciation of Cm in the presence of Th by TRLFS.

6.2 Speciation of colloid-borne Cm in presence of Th by TRLFS

TRLFS spectra of Cm, without and with the presence of Th, are recorded at the abovementioned titrations for the generation of HAS-monosilanol and HAS-polysilanol. The result is illustrated in Fig. 53. Spectra shift due to Th are observed (compare in Fig. 53 the

upper part (Cm) with the lower part (Cm+Th)) in both cases, at generation of HAS-monosilanol as well as at the formation of HAS-polysilanol (compare left and right part of Fig. 53) and reflect an interaction of Th with Cm.

Peak deconvolution of a composite spectrum as illustrated by Fig. 54 clarifies the appearance of different Cm species. In the presence of Th and HAS-monosilanol (lower part, left), three Cm species, the free Cm^{3+} aquo-ion (emission peak at 593.8 nm) and two colloid-borne Cm-species, named as Cm-Th(I) at 598,0 nm and Cm-Th(II) at 603,6 nm are identified. Exactly the same species are found if, instead of monosilanol, polysilanol is used for colloid generation (lower part, right). The result is in clear contrast to the behaviour of Cm without the presence of Th (upper part), which also shows the species at 593.8 nm and 598.5 nm, namely the Cm^{3+} aquo-ion and the Cm-HAS(I) but two further different colloid-borne Cm-species, one at 601.8 nm, named Cm-HAS(II), and another at 606.8 nm, unique for HAS-polysilanol and corresponding to the completely incorporated Cm species, namely Cm-HAS(III).

The fraction of each Cm species as a function of pH, as shown in Fig. 55, indicates roughly similar incorporation patterns for Cm with or without Th after replacing Cm-Th(II) either by Cm-HAS(II) or by Cm-HAS(III) depending on the original Si species at HAS formation.

A further characterization of Cm-Th(I) and Cm-Th(II) is made by the measurement of the fluoresence relaxation time which can be related with the number of Cm coordinated water molecules. Cm-Th(I) and Cm-Th(II) have a relaxation time of 134.0±1.8 μs and 342.9±8.6 μs (mean values for HAS-monosilanol- and HAS-polysilanol colloid-borne Cm) respectively, which correspond to four and one or no water molecules remaining in the coordination sphere of Cm.

Table 2 gives an overview of the characteristics of the different Cm-species. Therefrom we conclude that the affinity of Cm(III) for Th(IV) is higher than for mono- or even polysilanol. It infers a binding of Cm to Th and corroborates the above outlined results from radiometric measurements (see section 6.2). We postulate that a complexed form of Cm and Th is conucleating with Si and Al at colloid formation. The Cm-Th complex has a complex or „mixed“ behaviour at its interaction with HAS colloids in statu nascendi. The ambivalent behaviour of Cm+Th seems to resemble more that of Am at low pH from 4 to 6 and that of Th at neutral pH from 6 to 9. In the latter case, Cm is incorporated indirectly into the colloids via its

strong binding with Th and becomes more stably incorporated into colloids, in line with the stronger binding of Al with Th as compared with Si (cf. section 5.3).

6.3 Stability of pseudocolloids of (Am+Th)

The fact that the simultaneous interaction of Th and Am with HAS colloids in statu nascendi leads on the one side to a general somewhat lower quantity of incorporated activity in the colloidal fraction (cf. section 6.1), but on the other side to a stronger binding of Cm to the colloids (cf. section 6.2), encourages us to test the stability of the corresponding pseudocolloids of (Th+Am) by means of desorption experiments. The pseudocolloids are therefore generated at pH 5, 7 and 9 on the basis of mono- and polysilanol, conditioned in their mother solution for 7 days, and separated by ultrafiltration. The desorption consists of four washing procedures, three of them restore the original samples through addition of separately prepared inactive ultrafiltrates of the same composition as well as pH, and one uses bidistilled water at pH 6. The contact time with each wash-water is 1 day. The activity fraction remained in colloids after desorption and related to the originally incorporated fraction is evaluated. The result is shown in Figs. 56 and 57 for pseudocolloids from HAS-monosilanol and HAS-polysilanol, respectively, and compares the stable colloid-borne activity fraction (%) of Am (upper part) and of Th (lower part) in the separate samples (only Am or only Th) with that in the mixed sample (Am+Th). The conclusion of irreversible binding of Th as well as Am to HAS colloids remains valid, independently of their separate or simultaneous incorporation.

Conclusions of section 6

Tri- and tetravalent actinides such as Am(Cm) and Th, participating simultaneously in the HAS colloid generation, either on the basis of mono- or polysilanol, show a „mixed" behaviour of incorporation into the colloids. The underlying reason is the high affinity of Th for Cm, in line with its high affinity for Al. This characteristic is indirectly visible from the activity distribution in the 3 phases, ionic, colloids and precipitate, and directly proven by comparing the TRLFS speciation of Cm without and in the presence of Th at incorporation in HAS colloids in statu nascendi. Differences in incorporation patterns as well as in type and number of Cm species, as previously observed at the conucleation of Cm (without Th), Al and either mono- or polysilanol, are cancelled out if Cm is accompanied with Th. In the case of

(Cm+Th), only two Th-borne Cm species, namely Cm-Th(I) at 590 nm and Cm-Th(II) at 603.6 nm, with fluorescence life times of 134.0 μs and 342.9 μs, corresponding to four and no waters in the coordination sphere of Cm, respectively, are identified for both, HAS-mono- as well as HAS-polysilanol. The interaction behaviour of the Cm-Th complexes with HAS colloids resembles more that of Cm(Am) at low pH from 4 to 6 and more that of Th at neutral pH from 6 to 9.

The stability of the generated pseudocolloids against desorption with inactive medium remains, notwithstanding Cm-Th complex formation and altered incorporation mechanism, almost unchanged. Consequently, the statement of irreversible Am(Cm)- and Th- colloid bindings remains valid, also in the case of their simultaneous incorporation.

7 Behaviour of aged aluminosilicate colloids in presence of tri- or tetravalent actinides

The interaction of actinides with aluminosilicate colloids in statu nascendi has been used to simulate the formation of pseudocolloids through conucleation. An appropriate model to study the generation of pseudocolloids by the alternative way of actinide sorption to colloids may be the use of aged aluminosilicate colloids. Fig. 58 illustrates the corresponding experimental pathways.

7.1 Influence of colloid age on incorporation of Am and Th

HAS colloids are synthesized through conucleation of Si and Al on the basis of mono- as well as polysilanol under the optimum conditions I and II (see section 4.3) at six different pH´s from 4 to 9. After different sample conditioning or colloid aging times, namely 1, 7 and 24 days, each co-nucleation sample is spiked either with Am or with Th to achieve a final concentration of $5x10^{-8}$ mol l^{-1}. After activity contact time from 3 hours up to 35 days, the Am or Th fraction incorporated in colloids is determined. Fig. 59 illustrates the result of the incorporation of either Am (left part) or Th (right part) into the HAS-monosilanol (upper part) as well as HAS-polysilanol colloids (lower part) of different age after an activity contact time of 35 days and includes the corresponding results for HAS colloids in statu nascendi for the purpose of comparison. Aged colloids (e.g. from 7 days) are not tied up to bind Am, but the af-

finity for Th is unchanged or even higher, suggesting a displacement mechanism of Si in HAS.

The influence of the activity contact time on sorption into the colloids is further analyzed by comparing the status after 3 hours with that after 35 days (Fig. 60). Fig. 60 shows the result for Am and Fig. 61 the result for Th. As far as Am is concerned, we observe that aged HAS-monosilanol colloids (Fig. 60, upper part) loose their sorption capacity for Am from the very beginning, e.g. already after 7 days aging and 3 h activity contact time, whereas 7 days aged HAS-polysilanol colloids (Fig. 60, lower part) initially sorb Am, desorbing it again with time. As far as Th is concerned (Fig. 61), different sorption patterns as well as kinetics for Th sorption into HAS-mono- and HAS-polysilanol (compare upper and lower part of Fig. 61) reflect correspondingly different sorption mechanisms. In the case of HAS-monosilanol (Fig. 61, upper part), the Th incorporation mechanisms either through sorption or condensation (compare aged HAS with HAS in statu nascendi) are very similar. Aged HAS-polysilanol colloids, however, (Fig. 61, lower part) sorb Th much faster than HAS-polysilanol colloids in statu nascendi, which may be related with the omitted waiting time of colloid formation.

7.2 Influence of colloid age on stability of pseudocolloids of Am(Th)

Activity desorption with inactive medium

The pseudocolloids of Am and Th, which have been generated from 27 days aged HAS-polysilanol colloids at pH 5, 7 and 9 after a contact with activity during ≥35 days, are subjected to a desorption procedure consisting of three one-day-equilibrations with ultrafiltrate from duplicate but inactive samples. The stable colloid-borne activity fractions (%) are evaluated and the result is shown for Am and Th in Fig. 62b and Fig. 62c, respectively. Obviously, a small amount of incorporated Am fraction as well as the almost quantitatively incorporated Th fraction (cf. Fig. 59) are irreversibly bound. An exception is the association of Am at pH 5, which is a completely desorbed. Less aged pseudocolloids of Am at pH 5, e.g. 7 days old at the moment of contact with activity, keep still a 65% of the incorporated Am after desorption (Fig. 62a). We assume that some Am which is irreversibly bound in aged colloids is nothing but a reflection of a non completed colloid formation. The irreversible incorporation of Th, however, is not dependent on conuleation. The high affinity of Th for Al immediately displaces Si out of the HAS colloids and causes the most stable incorporation at all pH.

Activity desorption with EDTA

The stability of Th sorption into aged colloids is further tested with the aid of EDTA. Desorption experiment is performed as follows. Al is condensed with monosilanol as well with polysilanol (conditions I and II) at pH 5, 7 and 9 for colloid formation and the samples are conditioned for 27 days. Th is than introduced to make a final concentration of 4.8×10^{-8} mol l^{-1}. After a contact time with Th of 35 days, aliquots of each sample are taken to evaluate the incorporated Th activity fraction related to the input Th activity, and EDTA is added to an end concentration of 1×10^{-4} mol l^{-1}. After different contact times with EDTA, the remained or „EDTA-stable" activity fraction as compared with the initially incorporated Th fraction is determined. Fig. 63 shows the result of the Th desorption kinetics from aged pseudocolloids with EDTA. Th sorbed to either aged HAS-mono- or HAS-polysilanol colloids shows fast EDTA desorption kinetics at pH 5 within the first three days. However, a $\geq$ 20% fraction of incorporated Th remains even after 30 days contact time with EDTA. At neutral pH (7-9), Th sorbed to HAS-polysilanol colloids (Fig. 63, lower part) cannot be displaced by EDTA, in contrast to Th associated with HAS-monosilanol colloids (Fig. 63, upper part), which is at least partially (a 50%) desorbable within a few days of contact time with EDTA. This and other experiments with competitive ligands for the better comprehension of the formation of different colloid-borne Th species, leading to distinct overall stabilities of the pseudocolloids of Th, are still in progress.

Conclusions of section 7

Tri- and tetravalent actinides, e.g. Am and Th, are incorporated into HAS colloids, not only at the moment of colloid generation through conucleation, but also through sorption on aged colloids as they may exist in the aquifer system either from condensation or dispersion. The sorption of Am is small and merely the result of a still proceeding colloid formation under the given experimental colloid aging times ($\leq$ 27 days). The sorption of Th into HAS colloids, however, is almost independent of the colloid age. The underlying reason is the existence of different incorporation pathways for Th. If present at the moment of colloid formation, Th follows the conucleating behaviour of either mono- or polysilanol with Al. Later, Th interacts with preformed HAS colloids by displacing Si in a very fast sorption process. Th sorption is mosty pronounced for colloids, formed from polysilanol, reflecting the stronger

affinity of the Th-oxyhydroxide anionic ligand for the Al^{3+} cation, a characteristic which has been observed from a number of other experiments as described in previous sections.

The corresponding pseudocolloids of Th are extremely stable against desorption with inactive medium, and the Th-(aged HAS colloid)-bindings are called irreversible. Their decreasing stability against desorption with EDTA with decreasing pH, e.g. from 100% and 50% at neutral pH (7-9) for HAS generated from poly- and monosilanol, respectively, to a 20% at pH 5 for both HAS after 35 days EDTA contact time, reflects the existence of several colloid-borne Th species. Isomorphic substitution of Th for Si through sorption on aged HAS-polysilanol colloids at neutral pH is ascertained.

8. Tri- and tetravalent actinides: tracers for the aluminosilicate colloid generation

In the previous considerations, actinides have been the main subject of interest. Colloids have been seen as vehicles, which may bind actinides irreversibly and transport them without hindrance in the geosphere. Now we turn our interest to the colloids and consider the irreversibly bound actinides, Am(III) and Th(IV) as tracers for Al(III) and Si(IV), respectively, in order to better understand the process of aluminosilicate colloid formation.

8.1 Colloid and pseudocolloid generation mechanisms

HAS-monosilanol colloids

In recent publications, Doucet et al.[54,55] describe two types of HAS, formed from undersaturated Si in acidic solutions at pH = 6 and differentiated by NMR spectroscopy, and visualize their structures by AFM. One is rectangular with 25 nm length and another has a discoid shape with 18 nm diameter. They correlate the different structures as well as distinct Si/Al ratios in HAS, namely 0.5 and 1.0, with different Si/Al concentratio ratios in the mother solutions, and postulate a reaction mechanism for the formation of HAS via the competitive condensation of silicic acid $Si(OH)_4$ at a hydroxylaluminum template. Our findings, e.g. HAS colloids with a Si/Al atomic ratio of 0.7 (cf. section 3.5), are in good agreement with the mentioned concept for HAS formation. Therefore, we propose a similar reaction mechanism, which has been adapted to our experimental conditions for HAS colloid generation by titration of Al dissolved in acid with Si dissolved in base to beyond acid (pH = 4 – 9), and which

selects such HAS colloids capable to incorporate trivalent actinides. Fig. 64 illustrates the template formation [54,55]: If Al is in excess, Al hydrolyzes, dimerizes and builds a hydroxy-alumino template. $Si(OH)_4$ condensates at the preformed template under formation of a hydroxy-aluminosilicate (Si/Al ratio = 0.5). If Si is in excess, HAS(I) acts as a template for further reactions with $Si(OH)_4$ and forms HAS(II) with Si/Al = 1. In HAS(II), 50% of the Al has changed from the octahedral to the tetrahedral geometry. This kind of nucleation has to build up a surface on ist own, starting from a dimeric Al template. Fig. 65 illustrates the mentioned self catalyzing reaction, less efficient to incorporate trivalent actinides (An(III)) as compared with Al, allowing only bidentate and tridendate bindings to the colloids.

HAS-polysilanol colloids

The aluminosilicate colloids, which have been synthesized from HAS-polysilanol and from HAS-monosilanol are quite similar, e.g. both, formed out of mother solutions with a Si/Al concentration ratio of 100 have a Si/Al atomic ratio of about one (cf. section 3.5). Their completely different behaviour at the interaction with actinides, however, e.g. different incorporations patterns as well as incorporation kinetics for Am and Th, different colloid-borne Cm species as identified by TRLFS, different stability characteristics, clearly reveal distinct reaction mechanisms for the HAS-monosilanol and the HAS-polysilanol colloid generation. We propose an inner surface complexation model for the formation of HAS-polysilanol colloids, which takes into account the high affinity of polysilanol for the Al^{3+} cation [56], allows for isomorphic substitution of Cm for Al in the colloidal aluminosilicate structure as well as for the growth of Th into the colloids with time. Fig. 66 shows the consecutive steps: (1) the replacement of coordination water of Al (or Cm) by Si-polysilanol-anions; (2) the strong Al-binding weakens the Si-O-binding; (3) a product with an Si/Al ratio = 1 is splitt off. Th can either copolymerize with Si and form poly-Si(Th)- anions (Fig. 67) or displace Si in the HAS product, depending on wether the interaction of Th with Si and Al is simultaneous or a posteriori.

8.2 Role of Si and Al in colloid formation

The suggestion of Exley et al. [80,81] that the mechanim of HAS formation at low pH involves the poisoning of aluminium hydroxyde polymerization by silicic acid, bases on an

older mechanistically proposal of Birchall [82] to describe the retardation of ordinary portland cement (calcium hydroxide lattice) by sugars. The applicative know-how is even older and dates back to the construction of the chinese wall and the use of rice water as an additive in the mortel. Inspired by such points of view, we postulate that the HAS colloid formation as we observed at neutral pH (≥ 7) results from the reverse effect, namely the inhibitory effect of small amounts of Al on the polymerization of Si, which is present in the mother solution in a hundredfold Al-concentration. Fig. 68 visualizes the conception. Elements with high oxidation state such as Si(IV) neutralize their positive charge by surrounding themselves to a maximum extend with oxygens in the processes of hydration, hydrolysis and polymerization. Precipitation is the inevitable consequence. In the presence of Al, an isomorphic substitution of Al for Si takes place. Negative charges are induced into the forming silicate structure. The mutual repulsion between HAS particles hinders a further aggregation, the process which corresponds to an extremely retarded polymerization of Si through the binding of Al. We may say that an Al-controlled polymerization of Si enables kinetically the thermodynamically unfavourable colloidal state. Such a stabilization of the colloidal state has been formulated in theoretical terms by the DLVO theory (see section 2.1). The Al effect is de facto a shift of the equilibrium $Si_{solution} \Leftrightarrow Si_{colloids} \Leftrightarrow Si_{precipitate}$ from the right to the left.

To test the hypothesis, the effect of Al is analyzed under our experimental working conditions for aluminosilicate colloid formation, e.g. the behaviour of a 2.5 times oversaturated Si solution ($5x10^{-3}$ mol l^{-1}) (100%) at pH 7 in presence of 100% Al ($5x10^{-3}$ M) and 1% Al ($5x10^{-5}$ M) at depolymerization and polymerization, respectively. The experimental approaches as shown in Fig. 26 and molybdenum-tests for the quantification of mono- and polysilanol are used. The result is illustrated in Fig. 69 and shows that addition of minute amounts of Al (1% of Si) enhance at first the polymerization rate of Si but shift the equilibrium between mono- and polysilanol in favour of monosilanol ($\Delta = 10\%$). The fact corroborates the hypothesis of the inhibitory effect of the Al binding on the polymerization of Si. Fig. 69 further demonstrates the instantaneous reaction of Al with polysilanol, both present in equal concentration, and the complete inhibition of the depolymerization of Si through aluminosilicate formation. The findings not only infer the formation of the aluminosilicate binding, but they also confirm that the chemical affinity of the Al^{3+} ion towards complexation is preferentially marked with polysilanol [23,56].

The Al effect is further pursued radiochemically from Am as illustrated by Fig. 70. To a constant concentration of dissolved Si ($1.3x10^{-3}$ M) in base, increasing concentrations of Al

dissolved in acid are given and the bebaviour of Am, added as a tracer, is observed. At pH 5 and low Al-concentration, Am is in the precipitate. Through addition of more and more Al, Am migrates from the precipitate into the colloids and even to the solution. The same happens at pH 8: at increasing the Al concentration, Am is transferred from the precipitate to the colloids, and than returns to the precipitate. The explanation: The equilibrium $Am(Al)_{solution} \Leftrightarrow Am(Al)_{colloids} \Leftrightarrow Am(Al)_{precipitate}$ is shifted to the left through binding of Am(Al) with Si and indirectly through the inhibition of the polymerization of Si by Al. Once Si is saturated with Al, the overlapping hydrophobic effect of excess, non-binding Al drives the colloidal HAS including the colloid-borne Am into precipitate. In theoretical terms, the process is called the „colloid destabilization by decrease of the thickness of colloidal electric double layer through increase of the ionic strength of solution“ (see section 2.1). The experiment nicely shows the dual character of Al, either inhibitor of the polymerization of Si or activator of the agglomeration of HAS colloids, and demonstrates why colloids are built only under well-tuned parameter conditions, which we have called „optimum“ conditions. In nature, such conditions are obviously not the exception but the underlying rule; otherwise we would not find colloids in all groundwater.

Conclusions of section 8

The high oxidation state of Si(IV) induces polymerization. Doping the Si(IV) mother solution with Al(III) programms the end of polymerization at colloidal size. Stabilization of the colloidal state is due to isomorphic substitution of Si for Al, inducing thereby negative charges into the silica structure. Repulsion of the negatively charged particles and an extreme retardation of the Si polymerization is the consequence.

Two different mechanisms for colloid formation are postulated on the basis of the interaction of tri- and tetravalent actinides with HAS colloids in statu nascendi. One model starts from monosilanol condensing with Al in a self catalyzing template mechanism, which is not very efficient to bind tri- or tetravalent actinides. The other is an inner surface complexation model which starts from a preformed and very effective polysilanol surface for catalyzing the conucleation of Si and Al and proceeds under expulsion of the HAS product. In such a process, tri- and tetravalent actinides easily substitute isomorphically for Al and Si, respectively.

9 Actinide analogs of aluminosilicate colloids

The controlled polymerization of Si to the colloidal size through binding with Al is understood as a play of elements with high and different oxidation state and the induction of charge. The question whether such a mechanism is unique for Si and Al or generally valid, for example also for tri-and tetravalent actinides, motivates us to search for colloid formation at the coprecipitation of Th and Am.

9.1 Parameter screening for colloid formation of Th and Am

Solubility data for amorphous (am) $Th(OH)_4$ [83] and $Am(OH)_3$ [66] as a function of pH are given in Fig. 71, lower and upper part, respectively. Oversaturation with colloid formation within the pH range from 4 to 9 might be expected in a rather broad concentration range of about 10^{-9} to 10^{-6} mol l^{-1} for Th and 10^{-9} and 10^{-7} mol l^{-1} for Am. A screening experiment to ascertain conditions for colloid formation is conducted for a corresponding variety of the initial Th and Am concentrations and their different ratios (from 0.1 to 6.5). Each coprecipitation sample is prepared by titrating an acid solution of Th and Am in 3x 10^{-2} mol l^{-1} HCl with 3x 10^{-2} mol l^{-1} NaOH (suprapur, Merck) to a preset pH. After different conditioning times, the distribution of Th as well as of Am in the three phases (ionic, colloids and precipitate) is determined. Blanks with only Th or only Am are also made for the purpose of comparison.

Figs. 72-75 show the result for 4 levels of Th concentration, i.e. at 1x10^{-9}, 7.0x10^{-9}, 4.6x10^{-8}, 3.2x10^{-7} mol l^{-1}, each of them combined with Am to cover the above indicated screening area, as well as for the corresponding separate samples (only Am or only Th). The figures represent the activity fraction (%) in the colloidal phase after 3 hours conditioning time for the mixed and the separate samples of Th and Am, as a function of the pH. Under all analyzed conditions, the changing behaviour of „only Th“ as well as „only Am“ when accompanied by Am (measurement of Th in (Th+Am) sample) or Th (measurement of Am in (Th+Am) sample), respectively, is striking. Especially at pH = 6 – 9, Th starts to behave like Am and vice versa. What more is, Th as well as Am, are transferred from the precipitate to the colloidal state, only through mutual interaction. This is a clear indication for the binding of Th with Am, which will be verified with TRLFS (see next section 9.2). It is also the expression of the mutual inhibitory effect on their polymerization. The patterns for incorpora-

tion into the colloidal phase for the mixed and single samples of Th and Am are also different in the acidic region pH = 4 to 6. In this region, Am is well soluble and Th shows a sharp solubility decrease (see Fig. 71). It is therefore amazing to find some Th and even Am in the colloidal phase of the separate samples. The effect might be partly due to „impurities“ in the samples. Ubiquitous elements like Si may be present in concentrations, which are comparable to the solubility concentrations of actinides, and therefore not negligible. However, the comparison of the behaviour of Am and Th, separately, with that of the (Am+Th)-mixture under the exactly same conditions is still allowed and can give useful information.

Fig. 76 summarizes the results given in Figs. 72-75 without the blanks and shows the activity in the colloidal fraction (%) after 3 hours (Fig. 76, left part) and after 35 days (Fig. 76, right part) in order to allow a better comparison of colloid formation, not only at different concentration levels and ratios, but also after an increased sample conditioning time. The view of activity incorporation into the colloidal phase after 3 hours (Fig. 76, left part) clearly shows the similar behaviour of Th and Am in the mixed samples at neutral pH at all concentration levels of Th. At pH = 4 – 6, however, Th and Am behave differently. At increasing concentration, Th is oscillating between the colloidal phase and the precipitate, whereas Am is oscillating between the colloidal phase and the solution. The view of activity in colloids after 35 days (Fig. 76, right part) reveals that the colloids, which have been generated at neutral pH at relatively high concentrations of Th and Am as compared with their solubilty concentrations are quite unstable as a function of time. The fact may be due to the lower induced polarization by substituting Th(IV) for Am(III) as compared with Si(IV) substitution for Al(III), or reverse. Another reason for the low colloid stability may be related with the concentration levels of actinides we have used: too high to form stable colloids, but too low as compared with system impurities, which interactions become visible now.

In the region of higher solubility of Th and Am, namely at pH = 4 - 5, we observe an interesting colloid stabilization with time. Let us take the example of the sample with Th at $10^{-7.3}$ mol l^{-1} and Am at $10^{-8.1}$ mol l^{-1} (ratio Th/Am = 6.122) at pH = 4. Colloid stabilization (compare corresponding left and right parts of Fig. 76) is expressed not only by an increased activity in the colloidal fraction with time but also by a synchronization of the polymerization of Am and Th as expressed by a pH shift for the maximal Am-activity after 35 days. Fig.77 illustrates the corresponding kinetics and illustrates the partition of the activity in the three phases (soln / coll. / prec.). The upper part of Fig. 77 shows the behaviour of the separate Th and Am samples (Th at the left and Am at the right part of Fig. 77). Th is fully precipitated at

all times. Am is dissolved at 60% but becomes 60% colloidal with time. The middle part of Fig. 77 gives the kinetic behaviour of Th and Am in the mixed sample and shows that Th is transferred from the precipitate to the colloidal phase and even to the solution only through mixing (binding) with Am. The effect of mixing Th with Am is the partial inhibition of polymerization (precipitation) of Am in favour of Am in colloids Am and in solution. After some days, the polymerization kinetics of Th and Am become synchronized, both with a 60% in the colloidal phase. After 89 days we calculate a colloidal Th/Am atomic ratio = 7.88, reflecting almost the Th/Am concentration ratio in the mother solution, which is 6.12.

The possibility to achieve a better colloid stabilization by substituting tri- or tetravalent cations for divalent cations in order to increase the induced polarization is further analyzed. Therefore Mg is added in a concentration of 10^{-2} mol $l^{-}1$ to the mixed (Th+Am) sample (Fig. 77, middle part) at pH = 4 with Th at $10^{-7.3}$ mol l^{-1} and Am at $10^{-8.1}$ mol l^{-1}. The Mg-effect is shown in the lower part of Fig. 77. The equilibrium of Th in the mixture is shifted in favour of the precipitate. Only 20% instead of 60% of the original Th remains colloidal, but very stable with time. Am is colloidal at about 60% and shows a synchronized behaviour with Th from the very beginning. The colloids have now an atomic Th/Am ratio, e.g. after 111 days of 2.17, instead of 7.88 for the analog sample without Mg. The experiment clearly demonstrates that the colloid composition and the related colloid stability can be directed by divalent cations in the medium. This interesting effect will be further analyzed.

9.2 Interaction of Th with Cm analyzed by TRLFS

From the previous radiometric experiments coupled with ultrafiltration, we have found conditions where Th and Am conucleate, and by doing so, stabilize actinides into the colloidal state. We now want to verify spectroscopically the interaction of Cm with Th with the aid of TRLFS, directly at the titration of an acid solution ($3.5x10^{-7}$ mol l^{-1} Th and $5x10^{-8}$ mol l^{-1} Cm in 0.03 mol l^{-1} HCl) with 0.03 M NaOH (suprapure, Merck). The fluoresence spectra in the course of the titration are shown in Fig. 78 (upper part) and the deconvoluted spectra in Fig. 78 (middle part). Two Th-borne Cm species are observed, namely Cm-Th(I) and Cm-Th(II) with emission peaks at 598.0 nm and 604.8 nm, respectively. The fluorescence life times are also measured to ascertain the number of hydration waters molecules bound to Cm. Cm-Th(I) and Cm-Th(II) have a relaxation time of 135.5 μs and 331.0 μs, corresponding to 3.9 and 1.1 remaining water molecules of Cm, respectively. The pentadentate binding for the Cm-Th(I)

species and the complete incorporation of Cm into the structure of Th for the Cm-Th(II) species are thereby ascertained. Overall speciation results are summarized in Fig. 78 (lower part) for the free Cm ion as well as the Th bound Cm species as a function of pH. The Cm^{3+}-aquo-ion is predominating in the low pH region from 1 to 4. At the same time the Cm-Th(I) species is built to a maximum of 25% at pH = 5 – 6. The incorporated species Cm-Th(II) emerges from pH 4 and increases its fraction sharply at pH 6 to more than 95% in the pH region from 6 to 9. The colloid-borne Cm species, as identified by TRLFS, correspond to the optimum regions for colloid formation, as identified in the screening experiment (cf. Fig. 76), which corroborates spectroscopically the indications from radiometric measurements (section 9.1) that „americiothoronate“ colloids are generated. We also remark that Cm-Th(I) and Cm-Th(II) without HAS are very similar, although not completely same, as compared to the Cm-Th(I) and Cm-Th(II) which are found in presence of HAS (see section 6.2, Table 2).

The question whether the americiothoronate binding is a conditio sine qua non for colloid formation is still open. We expect more information from the analysis of actinide colloid formation with LIBD, as described in the following.

9.3 Interaction of Th with Eu traced by LIBD

In a similar titration experiment as performed for the TRLFS measurement, we trace colloid formation directly at the titration of 6.5×10^{-7} mol l^{-1} Th with 1×10^{-7} mol l^{-1} Eu in the pH range of 1 to 10. Eu is used as inactive substitute for Am(Cm). We compare the breakdown probability as a function of pH for four samples: (1) blank without Th and Am; (2) Eu only; (3) Th only; (4) mixture of Th+Eu. Fig. 79 shows the result. The relatively high background at pH ≥ 6 resulting even from suprapure chemicals or from leaching of the vessel walls of the LIBD instrumentation limits the observation window to the low pH region. However, the result is clear. At pH = 4 – 5, the generation of colloids by mixing Th and Eu, clearly surpasses a certain colloid formation in the separate Th and Eu samples and corroborates the previous findings of colloid generation through polarization at heterogeneous nucleation (polymerization) of elements with different oxidation state and therefore with different rates of polymerization (see section 8.2). Comparing the present result with the result of radiometric measurement as shown in Fig. 7 and Fig. 77, we may even assume that the europiothoronate colloids as detected by LIBD are similar to the americiothoronate colloids formed at pH 4 after 3 hours with a Th/Am activity fraction ratio of 59.4% / 6.4%, multiplied with the Th/Am

concentration ratio in the original solution, namely 6.12, giving the atomic Th/Am ratio in colloids: $(Th/Am)_{colloids} = 57$. Investigations on this subject are currently pursued. The important result leads to a new view of actinide colloids and also to a new definition of „real colloids“, which might quite different from what we have been used to in the past.

Conclusions of section 9

Americio- and europiothoronate colloids have been synthesized in analogy with aluminosilicate colloids. The colloid generation is explained as a controlled polymerization of actinides of one oxidation state through conucleation with actinides of different oxidation state. The control consists of the retardation of polymerization through mutual binding, as confirmed by TRLFS, and the stabilization of the colloidal state, as shown by LIBD, through polarization of the particles. The hypothesis that one element, present in a single oxidation state, cannot build „real colloids“ of actinides will be further verified.

The Th/Am atomic ratio in the americiothoronate colloids is, in contrast to that in HAS colloids, the same as the Th/Am concentration ratio in the mother solution. Divalent cations, such as Mg can alter the Th/Am atomic ratio in the colloids and influence the colloid stability correspondingly.

10 Summary

Migration of colloid-borne actinides in the geosphere is a well recognized, but hitherto non-quantifiable fact, that still questions the safety of nuclear repositories. The underlying reason is pour knowledge about the mechanisms of colloid formation, colloid stabilization and hence of colloid/actinide interaction. The present investigation concentrates on whether and how tri- and tetravalent actinides are incorporated into the colloidal phase, either through formation of real colloids or by binding to natural aquatic colloids, e.g. aluminosilicate colloids. The irreversibility of such processes is a conditio sine qua non for the colloid facilitated actinide migration and therefore a central question in this study.

The first part of the work deals with the synthesis of aluminosilicate colloids under normal conditions of temperature and pressure from supersaturated mother solutions through conucleation of Si(IV) and Al(III). It includes the identification, analysis and intercorrelation of the thermodynamical and kinetic solubility parameter of Si and Al on theoretical and ex-

perimental basis, as well as the characterization of the generated colloids. In an elaborated parameter screening experiment, optimum conditions for the formation of aluminosilicate colloids are recognized from the behaviour of Am, added as a tracer in the condensation process of Si and Al. The optima are reflected by maxima of Am activity in the colloidal fraction of mother solutions made at pH 5 - 6 and pH 8 - 9, with a Si/Al concentration ratio of 100, but at two different Si concentration levels, namely in a slightly undersaturated and in a 6.5 times oversaturated solution, containing monosilanol and polysilanol, respectively. The corresponding colloids, as characterized by LIBD, AFM and SEM-EDXS, all belong to a unique colloid type which is very similar to the natural aquatic colloids of the imogolite type with a Si/Al atomic ratio of ca. 1, namely hydroxy aluminosilicate (HAS) colloids. The particle size is 10 - 50 nm and the number density amounts to $10^{11} – 10^{14}$ particles per litre.

The second part of this study investigates the interaction of trivalent actinides with HAS colloids in formation (in statu nascendi) and comprises the speciation of colloid-borne Cm with TRLFS, stability tests of the generated pseudocolloids of Am(Cm) by means of LIBD and desorption experiments, and determination of the capacity of HAS colloids to bind Am(Cm). The TRLFS analysis shows a red shift of the typical fluorescence emission band of the Cm^{3+} aquo-ion at 593.8 nm to 598.5 nm, 601.8 nm and 606.8 nm indicating the formation of three colloid-borne Cm species, namely Cm-HAS(I), Cm-HAS(II) and Cm-HAS(III), respectively. The spectral shift is proven to be characteristic for the interaction of Cm with Si. The respective increased fluorescence relaxation times from 65.2 μs for the Cm aquo-ion to 83.5 μs, 88.3 μs and 518.0 μs, are correlated with the number of replaced Cm coordination waters through silanols, and reveal the three colloid-borne Cm species as a bidentate, a tridentate and a completely incorporated Cm into the aluminosilicate structure of colloids. The relative Cm species distribution as a function of pH at the two above mentioned concentrations of Si for optimum colloid formation shows that the binding strength of Am(Cm) to HAS colloids increases with increasing pH and increasing concentration of Si. The effect is correlated with the faster polymerization kinetics of Si at high pH and high Si concentration, as demonstrated by a number of molybdenum tests for the quantification of the polysilanol fraction as a function of time under our experimental conditions for colloid generation. The isomorphic substitution of Am(Cm) for Al in the aluminosilicate colloid structure is further correlated with the interfacial energy of polysilanol, which seems to be necessary to overcome the activation energy barrier for the complete incorporation of Am(Cm). The explanation is corroborated by the fact that Cm-HAS(III) is also built at increased temperature, e.g. 5 days at 90°C, from

undersaturated Si (monosilanol) as an alternative way to provide activation energy. The generated pseudocolloids of Am(Cm), corresponding to the Cm-HAS(II) and Cm-HAS(III) species are extremely stable as a function of time, against desorption with inactive medium (irreversible Am(Cm)-colloid binding), and at increased temperature. Their formation is, however, pH reversible, and in line with the relatively low stability of Cm-HAS(I) built at pH 5-6. The maximum capacity of HAS colloids to incorporate Am(Eu) is reached for HAS colloids, generated from polysilanol at pH 8 - 9 when about one third of the Al in colloids is substituted by Am(Eu) and the HAS colloids start loosing their original identity.

The third topic of investigation is the interaction of tetravalent actinides with HAS colloids in statu nascendi, and includes the determination of the activity incorporation patterns as well as kinetics for Th, stability tests of the generated pseudocolloids of Th, and determination of the capacity of HAS colloids to bind Th. The incorporation of Th into HAS colloids increases with increasing time, pH and Si concentration, and reflects the polymerization kinetics of Si. The behaviour of Th is yet different from that of Si: the fraction of Th migrating from the mother solution into the colloids is a hundred times higher than that of Si, namely 100% and 1%, respectively, indicating a much higher affinity of Th-oxyhydroxide for the Al^{3+} cation in comparison with mono- and even polysilanol. The pseudocolloids of Th show a high resistance against desorption with inactive medium. The Th-HAS bindings are therefore considered to be irreversible. The incorporation of Th differs from that of Am as far as pH dependency, kinetics, quantity as well as stability are concerned. The general tendency ist that Th incorporates slower, more and in a broader pH region as compared with Am. Colloid-borne Th, unlike colloid-borne Am, stabilizes the HAS colloids. The highest concentration of Th, possibly hold by HAS colloids, is given at colloid formation from polysilanol at neutral pH from 6 to 9, and after a conditioning time of several days. In that case about 80% of the Si in colloids is substituted by Th. Since the Si/Al atomic ratio in colloids is ca. 1, the Al concentration in the mother solution can serve as an indicator for the amount of potentially incorporated Th in the colloids.

The fourth part of this study analyzes the interaction behaviour of a mixture of tri- and tetravalent actinides with HAS colloids in statu nascendi by comparing it with their separate behaviour. To this purpose, Am(Cm) and Th activity phase distribution patterns, time-resolved laser fluoresence spectra shifts, Cm species distributions and activity desorption measurements are evaluated. Incorporation of Am as well as of Th out of their mixture still takes place. Differences in incorporation patterns as well as in type and number of Cm spe-

cies, as previously observed at the formation of HAS colloids, either from mono- or polysilanol, are cancelled out if Cm is accompanied with Th. Only two colloid-borne Cm species, namely the Th-borne Cm species, Cm-Th(I) at 590.0 nm, and Cm-Th(II) at 603.6 nm, with fluorescence life times of 134.0 μs and 342.9 μs, corresponding to four and no waters in the coordination sphere of Cm, respectively, are now identified. They reflect the interaction behaviour of Cm-Th complexes with HAS colloids. This interaction resembles more that of Cm(Am) at low pH from 4 to 6, and more that of Th at neutral pH from 6 to 9. The stability of the generated pseudocolloids against desorption with inactive medium remains, notwithstanding the Cm-Th complex formation, almost unchanged. Consequently, the (Cm+Th)-HAS bindings are irreversible.

The fifth topic of this work concerns the incorporation behaviour of tri- and tetravalent actinides into aged HAS colloids through sorption, and comprises the evaluation of Am and Th activity incorporation patterns as well as stability tests of the corresponding pseudocolloids. Aged colloids are not tied up to sorb Am. Their capability to sorb Th, however, is high, and comparable to that of HAS colloids in statu nascendi. The high stability of the pseudo-(aged)-colloids of Th against desorption with inactive medium corresponds to irreversible Th-(aged HAS colloid)-bindings. A gradually decreasing stability against desorption with EDTA, from 100% to a 20% after 35 days EDTA contact time, reveals different colloid-borne Th species with decreasing Th-colloid binding strength in the order: Th-HAS-polysilanol (pH 7-9) (containing Th isomorphically substituted for Si) > Th-HAS-monosilanol (pH 7-9) > Th-HAS-poly-silanol or Th–monosilanol (pH 5).

The sixt part of the work is the trial to find out how colloids are thinking by reviewing the gained results from the standpoint of colloids, traced by actinides, and to postulate mechanisms for colloid formation. Key words of colloidal language are „controlled polymerization“ through „polarization“ and „optimal conditions“. They are elaborated in the experimentally corroborated conception. The high oxidation state of Si(IV) induces polymerization. Doping the Si(IV) mother solution with Al(III) programms the end of polymerization at colloidal size. Stabilization of the colloidal state is due to isomorphic substitution of Si for Al, inducing thereby negative charges into the silica structure. Repulsion of the negatively charged particles and an extreme retardation of the Si polymerization is the consequence. An optimal Si/Al ratio in the mother solution is prerequisite to stable HAS colloids. An excess of Al promotes colloid agglomeration through solvation effect. Two different mechanisms for colloid formation are postulated on the basis of the interaction of tri- and tetravalent actinides with HAS

colloids in statu nascendi. One model starts from monosilanol condensing with Al in a self-catalyzing template mechanism, which is not very efficient to bind tri- or tetravalent actinides. The other is an inner surface complexation model which starts from a preformed and very effective polysilanol surface for catalyzing the conucleation of Si and Al and proceeds under expulsion of the HAS product. In such a process, tri- and tetravalent actinides easily substitute isomorphically for Al and Si, respectively.

The seventh and last part of this study is devoted to the question whether actinide analogs of aluminosilicate colloids such as americiothoronate colloids do exist, also without the aid of Si or Al. This part contains a parameter screening experiment for colloid formation out of supersaturated solutions of Th and Am, based on activity measurements in the ionic, colloidal and precipitated fraction, speciation of colloid-borne Cm with TRLFS, and monitoring of colloid formation by LIBD. Optimum conditions for the formation of stable amerciothoronate colloids are found at pH 4 – 6, for several Th concentration levels between 10^{-9} and 10^{-6} mol l^{-1} , and at pH 9, for one Th concentration namely 10^{-9} mol l^{-1}, each of them combined with Am to give a Th/Am ratio in the mother solutions between 0.1 and 6.5. The optima are correlated with two colloid-borne Cm species, Cm-Th(I) at 598.0 nm and Cm-Th(II) at 604.8 nm, with fluoresence life times of 135.5 μs and 331.0 μs, corresponding to four and no water molecules in the coordination sphere of Cm, respectively. The species are very similar to those found at simultaneous incorporation of Am(Cm) and Th in HAS colloids in statu nascendi. LIBD measurements corroborate that precipitating Th, mixed with precipitating Eu, are transferred into the colloidal state through Th-Eu-binding. The Th/Am atomic ratio in the americiothoronate colloids is the same as the Th/Am concentration ratio in the mother solutions. We propose therefore a simple conucleation of Th with Am(Cm, Eu) as a binding mechanism. This is in contrast to the nucleation mechanism of Si with Al, namely the formation of a solid solution, with ($Si/Al_{coll.} = 1$) << ($Si/Al_{soln} = 100$). Divalent cations, such as Mg, can alter the Th/Am atomic ratio in the colloids and influence the colloids stability correspondingly. The Mg effect is shown to be an effect on the polymerization rate of Th (retardation through binding) as well as on the polymerization rate of Am (acceleration through solvation effect). Investigations on this subject are continued, since they may lead to a new view of actinide colloids, to a new definition of „real colloids“, which is quite different from the one we have been used to in the past, and especially to a better understanding of the fundamental rules for colloid stabilization in general.

11 References

[1] S. Yariv, H. Cross, Geochemistry of Colloid Systems, Springer, Berlin, 1979.

[2] J.F. McCarthy and C. Degueldre, in: J. Buffle and H.P. Van Leeuwen (Eds.), Environmental Particles, Lewis publishers, Boca Raton, 1993, p. 248

[3] P. Cloos, A.J. Leonard, J.P. Moreau, A. Habillon, J.J. Fripiat, Clays Clay Miner. 17 (1969) 270.

[4] C. Clark-Monk and B. Ellis, J. Colloid Interface Sci. 44 (1979) 37.

[5] J. Duan, J. Gregory, Colloids Surf. A 107 (1996) 309.

[6] J.I. Kim, Radiochim. Acta 52/53 (1991) 71.

[7] M. Bouby, T. Ngo Manh, H. Geckeis, F. Sherbaum, J.I. Kim, Radiochim. Acta 90 (2002) 727.

[8] J.I. Kim, P. Zeh, B. Delakowitz, Radiochim. Acta 58/59 (1992) 147.

[9] J.I. Kim, B. Delakowitz, P. Zeh, D. Klotz, D. Lazik, Radiochim. Acta 66/67 (1994) 165.

[10] M. Schnitzer and S.U. Kahn, Humic Substances in the Environment, Marcel Dekker, New York, 1972.

[11] M. Buleva, I. Petkanchin, Colloids Surf. A 151 (1999) 225.

[12] J.I. Kim, D.S. Rhee, G. Buckau, A. Morgenstern, Radiochim. Acta 79 (1997) 173.

[13] C. Degueldre, I. Triay, J.I. Kim, P. Vilks, M. Laaksoharju, N. Miekeley, Appl. Geochem. 15 (2000) 1043.

[14] J.I. Kim, MRS Bulletin 19 (1994) 47.

[15] J.I. Kim, Nuclear Engineering and Design 202 (2000) 143.

[16] A.B. Kersting, D.W. Erfurd, D.L. Finnegan, D.J. Rokop, D.K. Smith, J.L. Thompson, Nature 397 (1999) 56.

[17] H. Geckeis, R. Klenze, J.I. Kim, Radiochim. Acta 87 (1999) 13.

[18] Th. Stumpf, A. Bauer, F. Coppin, J.I. Kim, Environ. Sci. Technol. 35 (2001) 3691.

[19] Th. Rabung, Th. Stumpf, H. Geckeis, R. Klenze, J.I. Kim, Radiochim. Acta 88 (2000) 711.

[20] J.I. Kim, Mater. Res. Soc. Symp. Proc. 294 (1993) 3.

[21] R. Artinger, W. Schüßler, T. Schäfer, J.I.Kim, Environ. Sci. Technol. 36 (2002) 4358.

[22] R. Artinger, Th. Rabung, J.I. Kim, S. Sachs, K. Schmeide, K.H. Heise, G. Bernhard, H. Nitsche, J. Contam. Hydrol. 58 (2002) 1.

[23] T.W. Swaddle, Coord. Chem. Rev. 219-221 (2001) 665.
[24] W. Bernotat, X. Le Gal, J.L. Crovisier, European Union of Geosciences, J. Conf. Abstracts, Vol. 6 No. 1, EUG XI Strasbourg, France, 6-12 April 2001, p. 660.
[25] J.I. Kim, K. Gompper, K.D. Closs, G. Kessler, D. Faude, J. Nucl. Mater. 238 (1996) 1.
[26] J.I. Kim, R. Klenze, H. Wimmer, Eur. J. Solid State Inorg. Chem. 28 (1991) 347.
[27] F.J. Scherbaum, R. Knopp, J.I. Kim, Appl. Phys. B - Lasers and Optics 63(3) (1996) 299.
[28] T. Bundshuh, W. Hauser, J.I. Kim, R. Knopp, F.J. Scherbaum, Colloid. Surf. A 180 (2001) 285.
[29] T. Bundshuh, R. Knopp, J.I. Kim, Colloids Surf.A 177 (1) (2001) 47.
[30] K. Kitamori, K. Yokose, M. Sakagami, T. Sawada, Jpn. J. Appl. Phys. 28 (7) (1989) 1195.
[31] C. Walther, C. Bitea, W. Hauser, J.I. Kim, F.J. Scherbaum, Nucl. Instrum. Methods Phys. Res. B 195 (2002) 374.
[32] C. Bitea, C. Walther, J.I. Kim, H. Geckeis, T. rabung, F.J. Sherbaum, D.G. Cacuci, Colloids Surf. A, in press.
[33] R.J. Hamers, J. Phys. Chem. 100 (1996) 13103.
[34] F.J. Giessibl, Science 267 (1995) 68.
[35] M. Plaschke, J. Römer, J.I. Kim, Ultramicroscopy 75 (1998) 77.
[36] M. Plaschke, T. Schäfer, T. Ngo Manh, R. Knopp, H. Geckeis, J.I. Kim, Anal. Chem. 73 (2001) 4338.
[37] M. Plaschke, J. Römer, J.I. Kim, Environ. Sci. Technol. 36 (2002) 4483.
[38] M. Stumm, Aquatic Chemistry, Wiley-Interscience, New York, 1981.
[39] M. Stumm, Chemistry of the Solid-Water interface, Wiley-Interscience, New York, 1992.
[40] K.S. Birdi, Surface and Colloid Chemistry, CRC, New York, 1997.
[41] H.-D. Dörfler, Grenzflächen- und Kolloidchemie, VCH, Weinheim, 1994.
[42] D.J. Shaw, Introduction to Colloid and Surface Chemistry, Butterworth-Heinemann, Oxford, 1991.
[43] D.F. Evans, H. Wennerström, The Colloidal Domain – Where Physics, Biology and Technology Meet, VCH, Weinheim, 1994.
[44] R. Klenze, J.I. Kim, H. Wimmer, Radiochim. Acta 52/53 (1991) 97.
[45] Th. Fanghänel, J.I. Kim, J. Alloys Compd. 271-273 (1998) 728.

[46] J.V. Beitz, Similarities and differences in trivalent lanthanide- and actinide molecules, in Handbook of Physics and Chemistry of the Actinides, Vol.18, K.A. Gschneider, Jr, L. Eyring, G.R. Choppin, G.H. Lander (Eds), North-Holland Phys. Publ., Amsterdam, p.120, 1994.

[47] D.S. Kliger, Ultrasensitive Laser Spectroscopy, Academic Press, New York, 1983.

[48] A.B. Yusov, J. Radioanal. Nucl. Chem. Articles 143 (1990) 287.

[49] Y. Kato, G. Meinrath, T. Kimura, Z. Yoshida, Radiochim. Acta 64 (1994) 107.

[50] Ch. Moulin, P. Decambox, V. Moulin, J.G. Decaillon, Anal. Chem. 67 (1995) 348.

[51] P. Schachtschabel, H.-P. Blume, C. Brümmer, K.-H. Hartge, U. Schwertmann, Lehrbuch der Bodenkunde, Ferdinand Enke Verlag Stuttgart, 1992.

[52] K. Wada, in J.B. Dixon, S.B. Weed (Eds.), Minerals in Soil Environments, Soil. Sci. Soc. Am., Madison (Wisc.), 1989.

[53] V.C. Farmer, M.J. Adams, A.R. Fraser, F. Palmieri, Clay Min. 18 (1983) 459.

[54] F.J. Doucet, C. Schneider, S.J. Bones, A. Kretchmer, I. Moss, P. Tekely, C. Exley, Geochim. Cosmochim. Acta 65 (2001) 2461.

[55] F.J. Doucet, M.E. Rotov, C. Exley, J. Inorg. Biochem. 87 (2001) 71.

[56] P.D. Taylor, R. Jugdaoshing, J.J. Powell, J. Amer. Soc. 119 (1997) 8852.

[57] J.D. Rimstidt, H.L. Barnes, Geochim. Cosmochim. Acta 44 (1980) 1683.

[58] M. Sadiq, W.L. Lindsay, Colo. State Univ. Exp. Stn. Tech. Bull., 134 (1979) 1.

[59] W.L. Lindsay, Chemical Equilibria in Soils, Wiley-Interscience, New York, 1979.

[60] H.M. May, D.G. Kinniburgh, P.A. Helmke, M.L. Jackson, Geochim. Cosmochim. Acta 50 (1986) 1667.

[61] H.C. Helgeson, J.M. Delany, H.W. Nesbitt, D.K. Bid, Am. J. Sc. 278 (1978) 1.

[62] C.F. Baes, Jr, R.E. Mesmer, the Hydrolysis of Cations, Wiley-Interscience, New York, 1976.

[63] R.M. Smith, A.E. Martell, Critical Stability Constants, Vol.4, Plenum Press, New York, 1978.

[64] Th. Stumpf, Th. Rabung, R. Klenze, H. Geckeis, J.I. Kim, J. Colloid Interf. Sci. 238 (2001) 219.

[65] W.I. Bourcier, K.G. Knauss, K.J. Jackson, Geochim. Cosmochim. Acta 57 (1993) 747.

[66] V. Neck, Th. Fanghänel, J.I. Kim, Report: FZKA 6110, Forschungszentrum Karlsruhe, 1998.

[67] R.K. Iler, The Chemistry of Silica, Wiley-Interscience, New York, 1997.

[68] G. Lagerstrom, Acta Chem. Scand. 13 (1959) 722.
[69] R. Siever, Amer. Mineral. 42 (1957) 826.
[70] N. Ingri, Acta Chem. Scand. 13 (1959) 758.
[71] S.M. Elgawhary, L. Lindsay, Soil Sci. Soc. Am. Proc. 36 (1972) 439.
[72] G.B. Alexander, J. Am. Chem. Soc. 75 (1953) 5655.
[73] E.N. Rizkalla, G.R. Choppin in: K.A. Gschneider Jr, L. Eyring, G.R. Choppin, G.H. Lander (Eds), Lanthanides and Actinides Hydration and Hydrolysis, Handbook on the Physics and Chemistry of Rare Earths, Vol. 18, Elsevier Science B. V., p. 529, 1994.
[74] W.De, Jr. Horrocks, D.R. Sudnick, J. Am. Chem. Soc. 101 (1979) 334.
[75] T. Kimura, G.R. Choppin, J. Alloys and Comp. 213/214 (1994) 313.
[76] K.H. Chung, R. Klenze, K.K. Park, P. Paviet-Hartmann, J.I. Kim, Radiochim. Acta 82 (1998) 215.
[77] H.M. Kingston, S.J. Haswell, Microwave-Enhanced Chemistry, Fundamentals, Sample Preparation and Applications, Am. Chem. Soc., Washington, D.C., p.314, 1997.
[78] S.W. Sill, Anal. Chem. 36 (1964) 675.
[79] O. Alhassanieh, A. Abdul-Hadi, M. Ghafar, A. Aba, Appl. Rad. Isotop. 51 (1999) 493.
[80] C. Exley, J.D. Birchall, Polyhedron 11 (1992) 1901.
[81] C. Exley, J.D. Birchall, Polyhedron 12 (1993) 1007.
[82] J.D. Birchall, N.L. Thomas, Brit. Ceram. Proc. 35 (1984) 305.
[83] V. Neck, J.I. Kim, Radiochim. Acta 89 (2001) 1.

12 Publications, Reports, Conferences

Publications

[1] M.A. Kim, P.J. Panak, J.I. Yun, J.I. Kim, R. Klenze, K. Köhler: „Interaction of Actinides with Aluminosilicate Colloids in Statu Nascendi, Part I: Generation and Characterization of Actinide(III)-Pseudocolloids“; Colloids and Surfaces A: Physicochem. Eng. Aspects 216 (2003) 97-108.
[2] P.J. Panak, M.A. Kim, J.I. Yun, J.I. Kim: „Interaction of Actinides with Aluminosilicate Colloids in Statu Nascendi, Part II: Spectroscopic Speciation of Colloid-borne Actinides(III); Colloids and Surfaces A: Physicochem. Eng. Aspects 227 (2003) 93-103.

[3] M.A. Kim, P.J. Panak, J.I. Yun, A. Priemyshev, J.I. Kim: „Interaction of Actinides with Aluminosilicate Colloids in Statu Nascendi, Part III: Colloid Formation from Monosilanol and Polysilanol“; Colloids and Surfaces A: Physicochem. Eng. Aspects, in press.

[4] M.A.Kim, P.J. Panak, J.I. Yun, A. Priemyshev, J.I. Kim: “Interaction of tetravalent Actinides with Aluminosilicate Colloids: Generation of Th-Pseudocolloids”, in preparation.

[5] M.A. Kim, P.J. Panak, J.I. Yun, A. Priemyshev, J.I. Kim: “Interaction of Actindes with Aquatic Colloids and Generation of Actinide Pseudocolloids”; Annual Rep. BMWA (2003).

[6] M.A, Kim, P.J. Panak, J.I. Yun, A. Priemyshev, J.I. Kim: “Interaction of Actinides with Aquatic Colloids and Generation of Actinide Pseudocolloids; IAEA Waste Management Research Abstracts (WMRA), Vol. 28, Abstarct No. 4959.

[7] P.J. Panak, M.A. Kim, R. Klenze, J.I. Kim, Th. Fanghänel: “Interaction of Cm(III) with Aqueous Mono- and Polysilicates studied by Time-resolved Laser Fluorescence Spectroscopy (TRLFS); Colloids and Surfaces A: Physicochem. Eng. Aspects, submitted.

Ph.D. Thesis

[1] A. Priemyshev; “Colloid Formation of Americium and Thorium in the Water / Aluminosilicate Systems”, Fakultät für Chemie, Technische Universität München (2004).

Conferences

[1] 8th International Conference on the Chemistry and Migration Behaviour of Actinides and Fission Products in the Geosphere, Bregenz, Österreich (2001):
M.A. Kim, P.J. Panak, J.I. Yun, J.I. Kim, R. Klenze, K. Köhler, “Interaction of Actinides with Aluminosilicate Colloids in Statu Nascendi”.

[2] GDCh-Jahrestagung Chemie 2001, Würzburg (2001):
M.A. Kim, P.J. Panak, J.I. Yun, J.I. Kim, R. Klenze, K. Köhler, “Interaction of Actinides with Aluminosilicate Colloids in Statu Nascendi”.

[3] 6. Projektstatusgespräch zu BMBF/BMWA-geförderten FuE-Vorhaben auf dem Gebiet der Entsorgung gefährlicher Abfälle in tiefen geologischen Formationen, Karlsruhe, "Einfluß von Kolloiden auf die Migration von Actiniden".

[4] 9th International Conference on the Chemistry and Migration Behaviour of Actinides and Fission Products in the Geosphere, Gyeongju, Korea (2003):
M.A. Kim, P.J. Panak, A. Priemyshev, J.I. Kim, "Actinides on the Track of Groundwater Colloids".
M.A. Kim, P.J. Panak, J.I. Yun, A. Priemyshev, J.I. Kim, K. Köhler, "Interaction of Tetravalent Actinides with Aluminosilicate Colloids: Generation of Thorium Pseudocolloids".
P.J. Panak, M.A. Kim, J.I. Yun, J.I. Kim, "Interaction of Actinides with Aluminosilicate Colloids "in Statu Nascendi"; Spectroscopic Speciation of Colloid-borne Cm(III)."

[5] GDCh-Jahrestagung Chemie 2003, München (2003):
M.A. Kim, P.J. Panak, J.I. Yun, A. Priemyshev, J.I. Kim, K. K. Köhler, "Interaction of Actinides with Aluminosilicate Colloids: Colloid Formation by Mono-Silanol and Oligo-Silanol".
M.A. Kim, P.J. Panak, J.I. Yun, A. Priemyshev, J.I. Kim, K. Köhler, "Intercation of Tetravalent Actinides with Aluminosilicate Colloids: Generation of Thorium Pseudocolloids".
P.J. Panak, M.A. Kim, J.I. Yun, J.I. Kim, "Interaction of Actinides with Aluminosilicate Colloids in "Statu Nascendi": Spectroscopic Speciation of Colloid-borne Cm(III)".

[6] "Plutonium Futures – the Science Conference", Albuquerque, New Mexico, USA (2003):
J.I. Kim, M.A. Kim, P.J. Panak, J.I. Yun, "Aquatic Colloids of Actinides: How are they generated under natural Aquifer Conditions?".

[7] American Chemical Society, 22th National Meeting & Exposition, Anaheim, CA, USA (2004):
J.I. Kim, P.J. Panak, J.I. Yun, M.A. Kim, "Actinides on the Track of Aquatic Colloids: Speciation of Colloid-borne Cm(III)".

Acknowledgements

Thanks are due to Drs. D. Schild and J.Römer for XPS and EDX analyses, M.Plaschke for AFM analyses, H. Geckeis for ICP-MS measurements, C.M. Marquardt for providing the isotopes Am and Cm and C. Dardenne for the thermodynamic solubility calculation.

Annexe: Figures and Tables

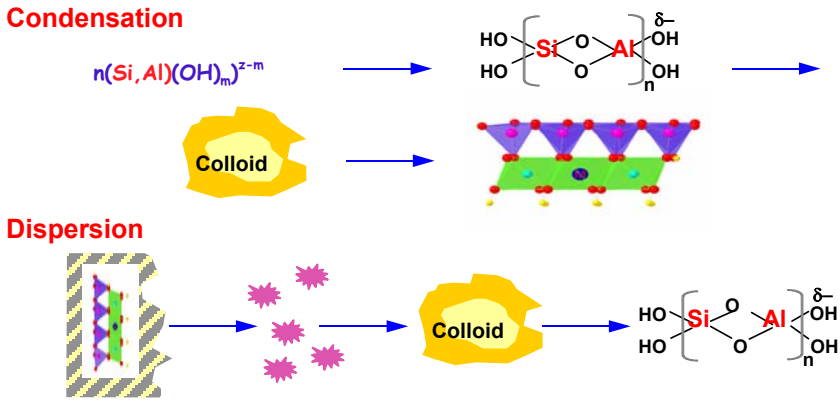

Fig. 1: General pathways for the formation of inorganic aquatic colloids such as aluminosilicate colloids.

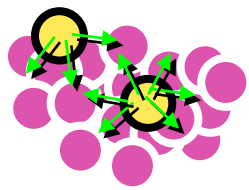

Fig. 2: Colloidal free energy stems from the imbalance of intermolecular forces exerted on molecules at the interface.

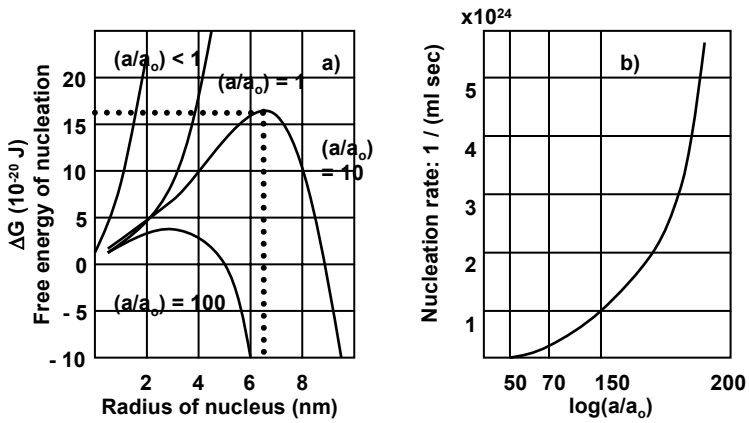

Fig. 3: (a) Free energy of nucleus formation calculated as a function of the radius for different supersaturated ratios (Eq.1). The maximum ΔG^* is the activation barrier to the generation of nuclei of radius r_j; (b) Nucleation rate calculated as a function of the critical supersaturation.

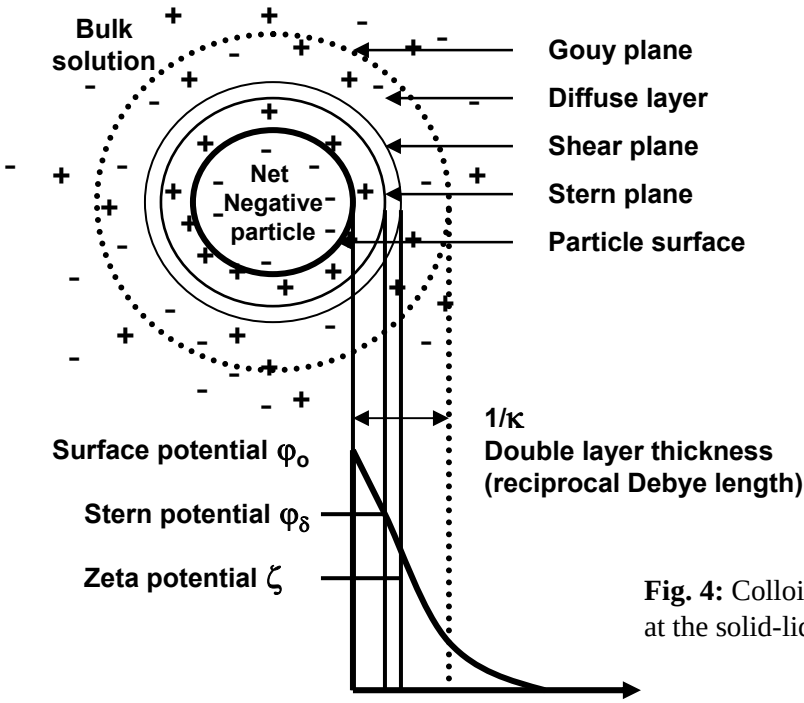

Fig. 4: Colloidal electric double layer at the solid-liquid interface.

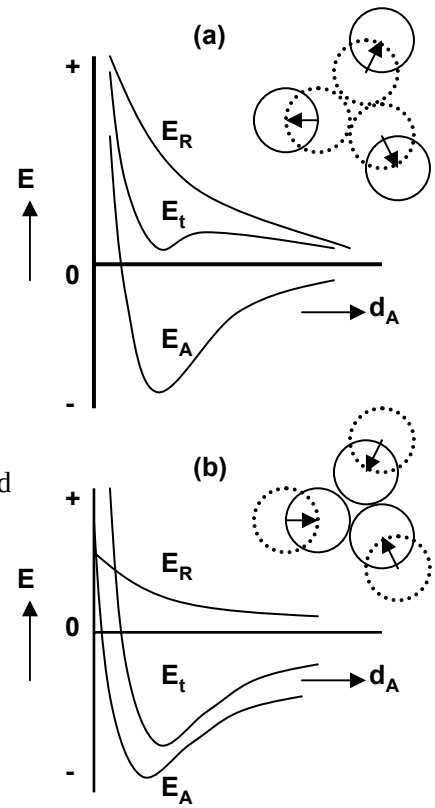

Fig. 5: Potential energy of particle-particle interaction (E_t) calculated as the sum of the electrostatic repulsive energy (E_R) and the van der Waals attractive energy (E_A) (Eqs. 7 and 8): (a) $E_R > E_A$: particle repulsion and colloid stabilization; (b) $E_A > E_R$: particle attraction and colloid agglomeration.

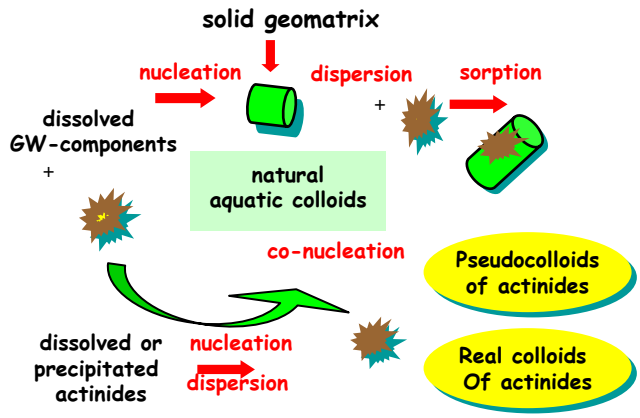

Fig. 6: General pathways for the transferation of actinides into the colloidal state by the formation of either real or pseudocolloids of actinides.

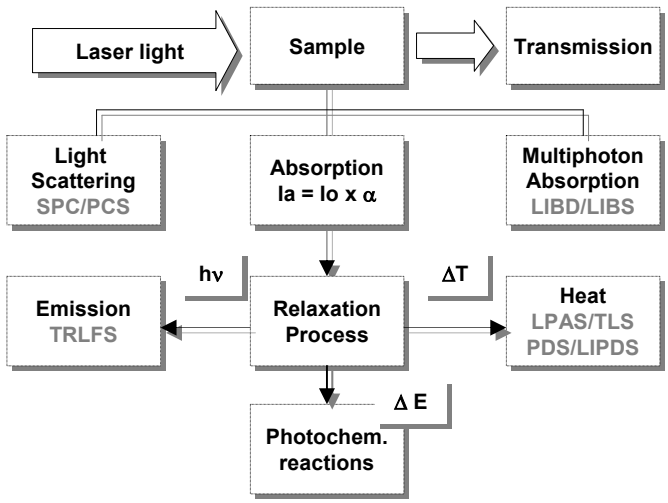

Fig. 7: Scheme of the basic principles of highly sensitive laser spectroscopic methods. Four categories are summarized as follows:

Photo-thermal spectroscopy
- LPAS: Laser-induced photo-acoustic spectroscopy
- LIPDS: Laser-induced photo-thermal displacement spectroscopy
- TLS: Thermal lensing spectroscopy
- PDS: Photo-thermal deflection spectroscopy

Luminescence spectroscopy
- TRLFS: Time-resolved laser fluorescence spectroscopy

Light scattering
- SPC: Single particle counting
- PCS: Photon correlation spectroscopy

Plasma generation
- LIBD: Laser-induced breakdown detection
- LIBS: Laser-induced breakdown spectroscopy

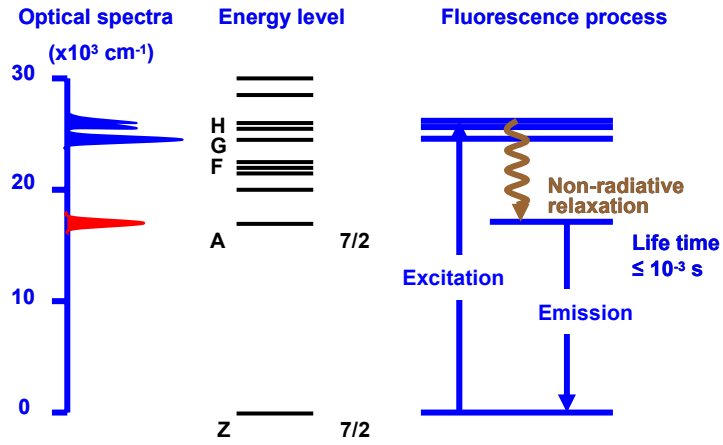

Fig. 8: TRLFS is based on the measurement of radiative relaxation of a light induced state e.g. of Cm(III).

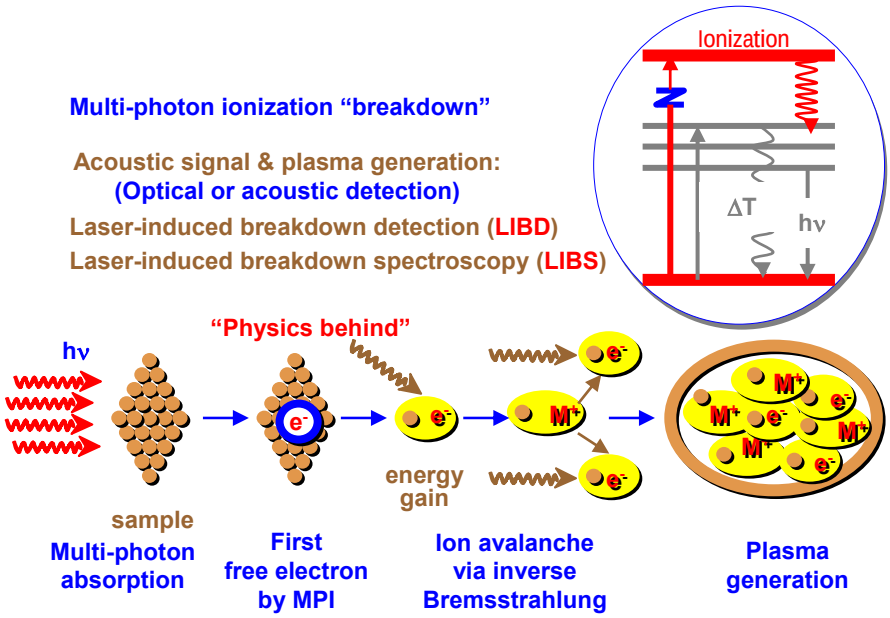

Fig. 9: Plasma generation of colloidal particles followed by plasma relaxation and ion-electron recombination accompanied by emission of white light (LIBD) and followed by atomic light emission of discrete wavelengths (LIBS).

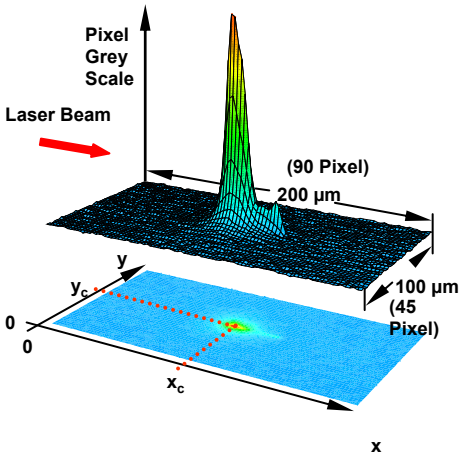

Fig. 10: A plasma light intensity contour of a single particle breakdown event (ø = 19 nm).

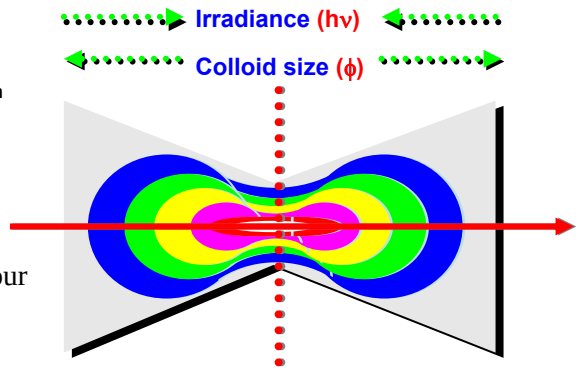

Fig. 11: Breakdown plasma generation in the laser beam focus area.

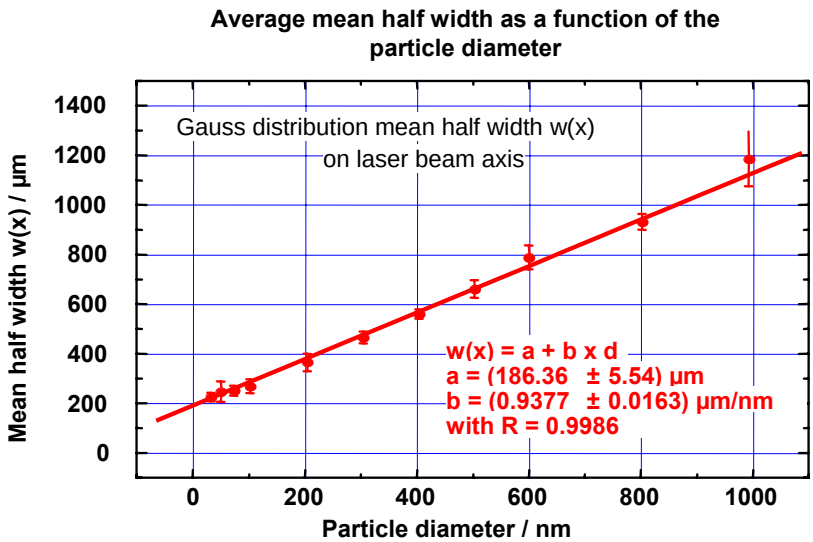

Fig. 12: LIBD particle size calibration with polystyrene reference particles.

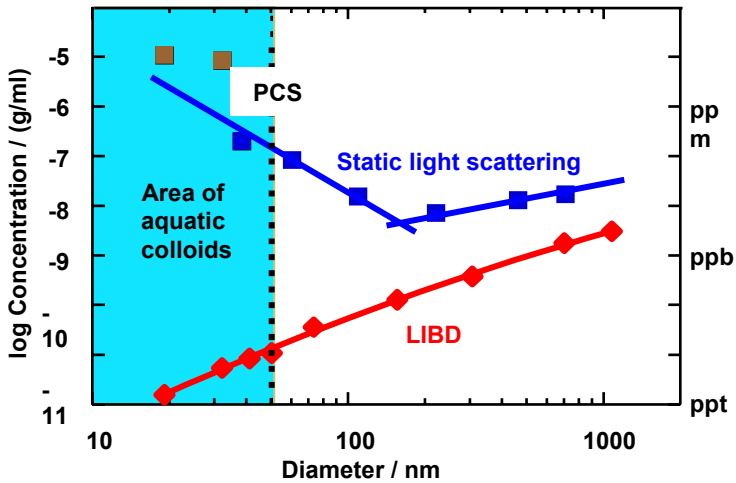

Fig. 13: The LIBD sensitivity: 10^4 – 10^7 times superior to light scattering methods. for aquatic colloids < 50 nm

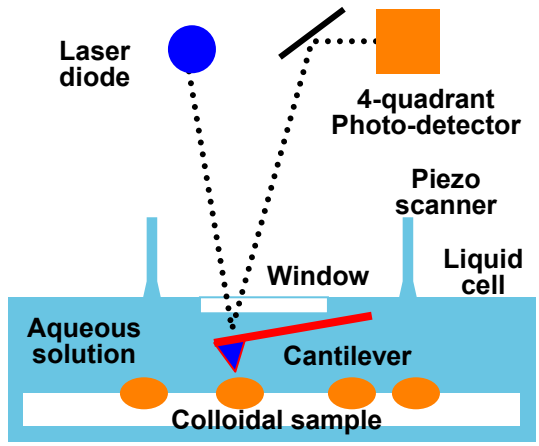

Fig. 14: Non-contact-mode atomic force microscopy (AFM) in aqueous solution with a laser-optical tip-sample distance control.

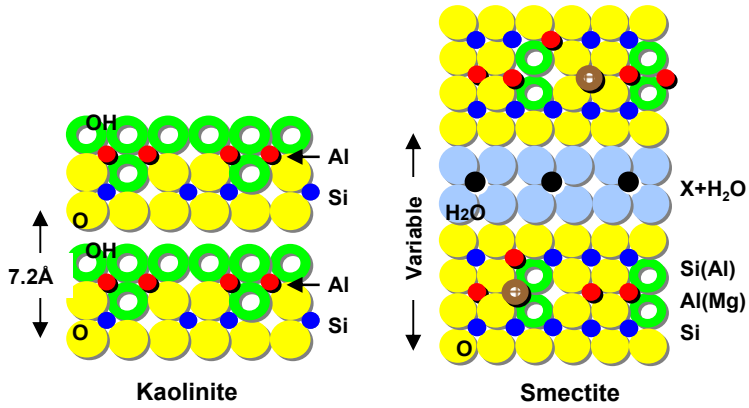

Fig. 15: Types of clay minerals based on the number and the sequence of tetrahadral (Si) and octahedral (Al) sheets: [TO]-kaolinite type; [TOT]-smectite type.

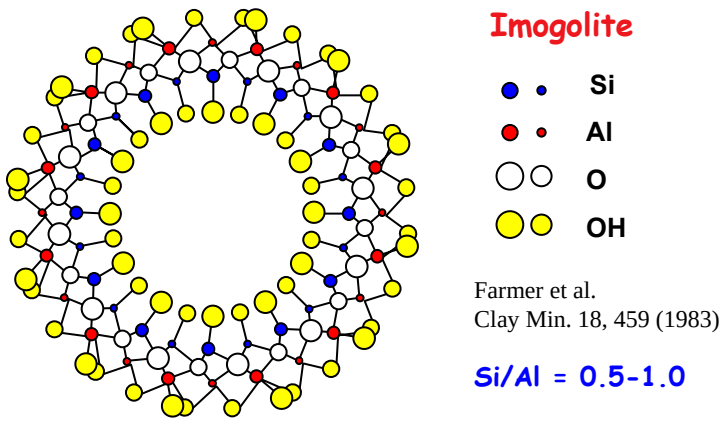

Fig. 16: Structure of imogolite (hydroxy-aluminosilicate or HAS) [53].

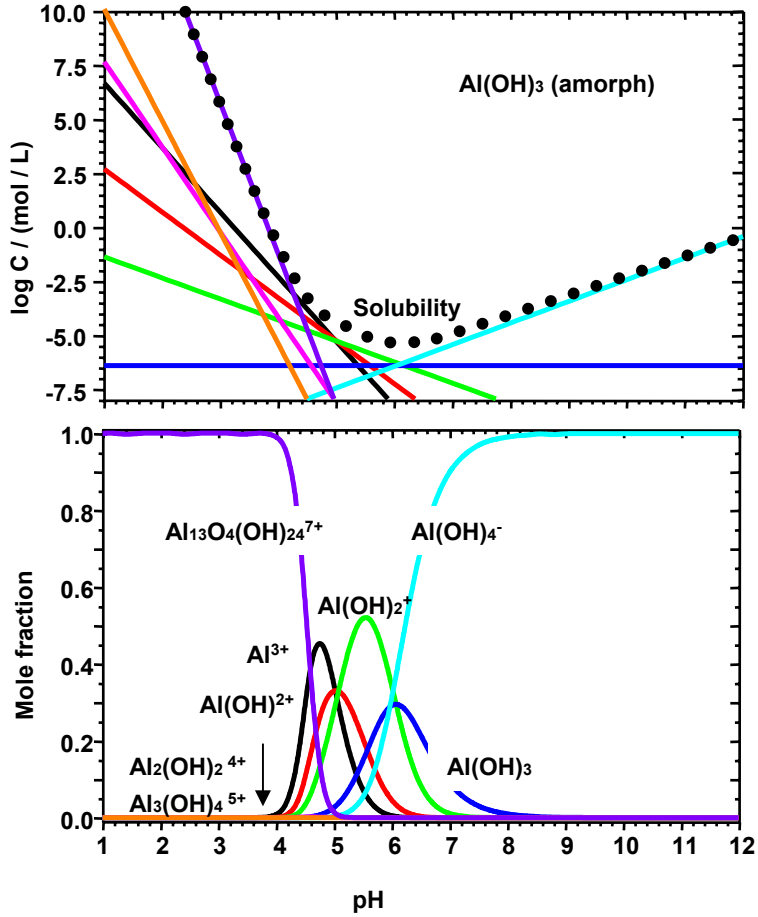

Fig. 17: Solubility of Al-hydroxide calculated by the data in refs [32-39] (upper part): Al species distribution as a function of pH (lower part).

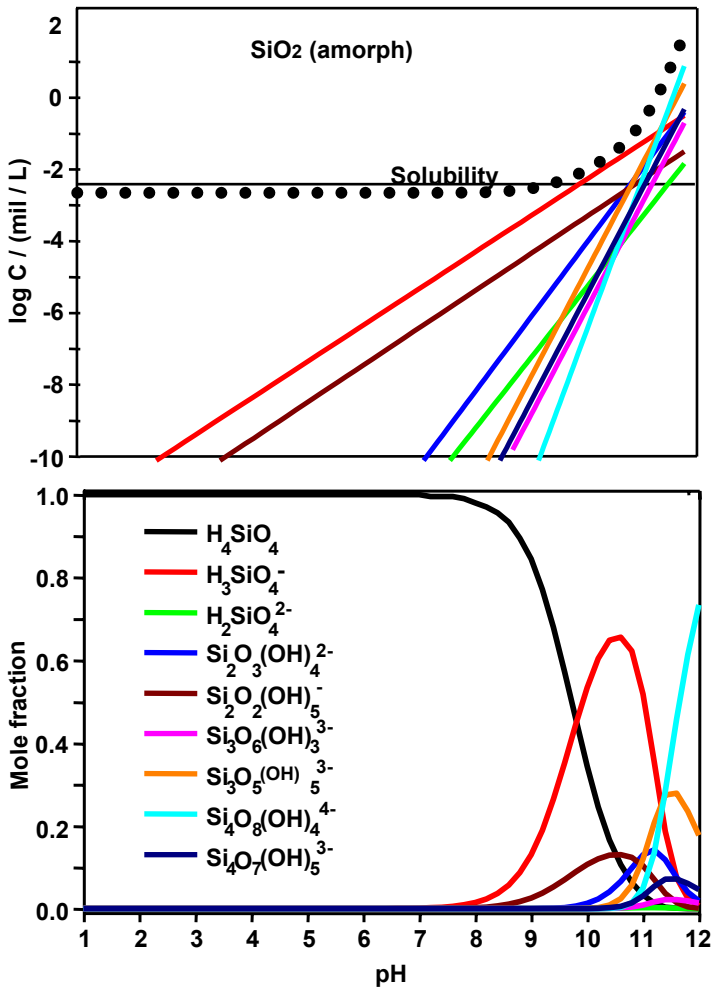

Fig. 18: Solubility of silica (amorph) calculated from the data in refs [32-39] (upper part); Si species distribution as a function of pH (lower part).

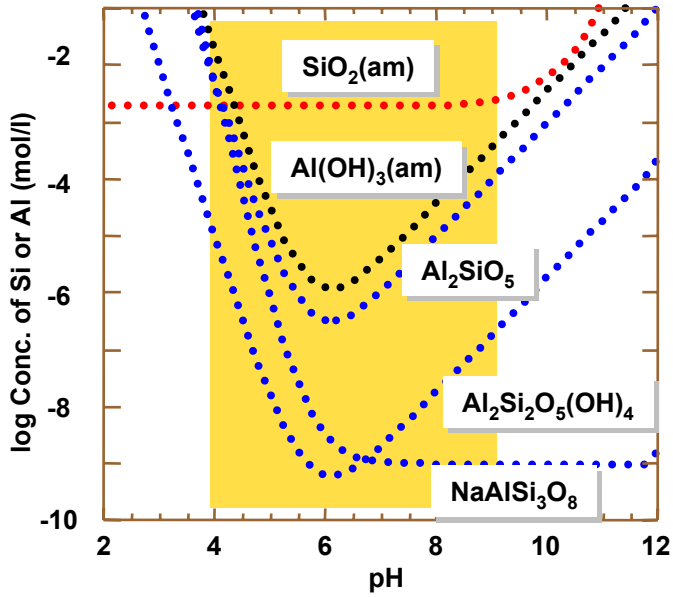

Fig. 19: Thermodynamic solubility of amorphous SiO_2, $Al(OH)_3$ and of some aluminosilicates calculated based on the available data in refs [32-39]: Al_2SiO_5 for sillimanite, $Al_2Si_2O_5(OH)_4$ for kaolinite and $NaAlSi_3O_8$ for low albite; the selected parameter screening area for aluminosilicate colloid formation is Indicated as coloured zone. Selection is made for the highest an lowest solubility of aluminosilicates.

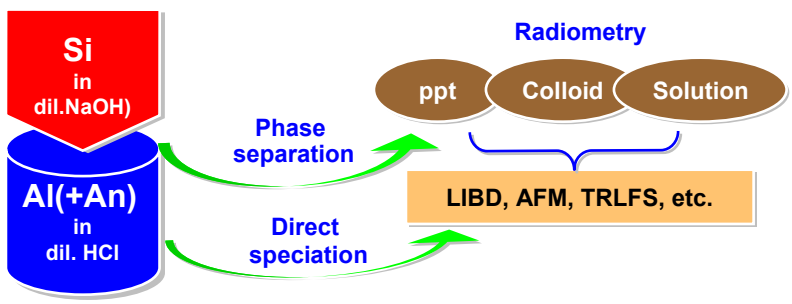

Fig. 20: Experiment of the parameter screening for the HAS colloid formation in the presence of Am(III) or Th(IV) by varying the individual element concentration and pH.

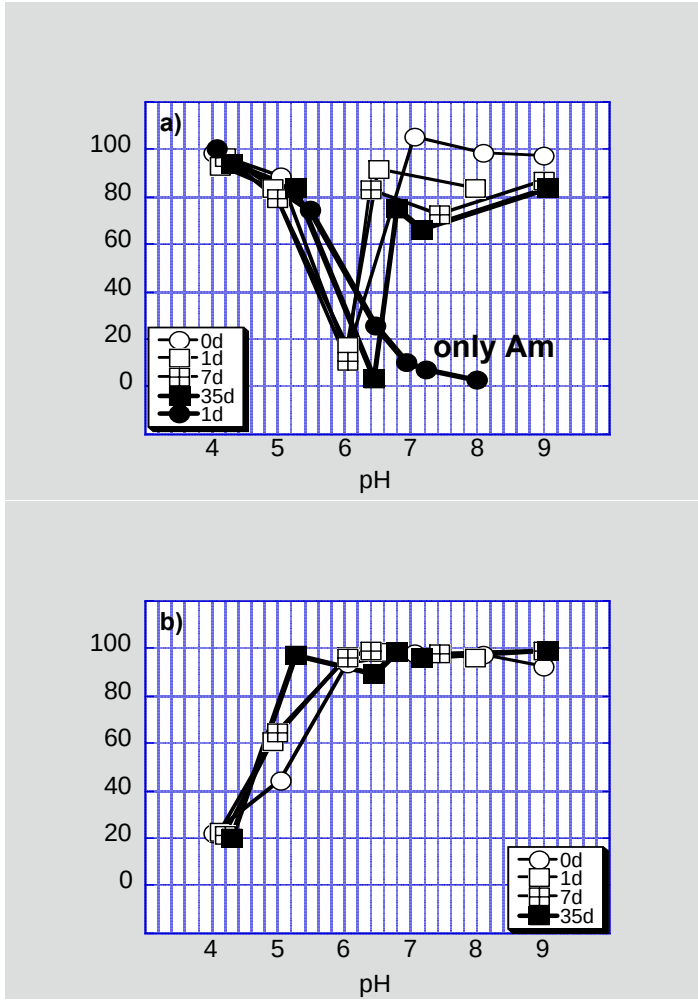

Fig. 21: The Am fraction in the filtrate from a 450 nm pore size filter as a function of pH (a) (normalized to the initial Am concentration); the colloid-borne Am fraction in the same filtrate (b). The sample solution is a mixture of 10^{-3} mol l^{-1} Si, 10^{-5} mol l^{-1} Al and 4.9x 10^{-8} mol l^{-1} Am, which is conditioned at different time. For comparison, the pure Am solution of 4.9x 10^{-8} mol l^{-1}, filtered at 450 nm pore size, is also shown for its fraction in solution.

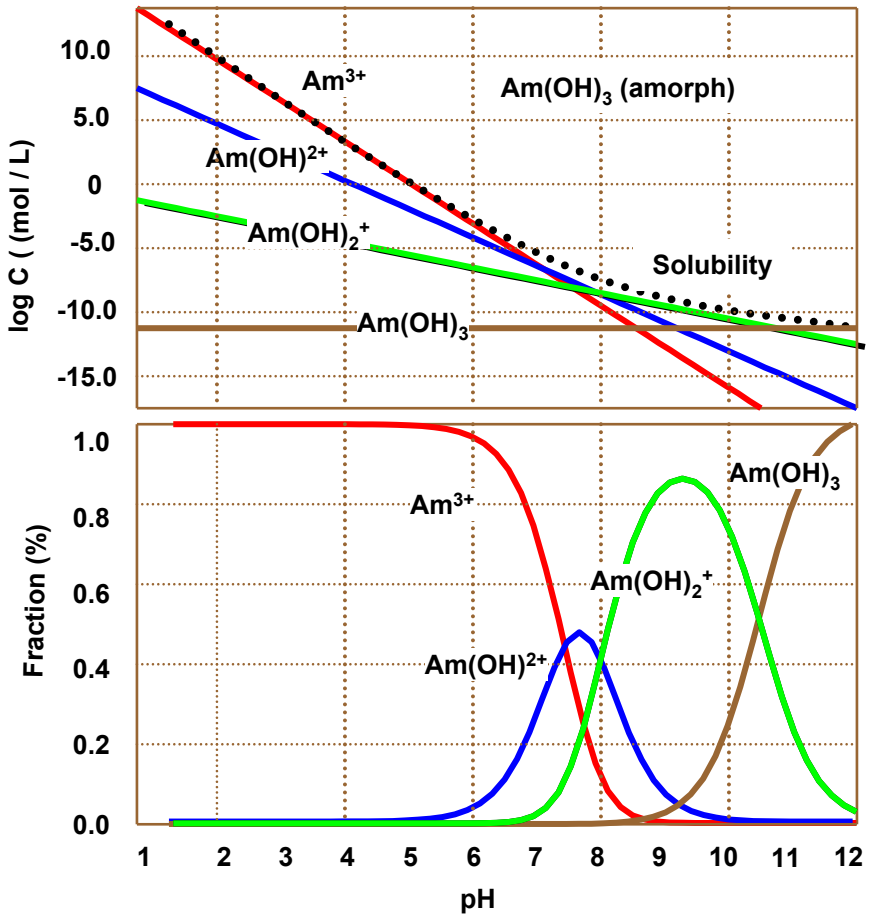

Fig. 22: Thermodynamic solubility and speciation of Am hydroxide calculated from the data in ref. [66]

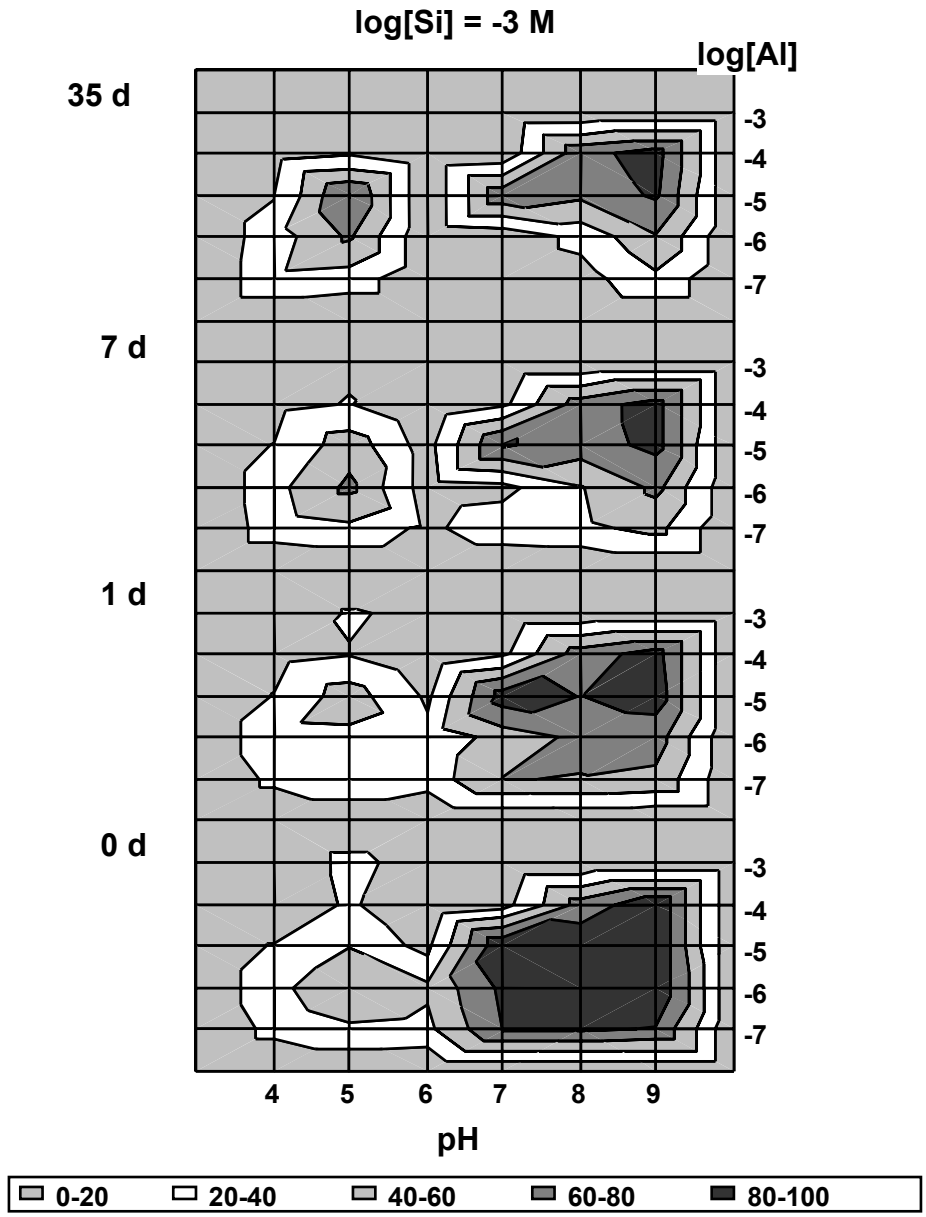

Fig. 23: Screening experimental results given as contour diagrams for the colloid-borne Am fraction (%) in mixture solutions of Al and Si. The Si concentration is maintained constant at 10^{-3} mol l^{-1}, while varying the Al concentration from 10^{-7} to 10^{-3} mol l^{-1} in the pH range 4-9.

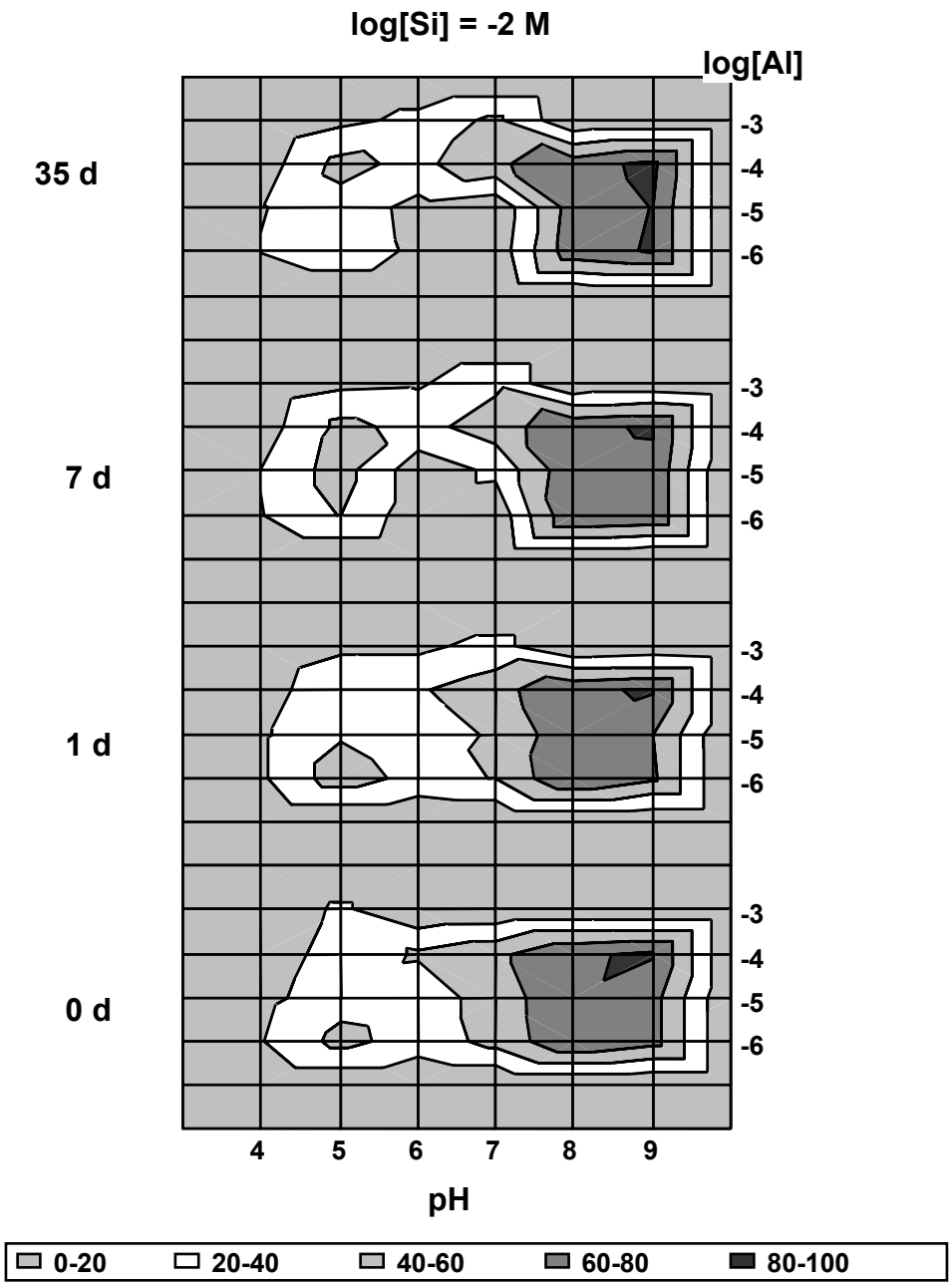

Fig. 24: Screening experimental results given as contour diagrams for the colloid-borne Am fraction (%) in mixture solutions of Al and Si. The Si concentration is maintained constant at 10^{-2} mol l^{-1}, while varying the Al concentration from 10^{-6} to 10^{-3} mol l^{-1} in the pH range 4-9.

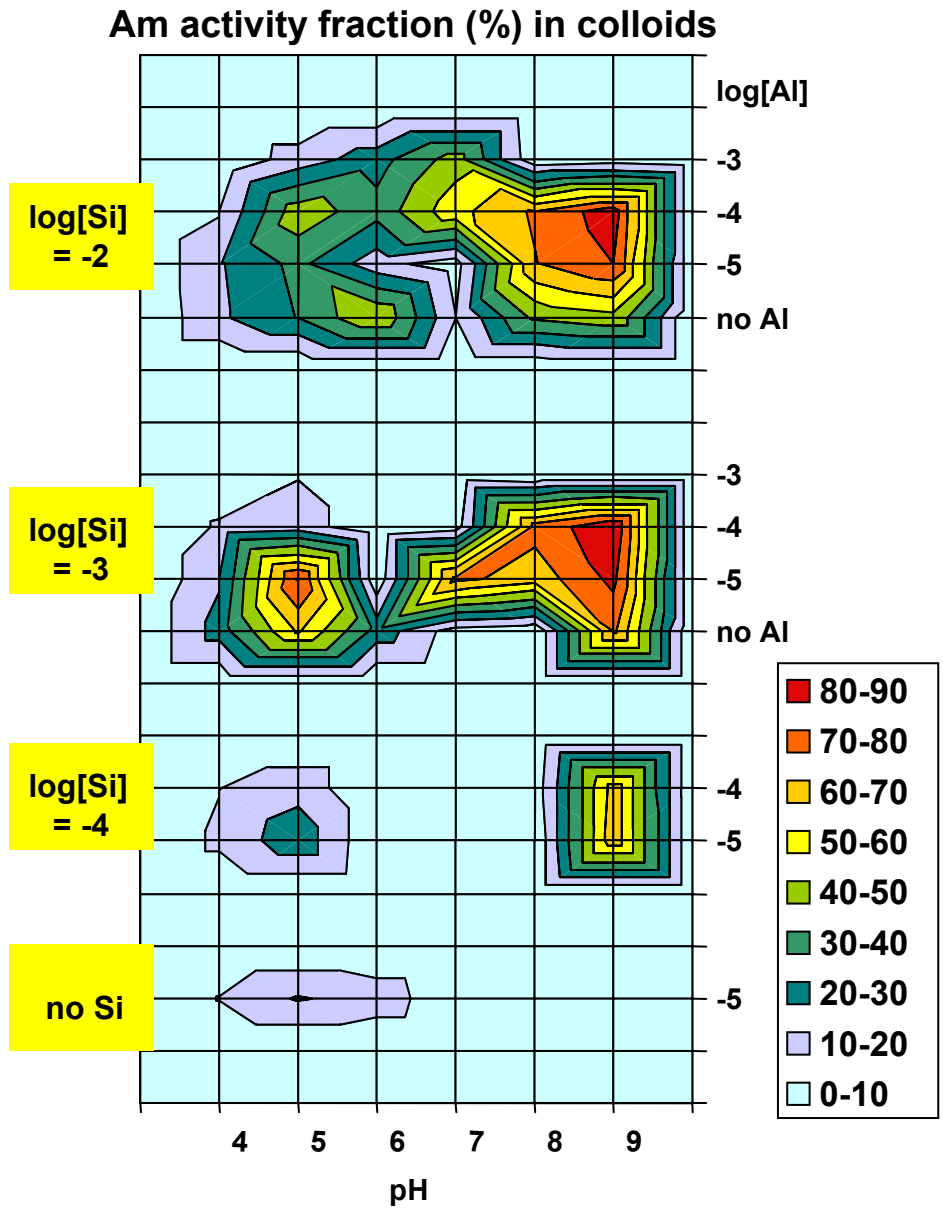

Fig. 25: A contour diagram of the colloid-borne Am fraction (z-axis) normalized to the initial Am concentration after 35 days of conditioning in different pH. Different Si and Al concentrations are indicated on the left and on the right y-axis, respectively.

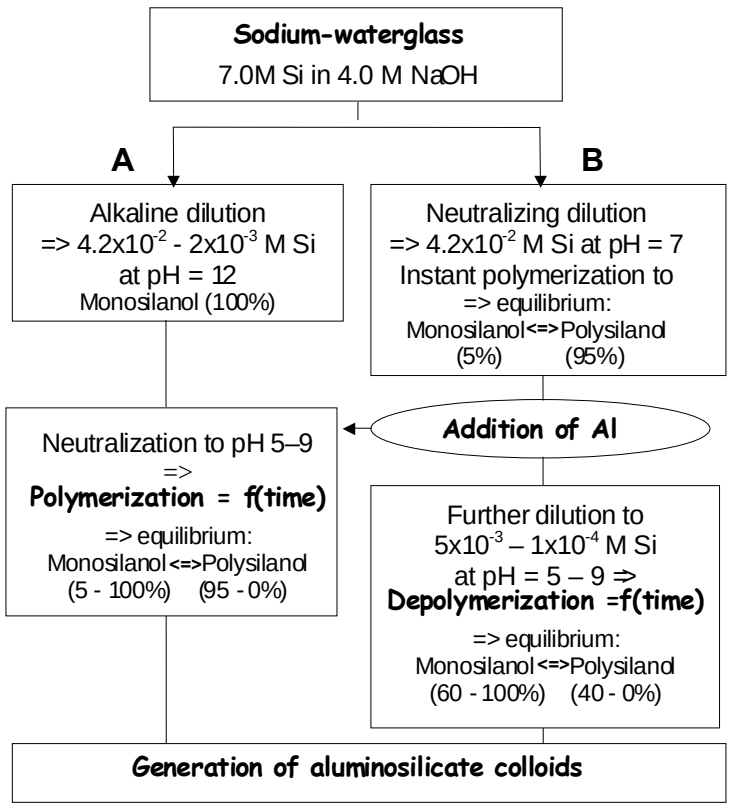

Fig. 26: Two experimental pathways for the generation of polysilanol and of hydroxy aluminosilicate (HAS) colloids from sodium-waterglass by (A): alkaline dilution and neutralization or (B): neutralization and dilution.

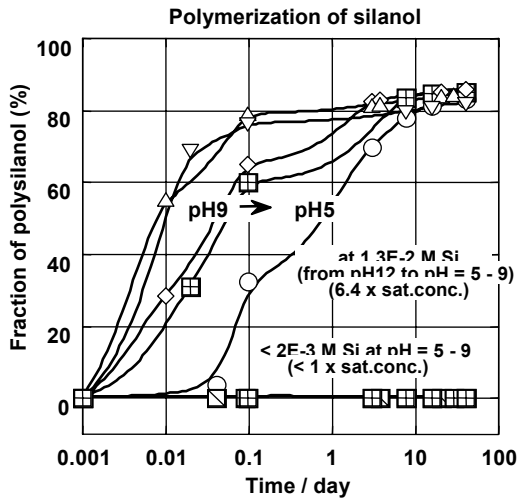

Fig. 27: The time dependent polymerization of silanol (silicic acid) at different pH for the Si concentration of $1.3x10^{-2}$ mol l^{-1} (6.4 times the saturation concentration of amorphous silica) (cf. approach A in Fig.26).

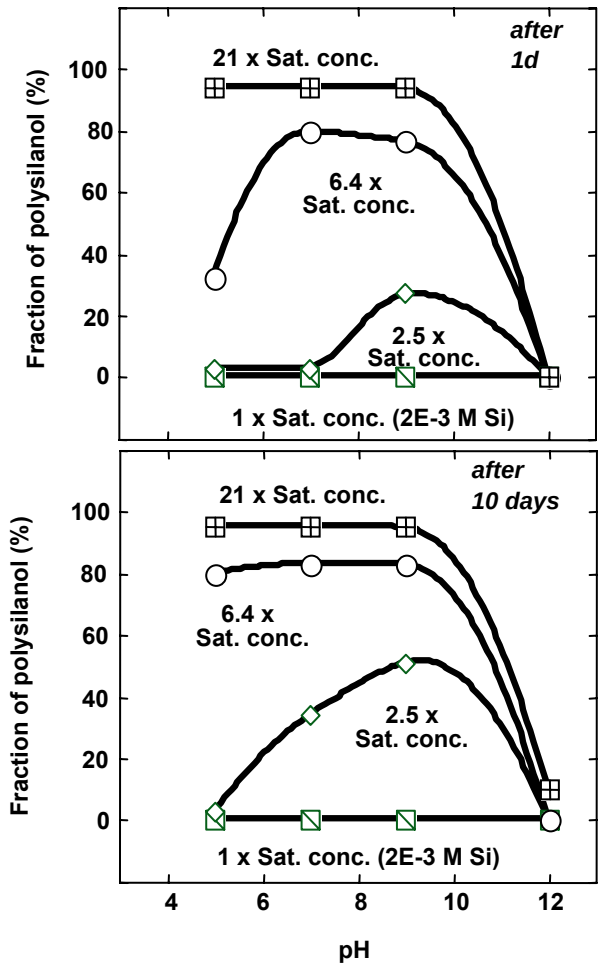

Fig. 28: The pH dependent polymerization of silanol at different initial concentrations after one day and 10 days of pH adjusting (the original solution at pH 12) (approach A in Fig.26)

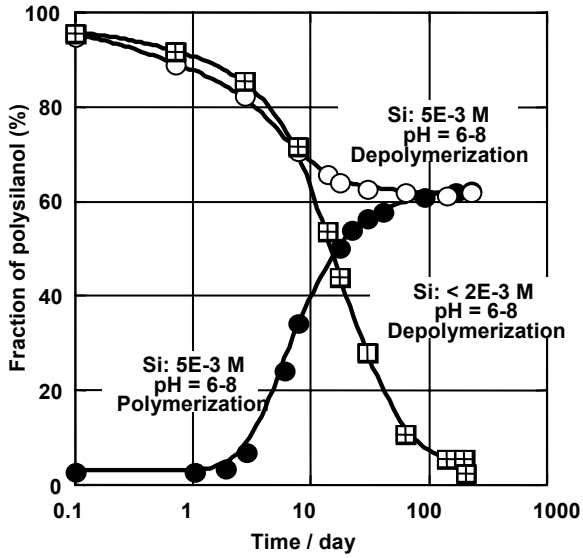

Fig. 29: Polymerization of silanol and depolymerization by dilution (approach A and B in Fig.25, respectively): an illustration of the reversibility under present experimental conditions.

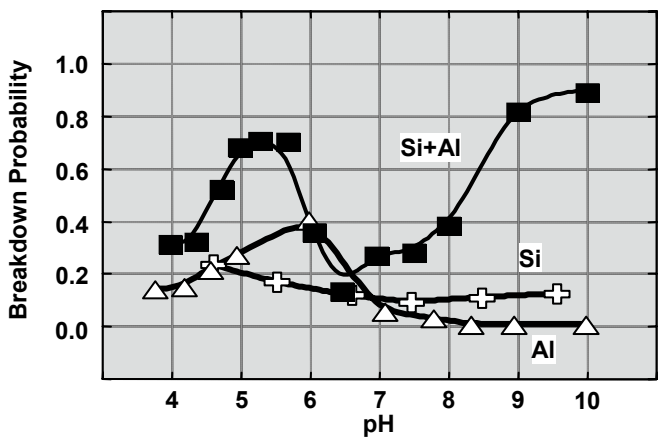

Fig. 30: Colloid generation observed by laser-induced breakdown detection (LIBD); (Si+Al): a titration of 10^{-5} mol l^{-1} Al in 0.03 M HCl with 10^{-3} mol l^{-1} Si in 0.03 M NaOH; (Si) and (Al): a titration of 0.03 M HCl with 10^{-3} mol l^{-1} Si in 0.03 M NaOH and of 10^{-3} mol l^{-1} Al in 0.03M HCl with 0.03 M NaOH

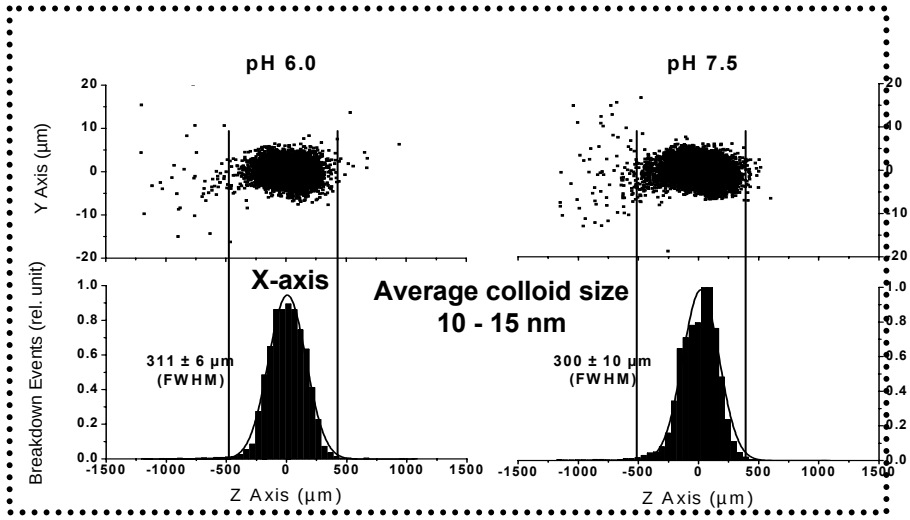

Fig. 31: LIBD experiment for the quantification of an average size of HAS colloids at pH 6.0 and 7.5: two-dimensional recordings of plasma light emission generated by breakdown of colloids within the laser beam focus volume (upper part) and statistical distribution of breakdown events on the z-axis. FWHM of breakdown event distribution is directly related to the average size of colloids of preponderance in solution.

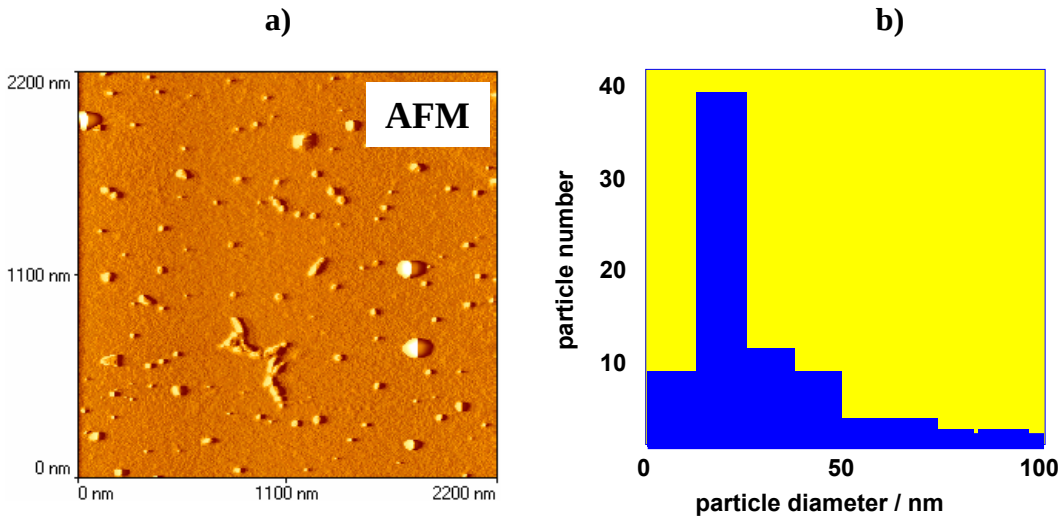

Fig. 32: Atomic force microscopic (AFM) characterization of colloids generated in a sample mixture of 10-3 mol l-1 Si and 10-4 mol l-1 Al at pH 7: (a) a non-contact mode AFM image of hydroxy aluminosilicate (HAS) colloids; (b) Size distribution of 70 particles (a mean particle diameter at about 27 nm and the maximal number at 19 nm).

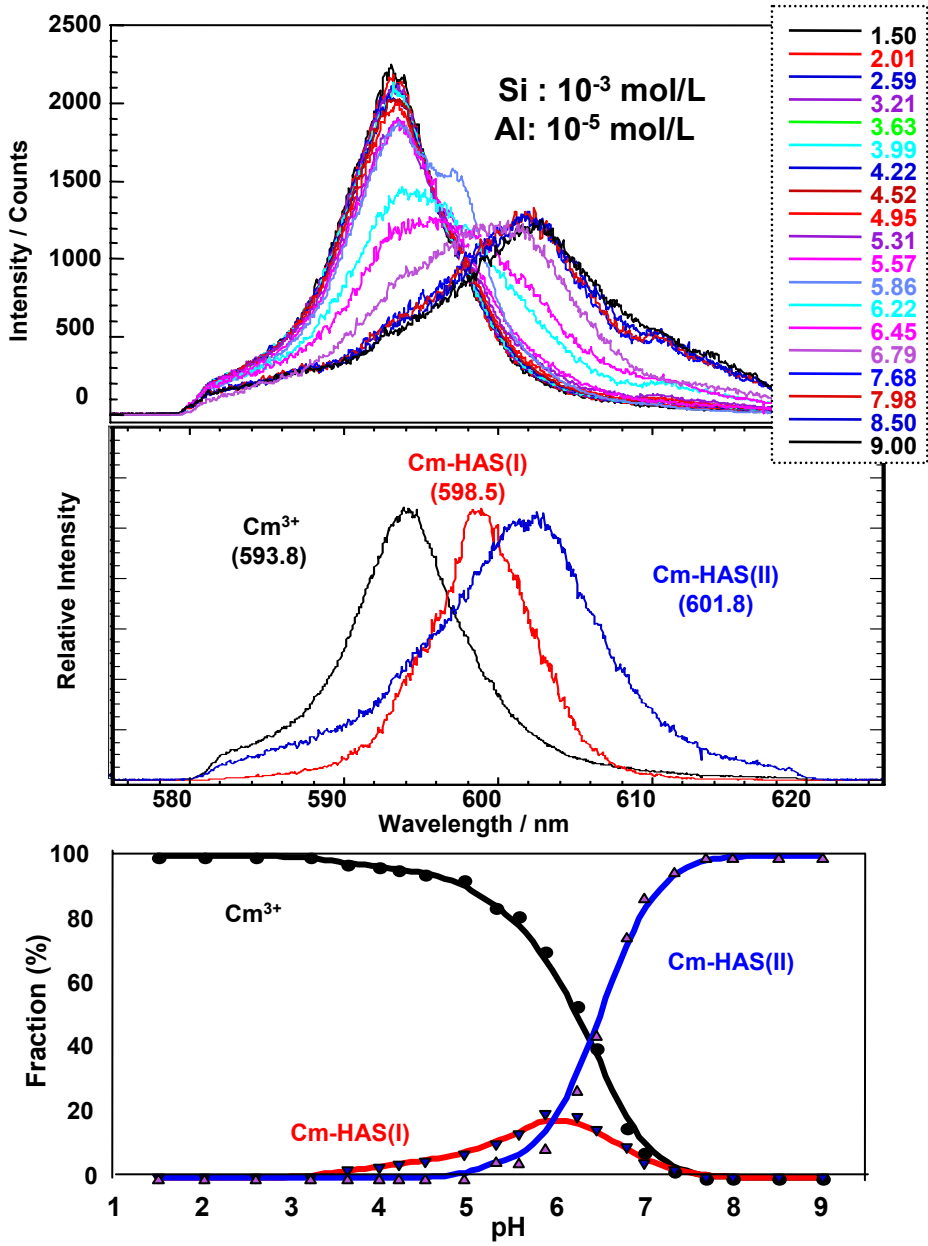

Fig. 33: Speciation of HAS colloid-borne Cm by TRLFS on the pH titration from 1 to 9 in a mixture solution containing 10^{-3} mol l^{-1} Si, 10^{-5} mol l^{-1} Al and 4.9×10^{-8} mol l^{-1} Cm: the pH dependent spectrum evolution (upper part) and the deconvoluted spectra of different Cm species present in the solution (middle part). The species distribution as a function of pH is illustrated in the lower part.

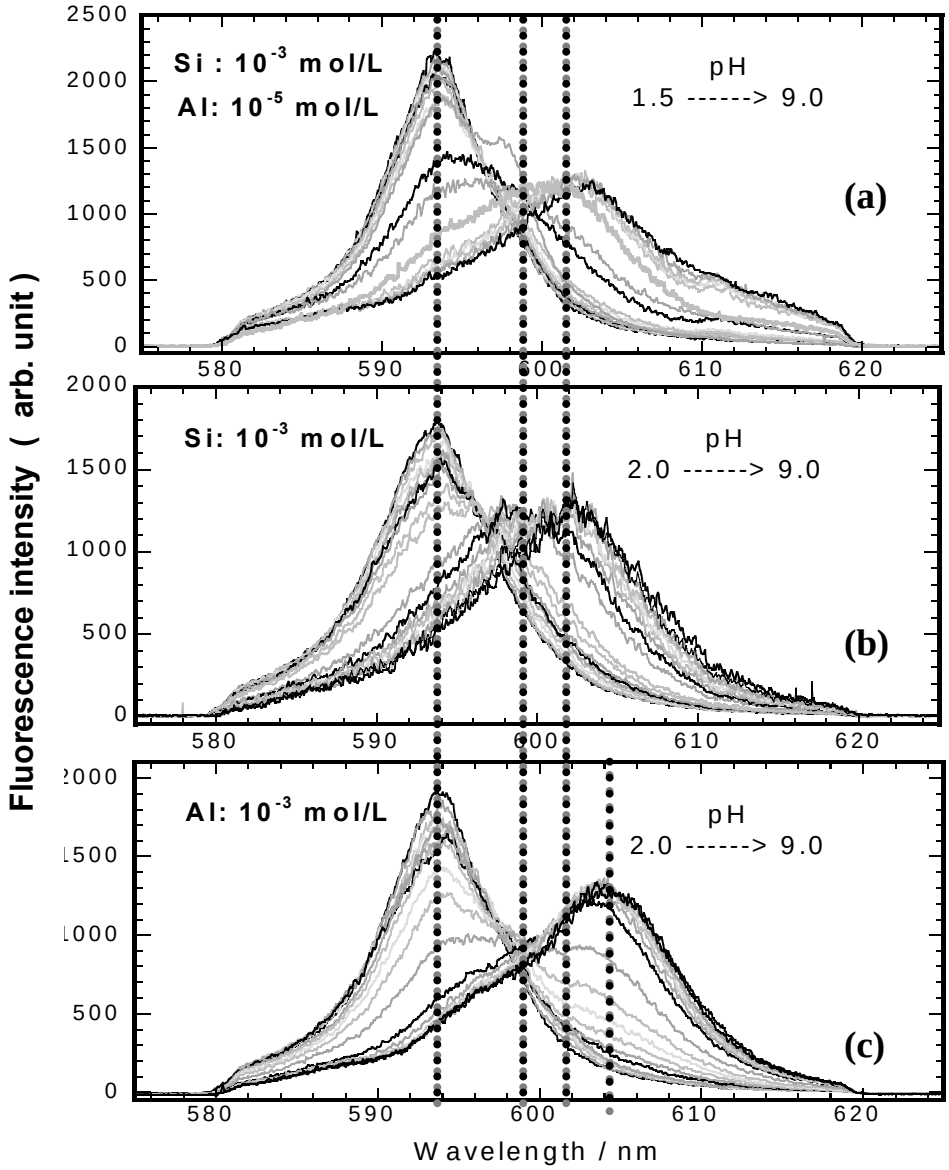

Fig. 34: Speciation of Cm by TRLFS in a mixture solution of 10^{-3} mol l^{-1} Si and 10^{-5} mol l^{-1} Al (a), in a pure Si solution of 10^{-3} mol l^{-1} (b) and in a pure Al solution of 10^{-3} mol l^{-1} (c). The solution pH is varied from 1.5 or 2.0 upwards to 9.0.

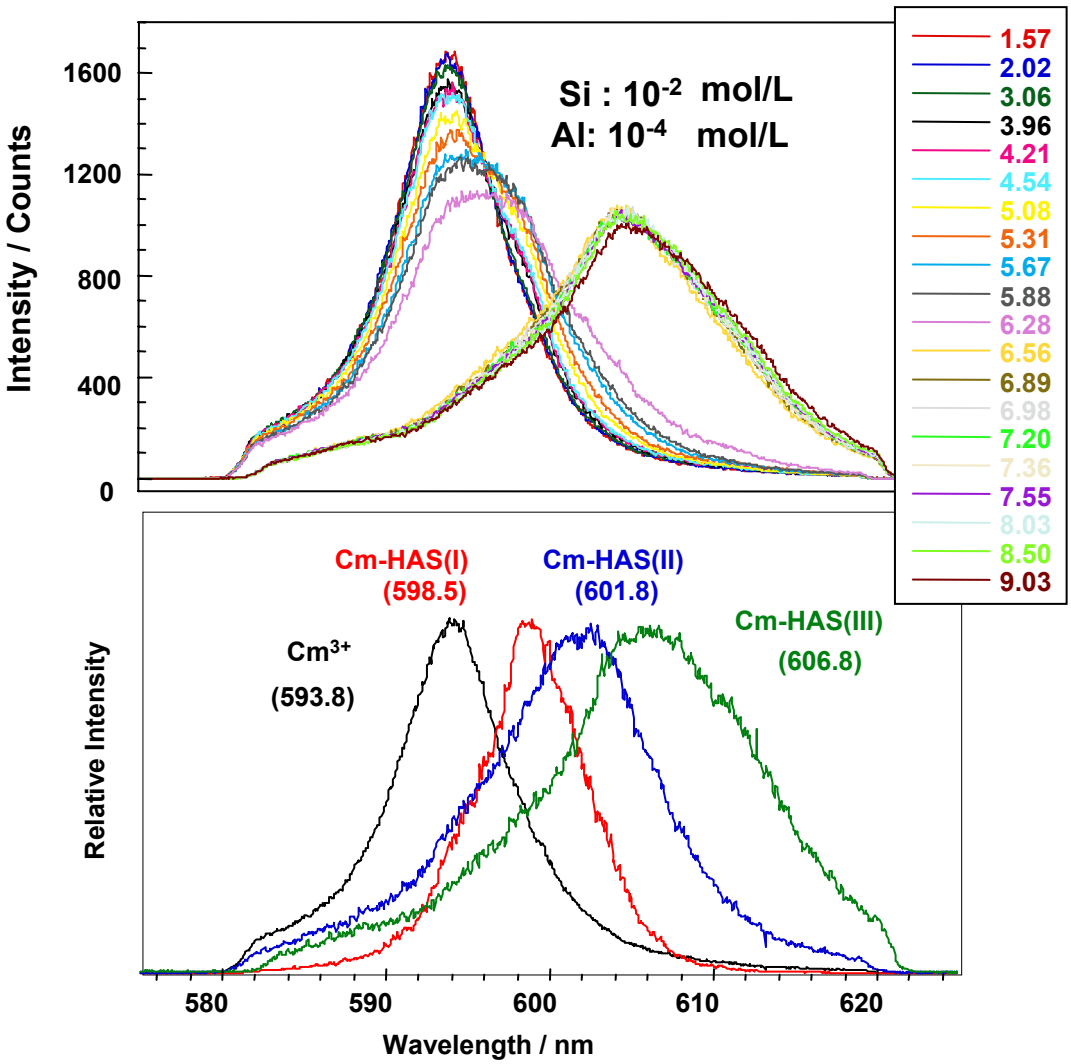

Fig. 35: Speciation of HAS colloid-borne Cm by TRLFS upon the pH titration from 1 to 9 in a mixture solution containing 10^{-2} mol l^{-1} Si, 10^{-4} mol l^{-1} Al and 4.9×10^{-8} mol l^{-1} Cm: the pH dependent spectrum evolution (upper part) and the deconvoluted spectra of different Cm species present in the solution (lower part).

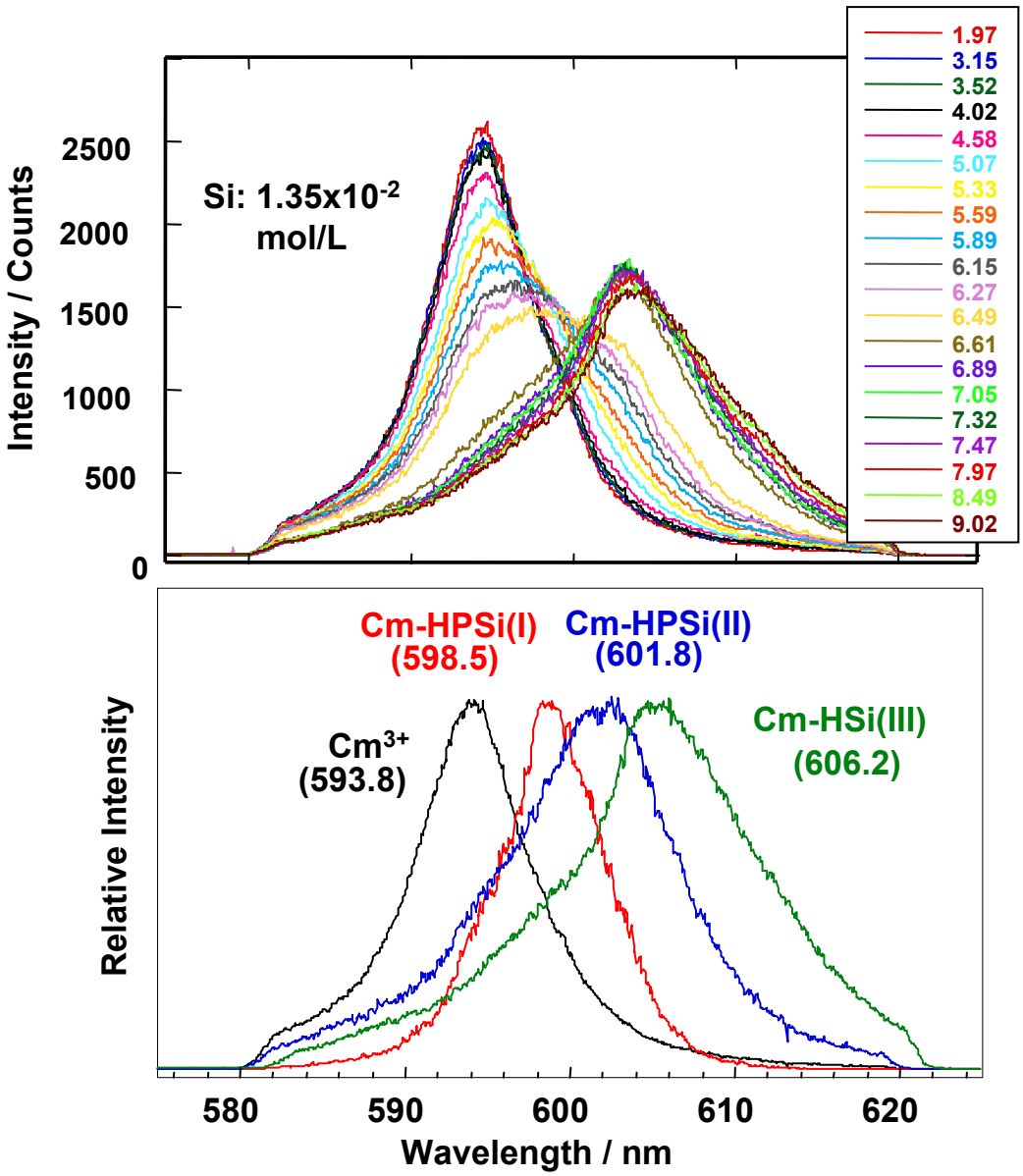

Fig.36: Speciation of Cm by TRLFS in a pure Si solution of 1.35×10^{-2} mol l^{-1}. The solution pH is varied from 2.0 upwards to 9.0: the pH dependent spectrum evolution (upper part) and the deconvoluted spectra of different Cm species (lower part).

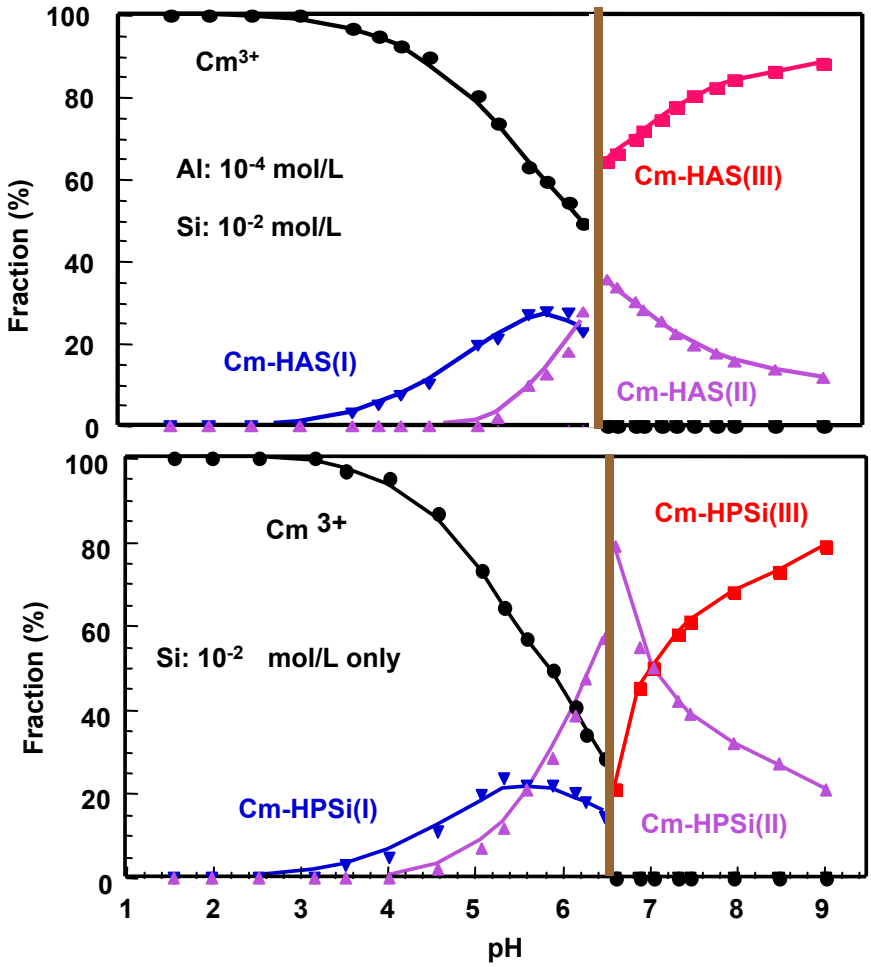

Fig. 37: The relative Cm species distribution as a function of pH in a mixture solution of 10^{-2} mol l^{-1} Si and 10^{-4} mol l^{-1} Al (upper part) and compared with that of a pure solution of 10^{-2} mol l^{-1} Si (lower part).

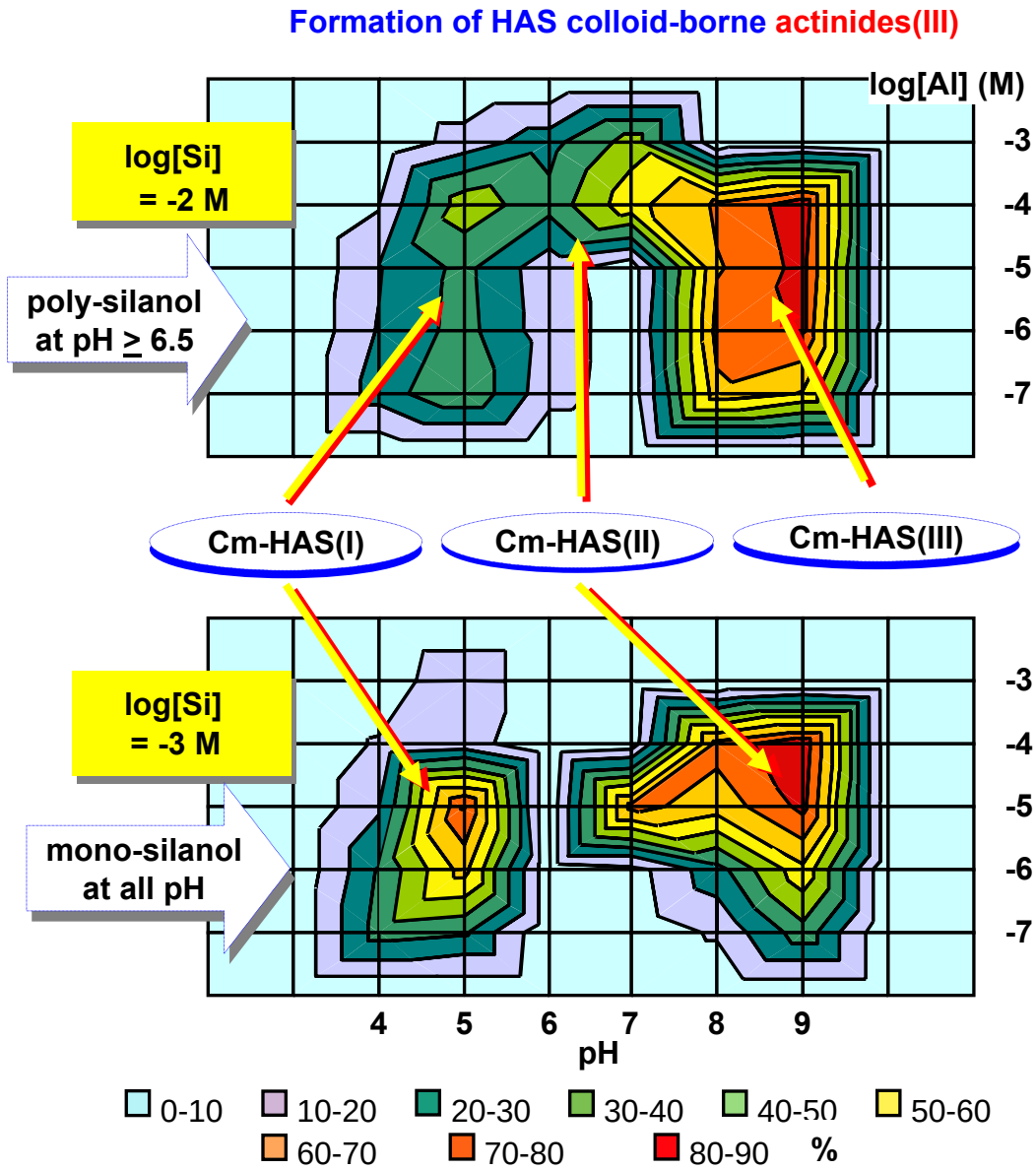

Fig. 38: : A contour diagram of the colloid-borne Am fraction (z-axis) normalized to the initial Am concentration after 35 days of conditioning in different pH. Different Si and Al concentrations are indicated on the left and on the right y-axis, respectively. The regions for the formation of different colloid-borne Cm(III) species, namely Cm-HAS(I) as a bidentate, Cm-HAS(II) as a tridendate, and Cm-HAS(III) as isomorphically substituted, are indicated by blue ellipses. The regions for the formation of different Si species, namely mono- and polysilanol are indicated by yellow arrows.

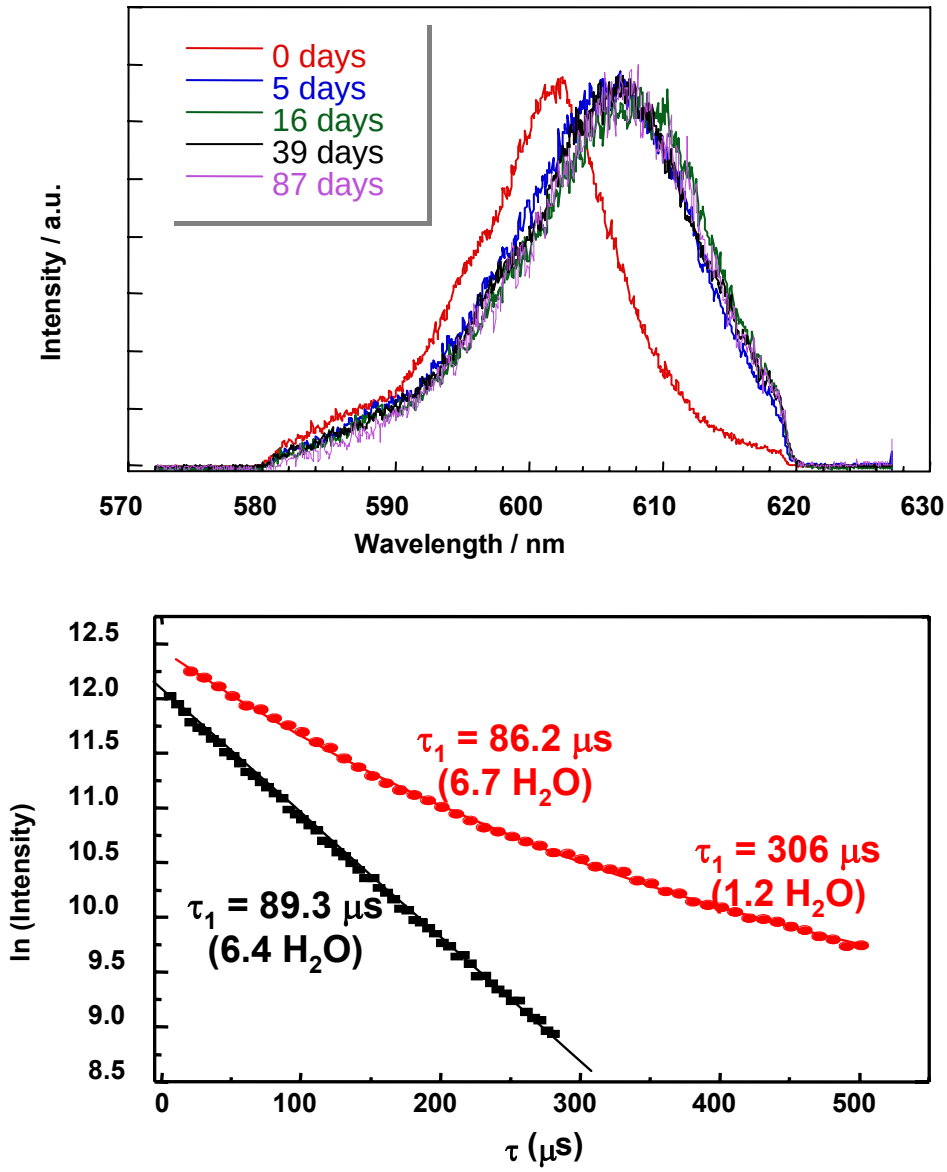

Fig. 39: Speciation of HAS colloid-borne Cm by TRLFS upon heating at 90°C from 5 up to 87 days of a mixture solution containing 10^{-3} mol l^{-1} Si, 10^{-4} mol l^{-1} Al and $5.0x10^{-8}$ mol l^{-1} cm: The time dependent spectrum evolution (upper part) and the fluorescence life times (lower part) before and after heating the sample.

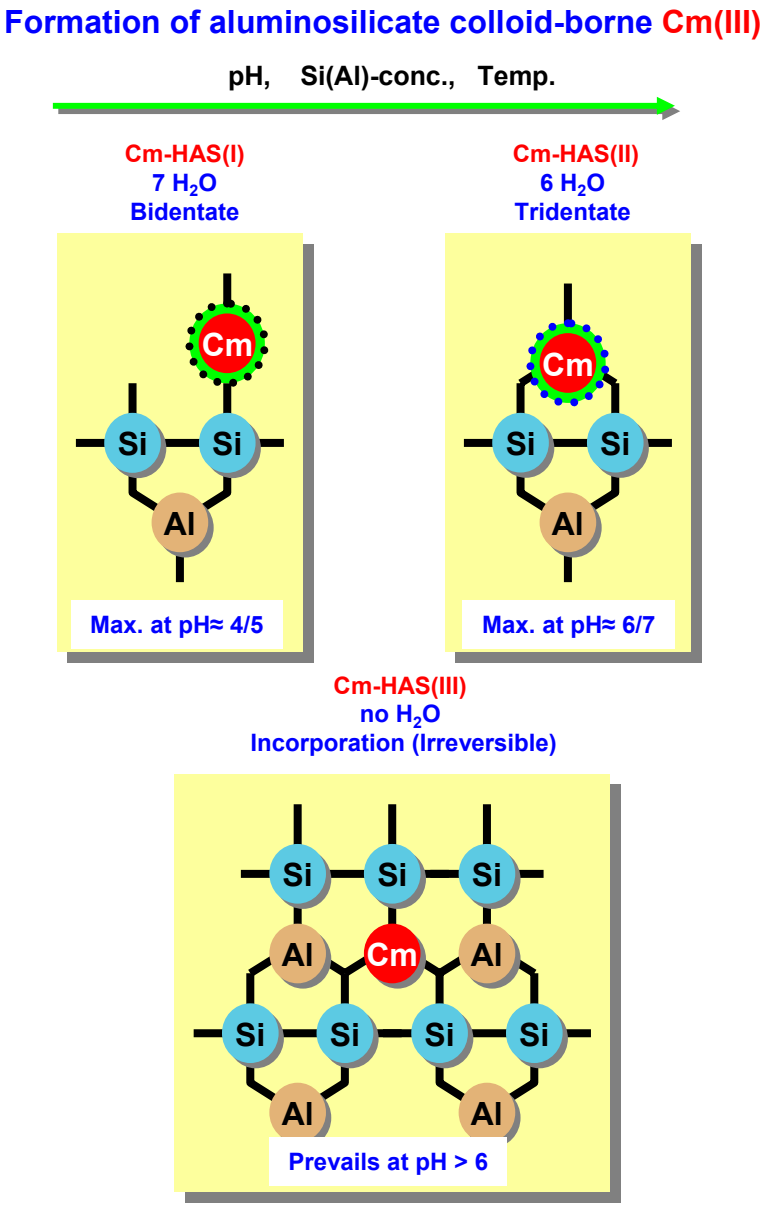

Fig.40: Illustrative overview for the formation of three colloid-borne Cm species.

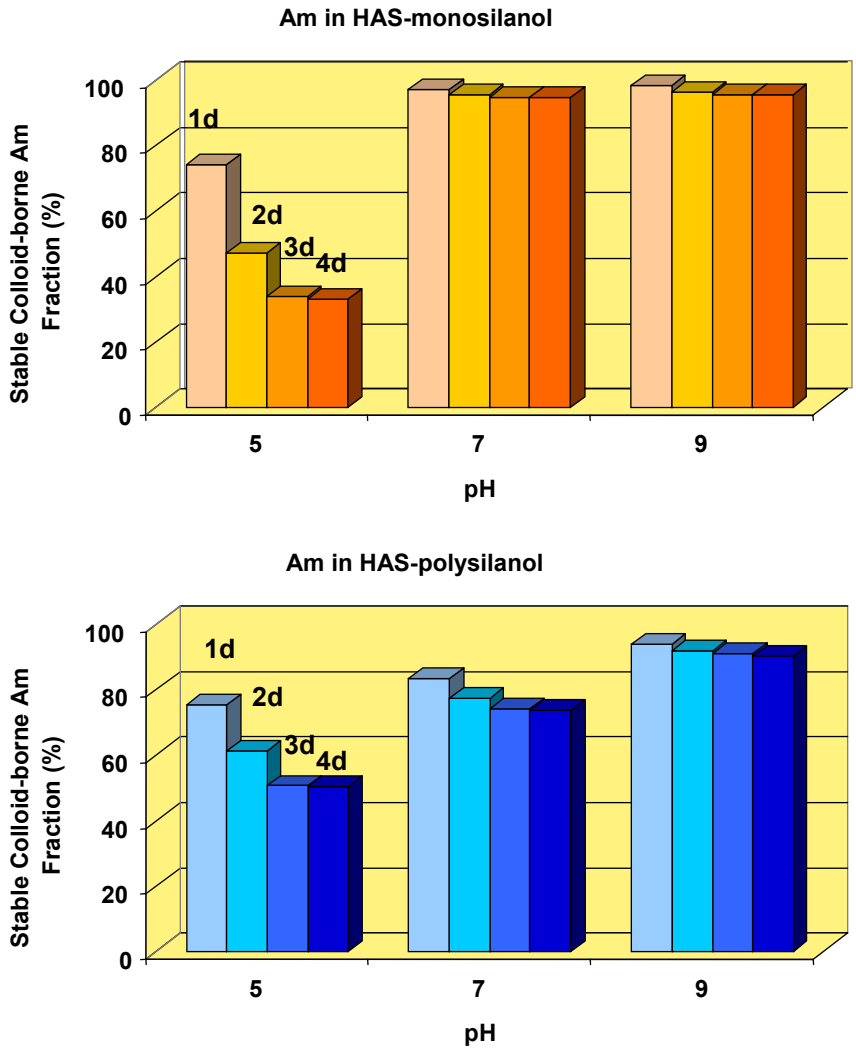

Fig.41: Colloid-borne Am fraction (%) in a sample after the desorption experiment. The initial sample is prepared at different pH with 10^{-3} mol l^{-1} Si, 10^{-5} mol l^{-1} Al and $5x10^{-8}$ mol l^{-1} Am (upper part) and 10^{-2} mol l^{-1} Si, 10^{-4} mol l^{-1} Al and $5x10^{-8}$ mol l^{-1} Am (lower part) and conditioned for 7 days prior to desorption experiment.

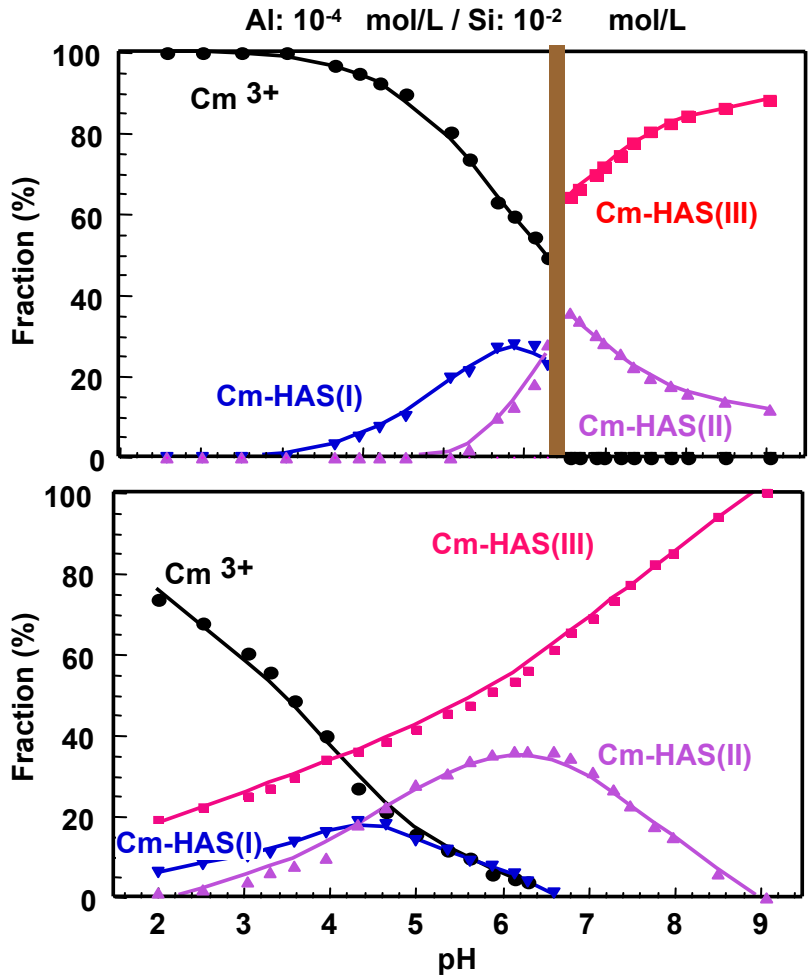

Fig. 42: The relative Cm species distribution upon pH titration from 9 to 2 (inverse titration) (lower part) and from 2 to 9 (upper part) in a mixture solution containing 1.3×10^{-2} mol l^{-1} Si, 10^{-4} mol l^{-1} Al and 4.9×10^{-8} mol l^{-1} Cm.

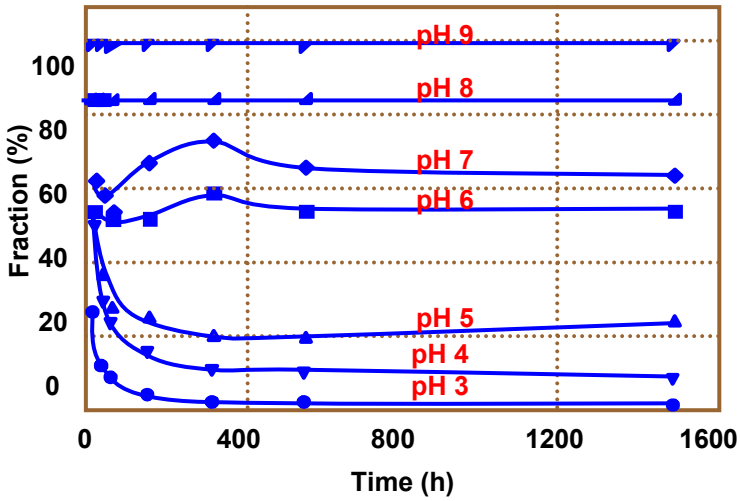

Fig. 43: Stability of the HAS colloid-borne Cm: Cm-HAS(III) as a function of time at different pH (cf. Fig.42).

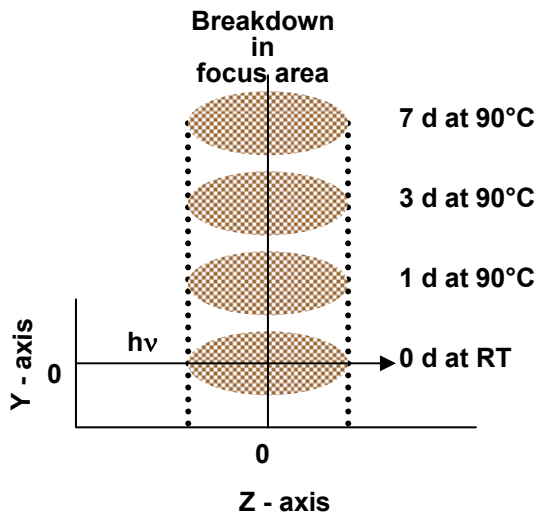

Fig. 44: LIBD experiment for the quantification of an average size of HAS colloids at pH 7.5 after heating to 90°C for different periods of time: two-dimensional recordings of plasma light emission generated by breakdown of colloids within the laser beam focus volume on which basis the average size of colloids of preponderance in solution can be estimated. The average size remains unchanged with time.

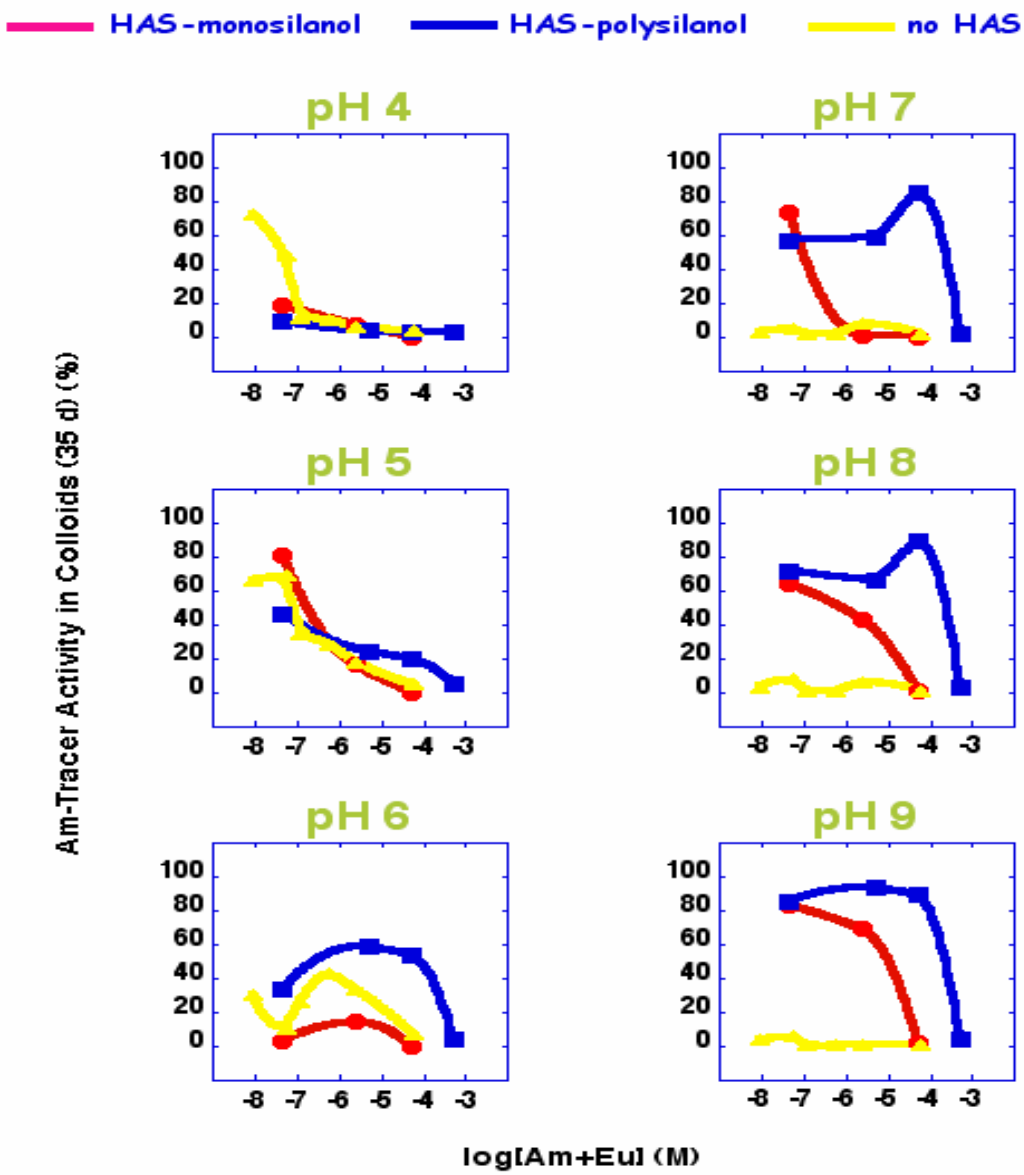

Fig. 45: Colloid-borne Am-activity fraction (%) as a function of the (Am+Eu)-concentration for different pH´s in three series of samples indicated as HAS-monosilanol, HAS-polysilanol and no HAS, respectively, and containing mixture solutions of:
(1): 10^{-3} mol l^{-1} Si, 10^{-5} mol l^{-1} Al, $5x10^{-8}$ mol l^{-1} Am, varied concentration of Eu;
(2): $1.3x10^{-2}$ mol l^{-1} Si, $1.5x10^{-4}$ mol l^{-1} Al, $5x10^{-8}$ mol l^{-1} Am, varied concentration of Eu;
(3): $5x10^{-8}$ mol l^{-1} Am, varied concentration of Eu.

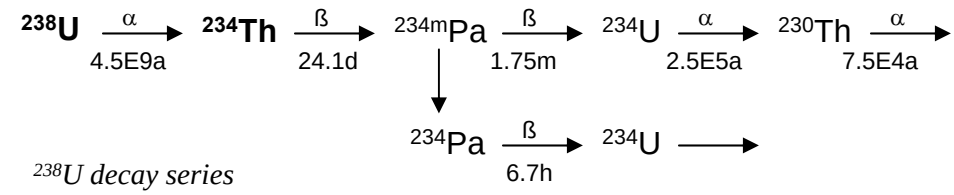

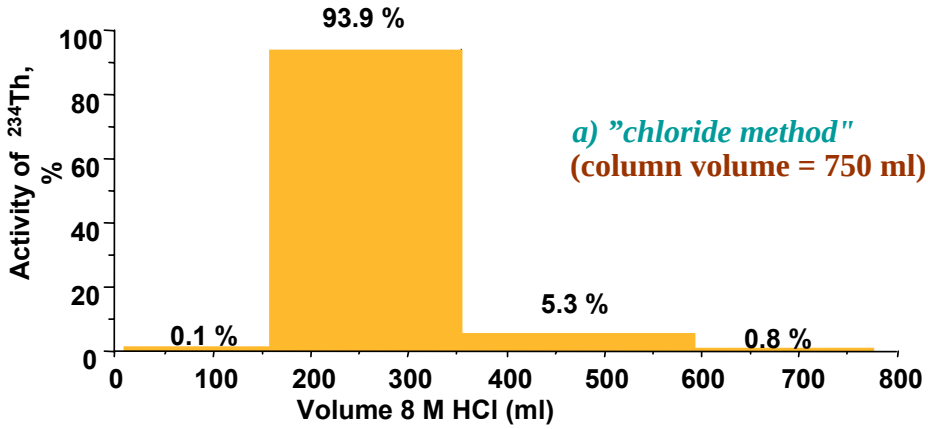

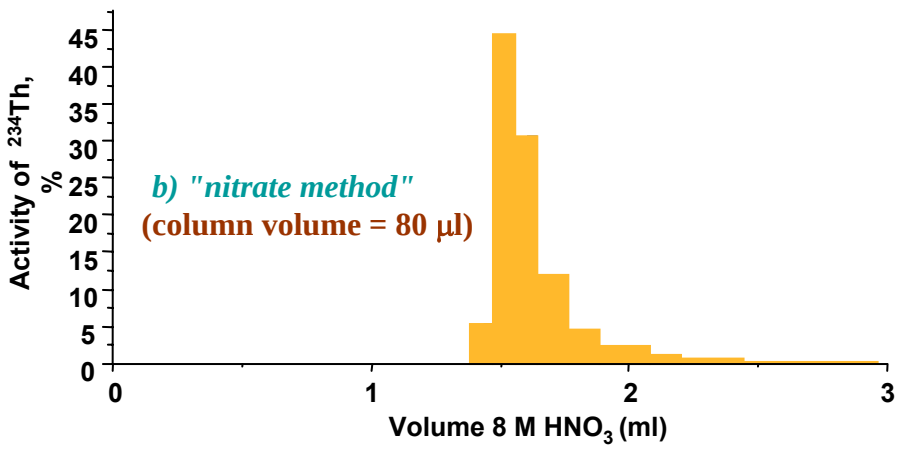

Fig. 46: Typical elution diagrams of 150 kBq 234Th at separation from 25 g uranylnitrate by chloride anion exchange (upper part) followed by nitrate anion exchange (lower part).

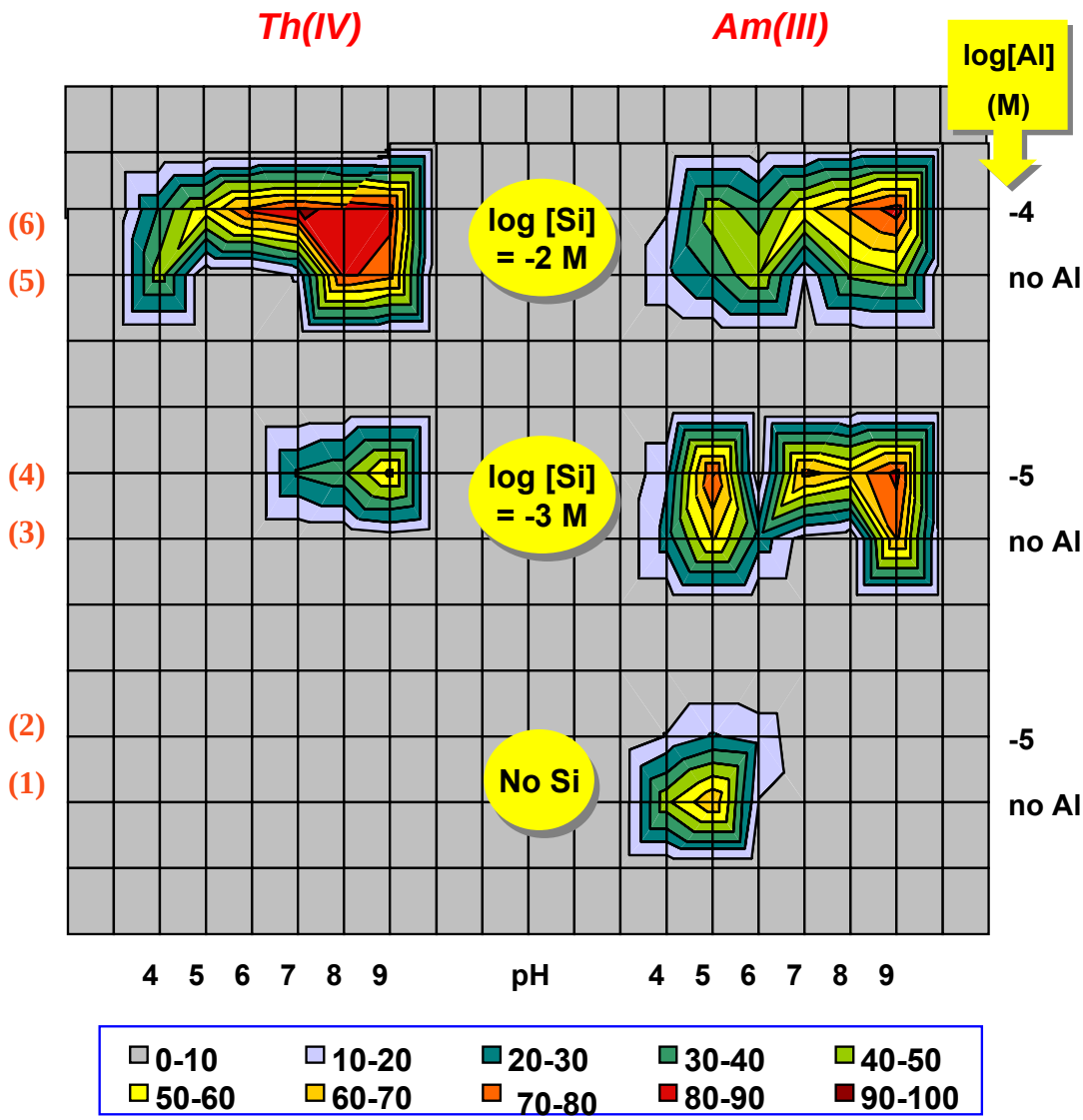

Fig, 47: A contour diagram of the colloid-borne activity fraction (%) (z-axis) normalized to the initial input activity after 35 days of sample conditioning time in different pH for Th (left part) and for Am (right part). Different Si and Al concentrations are indicated in the middle part of the fig. and on the right y-axis, respectively.

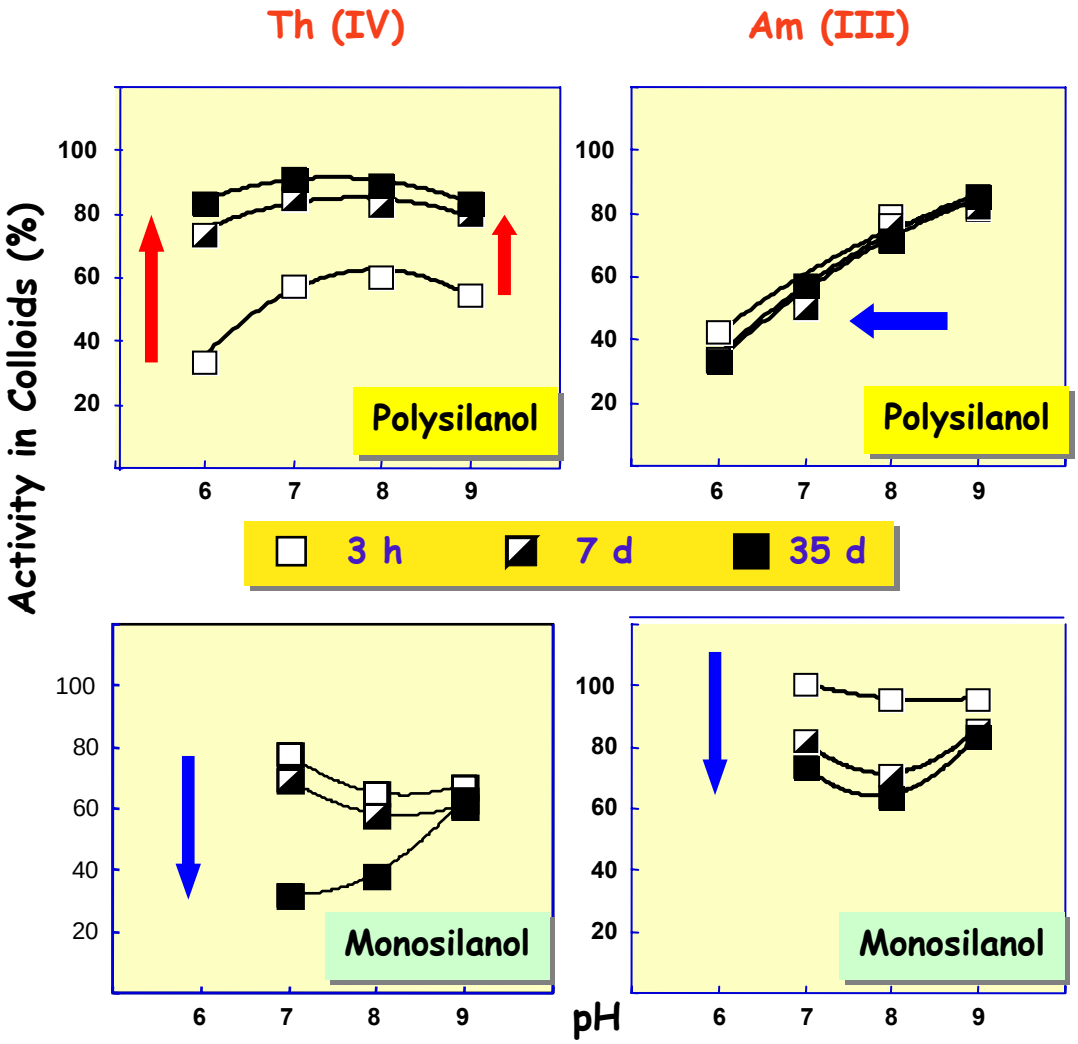

Fig. 48: Colloid-borne activity fraction (%) normalized to the initial activity as a function of pH after different sample conditioning times: Th- (left part) and Am- (right part) incorporated into HAS colloids generated from mono- (lower part) and from polysilanol (upper part).

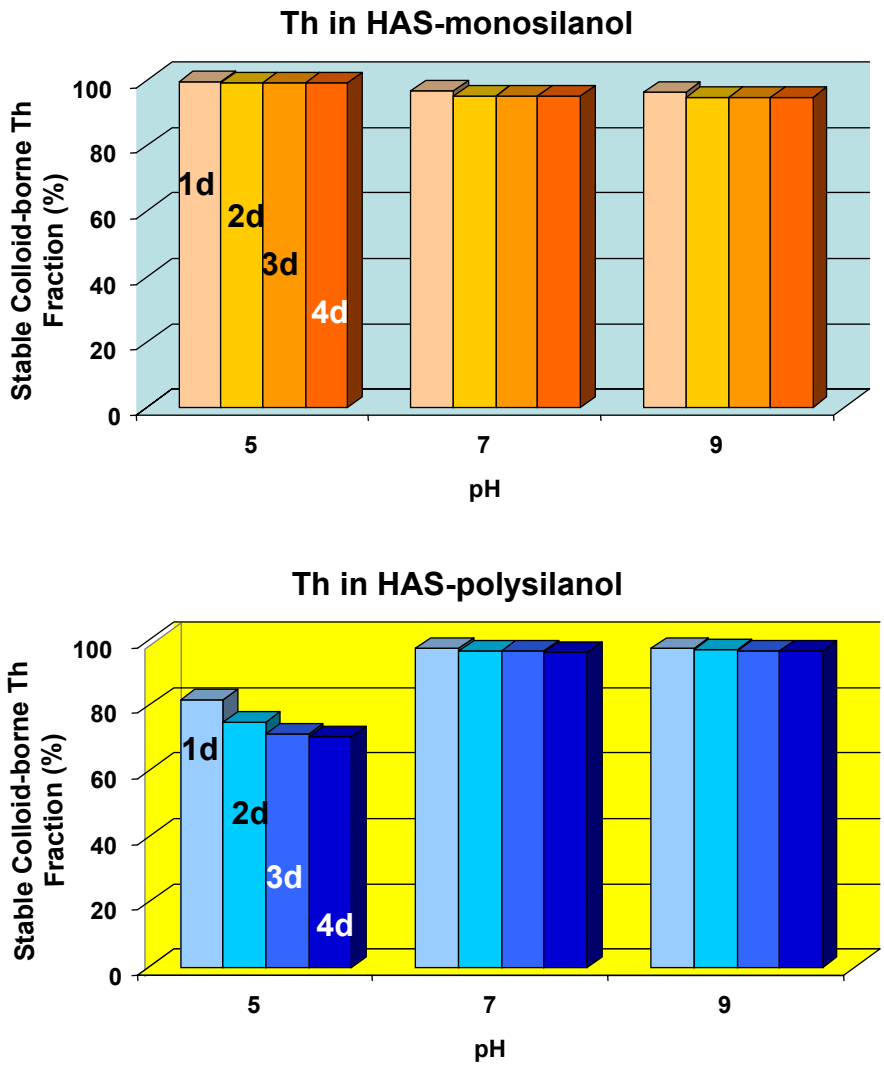

Fig. 49: Colloid-borne Th fraction (%) in a sample after the desorption experiment. The initial sample is prepared at different pH with 10^{-3} mol l^{-1} Si, 10^{-5} mol l^{-1} Al and $5x10^{-8}$ mol l^{-1} Th (upper part) and 10^{-2} mol l^{-1} Si, 10^{-4} mol l^{-1} Al and $5x10^{-8}$ mol l^{-1} Th (lower part) and conditioned for 7 days.

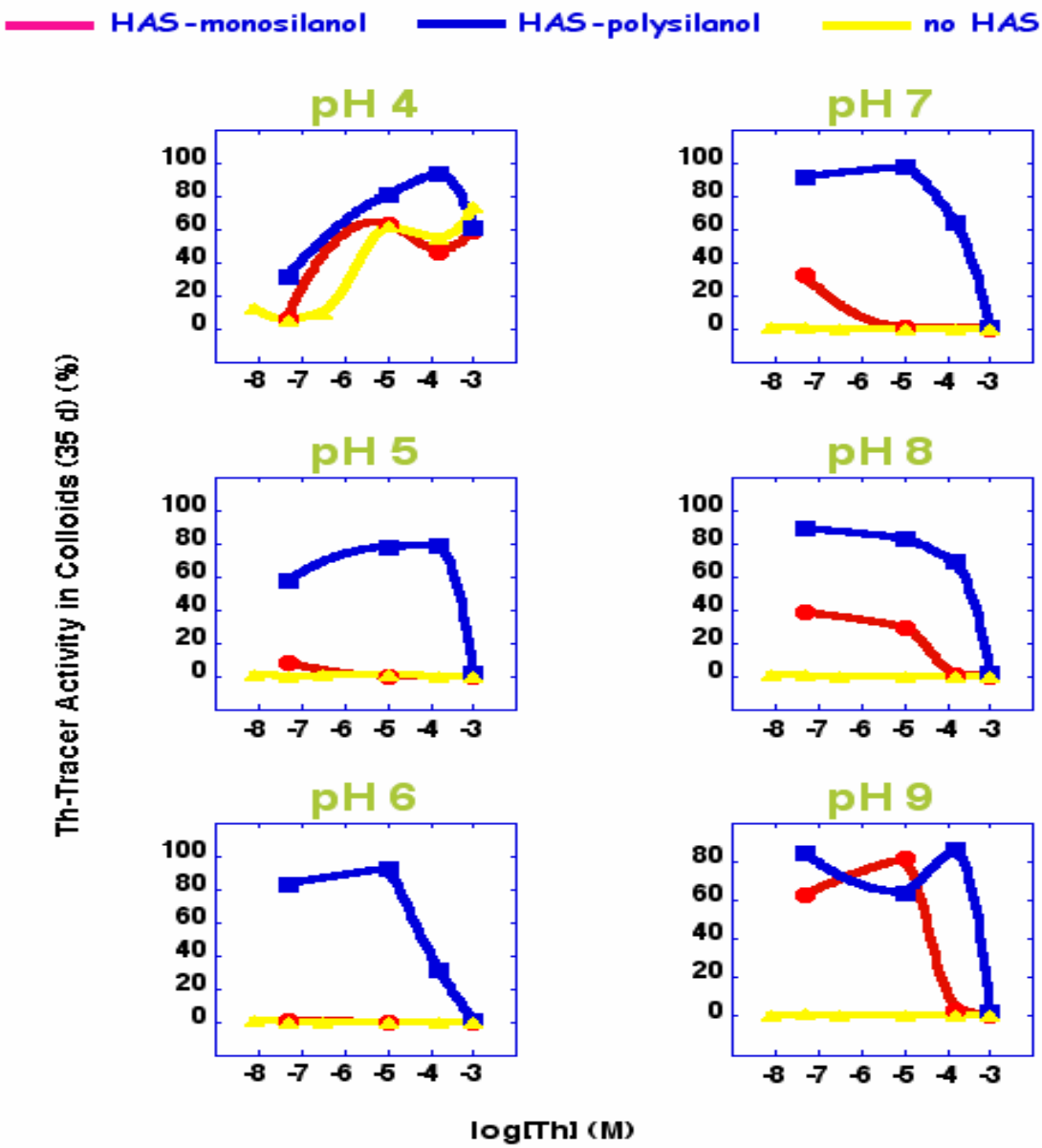

Fig. 50: Colloid-borne Th-activity fraction (%) as a function of the Th concentration for different pH´s in three series of samples indicated as HAS-monosilanol, HAS-polysilanol and no HAS, respectively, and containing mixture solutions of:
(1): 10^{-3} mol l^{-1} Si, 10^{-5} mol l^{-1} Al, $5x10^{-8}$ mol l^{-1}, varied concentration of Th;
(2): $1.3x10^{-2}$ mol l^{-1} Si, $1.5x10^{-4}$ mol l^{-1} Al, $5x10^{-8}$ mol l^{-1} Am, varied concentration of Th;
(3): Varied concentration of Th.

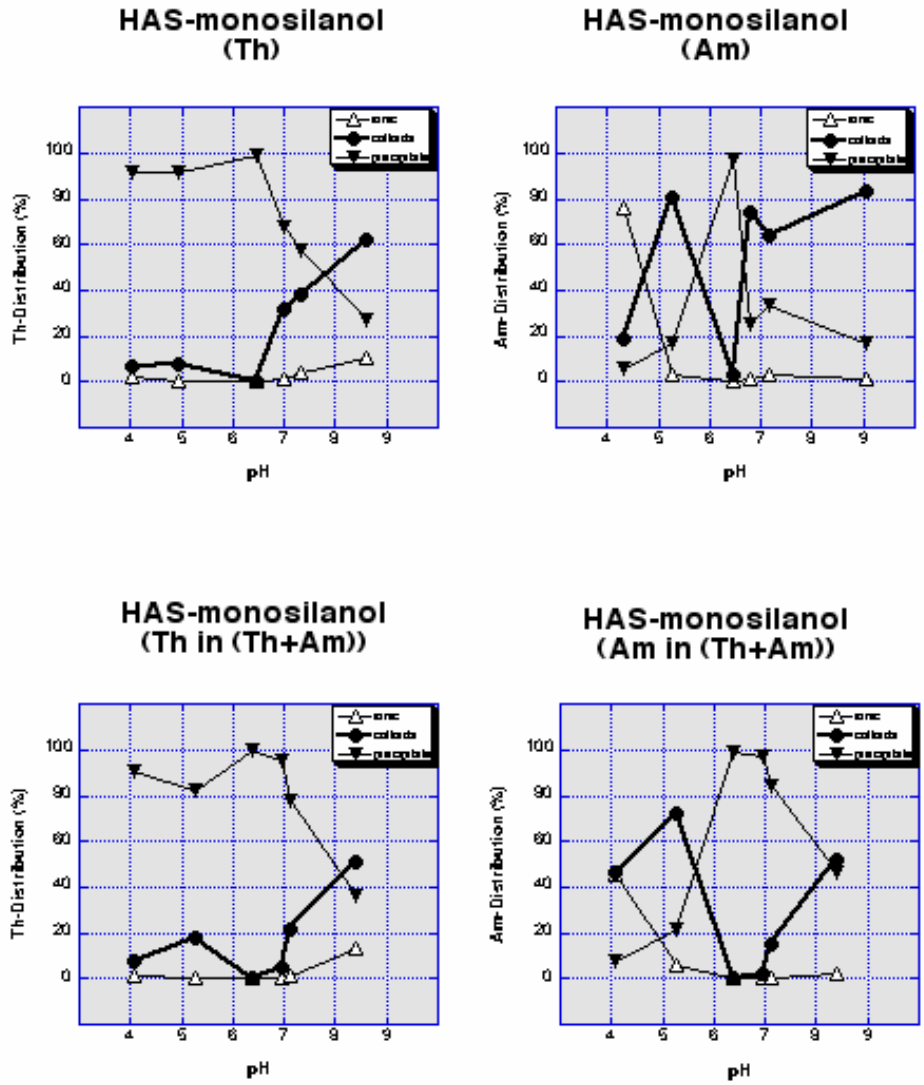

Fig.51: Activity fraction (%) in solution, colloids and precipitate as a function of pH for samples formed from HAS-monosilanol and containing solutions of:
(1): 10^{-3} mol l^{-1} Si, 10^{-5} mol l^{-1} Al, $5x10^{-8}$ mol l^{-1} Th (upper left part)
(2): 10^{-3} mol l^{-1} Si, 10^{-5} mol l^{-1} Al, $5x10^{-8}$ mol l^{-1} Am (upper right part)
(3): 10^{-3} mol l^{-1} Si, 10^{-5} mol l^{-1} Al, $5x10^{-8}$ mol l^{-1} Th, $5x10^{-8}$ mol l^{-1} Am (upper left and upper right part for Th and Am measurement, respectively).

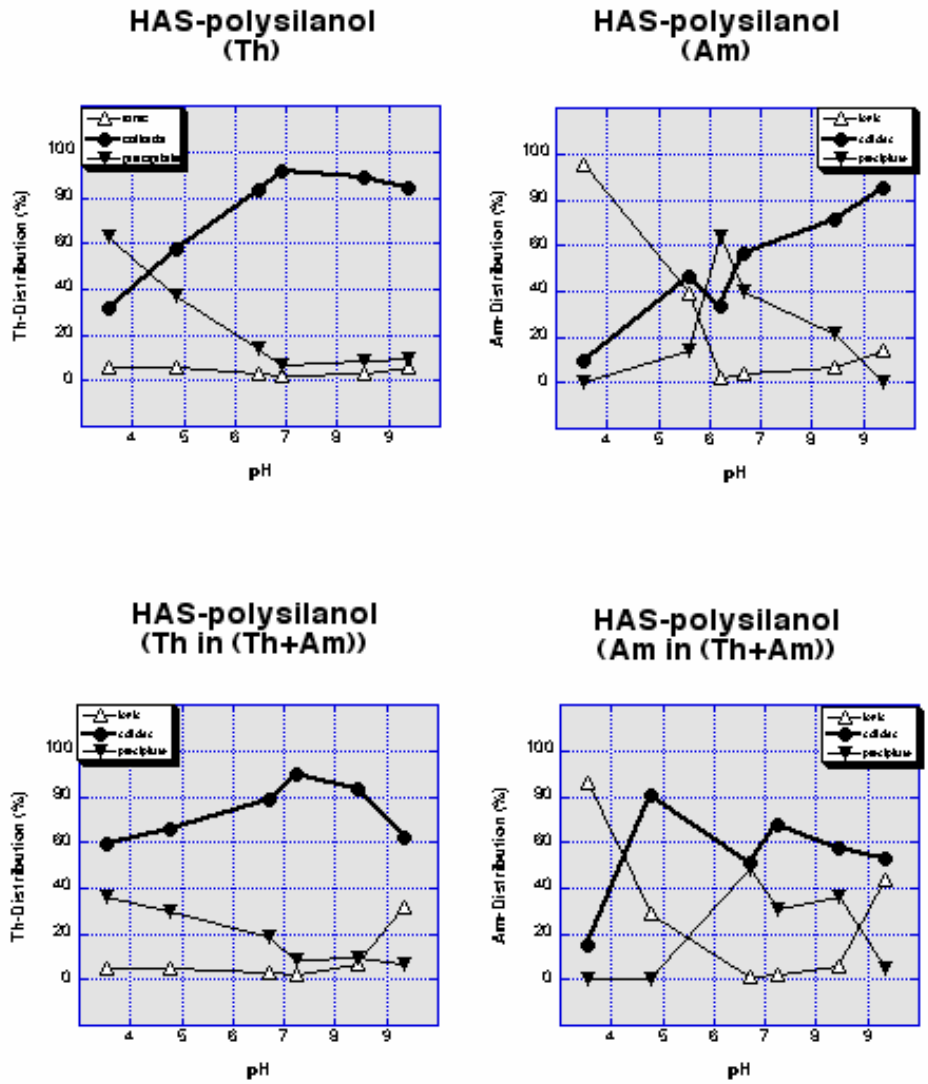

Fig.52: Activity fraction (%) in solution, colloids and precipitate as a function of pH for samples formed from HAS-polysilanol and containing solutions of:
(1): 1.3×10^{-2} mol l^{-1} Si, 1.5×10^{-4} mol l^{-1} Al, 5×10^{-8} mol l^{-1} Th (upper left part)
(2): 1.3×10^{-2} mol l^{-1} Si, 1.5×10^{-4} mol l^{-1} Al, 5×10^{-8} mol l^{-1} Am (upper right part)
(3): 1.3×10^{-2} mol l^{-1} Si, 1.5×10^{-4} mol l^{-1} Al, 5×10^{-8} mol l^{-1} Th, 5×10^{-8} mol l^{-1} Am (upper left and upper right part for Th and Am measurement, respectively).

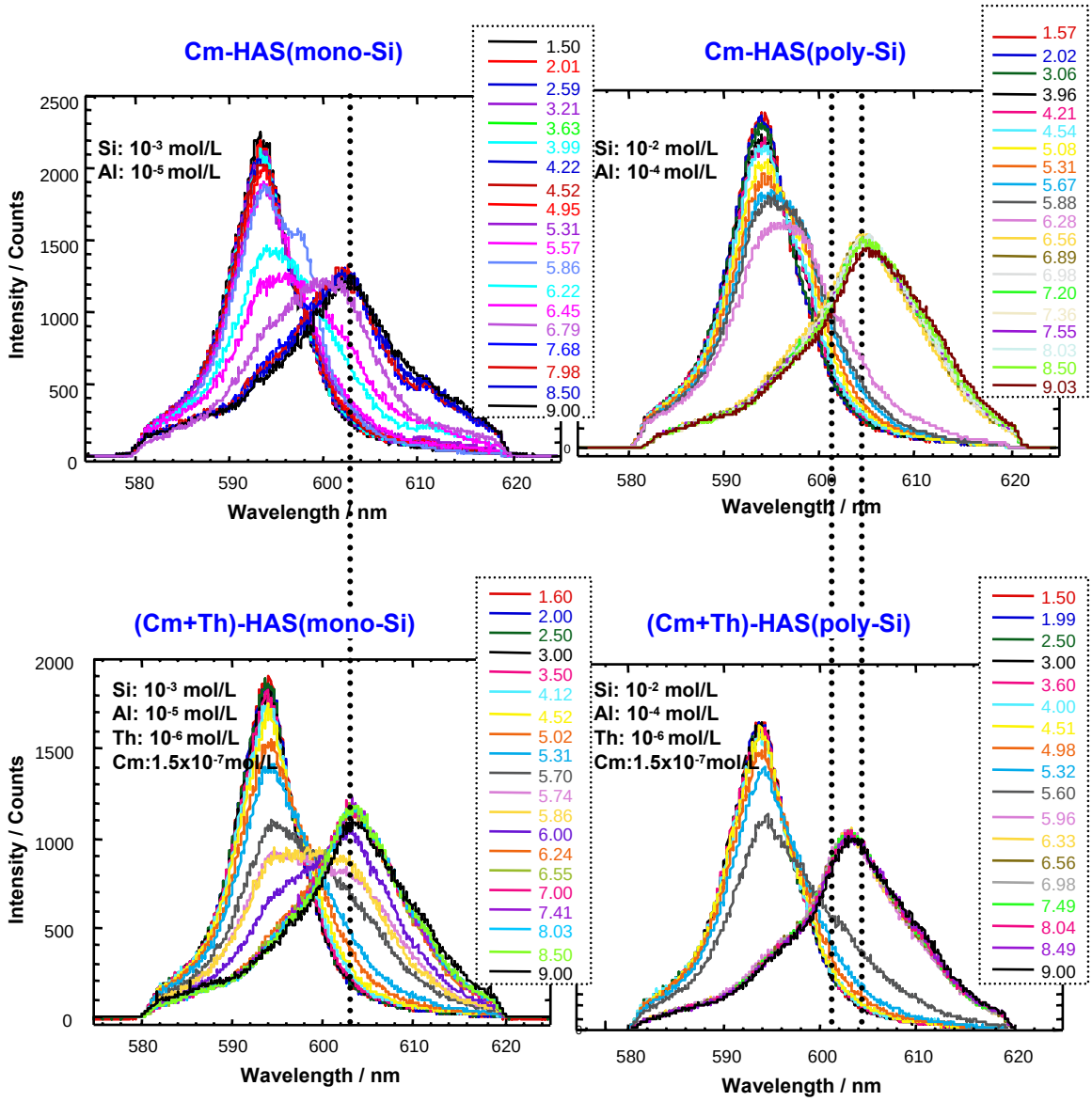

Fig.53: Speciation of HAS colloid-borne Cm by TRLFS on the pH titration from 1 to 9 in a solution containing mono-ilanol (left part) and in a solution containing polysilanol (right part) without (upper part) and with (lower part) Th addition: the pH dependent spectrum evolution.

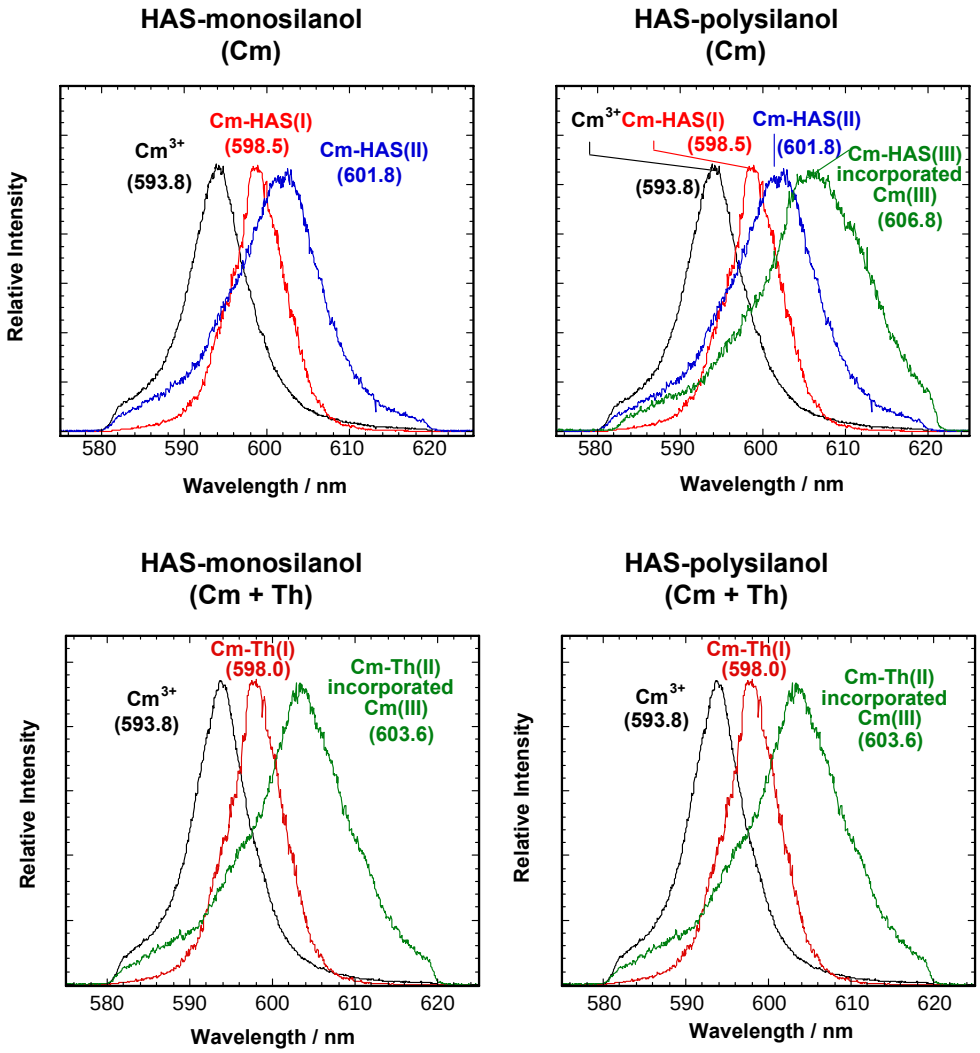

Fig.54: Deconvoluted spectra of different Cm species present in the solution (cf. Fig.53).

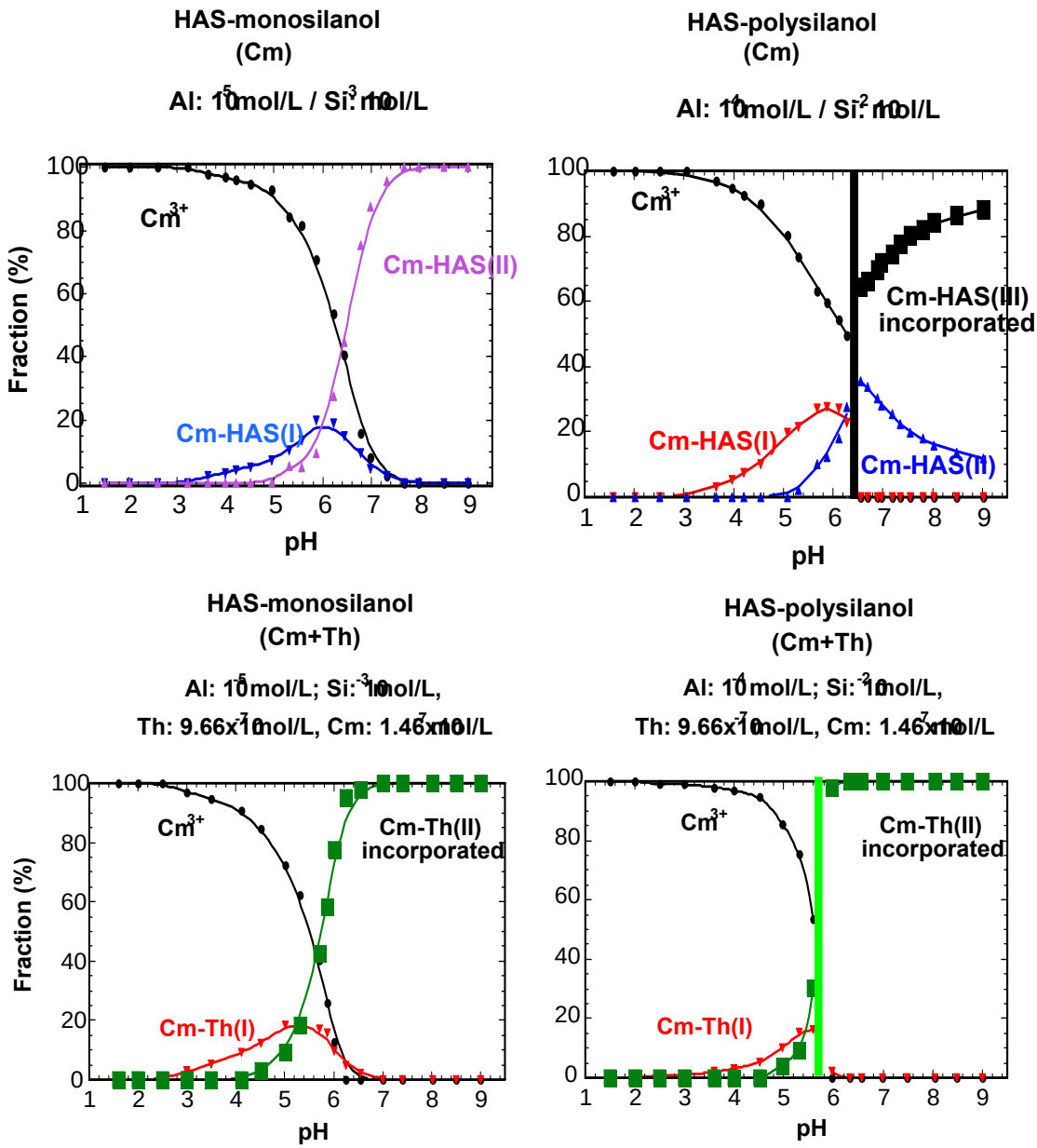

Fig.55: The relative Cm species distribution as a function of pH (cf. Figs 53 and 54).

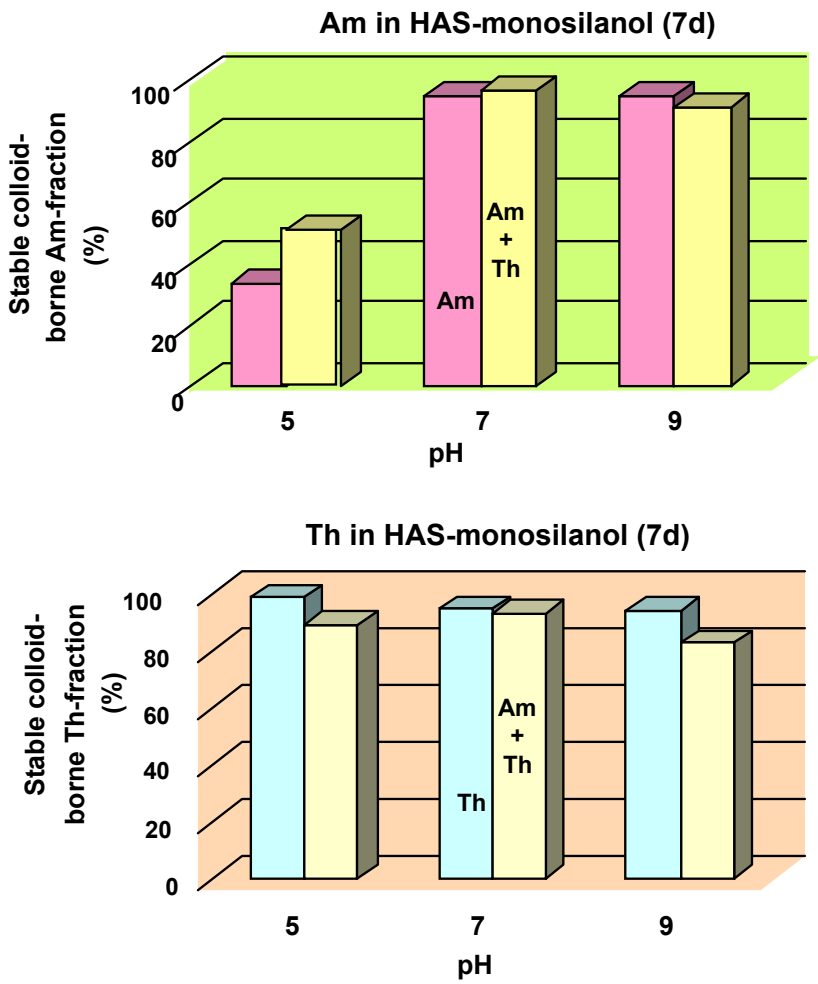

Fig. 56: Colloid-borne activity fraction (%) in a sample after the desorption experiment. The initial sample is prepared at different pH with 10^{-3} mol l^{-1} Si (monosilanol), 10^{-5} mol l^{-1} Al and $5x10^{-8}$ mol l^{-1} Am or Th or Th+Am and conditioned for seven days.

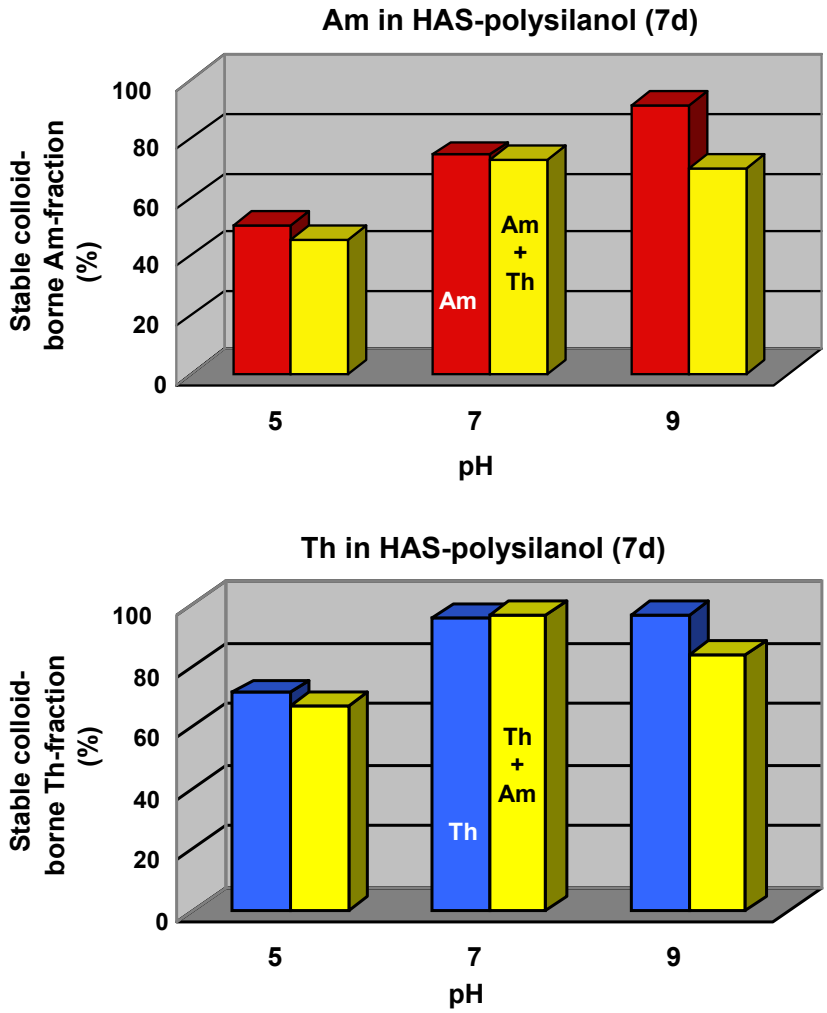

Fig. 57: Colloid-borne activity fraction (%) in a sample after the desorption experiment. The initial sample is prepared at different pH with 10^{-2} mol l^{-1} Si (polysilanol), 10^{-4} mol l^{-1} Al and $5x10^{-8}$ mol l^{-1} Am or Th or Th+Am and conditioned for seven days.

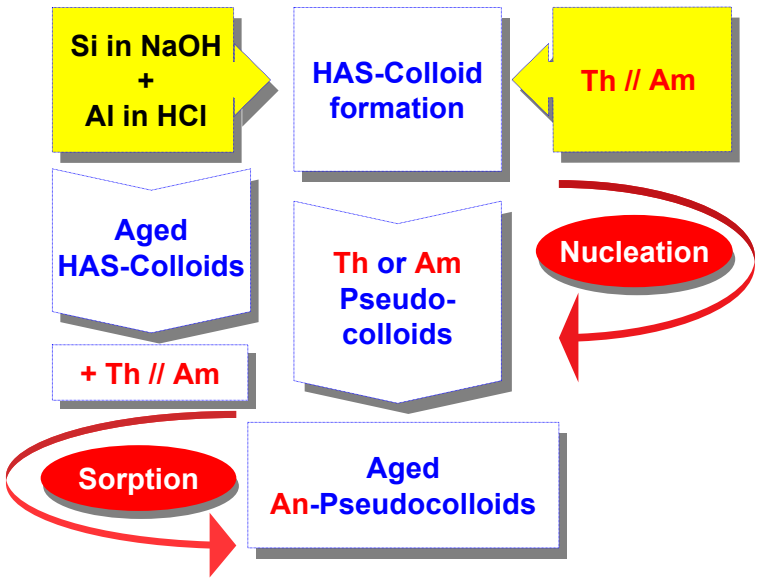

Fig. 58: Experimental interactions pathways of actinides with HAS colloids.

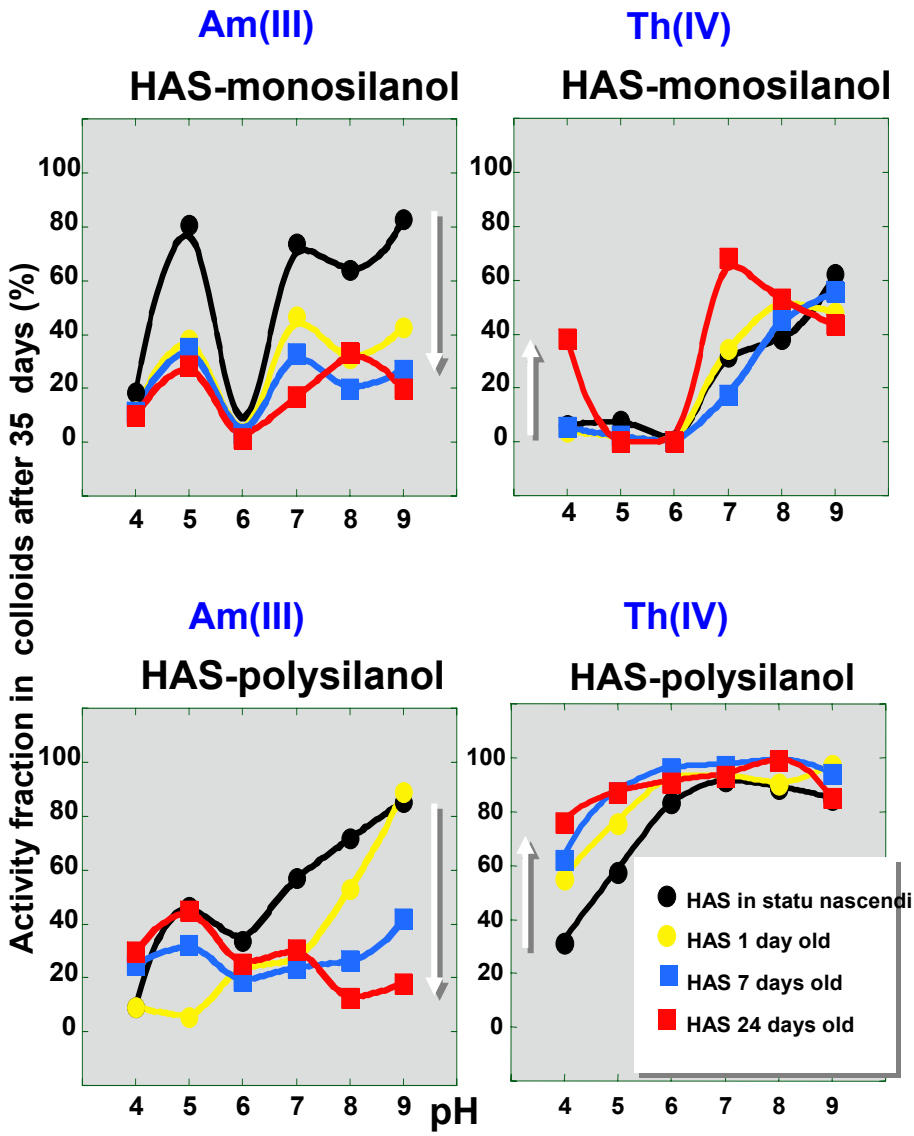

Fig. 59: Colloid-borne activity fraction (%) normalized to the initial activity as a function of pH after 35 days sample conditioning time for colloids of different ages (from 0 to 24 days): for Am (left part) and Th (right part) incorporation into colloids generated from HAS-monosilanol (upper part) and from HAS-polysilanol (lower part).

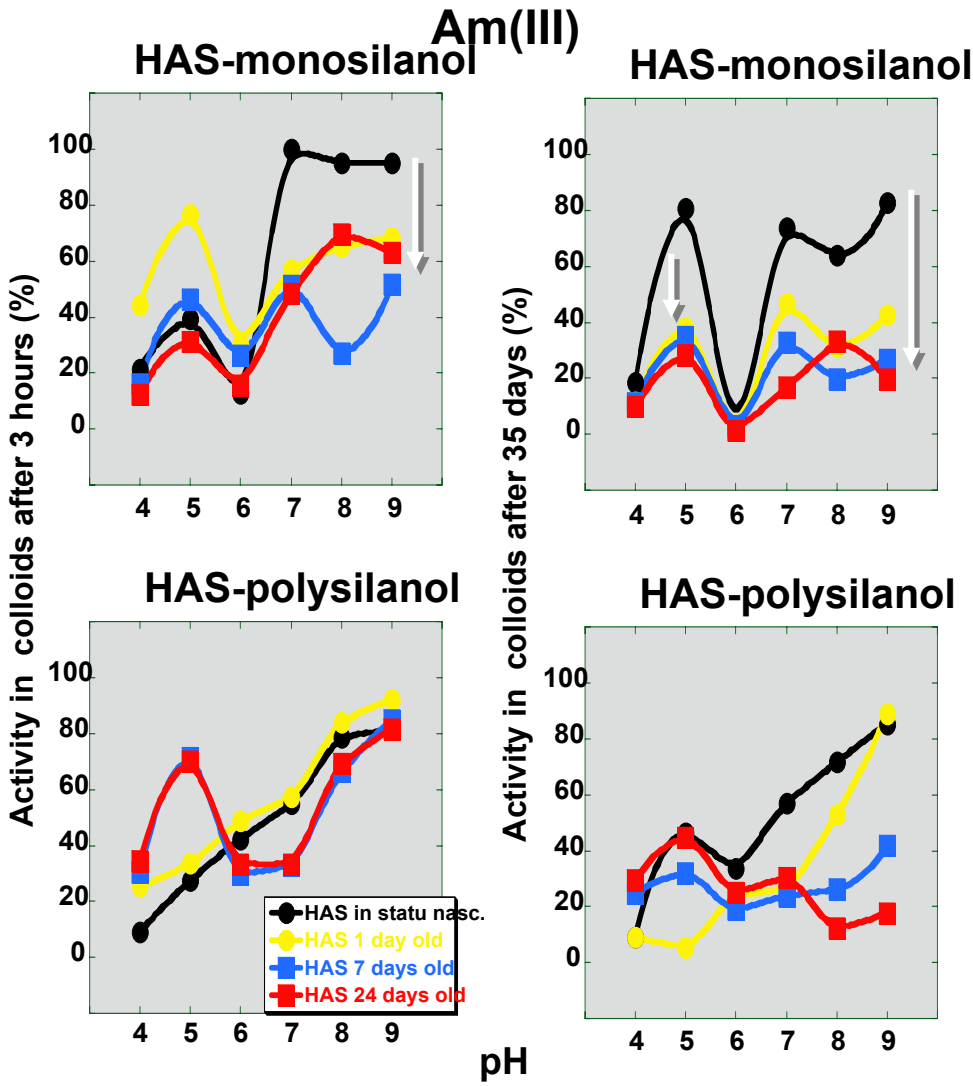

Fig. 60: Colloid-borne Am fraction (%) normalized to the initial activity as a function of pH after 3 hours and 35 days activity contact time (left and right part, respectively) for colloids of different ages (from 0 to 24 days) generated from HAS-monosilanol (upper part) and from HAS-polysilanol (lower part).

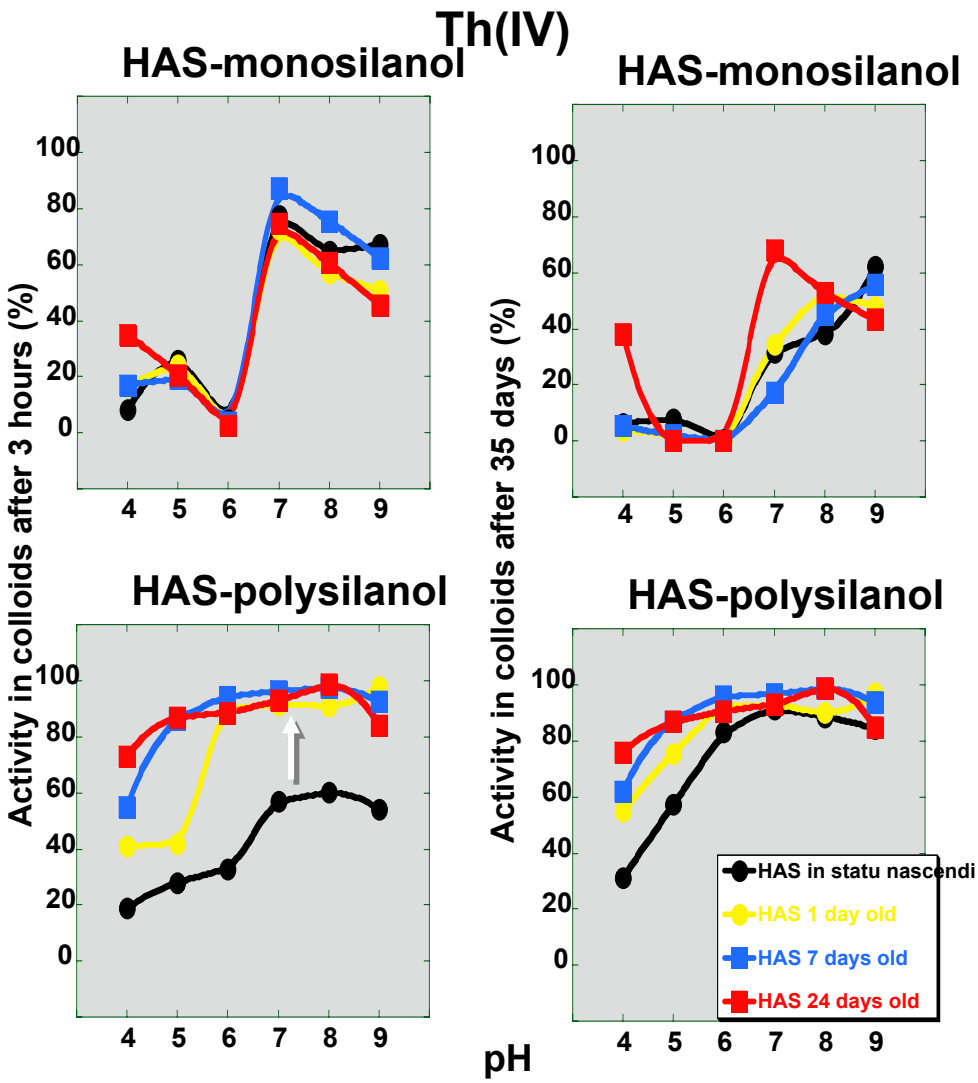

Fig. 61: Colloid-borne Th fraction (%) normalized to the initial activity as a function of pH after 3 hours and 35 days activity contact time (left and right part, respectively) for colloids of different ages (from 0 to 24 days) generated from HAS-monosilanol (upper part) and from HAS-polysilanol (lower part).

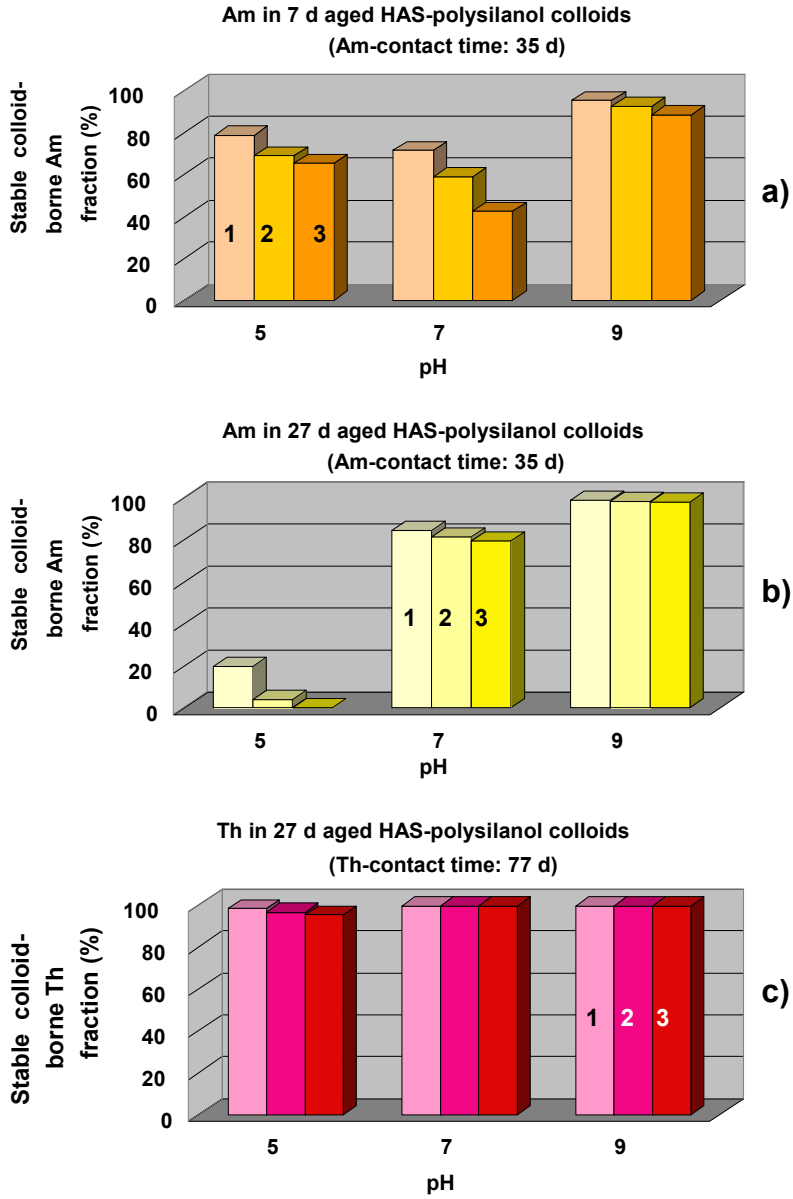

Fig. 62: Colloid-borne activity fraction (%) in a sample after the desorption experiment. The initial sample is prepared at different pH with 10^{-2} mol l^{-1} Si (polysilanol), 10^{-4} mol l^{-1} Al: (a) $5x10^{-8}$ mol l^{-1} Am is added after 7 days aging time and the Am contact time is 35 days; (b) $5x10^{-8}$ mol l^{-1} Am is added after 27 days aging time and the Am contact time is 35 days; (c) $5x10^{-8}$ mol l^{-1} Th is added after 27 days aging time and the Am contact time is 77 days. Desorption experiment is performed in three sequential equilibria each with fresh solution.

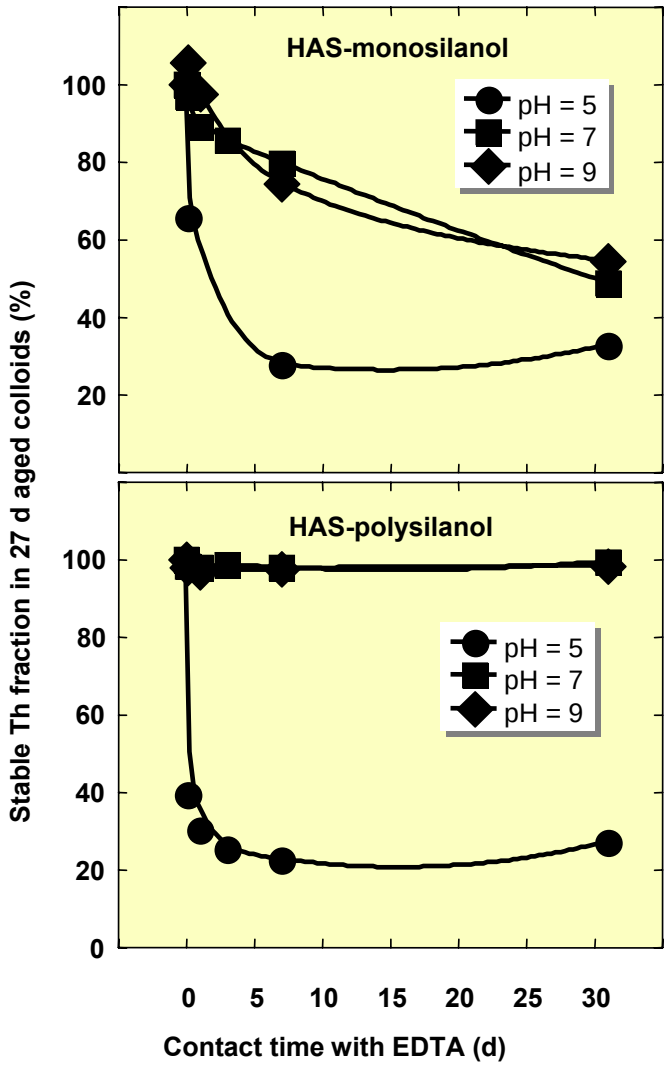

Fig. 63: Colloid-borne Th activity fraction (%) in a sample at desorption with $1x10^{-4}$ mol l^{-1} EDTA as a function of time. The initial sample is prepared at different pH with
(upper part): 10^{-3} mol l^{-1} Si (monosilanol), 10^{-5} mol l^{-1} Al
(lower part): 10^{-2} mol l^{-1} Si (polysilanol), 10^{-4} mol l^{-1} Al
After an aging time of 27 days, $4.8x10^{-8}$ mol l^{-1} Th is added; The Th contact time is 35 days.

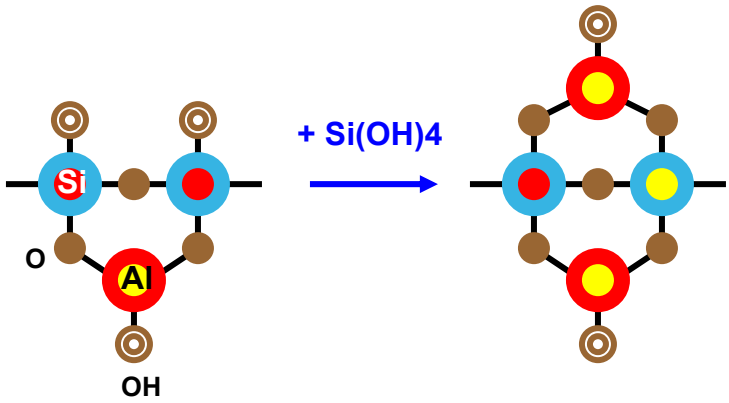

Fig. 64: Template mechanism for the formation of hydroxy aluminosilicates as proposed by Doucet et al. [Geochim. Cosmochim. Acta 65 (15) 2461 (2001)].

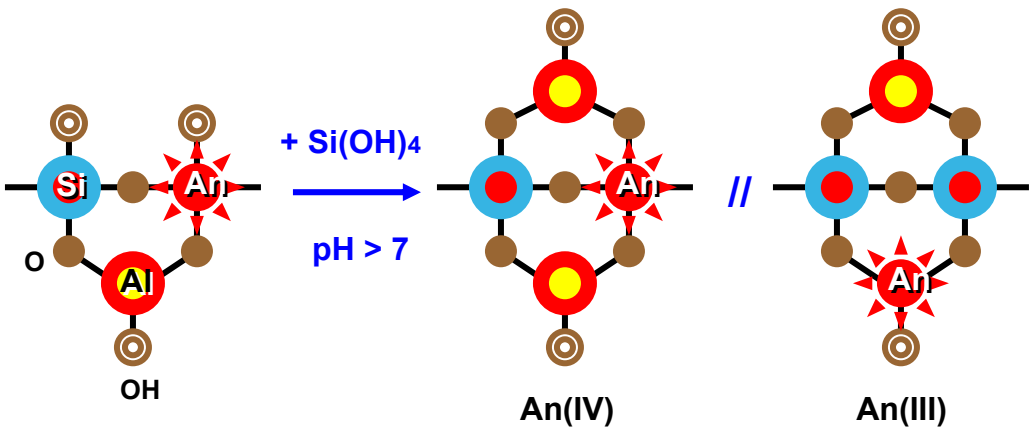

Fig. 65: Postulated mechanism for the formation of colloid-borne An(III) or An(IV) in HAS(monosilanol) colloids.

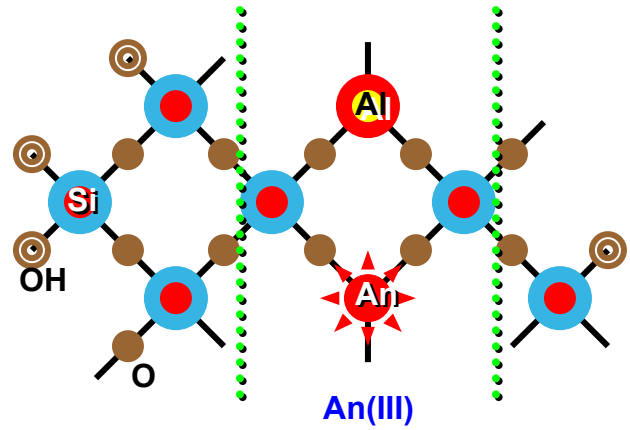

Fig. 66: Postulated mechanism for the formation of colloid-borne Am(Cm) from HAS(polysilanol) colloids with Si/Al atomic ratio: ca 1.

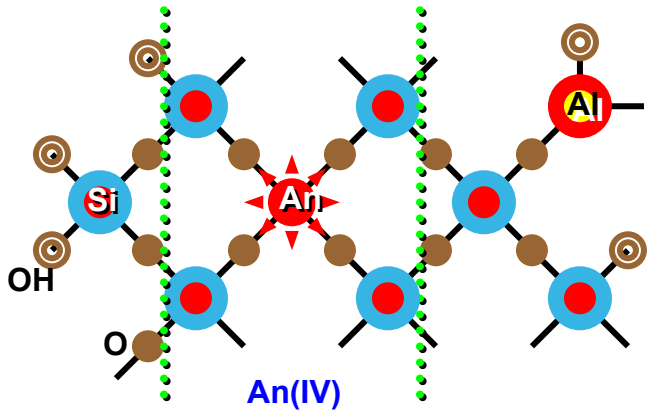

Fig. 67: Postulated mechanism for the formation of colloid-borne Th(IV) by heterogeneous nucleation with Si.

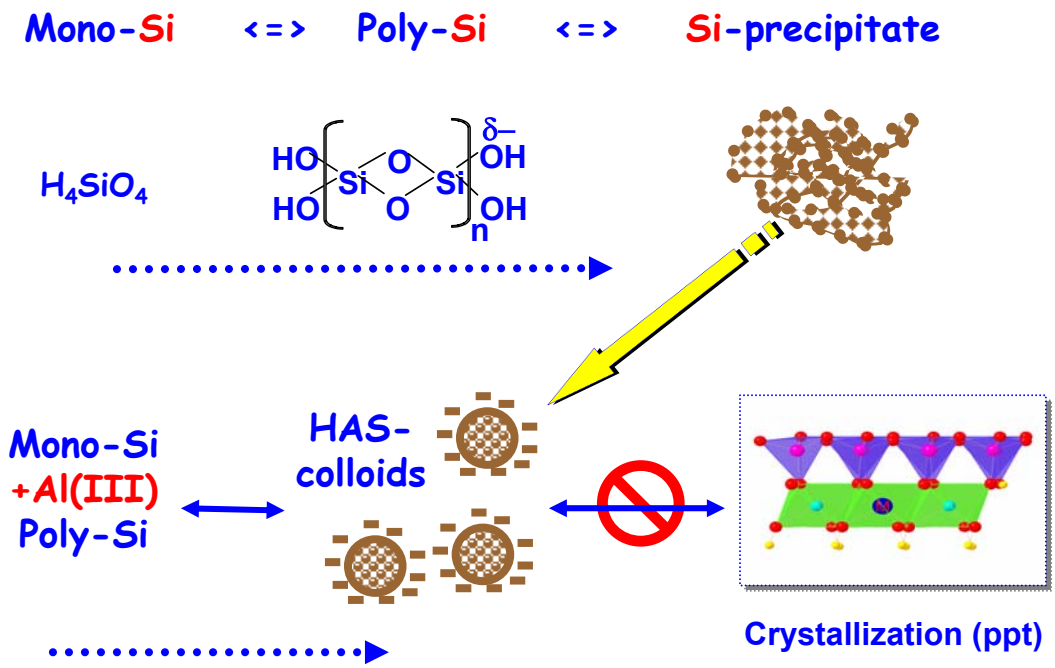

Fig. 68: Stabilization of HAS colloids through Al-controlled polymerization of Si.

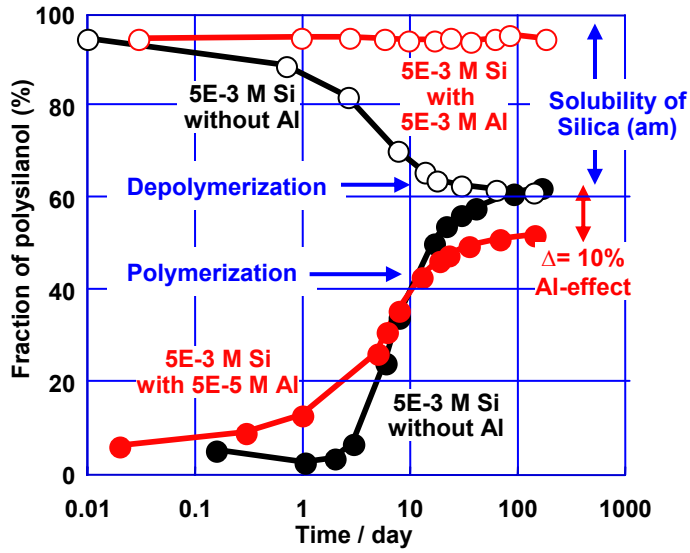

Fig. 69: The Al ion effect on the polymerization and depolymerization of Si, monitored by molybdenum tests.

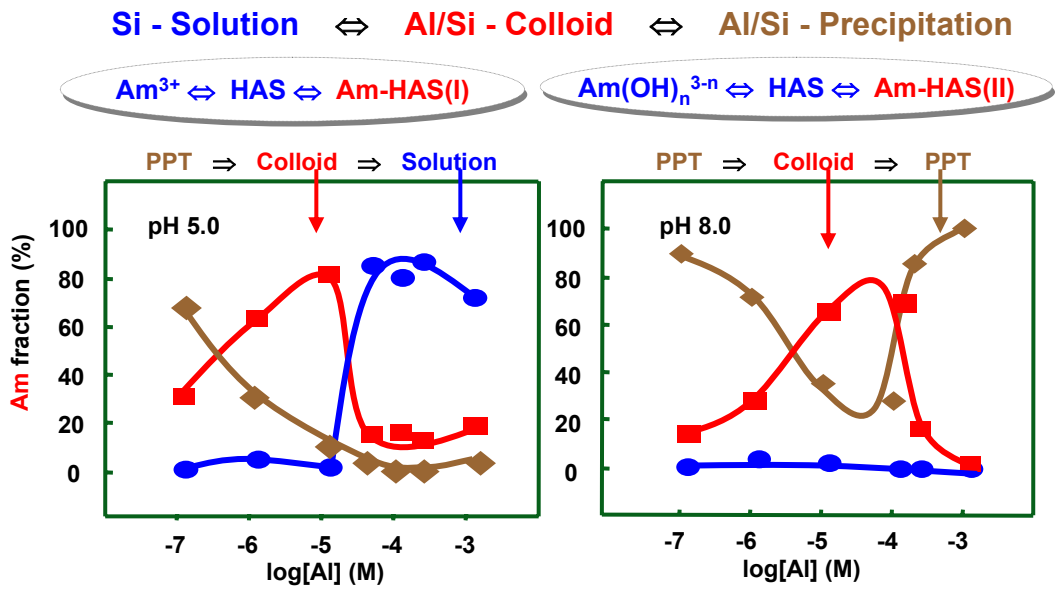

Fig. 70: Dual effects of Al on the formation of colloid-borne Am: (1) Binding with Si and HAS colloid formation (pH 5); (2) HAS colloid agglomeration via hydrophobic process.

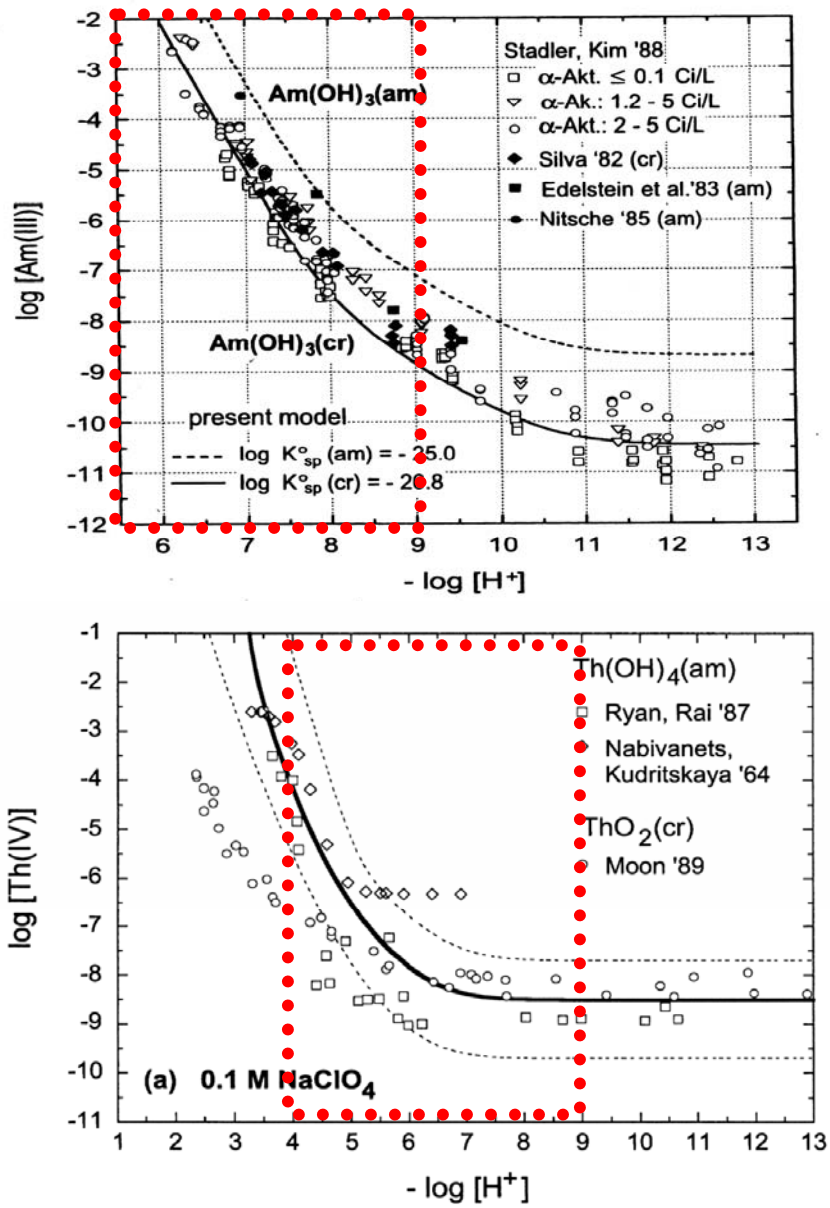

Fig. 71: Thermodynamic solubility of $Th(OH)_4$ (am) and $Am(OH)_3$ as a function of pH from literature. Conditions expected for colloid formation are indicated by dotted area.

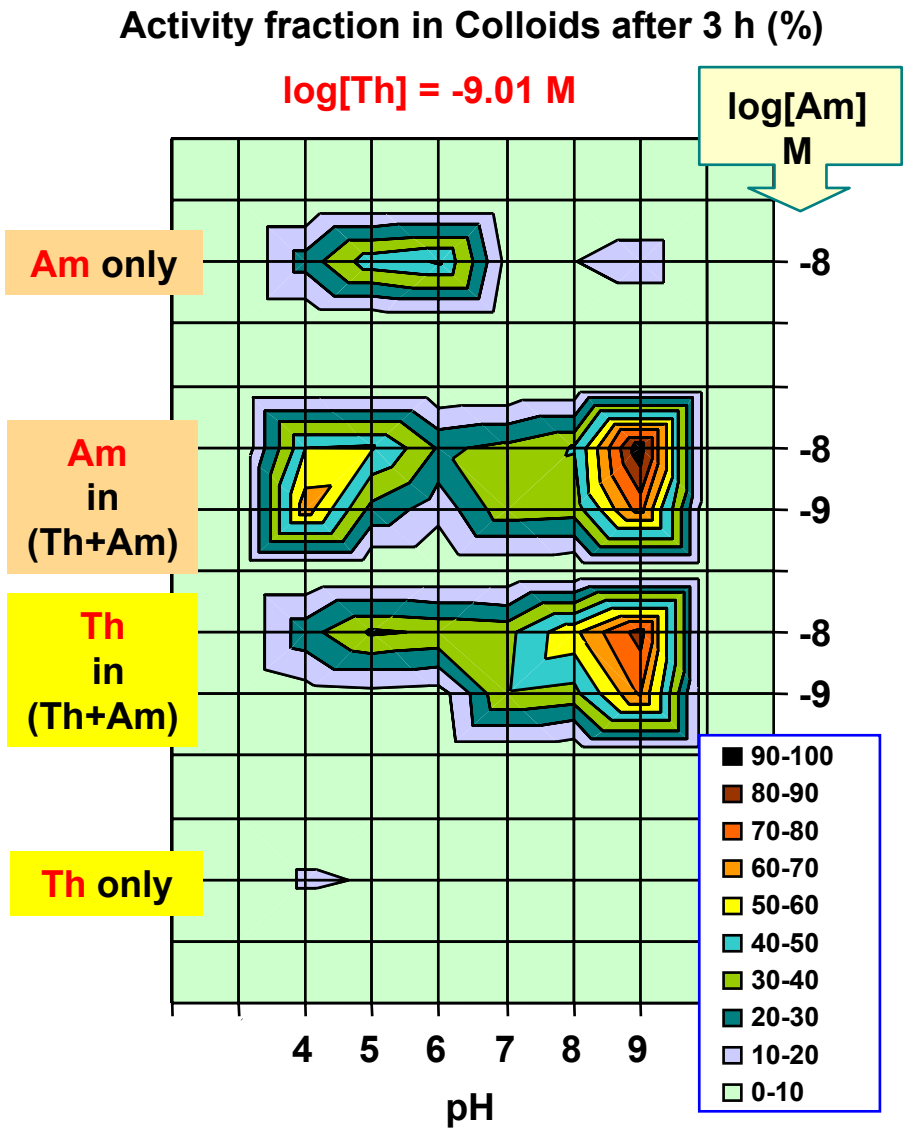

Fig. 72: Th and Am colloid-borne activity fraction (%) after 3 hours conditioning time in four sample series at different pH: two mixed samples containing $1x10^{-9}$ mol l^{-1} Th and $1x10^{-9}$ or $8x10^{-9}$ mol l^{-1} Am (Th+Am) and two separate samples containing $1x10^{-10}$ mol l^{-1} Th (Th only) and $8x\ 10^{-9}$ mol l^{-1} Am (Am only).

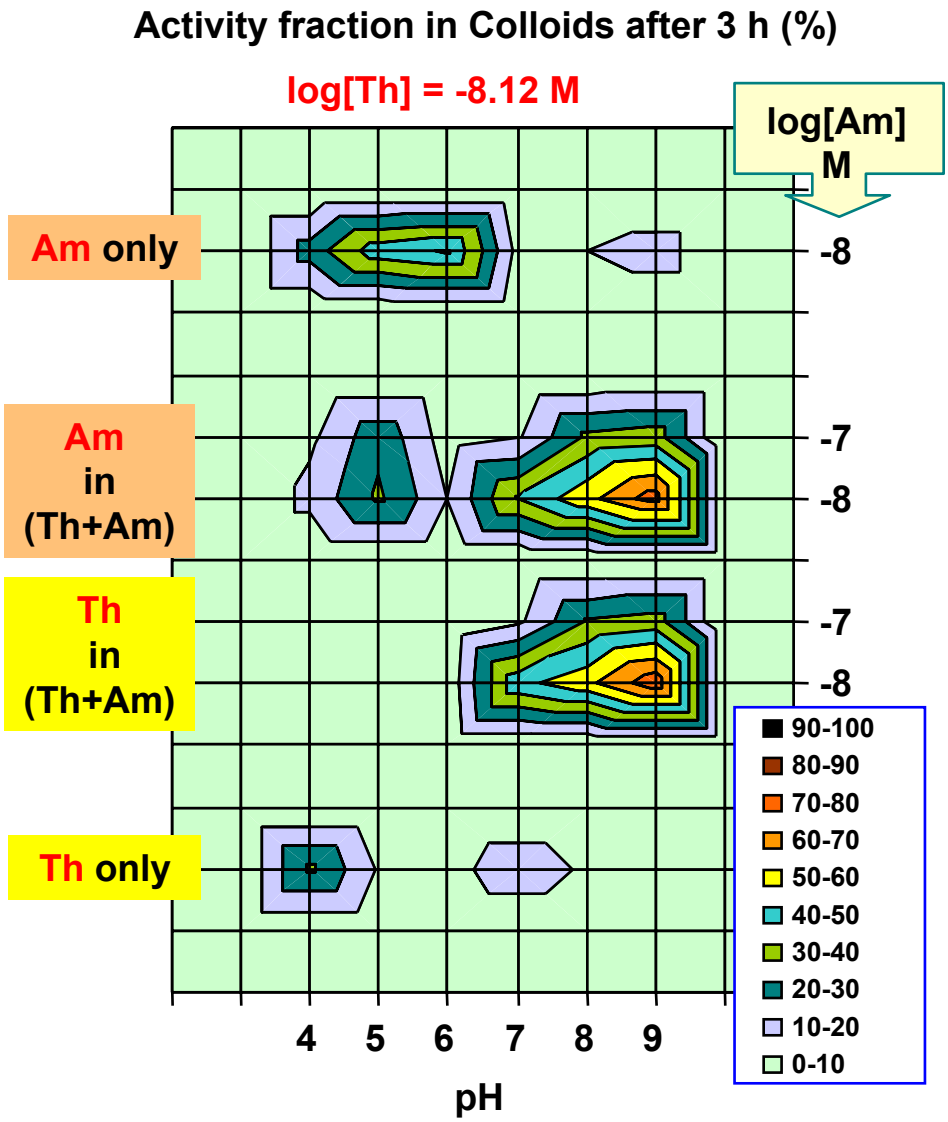

Fig. 73: Th and Am colloid-borne activity fraction (%) after 3 hours conditioning time in four sample series at different pH: two mixed samples containing $7x10^{-9}$ mol l^{-1} Th and $8x10^{-9}$ or $5.4x10^{-8}$ mol l^{-1} Am (Th+Am) and two separate samples containing $7x10^{-9}$ mol l^{-1} Th (Th only) and $8x10^{-9}$ mol l^{-1} Am (Am only).

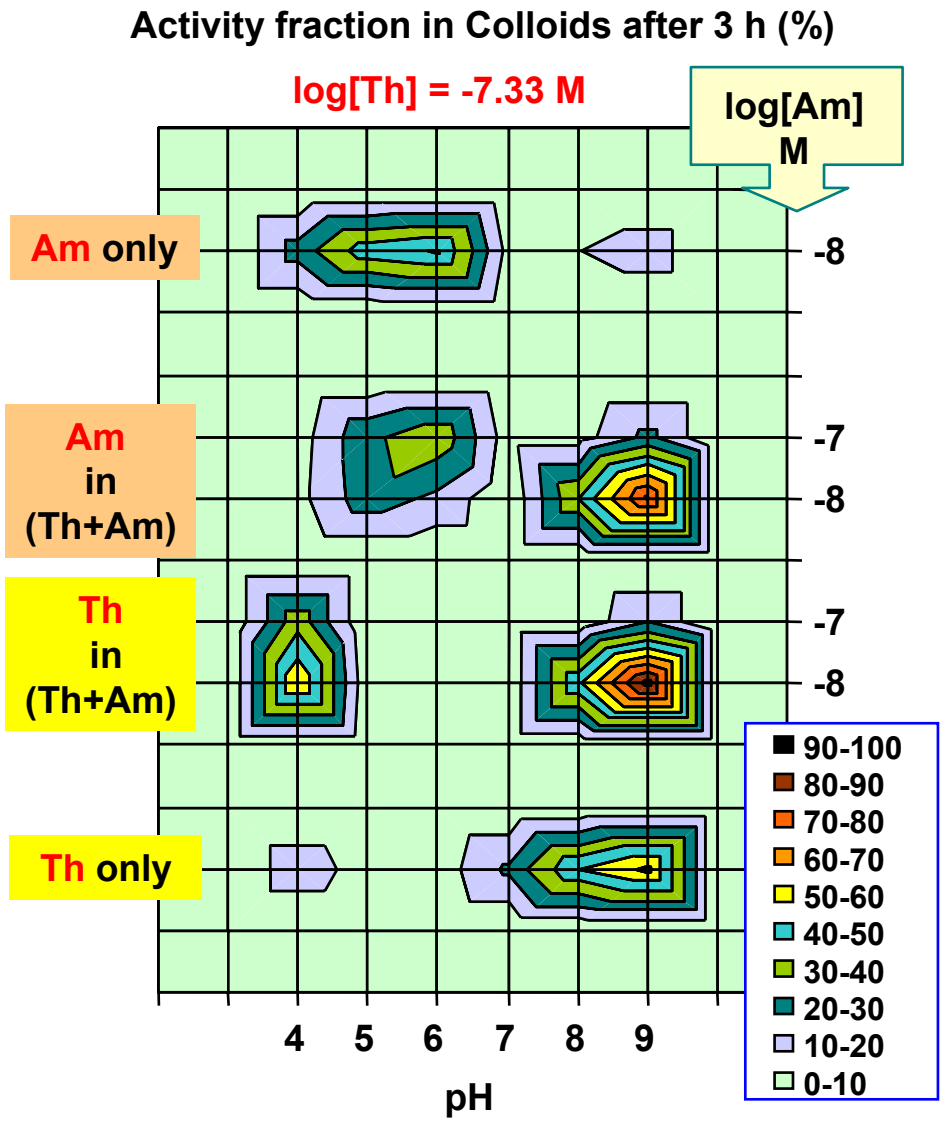

Fig. 74: Th and Am colloid-borne activity fraction (%) after 3 hours conditioning time in four sample series at different pH: two mixed samples containing 4.6×10^{-8} mol l^{-1} Th and 7×10^{-9} or 6×10^{-8} mol l^{-1} Am (Th+Am) and two separate samples containing 4.6×10^{-8} mol l^{-1} Th (Th only) and 1×10^{-8} mol l^{-1} Am (Am only).

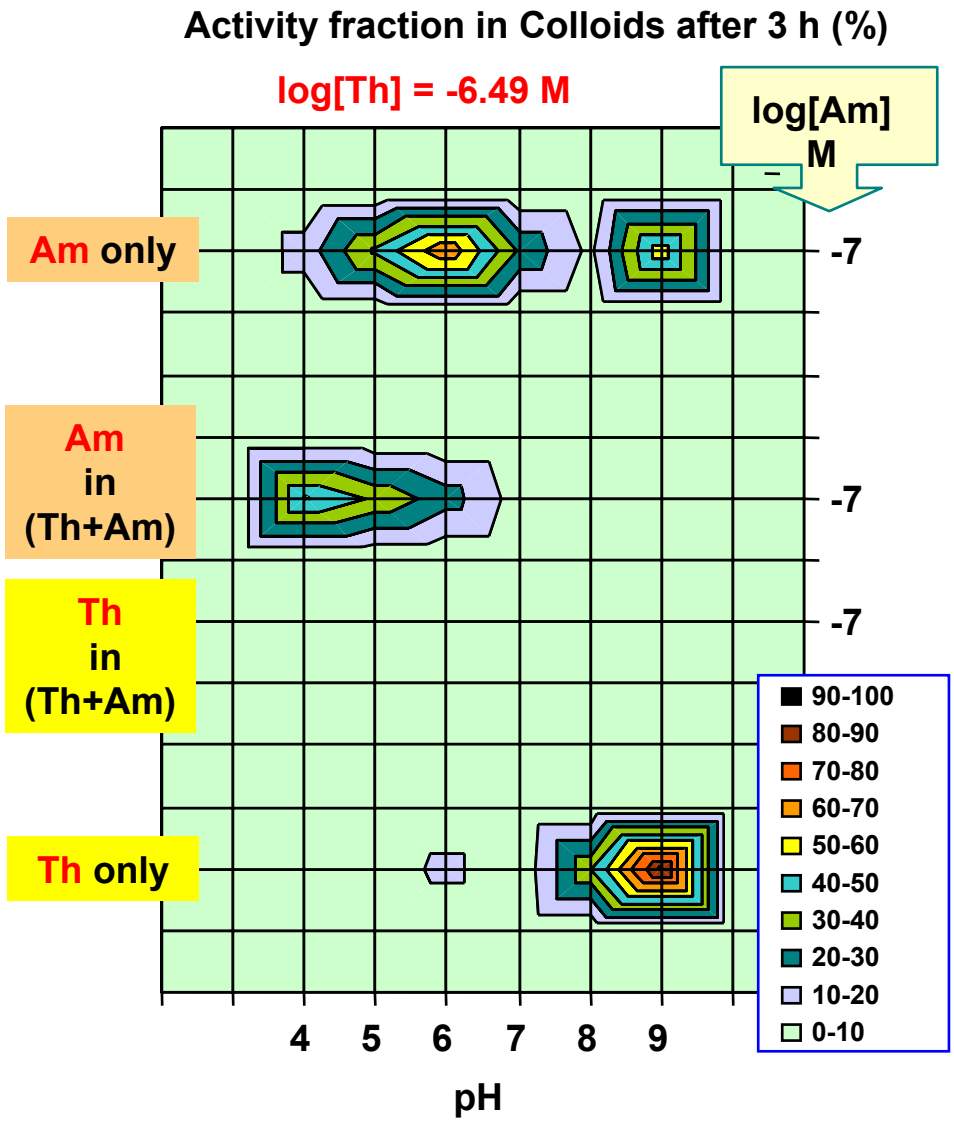

Fig. 75: Th and Am colloid-borne activity fraction (%) after 3 hours conditioning time in three sample series at different pH: two mixed samples containing 3.2×10^{-7} mol l^{-1} Th and 5×10^{-8} mol l^{-1} Am (Th+Am) and two separate samples containing 3.2×10^{-7} mol l^{-1} Th (Th only) and 5×10^{-8} mol l^{-1} Am (Am only).

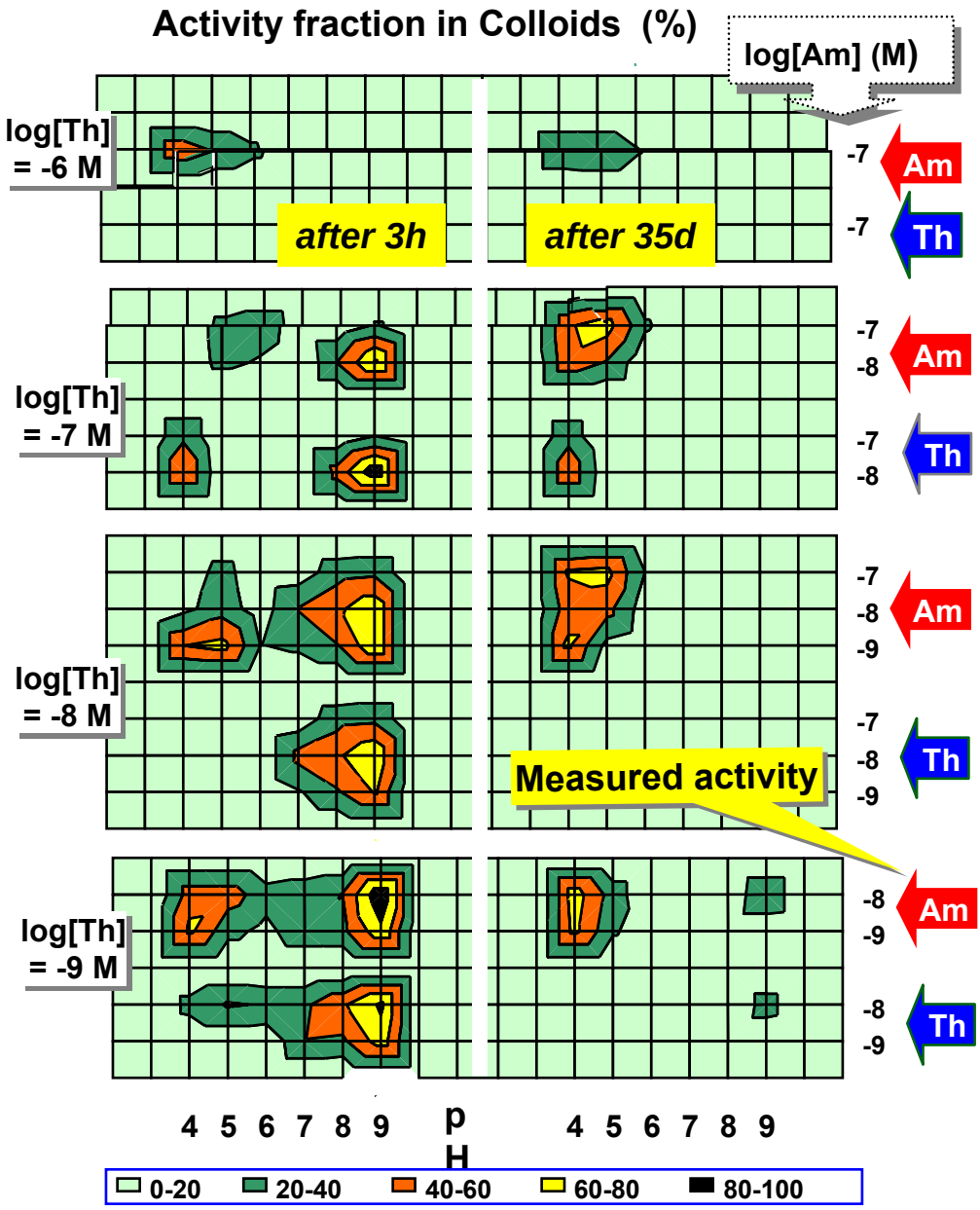

Fig. 76: Overview of Th and Am colloid-borne activity fraction (%) as shown in Figs. 72-75 (series of mixed samples (Th+Am), separate samples (Th or Am only)) at different pH after different sample conditioning times, 3 hours and 35 days as illustrated in the left and the right part of the figure.

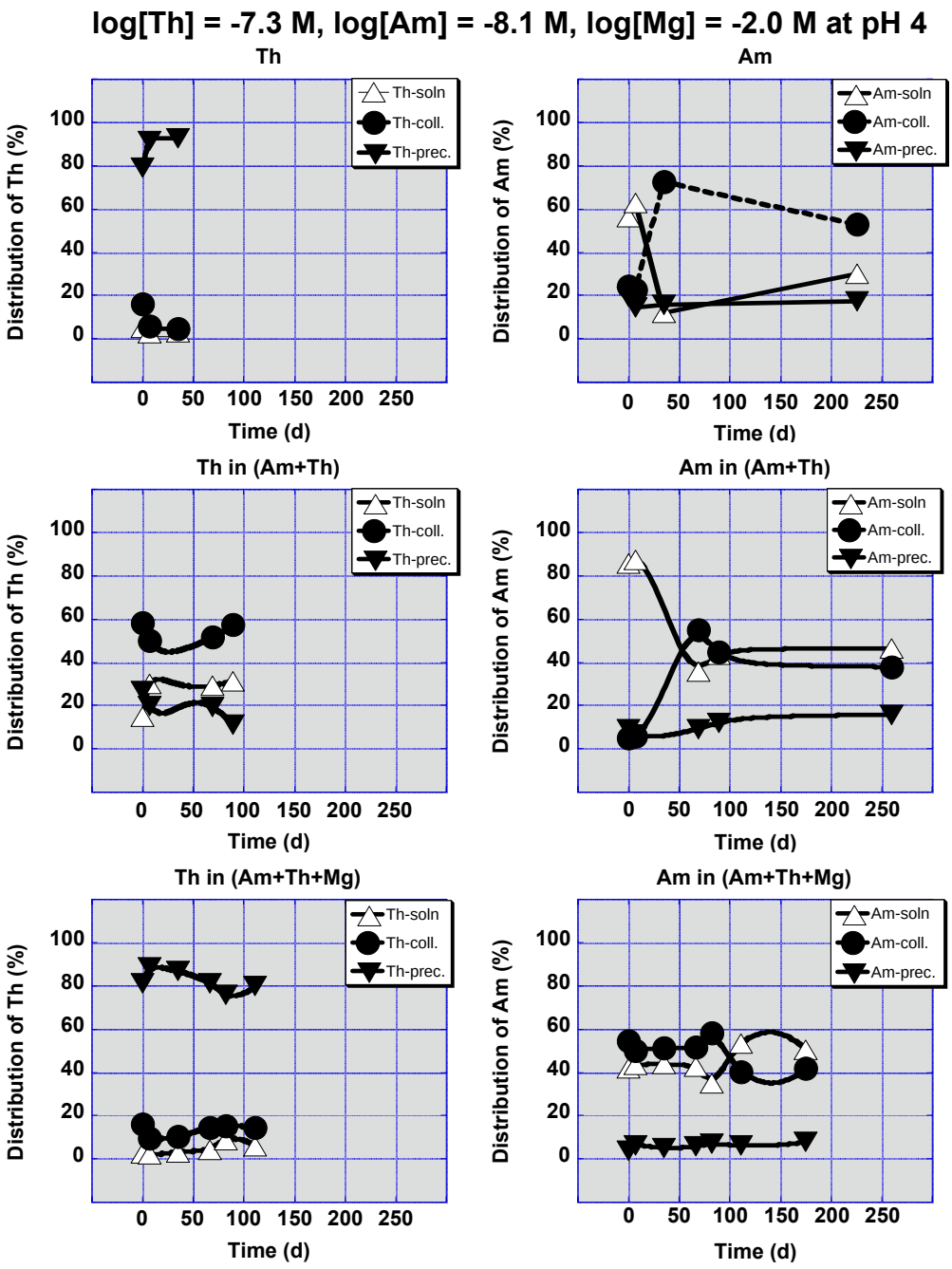

Fig.77: Colloid-borne activity fraction (%) as a function of the conditioning time without and with Mg: one mixed and two separate samples containing 4.6×10^{-8} mol l^{-1} Th and 7×10^{-9} mol l^{-1} Am (cf. Fig.76) at pH 4 (middle and upper parts) and for the mixed sample with addition of 10^{-2} mol l^{-1} Mg (lower part).

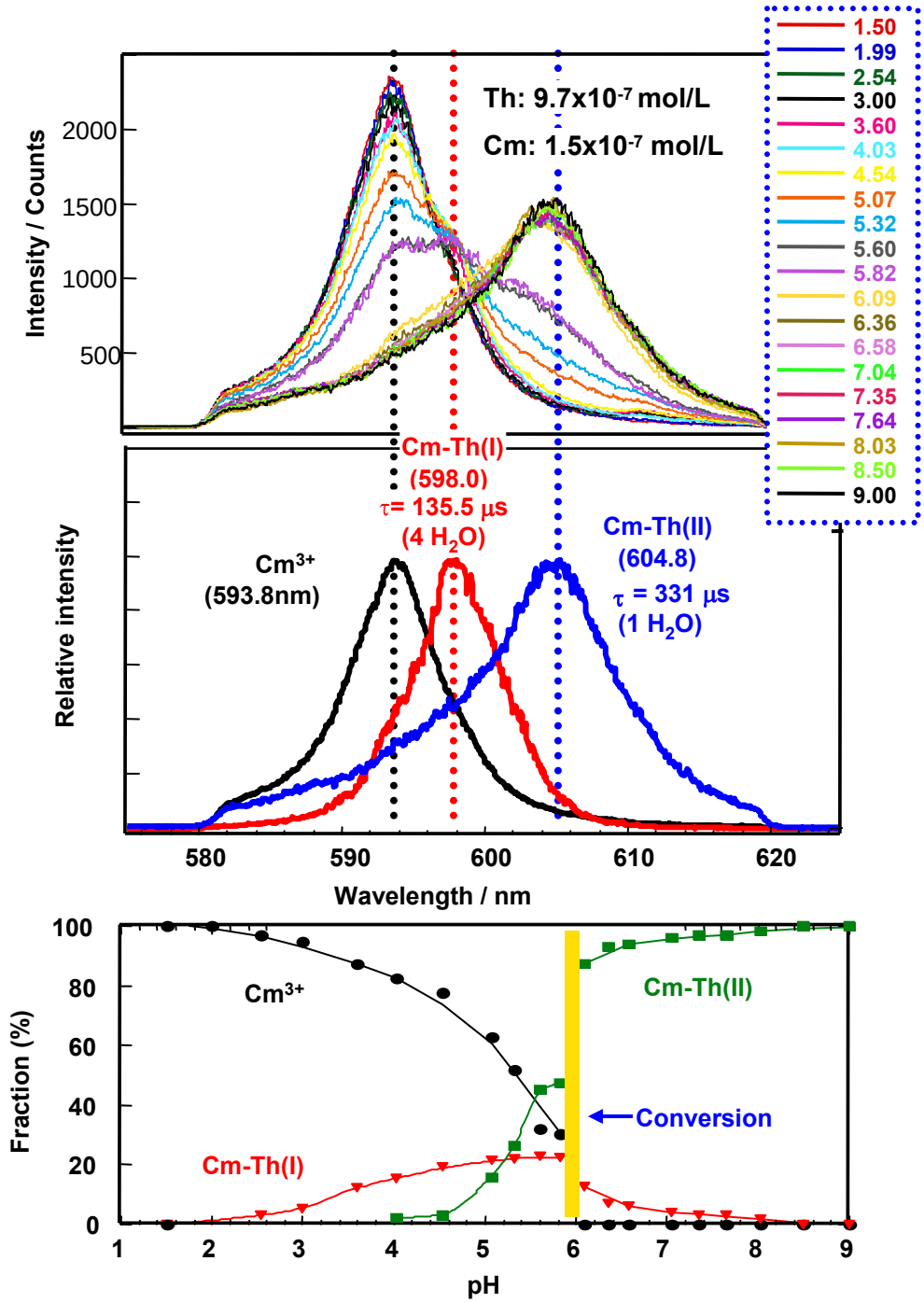

Fig. 78: Speciation of Th-borne Cm by TRLFS on the pH titration from 1 to 9 in a mixture solution containing 3.5×10^{-7} mol l^{-1} Th and 5×10^{-8} mol l^{-1} Cm: the pH dependent spectrum evolution (upper part) and the deconvoluted spectra of different Cm species present in the solution (middle part). The species distribution is given in the lower part.

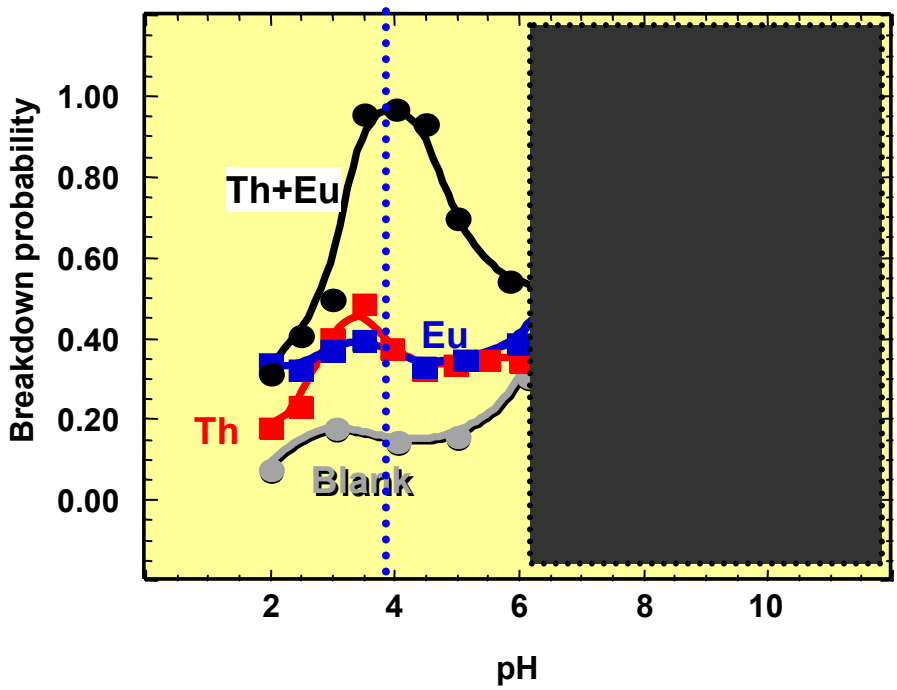

Fig. 79: Colloid generation observed by LIBD on the pH titration from 1 to 10 in a mixture solution containing 3.5×10^{-7} mol l^{-1} Th and 5×10^{-8} mol l^{-1} Eu (cf. Fig.78). Blank is water titrated by diluted HCl and NaOH. The latter contains colloidal impurities, which are however scavenged by Th for partial precipitation.

Table 1: Fluorescence emission properties of Cm in different solutions: a comparison. The Cm^{3+} aquoion has a emission peak at 593.8 nm with a life time of 65 μs and 9 inner sphere hydration water molecules

Solution	Parameter	Species (I)	Species (II)	Reference
Mixture of	Emission peak (nm)	598.5	601.8	this work
10^{-3} mol/l Si	Life time (μs)	83.5±3.7	88.3±5.2	
10^{-5} mol/l Al	H_2O molecule	6.9	6.4	
10^{-3} mol/l Si	Emission peak (nm)	598.5	601.9	this work
	Life time (μs)	85.5±6.1	88.1±8.5	
	H_2O molecule	6.8	6.5	
10^{-3} mol/l Al	Emission peak (nm)	598.2	604.1	this work
	Life time (μs)	82.0±2.9	110.5±6.7	
	H_2O molecule	7.1	5.0	
Colloidal	Emission peak (nm)	601.2	603.3	ref. 64
γ-Alumina	Life time (μs)	110	110	
	H_2O molecule	5.0	5.0	
Suspension	Emission peak (nm)	598.8	603.3	ref. 18
of smectite	Life time (μs)	110	110	
& kaolinte	H_2O molecule	5.0	5.0	
Colloidal	Emission peak (nm)	602.3	604.9	ref. 76
Silica	Life time (μs)	220±14	740±35	
	H_2O molecule	2.1	0	

Table 2: Comparison of colloid-borne Cm species without and with Th								
	HAS-Monosilanol					HAS-Polysilanol		
	Cm Species	Peak Max. (nm)	Relax. Time (μs)	Coord. Water (number)		Cm Species	Peak Max. (nm)	Relax. Time (nm)	Coord. Water (number)
Cm	Cm-HAS(I)	598.0	83.5	7		Cm-HAS(I)	598.5	83.5	7
	Cm-HAS(II)	601.8	88.5	6		Cm-HAS(II)	601.8	88.3	6
						Cm-HAS(III)	605.2	518.5	0-1
Cm+Th	Cm-Th(I)	598.0	132.8	4		Cm-Th(I)	598.5	135.3	4
	Cm-Th(II)	603.6	336.9	0-1		Cm-Th(II)	603.6	349.0	0-1